CHALMERS
UNIVERSITY OF TECHNOLOGY

Innovative timber floor

Development of a timber sandwich structure

Master's Thesis in the Master's Programme Structural Engineering and Building Technology

MATHILDA LARSSON
HENRIK MAYOR

Department of Civil and Environmental Engineering
Division of Structural Engineering
Steel and Timber Structures
CHALMERS UNIVERSITY OF TECHNOLOGY
Gothenburg, Sweden 2016
Master's Thesis BOMX02-16-109

MASTER'S THESIS BOMX02-16-109

Innovative timber floor

Development of a timber sandwich structure

Master's Thesis in the Master's Programme Structural Engineering and Building Technology

Mathilda Larsson

Henrik Mayor

Department of Civil and Environmental Engineering
Division of Structural Engineering
Steel and Timber Structures
CHALMERS UNIVERSITY OF TECHNOLOGY
Göteborg, Sweden 2016

Innovative timber floor
Development of a timber sandwich structure

Master's Thesis in the Master's Programme Structural Engineering and Building Technology

MATHILDA LARSSON

HENRIK MAYOR

Examensarbete BOMX02-16-109/ Institutionen för bygg- och miljöteknik,
Chalmers tekniska högskola 2016

Department of Civil and Environmental Engineering
Division of Structural Engineering
Steel and Timber Structures
Chalmers University of Technology
SE-412 96 Göteborg
Sweden
Telephone: + 46 (0)31-772 1000

Cover:
Timber sandwich floor with corrugated core.
Department of Civil and Environmental Engineering, Göteborg, Sweden, 2016

Innovative timber floor

Development of a timber sandwich structure

Master's thesis in the Master's Programme Structural Engineering and Building Technology

MATHILDA LARSSON
HENRIK MAYOR
Department of Civil and Environmental Engineering
Division of Structural Engineering
Steel and Timber Structures
Chalmers University of Technology

ABSTRACT

Timber has low bending and shear modulus, therefore serviceability limit state (SLS) requirements are often governing in design. The low stiffness makes it hard for timber floor systems to compete with concrete floors for long span (over 12 m) and/or high load (5-10 kN/m^2) applications. Timber floors also have a considerable structural height compared to concrete solutions. Sandwich structures provide high stiffness due to its geometric configuration. They have since the middle of the 20th century been implemented in a wide range of applications, however timber sandwich elements have not yet been used on a large scale in the building industry as load-carrying members.

The aim of this Master thesis was to investigate the possibilities and benefits of implementing sandwich technique in prefabricated timber floor systems. A concept of a timber sandwich floor was developed and two case studies were executed in order to evaluate the competitiveness of the concept. Only the structural part of floor systems was treated in the study.

Sandwich structures consist of two faces separated by a core. The core can be made in many different shapes. The corrugated core is considered most suitable for timber floors. The corrugation can be made by form-pressing veneers. Plywood, Kerto-Q and CLT are all found suitable material choices for the faces.

The best performance, with regard to deflection, of the sandwich floor is reached when the parallel direction of the corrugation and the main fibre direction of the face material are positioned along the short span. The positioning of the main fibre direction of the core material has in general low impact on the performance. Due to manufacturing, the corrugation will have curved corners; the curvature has low impact on the performance as long as it does not affect the number of corrugation cells. Supporting the floor on four edges instead of two edges yields significantly higher performance for a sandwich floor with aspect ratio 1:1.

In comparison to an existing timber floor system, the sandwich floor system can be designed with lower structural height and at the same time lower material volume. Unlike other timber floor systems, the sandwich floor can compete with concrete floor solutions for high load applications (5 kN/m^2).

Key words: Timber structures, floor systems, sandwich plates, corrugated core, deflection, first eigenfrequency

Innovativt träbjälklag
Framtagande av ett sandwichelement i trä

Examensarbete inom masterprogrammet Structural Engineering and Building Technology

MATHILDA LARSSON
HENRIK MAYOR
Institutionen för bygg- och miljöteknik
Avdelningen för konstruktionsteknik
Stål- och träkonstruktioner
Chalmers tekniska högskola

SAMMANFATTNING

Trä har låg böj- och skjuvstyvhet vilket gör att bruksgränstillstånd (SLS) oftast är dimensionerande vid design av träbjälklag. Den låga styvheten gör det svårt för träbjälklag att utmana håldäck när bjälklaget ska klara långa spann (över 12 m) och hög last (5-10 kN/m^2). Existerande träbjälklag har en betydligt högre konstruktionshöjd jämfört med håldäck. Sandwichelement har en hög styvhet tack vare sin geometriska utformning och började utnyttjas inom olika användningsområden under 1900-talet. Dock har inte träsandwichelement använts som konstruktionsdel i byggnader i större utsträckning.

Syftet med projektet var att undersöka möjligheterna och fördelarna av att implementera sandwichtekniken hos prefabricerade träbjälklag. Ett träbjälklags-koncept utvecklades och två fallstudier utfördes för att utvärdera konkurrenskraften mot existerande träbjälklag och andra material. Arbetet avgränsades till den bärande delen av trägolvet.

Sandwichstrukturer består av två flänsar som är separerade från varandra med en kärna i mitten. Kärnan kan utformas i olika former och material. En korrugerad kärna av formpressad faner anses effektiv ur produktionssynpunkt. Plywood, Kerto-Q och CLT är material som anses vara lämpliga för flänsarna.

Träsandwichbjälklaget uppnår den högsta kapaciteten, med hänsyn till nedböjning, när korrugeringens längsriktning och fibrernas huvudriktning är placerade längst det korta spannet. Huvudriktningen på fibrerna i kärnan har en liten inverkan på den totala kapaciteten. På grund av tillverkning kommer korrugeringen att ha rundade hörn vilket inte har någon påverkan på kapaciteten så länge rundningen inte påverkar antalet korrigeringsceller. Stöd på fyra kanter istället för två visar sig ge en väsentlig högre kapacitet när bjälklaget har sidoförhållandet 1:1.

I jämförelse med ett existerande träbjälklag kan träsandwichbjälklaget produceras med en lägre konstruktionshöjd och lägre materialvolym. Träsandwichbjälklaget visar sig, i jämförelse med existerande träbjälklag, kunna utmana betonggolv vid höga laster. Den låga vikten motsvarande 15 % av vikten hos håldäck är en fördel för träsandwichelement.

Nyckelord: Träkonstruktion, träbjälklag, sandwichelement, korrugerad kärna, nedböjning, första egenfrekvens

Contents

Preface

We both share a deep interest in timber structures and green building. This made us want to spend the spring 2016 learning and investigate more about new ways of constructing in timber. We hope that this project, the beginning of developing a new timber floor system, will contribute to timber structures and increase the possibilities and benefits of building with timber in the future. We both see timber structures as a key factor for green building.

This Master's thesis was carried out at the department of Civil and Environmental Engineering at Chalmers University of Technology. We would like to take the opportunity to thank Peter Nilsson who has contributed with his great knowledge in sandwich structures. We would also like to thank Rasoul Atashipour who has contributed to this Master's thesis with his deep knowledge in plate theory.

We would like to send great gratitude to our supervisor and examiner Mohammad Al-Emrani for his support, deep knowledge and encouragement with nutrition during the whole project.

Finally, we would like to thank our opponents Axel Steinert and Herman Mellegard for their inputs and comments to this thesis.

Gothenburg, May 2016

Mathilda Larsson

Henrik Mayor

Notations

Roman upper case letters

A_c	Area of core per unit width, [m^2/m]
A_f	Floor area, [m^2]
A_{ij}	In-plane stiffness coefficients, [N/m]
$A_{f.bot}$	Area of bottom face per unit width, [m^2/m]
$A_{f.top}$	Area of top face per unit width, [m^2/m]
B	Floor span in y-direction, [m]
D_{ij}	Stiffness coefficients used in plate constitutive equation, [Nm] and [N/m]
$D_{s.ij}$	Bending stiffness coefficients, [Nm]
D_{Qx}	Transverse shear stiffness in x-direction of sandwich plate, [N/m]
D_{Qy}	Transverse shear stiffness in y-direction of sandwich plate, [N/m]
D_x	Bending stiffness in x-direction of sandwich plate, [Nm]
D_y	Bending stiffness in y-direction of sandwich plate, [Nm]
D_{xy}	Torsional stiffness of sandwich plate, [Nm]
E_i	E-modulus in local material coordinate system, [Pa]
E_c	Modulus of elasticity of core material, [Pa]
E_f	Modulus of elasticity of face material, [Pa]
E_x	Axial stiffness in x-direction of sandwich plate, [N/m]
E_y	Axial stiffness in y-direction of sandwich plate, [N/m]
G_{ij}	Shear stiffness in local material coordinate system, [Pa]
G_c	Shear stiffness of core material, [Pa]
G_f	Shear stiffness of face material, [Pa]
G_v	Panel shear stiffness, [Pa]
G_r	Planar shear stiffness, [Pa]
G_{xy}	Horizontal shear stiffness of sandwich plate, [N/m]
I_c	Moment of inertia, around global neutral axis, of core per unit width, [m^4/m]
$I_{f.bot}$	Moment of inertia, around global neutral axis, of bottom face per unit width, [m^4/m]
$I_{f.top}$	Moment of inertia, around global neutral axis, of top face per unit width, [m^4/m]
I_x	Moment of inertia, around global neutral axis, in x-direction per unit width, [m^4/m]
K	Shear correction factor, [-]

L	Floor span in x-direction, [m]
M_{Ed}	Applied bending moment, [Nm]
M_{Rd}	Bending moment resistance, [Nm]
Q	Concentrated load, [N]
Q_k	Characteristic value of concentrated load, [N]
Q_d	Design value of concentrated load, [N]
R_c	Radius of core, [m]
T	Shear force, [N]

Roman lower case letters

b_{top}	Bond line length of upper part of corrugation per unit width, [m/m]
f_1	First eigenfrequency, [Hz]
f_{ii}	Compression/tension strength in local material coordinate system, [Pa]
f_{ij}	Shear strength in local material coordinate system, [Pa]
f_c	Horizontal component of corrugated core (or bond length), [m]
$f_{c.0.d}$	Compressive strength parallel to the grain, [Pa]
$f_{c.90.d}$	Compressive strength perpendicular to the grain, [Pa]
f_{md}	Design bending strength, [Pa]
$f_{t.0.d}$	Design tensile strength parallel to the grain, [Pa]
$f_{t.90.d}$	Design tensile strength perpendicular to the grain, [Pa]
$f_{v.d}$	Design shear strength, [Pa]
$f_{v.k}$	Characteristic shear strength, [Pa]
h	Distance between centroid of top face and bottom face, [m]
h_c	Height of core, [m]
h_h	Height of honeycomb core, [m]
h_{tot}	Height of sandwich plate, [m]
$k_{c.90}$	Factor taking into account the load configuration, possibility of splitting and degree of compressive deformation [-]
k_{def}	Deformation factor, [-]
k_{mod}	Modification factor, [-]
$l\alpha$	Length of inclined corrugation leg, [m]
l_c	Length of corrugation, [m]
m_{freq}	Mass per unit area, [kg/m^2]
p	Half corrugation length, [m]
q	Uniformly distributed load, [N/m^2]

q_k	Characteristic value of uniformly distributed load, [N/m^2]
q_d	Design value of uniformly distributed load, [N/m^2]
S	Shape factor based on the geometry of the corrugation, [-]
t_c	Thickness of core, [m]
$t_{f,top}$	Thickness of top face, [m]
$t_{f,bot}$	Thickness of bottom face, [m]
v	Impulse velocity, [m/s]
w	Deflection, [m]
w_c	Precambering, [m]
w_{1kN}	Deflection due to concentrated load with amplitude of 1 kN, [m]
w_{fin}	Final deflection (including creep) , [m]
w_{inst}	Instantaneous deflection, [m]
$w_{net,fin}$	Net final deflection (including creep and precambering), [m]

Greek lower case letters

α_A	Area reduction factor, [-]
α_c	Corrugation angle, [°]
γ_M	Material partial factor, [-]
$\mathbf{z}$	Damping ratio, [-]
λ	Buckling load factor, [-]
ν_c	Poisson's ratio of core material, [-]
ν_f	Poisson's ratio of face material, [-]
ν_{ij}	Poisson's ratio in local material coordinate system, [-]
ν_x	Poisson's ratio related to bending of sandwich plate, [-]
ν'_x	Poisson's ratio related to stretching of sandwich plate, [-]
ν_y	Poisson's ratio related to bending of sandwich plate, [-]
ν'_y	Poisson's ratio related to stretching of sandwich plate, [-]
σ_{ii}	Normal stress in local material coordinate system, [Pa]
$\sigma_{c.0.d}$	Design compressive stress parallel to the grain, [Pa]
$\sigma_{c.90.d}$	Design compressive stress perpendicular to the grain, [Pa]
$\sigma_{t.0.d}$	Design tensile stress parallel to the grain, [Pa]
$\sigma_{t.90.d}$	Design tensile stress perpendicular to the grain, [Pa]
τ_{ij}	Shear stress in local material coordinate system, [Pa]
τ_d	Design shear stress, [Pa]

$\tau_{x,top}$	Shear stress core/top face intersection in x-direction, [Pa]
$\tau_{x,bot}$	Shear stress core/top face intersection in x-direction, [Pa]
ψ_0	Factor for combination value of variable action, [-]
ψ_2	Factor for quasi-permanent value of variable action, [-]

1 Introduction

Sandwich elements provide high strength and stiffness by using material in an efficient way. This Master's thesis is about the development of a new timber floor system created as a sandwich structure. Timber sandwich elements have not been implemented as structural components in buildings on great scale and few studies on timber sandwich elements for building applications have been conducted. The thesis deals with a conceptual development of a sandwich floor and investigations on the structural behaviour and performance of the floor.

1.1 Background

In the beginning of the 1990s the restriction in Sweden against constructing timber buildings higher than two stories was eased. The growing environmental awareness in combination with the eased regulations on timber constructions have increased the interest for timber as building material for multi-story buildings. In the current trend of constructing multi-story timber buildings, there is a need for a new structural floor element that provides high stiffness and strength. Conventional timber floor systems used in Sweden today have large structural height and are prone to vibration problems. Many building objects in Sweden have height and not floor restrictions. Lower structural height of the floor opens the possibility to fit more floors in a multi-storey building with restricted height. Further on, the market for timber floors is almost non-existing for spans longer than 12 m or with imposed loads at 5-10 kN/m^2. If a timber floor system could span longer and carry higher loads, it will offer prospects of gaining market in a new field.

The serviceability limit state (SLS) criteria regarding deflection and vibration are often governing in design of the load-carrying structure of timber floors. The problems regarding deflection and vibrations can be overcome with a high stiffness to low weight structure. Timber is a lightweight material however it also has low bending and shear stiffness.

Sandwich elements provide high stiffness by using the material in a structurally efficient way. During the second part of the 20^{th} century sandwich elements have been implemented in a various range of fields. They have for example been used in the ship and aircraft industries and later on in bridge decks. Larger structures using sandwich elements are often made in steel or FRP. Timber sandwich elements are less common even though the military aircraft "Mosquito", considered to be the first sandwich structure, was made in timber. Sandwich elements in timber have not, on a large scale, been implemented in the building industry as load-carrying structures. By engineering the geometrical and material properties of these elements, timber sandwich structures with high stiffness can be produced to low material use.

1.2 Aim and objectives

In this Master's thesis a concept for a new timber floor system was developed. The aim was to investigate the possibilities and potential benefits of implementing sandwich technique in prefabricated timber floor systems.

The structural behaviour of the new timber floor was evaluated with the objective to identify how design choices influence the performance. Two case studies were performed with the objectives to compare the performance with an existing floor system and to see if the new floor system could offer prospects to gain a new market for timber floors.

1.3 Method

The process of developing a concept for a new timber floor and investigating the behaviour and performance of the floor was divided into four parts. The parts, with their different methods and the targeted outcome, are presented below.

Literature study
The following parts were covered in the literature study:

- Engineered wood products.
- Conventional floor systems used in Sweden today.
- Existing sandwich floor structures.
- Overview of sandwich structures, both regarding structural behaviour as well as history and application.
- Research done on sandwich elements made of timber or wood-based products, independent of application area.
- The dynamic behaviour of timber floors.
- Design requirements for timber floor structures.

The outcome of the literature study was to:

- Present an overview of existing conventional timber floor systems and their maximum span and structural height.
- State the design requirements for timber floors.
- Relate the dynamic behaviour of timber floors to the vibration requirements.
- Demonstrate possible timber sandwich floor solutions.
- Compile important information and design guidelines of timber sandwich structures.

Concept development
This part aimed to present and evaluate promising sandwich configurations and material possibilities. The evaluation was based on a qualitative assessment focusing on manufacturing costs and methods in relation to structural performance. The outcome of the concept development was a sandwich configuration with determined wood-based material to study further.

Structural behaviour investigation
The structural behaviour of the timber sandwich floor was investigated by creating FE-models in Abaqus/CAE. Different aspect ratios and cross-sections were investigated. The preliminary dimensions of the cross-sections were generated with analytical calculations which accuracy was investigated by comparing the analytical performance with numerical models.

The main target of this study was to give an intention of how the structural performance was influenced by geometrical and material aspects. Further, to ensure that the analytical calculations could be used when generating preliminary dimensions of the cross-section.

Case studies
The gained knowledge from the structural behaviour investigation was used in this phase when generating concepts in two case studies. In the first case study was the sandwich floor compared with an existing timber floor system. The second case study dealt with a more complex scenario, to carry high load was a requirement and a lightweight structure was desired due to constrains in the construction process. In both case studies the performance of the sandwich floor was validated with FE-models in Abaqus/CAE.

The outcome of the first case study was to see if the sandwich floor could be designed with lower structural height than the existing floor. The second case study was performed to see if the sandwich floor could be applied for high load applications.

1.4 Limitations

This project focused on developing a new structural timber floor with a technique that is new for the building industry and with little research conducted in the field. Therefore it was necessary to narrow down the project and following limitations were made:

- The study focused only on the structural performance of the floor system; therefore the acoustical performance was not treated even though acoustics often are an important factor for floors.
- The fire performance of the floor was not evaluated.
- The choice of material of the new floor system was limited to wood-based products available on the market in the Nordic countries.
- A more detailed cost estimation of the manufacturing of the sandwich floor was not performed.
- The new timber floor was designed with regard to requirements for high frequency floors and transient loading.

2 Literature study

The following chapter is divided into different parts. First a presentation is given of different engineered wood products and how they can be shaped. This is followed by general information about timber floor systems and a presentation of prefabricated floor systems available on the Swedish market today. Thereafter sandwich structures are introduced; how they work, history, applications, available timber sandwich floors and different core configurations. Finally, criteria regarding vibration and deflection of timber floors and loading on floors are presented.

2.1 Engineered wood products

Different to sawn timber, which is more or less cut down trees sawn into desired dimensions, engineered wood products (EWPs) are in a greater extent processed and engineered. Advantages with processing wood are the possibilities to (Gard, 2015):

- Homogenizing properties, both physical and mechanical, in desired direction (longitudinal, transverse or radial).
- Synthesizing needed properties like shape, dimensions and mechanical properties.

EWPs can be divided into subgroups based on the form of wood they are produced from (Gard, 2015):

- Sawn timber boards
- Veneers
- Strands
- Particles
- Fibres

Most EWPs used today have been developed during the 20th century where most products have been invented in North America (Johansson M. , 2011). In Figure 2.1 common EWPs are categorized under the form of wood they are made from.

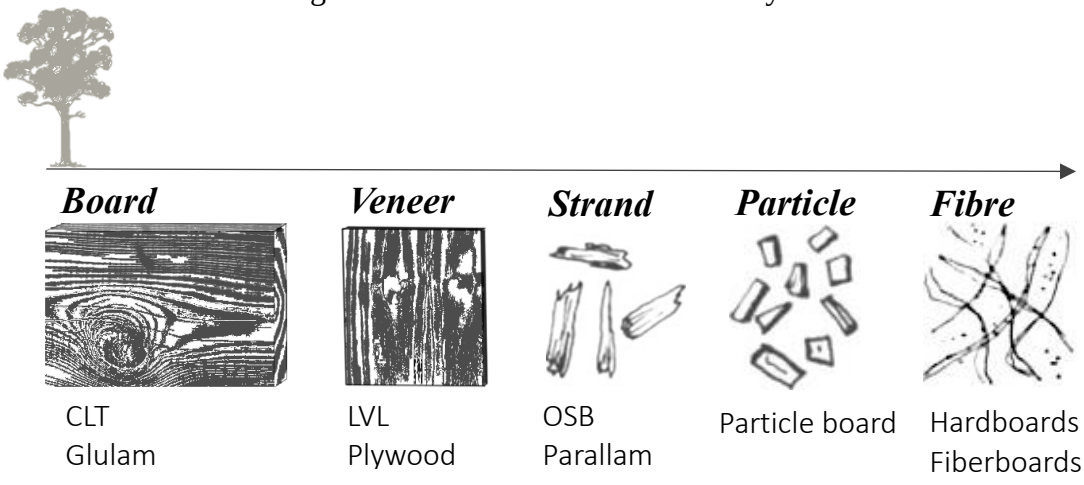

Figure 2.1: EWPs made from different type of wood.

The strength as well as other properties of timber varies to a great extent between different trees and even within a tree. It is therefore important to classify timber into specific strength classes with mechanical or visual grading. The variability of strength within the member and class is taken into account in Eurocode when using the partial factor for material properties. A material partial factor of 1.3 is used for solid timber while a factor of 1.25 is used for glued laminated timber and a factor of 1.2 is used for plywood (EN 1995-1-1, 2004). From the partial factors it can be concluded that the variability of strength is lower in plywood and glued laminated timber material than solid timber. This can be explained by the difference in production where plywood and glued laminated timber are made out of smaller parts of timber which are assembled together. Consequently these products avoid concentrations of defects, like knots and fibre distortion, in a larger range than solid timber. A more detailed description of some common EWPs follows below.

2.1.1 EWPs made from boards

These products are made from sawing timber into boards and then glue them together into beams or panels.

Glued laminated timber (Glulam)
Glulam consists of several laminations (at least four) adhesively bonded to each other with all fibres in axial direction. Normal straight glulam beams in Sweden are made of laminates with a thickness of 45 mm. Glulam beams are normally up to 215 mm wide but can be made wider by gluing beams to each other. The strength with regard to size is similar for glulam and solid wood but the variability in strength is lower for glulam (Johansson M. , 2011).

Glulam is mainly used for beams. The characteristic glulam bending strength is higher than the characteristic tensile strength of a single laminate. A reason for this is the alternative stress path provided by adjacent laminations. Commonly five different strength classes are used for glulam; GL20, GL24, GL28, GL32 and GL36. Glulam can also be manufactured with boards of different strength classes where the stronger timber is placed in the high stress regions in order to achieve higher material efficiency, this is called combined glulam (Colling, 1995)

Cross-laminated timber (CLT)
Similar to glulam, CLT is made from sawn timber boards. Different to glulam, the boards in CLT are placed with the fibres perpendicular to the layer above and below. CLT panels can be made of 3, 5, 7 or even more layers and the layers can vary in size. They can be made with maximum dimensions of 300 mm in thickness, 3 m in width and 24 m in length. The strength parameters are set by the manufacturer. The layers are often bonded with adhesives but can also be connected with nails or screws. CLT panels have for example been used as load-bearing walls and floor diaphragms (Johansson M. , 2011).

Forming of boards
It is possible to create curved glulam elements. The curvature depends on the thickness of the laminates and the strength class. A laminate thickness of 45 mm and a strength class of GL32 can provide a bending radius of 7 m (Nordic Wood, 2001).

2.1.2 EWPs made from veneer

Veneers are thin layers of wood, usually in the size range 2-4 mm. Veneers are obtained through rotary peeling of logs (Johansson M. , 2011).

Laminated veneer lumber (LVL)
LVL is made by gluing veneer sheets together and hot press the mat in temperatures around 150^{o}C (Ranta-Maunus, 1995). Normal LVL has all the fibres in longitudinal direction; however the fibres can also be placed perpendicular to each other. For example, the Finish LVL product Kerto-S has all the fibres in same direction while Kerto-Q has 80% of the fibres in one direction and 20% of the fibres perpendicular to the other fibres. This creates more stiffness in transverse direction which can be beneficial for some structural applications. LVL can be fabricated in up to 3 m in width and 24 m in length (Johansson M. , 2011). Standard thicknesses of LVL-Kerto are in the range of 27-75 mm (Ranta-Maunus, 1995).

LVL can be used as beams, plates, members of trusses or shells (Ranta-Maunus, 1995). It has in general high bending, tension, compression and shear strength and relatively high modulus of elasticity (Johansson M. , 2011). Ranta-Maunus (1995) suggests that LVL should be used where high strength and dimensional stability is needed. A beam made of Kerto-S has a characteristic bending strength of 44 MPa (Metsä Wood, 2013) which is significantly higher than the strength for common solid timber. The statistical variation in strength is smaller for LVL than glulam. The durability of LVL is similar to natural wood and the fire resistance is equivalent to glulam (Ranta-Maunus, 1995).

Plywood
Plywood is manufactured in a similar fashion as LVL, but different to LVL the veneers are laid up with fibres perpendicular to each other. The number of veneers is always odd so the first and the last layer have fibres in the same direction. The veneers are bonded with different kinds of adhesives. Structural plywood is in Sweden often produced in sheets with the dimensions 1200x2400 mm^2 or 1220x2440 mm^2 with a thickness of 12 mm or 24 mm (Johansson M. , 2011). The Swedish plywood P30 has, in the strong direction, the characteristic bending strength 23 MPa for 12 mm thickness and 21.6 MPa for thickness 24 mm. However the strength properties depend on the wood it is made from. The density of plywood varies between 350 kg/m^3 to 550 kg/m^3 which give an indication of the strength range. Plywood can for example be used as faces or webs in beams, as diaphragms or as wall panels (Steck, 1995).

Differences can be identified when comparing plywood and its constituents. The density of plywood is higher than the original wood; the density difference is dependent on the amount of adhesive and pressing. Creep deformation is slightly larger in plywood, the increase in creep is related to the glue lines. The deformation of plywood when subjected to compression perpendicular to the fibres is smaller (Steck, 1995).

Forming of veneers
The shape of the veneers can be influenced by temperature, moisture and time. Different methods, such as extrusion, roll-forming, press baking, hot-pressing and matched die take these parameters into account in different ways when forming the

veneers. To avoid cracks when curving the veneers the design, radius-to-thickness ratio and fibre direction, have some restrictions (Srinivasan, Bhattacharyya, & Jayaraman, 2007). Srinivasan et al. (2007) have performed tests on the formability of veneers and conclude that a three-veneer sheet is more suitable to curve compared to a two-veneer sheet. They further conclude that the minimum ratio between the bending radius and veneer thickness must be six or larger if the fibres of the outer veneers are perpendicular to the bending axis.

Veneers can be formed into corrugated 3D structural plates. It is the thickness of the veneers that set the limit for the radius of curvature of the corrugation (Hunt, 2004). According to Hunt (2004) several U.S. patents describe corrugating processes and apparatus.

In the hot-pressing process veneer sheets are placed in a moulding press in desired order with glue in between the sheets. At least one sheet should be placed with the fibre direction perpendicular to the other sheets for improved shape stability. After forming in the moulding press the veneer product is heated to the hardening temperature of the glue. The product is then removed from the mould to cool and dry. The process in the moulding press takes about three minutes (Magnevik, 2006).

Plywood can be formed-pressed directly. It also exist plywood products that facilitates the form-pressing like UPM Grada 2000 (UPM, 2014). However UPM Grada is more expensive than conventional birch and conifer plywood from the same manufacturer (CEOS, 2016).

Kavermann (2013) used a matched die process to bend plywood. He observed some forming issues; variation in profile height, delamination and damage of the outer veneers. Cracking of the outer veneers is more evident when the outer fibres are placed parallel to the bending axis. According to Kavermann (2013) roll-forming is a more efficient manufacturing method for large scale production of bent plywood than matched die process.

2.1.3 EWPs made from strands, particles and fibres

Strands, particles and fibres are all smaller wood elements than boards and veneers. Products are made by these elements in industrialised processes where the elements are glued to each other. The strength of the products is to a great deal dependent of the manufacturing process and also on the type and amount of adhesive (Johansson M. , 2011). A disadvantage with products made from strands, particles and fibres is that they consume more energy in the processing than solid timber. However they have the clear advantages that they can be produced from waste from other wood processes or from fast growing small trees (Griffiths, 1995).

Parallel strand lumber (Parallam)
Parallam is a beam-like product. The product is made by peeling logs into veneers and then cut the veneers into strands. The strands are glued together and cured under heat and pressure. The final beam product has maximum dimensions of 20 m in length, 480 mm in depth and 285 mm in width. Parallam has similar characteristic bending strength as LVL and is often used as high strength beams (Ranta-Maunus, 1995).

Oriented strand boards (OSB)
OSB is made from thin wood strands from small-diameter logs. The product consists of 95% strands and 5% adhesives bonded under heat and pressure. The fibres are oriented in the longitudinal direction on the outside of the board and randomly oriented on the inside. This is done to give the board better mechanical properties (Johansson M. , 2011).

OSB products are often used as panels with dimensions 1200x2400 mm^2 and 6 mm or 25 mm in thickness. However much larger panels can be manufactured, up to 25 x 3 m^2 and 75 mm in thickness. The panels can be used for structural applications by bonding them to each other in a similar way as CLT (Johansson M. , 2011).

Solid timber has an anisotropy about 40:1 while OSB has an anisotropy about 2.5:1, where the anisotropy is a ratio of the strength in longitudinal and transversal directions. Unless the OSB is heavily densified, the strength and stiffness are significantly lower than solid timber (Griffiths, 1995).

Particleboard and chipboard
Particleboards are produced from wood particles like sawdust while chipboards are produced from chips which are smaller than strands but larger than particles. Chipboards are normally produced of 85% chips and 15% adhesives (Johansson M. , 2011).

Fibreboards
Fibreboards can be produced either with hot-pressing or wet-process manufacturing. In hot-pressing adhesive is used as binder, in wet-process manufacturing the lignin in the wood is used as binder. Masonite is a structural element manufactured with the latter method (Johansson M. , 2011).

Forming of strands, particles and fibres
Hunt (2004) presents some manufacturing processes to make corrugated cores from wood flakes. He states that the strength can be increased and the formability eased by aligning the flakes in the direction of the corrugation. Hunt (2004) presents several patents where particles and fibres are processed into different 3D structures like corrugated structures, two-direction pyramid-like structures and open grid structures. He states that wood fibres can be shaped more freely than veneers.

2.2 Timber floor systems

The governing structural design criteria for the load-bearing floor systems are often deflection and vibration in serviceability limit state. However, the design of a floor system is also dependent on fire resistance, sound performance and integration of technical installations. Floor systems generally have a complete separation of the structural part and ceiling to meet the acoustic requirements (Johnsson, 2011).

Prefabricated timber floor systems used in Sweden today are commonly two-edges simply supported and the structural action is consequently in one-way (Träguiden, 2014). Brandin & Oscarsson (2015) state that it could be beneficial with regard to vibration to use a four-edges simply supported floor system that allows a two-way action.

In order for timber floor systems to compete with concrete floor systems, like hollow core floor slabs, in a greater extent Risberg (2016) says that the industry needs to learn how to use timber and that engineers in general have limited knowledge about timber structures. According to Johansson (2016) the choice of concrete before timber is influenced by tradition and habit. Further on Risberg (2016) says that when spans are long, over 12 m, there exist few timber floor solutions today. Johansson (2016) states that it is hard to use timber floor systems, in for example industry buildings, where the imposed load is 5-10 kN/m^2.

2.2.1 Services in timber floor systems

In case of good planning, sewer pipes and horizontal ducts can be placed between the webs of a floor system. The possibility of making holes in the webs is small so the pipes and ducts need to be parallel to the webs in order to integrate them in the structure. Placing pipes outside the load-bearing structure creates more freedom regarding the direction of pipes and ducts, however the spacing between the structural part and the ceiling needs to be larger and therefore the total height of the floor system becomes higher. Electrical services can be placed under the floor system without significantly increase the total height (Martinsons, 2006).

2.2.2 Wall-floor connection

A floor can either be laid on top or hung on load-bearing walls. Both types of connections contain difficulties that have to be dealt with. When the floor is laid on top of the wall large compression forces perpendicular to the fibres are present, air tightness is more difficult to achieve and horizontal forces need to pass the floor element. When the floor is hung, hangers need to be used and this can result in weaker joints with risk for additional deflection (Johnsson, 2011).

To achieve sufficient acoustic performance, the transfer of vibration from floors to walls should be avoided. Therefore some kind of vibration damping is needed in the joint (Johnsson, 2011).

2.2.3 Timber floor systems on the Swedish market

In the literature study four different floor systems from three different manufacturers, established on the Swedish market, were identified. All four systems have one-way action.

Martinsons floor systems
Martinsons have different types of floor systems consisting of a CLT upper plate, web and bottom flange of glulam. Two of Martinsons floor systems are illustrated in Figure 2.2 and have a structural height of 346 and 410 mm and can span 6.5 and 8.5 m respectively (Martinsons, 2012).

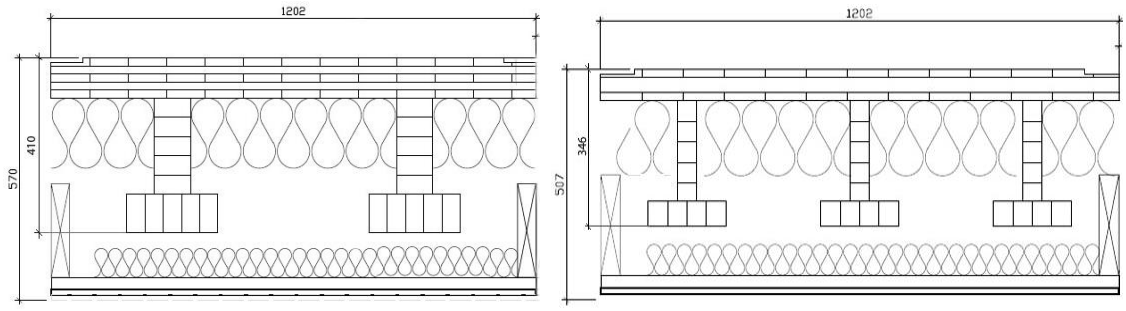

Figure 2.2: a) Marinsons floor system MBK-12-02 and b) MBK-03-02 (Martinsons, 2012).

Kerto-Ripa

Kerto-Ripa, illustrated in Figure 2.3, is produced by Metsä Wood and is a part of Moelven's Trä8 system, a complete prefab building system. The upper and lower plates are made of Kerto-Q while the ribs are made of Kerto-S (Moelven, 2016). The floor system can span up to 8 m (Metsä Wood, 2016).

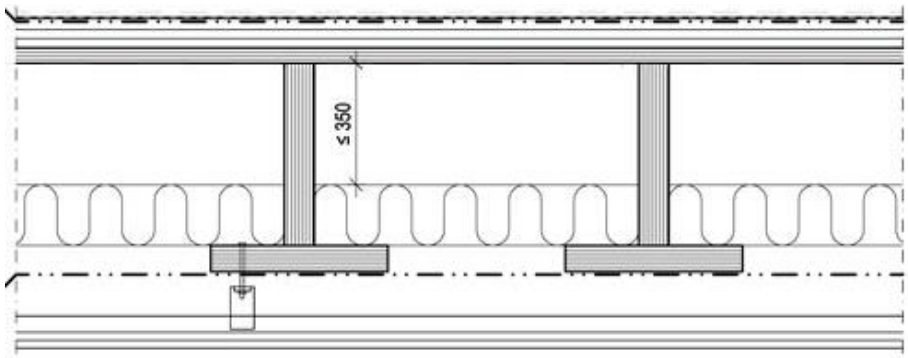

Figure 2.3: Kerto-Ripa floor system (Metsä Wood, 2016).

Masonite M101

Masonite produces a floor system where the main load is carried by I-beams. The upper and lower plates are not integrated with the flanges. The flanges of the I-beam consist of solid wood while the web consists of OSB, the cross-section is illustrated in Figure 2.4. The height of the I-beams can vary between 200 and 450 mm and span 3.7 to 9.1 m with a spacing of 400 mm. A fibreboard and gypsum board is placed on top and below the beams making the total height of the floor system 494 mm (Masonite Beams AB, 2010).

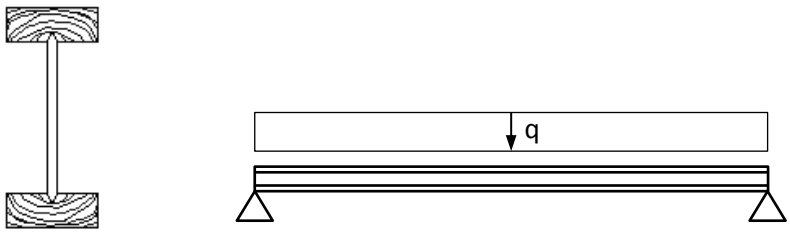

Figure 2.4: Masonite beam used in M101 floor system.

2.3 Sandwich structures

A sandwich plate consists of two thin faces of relatively high strength which are separated by a low density core. These plates have a high strength to weight ratio and can be made out of different materials.

2.3.1 The sandwich effect

A sandwich element has a high bending stiffness due to its specific arrangement of material. When it is subjected to bending the majority of the normal stress is carried by the faces while the shear stress is carried in the core (Allen, 1969). The bending stiffness can be increased by placing the faces further away from the neutral axis. For example, if the distance between the faces is 20 times the thickness of one face, the flexural rigidity is increased about 300 times (Vinson J. , 2001), which is illustrated in Figure 2.5. However the core must be stiff and strong enough to resist shear. The function of the core stiffness is furthermore to keep the faces nearly flat to avoid local buckling. The faces and the core need to be connected to each other to allow force transfer and obtain composite behaviour. The connection is often made with adhesives (Allen, 1969). A sandwich structure can be analysed using beam or plate analysis depending on if the structure acts in one or two ways (Zenkert, 1997).

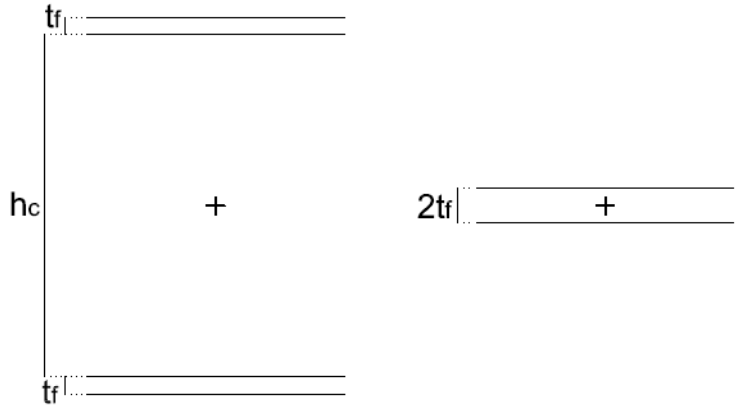

Figure 2.5: The flexural rigidity is increased by placing the faces away from the neutral axis. If $h_c/t_f=20$ the flexural rigidity is increased about 300 times compared to a monolithic structure with thickness $2t_f$.

2.3.2 History and application of sandwich structures

Nowadays sandwich structures are found in many different applications like satellites, aircrafts, ships, automobiles, rail cars, wind energy systems and bridge construction (Vinson J. R., 2005). In literature Fairbairn is often denoted the first person to have described the concept of sandwich structures, which he did 1849 in England (Vinson J. R., 2005), (Allen, 1969). However the concept was first used in a major structure almost 100 years later, in the British Second World War aircraft "Mosquito" by De Havilland (Allen, 1969). In 1944 the first research paper concerning sandwich elements was published and during the following period of ten years several papers dealing with theoretical analysis of sandwich elements were published (Zenkert, 1997). In the beginning of the 1950s honeycomb core materials were developed, primarily for the aerospace industry (Zenkert, 1997) and in the 1960s the U.S. Naval Air Engineering Center sponsored research concerning fiberglass sandwich structures

in order to compete in weight with conventional aluminium aircraft construction (Vinson J. R., 2005). During the 1970s research began in Sweden about the use of composite sandwich structures for naval ship hulls (Vinson J. R., 2005). Since the mid-seventies focus has changed from theoretical research to optimizations based on finite elements analysis (Zenkert, 1997). Since 1999 there is a journal fully devoted to sandwich structures, the "Journal of Sandwich Structures and Materials" (Vinson J. R., 2005).

2.3.3 History and application of timber sandwich structures

As mentioned in Chapter 2.3.2 sandwich structures were first used in the British military aircraft "Mosquito". As it happens to be, the sandwich elements used in the "Mosquito" were made out of timber, which can be seen in Figure 2.6 (Vinson J. R., 2005).

Figure 2.6: The wood fuselage of the "Mosquito" (Hisgett, 2012).

The design of the aircraft was presented in 1939 and the aim was to create an aircraft that did not further strain the metal industries. The entire fuselage was made of a balsa-plywood sandwich. The lightweight balsa wood was placed between two 3-ply spruce or birch faces, where spruce was used at the front of the fuselage and birch at the end (Ricker, 2005). During the 1950s several publications of analysis of sandwich structures emanated from U.S. Forest Products Laboratory (USFPL). They were associated with wood products and the research was focused on orthotropic materials like wood (Vinson J. R., 2005). USFPL has in a report from 1959 by Markwardt & Wood documented the use of sandwich plates in building construction. In the so-called Acorn House, built 1948, sandwich plates made of wood and paper were used both in the floor and roof structure. The plates consisted of an impregnated corrugated paper honeycomb core bonded to plywood faces from Douglas-fir. The height of the core was approximately 38 mm and the thicknesses of the faces were 10 mm. The floor plates spanned about 1.5 m (Markwardt & Wood, 1959). It seems as the development of sandwich elements during the latter part of the 20th century primarily has been related to other materials than wood. As the interest and demand of sustainable materials has increased, publications from the last ten years can be found dealing with wood sandwich plates, for example (Labans & Kalnins, 2011),

(Kavermann, 2013), (Li, Hunt, Gong, & Cai, 2014) and (Klimek, Wimmer, Brabec, & Sebera, 2015). The proposed plates are in general developed to carry smaller loads than floors.

2.3.4 Failure of sandwich structures

The critical failure modes for sandwich structures are influenced by geometry, material properties, design and how the structure is loaded. Zenkert (1997) states the most common failure modes and highlights the importance of being aware of these when analysing and designing sandwich structures. The failure modes are illustrated in Figure 2.7.

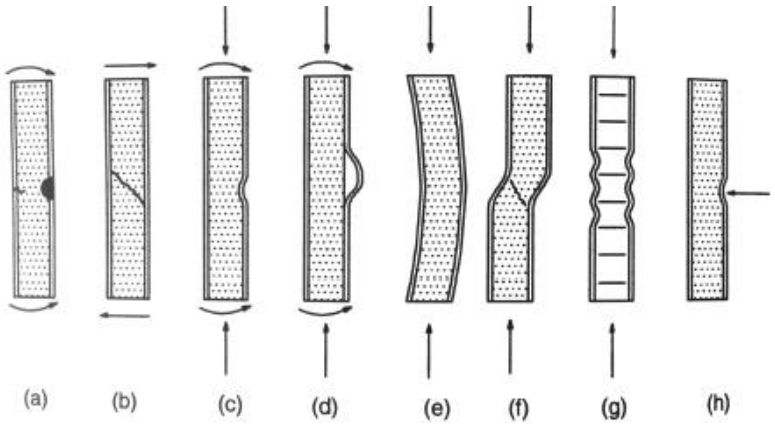

Figure 2.7: Failure modes: a) Face yielding/fracture, b) core shear failure, c) and d) face wrinkling, e) general buckling, f) shear crimping, g) face dimpling, h) local indentation. (Zenkert, 1997).

One of these modes is general buckling that often occurs if the structure is too slim or the core is not rigid enough. This may not always causes the structure to fail but reduces the capability. Face wrinkling occurs when the structure is subjected to an in-plane compressive load and/or the face is in compression during bending. This failure mode is characterized by the small wavelengths on one or both faces. Debonding takes place when the face to core bonding fails and is often difficult to detect. It is therefore important to avoid this failure mechanism by choosing a superior adhesive (Zenkert, 1997).

2.3.5 Timber sandwich floor systems on the European market

Three different sandwich timber floor systems available on the European market have been identified. Both Kielsteg and Lignatur utilises one-way action. Information about the structural performance of DendroLight has not been found.

Kielsteg
Kielsteg is a sandwich floor system from Austria with a V-similar core made out of plywood or OSB, illustrated in Figure 2.8. The product is described to be suitable as roof or floor systems where larger spans are required since the system can span up to 35 m as roof structure. As floor structure it fulfils vibration and deflection criteria for a span of 9.5 m with a structural height of 485 mm. The faces are made of C24 graded timber and are joined with the core by adhesive bonding under pressure. The standard

heights are between 228 and 800 mm and different fire resistance classes can be achieved using additional cladding on the bottom surface (Kielsteg, 2015).

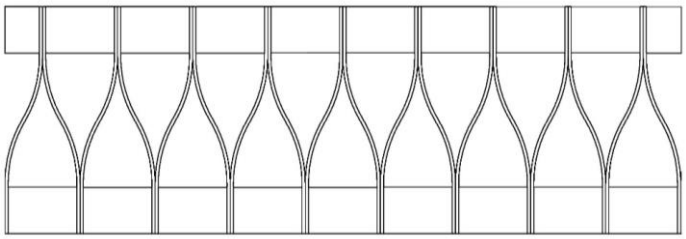

Figure 2.8: Illustration of the Kielsteg sandwich floor with V-formed core.

Lignatur

Lignatur element is a sandwich similar structure from Switzerland where the structure is divided into several box elements which is illustrated in Figure 2.9. The closed structure is made out of C24 graded timber. When used as floor structure it can span 4.5-10 m with a height of 120-480 mm. The structure can be combined with additional members to fulfil the acoustic and fire requirements in the actual building (Lignatur, 2014).

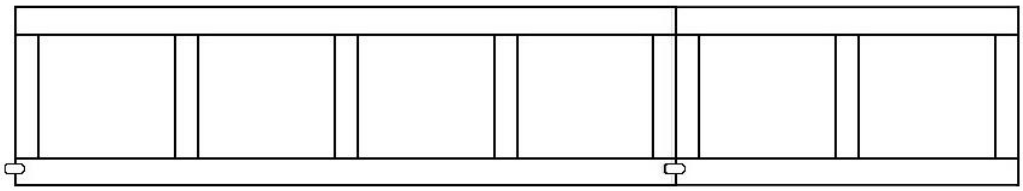

Figure 2.9: Illustration of the Lignatur sandwich floor system.

DendroLight

DendroLight is Latvian building block presented as ultra-light with high load-carrying capacity and good thermal and acoustic properties. It is illustrated in Figure 2.10. The building block is presented as suitable for floor structures. The cellular core material is sandwiched between solid wood or plywood layers, where the thickness of the faces is chosen based on application. The core consists of elements of solid wood glued together in perpendicular angles. It has standard heights between 36-112 mm. The maximum size of the plates is 10 m in length and 1.3 m in width (Dendrolight Latvija, 2016). No further information is given regarding the properties of DendroLight when used as a floor structure.

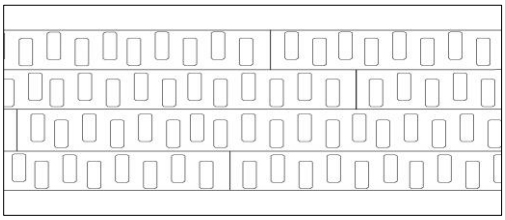

Figure 2.10: Illustration of the DendroLight sandwich building block.

2.4 Sandwich core configurations

Kavermann (2013) divides sandwich core configurations into three categories; honeycomb, corrugated and cellular cores. An additional configuration found in literature is grid cores (Fan, Meng, & Yang, 2006). In the subchapters below results from several research papers on investigations of core configurations for timber sandwich plates are presented. Most of the investigated plates have a structural height in the range of 10-80 mm. They are therefore not directly applicable to timber sandwich floor systems but can give an indication of different production methods, geometrical limitations, advantageous geometric ratios and design recommendations.

2.4.1 Cellular cores

Foam and balsa wood are two examples of cellular materials that have high stiffness-to-weight ratio. The faces are typically made in a different material such as OSB and the complete plate serves as a lightweight structure that is well insulated. Grenestedt & Bekisli (2003) have developed a different type of balsa block arrangement that allow the fibres to be oriented in 45^{o} to the normal of the core (see Figure 2.11). Their experiments proved the new arrangement to have 70% higher shear stiffness than a traditional arrangement of balsa blocks. The investigated core had a total height of 50 mm. It is developed for marine applications and ship hulls in particular.

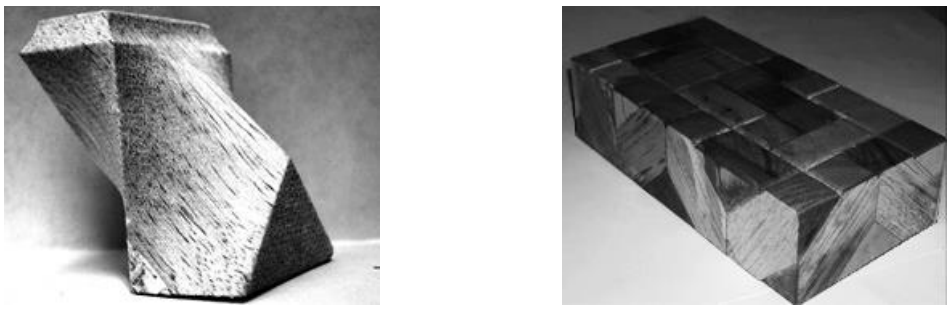

a) b)

Figure 2.11: a) illustrates a balsa block with 45^{o} fibre direction and figure b) illustrates the assembled core made out of several balsa blocks (Grenestedt and Bekisli, 2003).

2.4.2 Honeycomb cores

Honeycomb cores can be manufactured in a variety of materials and can be made in different shapes where the hexagonal shape is the most common (see Figure 2.12a). Hexagons with sharp corners can be made in paper or from wood fibres. Kavermann (2013) presents a honeycomb core structure that is possible to manufacture in plywood. It is made from sawn corrugated plywood plates that are placed vertically, as illustrated in Figure 2.12b. He concludes that the shear strength is influenced by the main fibre direction of the corrugations; the core has significantly higher shear strength if the main fibres are placed perpendicular to the bending axis. Kavermann (2013) compares the honeycomb core with a corrugated core (see Figure 2.16). He concluded that the honeycomb core out-performed the corrugated core in terms of out-of-plane properties. The specimens are loaded to failure. Foam reinforcement in the honeycomb core does not improve the structural behaviour.

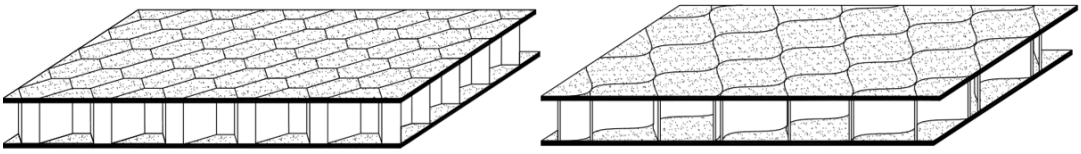

Figure 2.12: Illustration of a) a hexagonal honeycomb and b) a honeycomb possible to manufacture in plywood.

Frolovs et al. (2014) performed numerical investigations on a similar honeycomb core as the one studied by Kavermann (2013). In this honeycomb core straight ribs are placed between every second corrugated rib which is illustrated in Figure 2.13. They conclude that the anisotropy of the plate decreases when the number of waves per unit length increases. They measure the anisotropy as a ratio of bending stiffness in longitudinal and bending stiffness in transversal direction. The stiffness ratio decreases exponentially by increment of the number of waves per span. The anisotropy is also dependent on the depth of the waves. Frolovs et al. (2014) state that, due to high stiffness in both directions of their sandwich structure, it could be used for example in the structure of a roof or a ceiling panelling and as heavytruck floor.

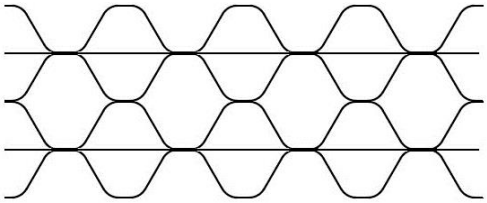

Figure 2.13: Illustration of a honeycomb core in plan view with straight ribs placed between every second corrugated rib.

Also a similar honeycomb in plywood is presented by Banerjee & Bhattacharyya (2011) and visualised in Figure 2.14. They perform a strength based optimization and present design maps. The design maps are based on failure criteria and not SLS criteria. For lower core depths, the core fails due to shear fracture. As the depth increases shear buckling becomes the governing failure mode. A balanced design of the core is when cell wall fracture and buckling occur at the same time. In theory this occurs when the cell thickness to cell radius ratio is equal to 0.027. The value is independent of loading and other geometrical parameters. The possible radius of the cells is dependent on manufacturing. Banerjee & Bhattacharyya (2011) have manufactured the sandwich structure as a response to the growing interest of stiff, strong and lightweight materials that are sustainable.

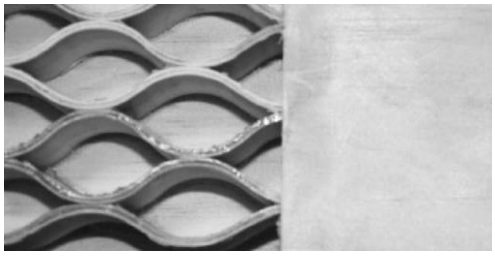

Figure 2.14: A similar honeycomb in plywood (Banerjee and Bhattacharyya, 2011).

2.4.3 Grid cores

Fan et al. (2006) present different types of grid structures which are illustrated in Figure 2.15. The simplest grid structure, bi-grid, was shown to have a lower shear and twisting stiffness than the other studied core types since it only has ribs placed in two directions. To get a more shear stiff structure at least three rib directions are needed. To make the manufacturing process more efficient and easy to assemble three ribs per intersection can be decreased to two ribs per intersection by using a kagome lattice grid, as Figure 2.15c illustrates. According to Fan et al. (2006) a kagome lattice core provides a stronger and stiffer structural pattern than honeycombs. They perform tests on kagome lattice structures made of carbon fibres.

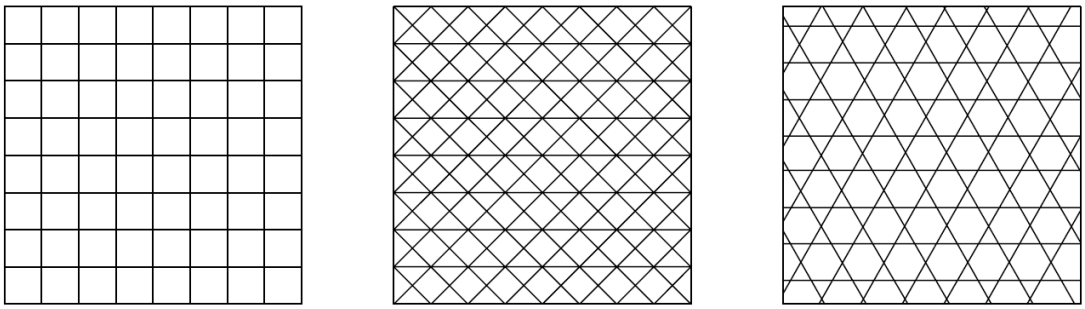

Figure 2.15: Illustration of a) bi-grid b) iso-grid and c) kagome lattice structure.

A timber kagome lattice grid sandwich plate is proposed by Klimek et al. (2015). The ribs are made of plywood and interlocked in the crossings. They state that the core to face bonding likely can be improved by using imprinted grooves in the faces. Klimek et al. (2015) mention that sandwich composite materials with high strength to low density are desirable for structural and aesthetic applications. They do not specify any specific application field for their sandwich structure.

Li et al. (2014) have performed investigations on a tri-axial core element made from either resin impregnated laminated paper or wood-fibre-based hardboard. The second material option has lower strength and stiffness than the first. The angle between the ribs is 60^{o} to create an equilateral triangle grid. The new sandwich structure is a part of a research program to develop sandwich plates made from wood-based composites that have low cost and possibility to adapt the performance to various applications. They further mention building construction materials and furniture as application areas with no added costs due to water resistance.

2.4.4 Corrugated cores

Corrugated cores in different materials such as steel, composite laminate and timber are common in research and the faces are usually made in the same material as the core. Plates with corrugated cores are generally easier and cheaper to manufacture than honeycomb structures (Kavermann, 2013). A typical corrugated core sandwich plate is illustrated in Figure 2.16.

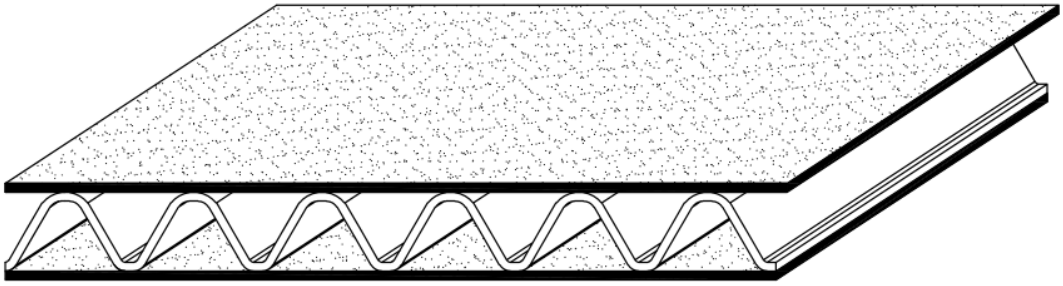

Figure 2.16: Illustration of corrugated sandwich plate.

The overall plate behaviour is dependent on the configuration and the geometric parameters of the core and can be optimized with regard to different aspects. According to Kavermann (2013) the faces should be placed so the main fibres are directed perpendicular to the corrugation as the core then provides relative support. He states that lightweight and sustainable plates, like the corrugated plywood sandwich, are desirable for many applications, for example as wall lining, ceilings and decorative furniture.

The corrugated core can be placed in a double layer to increase the height of the plate which is illustrated in Figure 2.17. Kavermann (2013) performs test on this type of core and the result shows marginally lower shear stiffness than a one layer core plate. The shear properties in bending parallel to the corrugation of the double layer core are increased with 25% with foam reinforcement. No bending tests with foam reinforcement were performed perpendicular to the corrugation but Kavermann (2013) claims foam would decrease the distortion of the core.

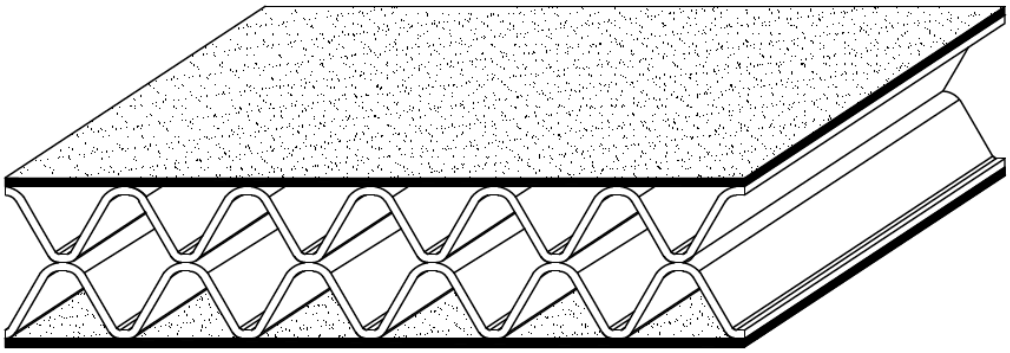

Figure 2.17: Illustration of double corrugated sandwich plate.

Labans & Kalnins (2011) made both numerical and experimental investigations on small sandwich plates with corrugated cores in plywood. They concluded that the plate stiffness is largely dependent on the corrugation angle and in an optimization process regarding weight to stiffness they found out that a corrugation angle of 60^{o} yields best result. Labans & Kalnins (2011) said that one promising direction for timber sandwich plates is as alternative for thick traditional plywood boards in several fields as the strength to density ratio is higher.

Sliseris & Rocens (2011) performed an optimization regarding bending of larger corrugated core sandwich plates with a height range of 200-350 mm and a span range

of 4-10 m. They concluded that deflection is often the leading design criteria. However for a span less than 6 m and a height greater than 300 mm shear stress is often the leading criteria. They say that traditional plywood sheets are not rational due to their slenderness and low load-carrying capacity. The load-carrying capacity of plywood plates could be increased by using a corrugated sandwich.

Extensive research has been done on corrugated cores for sandwich plates in steel. The cross-sectional notations are given in Figure 2.18. Chang (2004) concluded that a corrugated core should have a corrugation angle between 45°-70°, t_c equal to $t_{f.top}$ and $t_{f.bot}$, h_c/t_c about 20 and p/h_c between 1-1.2. Alwan & Järve (2012) showed that the stiffness decreases with increased h_c/t_c and p/h_c ratios. Similar studies have been performed on corrugated cores made of fibre reinforced polymers with same shape as in the Figure 2.18. Zhang et al. (2013) concluded that the specific bending strength increases when the corrugation angle, α_c, increases and the bond length, f_c, decreases.

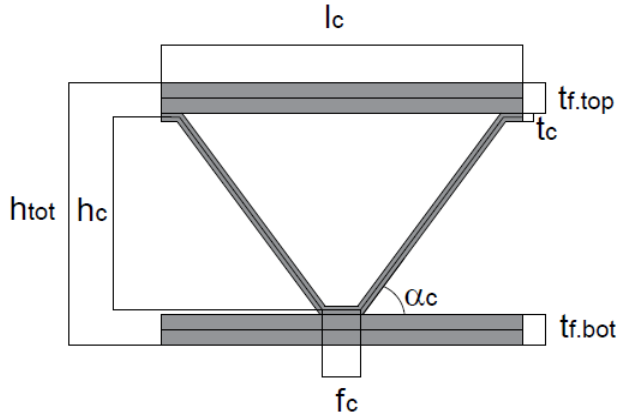

Figure 2.18: Notation of dimensions of corrugated steel sandwich plate. p is equal to half l_c.

2.5 Dynamic response of timber floors

The dynamics of floors in residential and office buildings is related to serviceability limit state and is therefore connected to the comfort and perceived safety of the users. Humans are sensitive to low-frequency vibrations and the most sensitive range is between 4 to 8 Hz, this range contains eigenfrequencies of some of the organs of the human body. As a consequence the lower limit of the first eigenfrequency of timber floors is set to 8 Hz in EN 1995-1-1 (2004). Important to remember is that the perception of vibrations is subjective and differs between persons and also what the persons are doing when they are subjected to vibrations. A person sitting still is more likely disturbed by vibrations than a person walking around (Brandin & Oscarsson, 2015).

Vibrations occur in a floor when it is subjected to dynamic loading, in other words a load that varies with time. The vibration response of the floor is dependent on both the load and the dynamic properties of the floor. Large vibration occurs when the frequency of the load is around the eigenfrequency of the structure (Brandin & Oscarsson, 2015).

2.5.1 Dynamic loading of floors

The dynamic load can be of two types; transient or continuous. Vibrations in office and residential building floors are often caused by human activities, like vibrations induced by footsteps, which more is related to transient loading (Brandin & Oscarsson, 2015). The impact load of a footstep has mainly a frequency between 0-2 Hz but with contributions up to 40 Hz. The first eigenfrequency of timber floors is often in the range 0-40 Hz (Ohlsson, 1988).

2.5.2 Dynamic properties of floors

The simplest dynamic model of a structure is a single degree of freedom system (SDOF). Three constants are found in the equation of motion of a SDOF system; mass, damping and stiffness. The eigenfrequency of the system is dependent on all of these constants. While mass and stiffness are relatively easy to determine for a structure, the damping properties are more difficult to quantify. Damping is for example dependent on the material damping, as well as the damping properties of the connections and supports (Brandin & Oscarsson, 2015).

2.5.3 Vibration requirements in timber floors

When regarding both Eurocode 5 and the Swedish National Annex following three requirements need to be fulfilled for timber floors (Brandin & Oscarsson, 2015):

1. The first eigenfrequency must be over 8 Hz

$$f_1 > 8\ Hz \tag{2.1}$$

2. The maximum instantaneous deflection is 1.5 mm when a concentrated load is applied in any point (taking load distribution into account)

$$w_{1kN} \leq 1.5\ mm \tag{2.2}$$

3. The maximum impulse velocity is limited when an unit impulse of 1 Ns is applied in a point, giving maximum response

$$v \leq 100^{(f_1 \zeta - 1)}\ m/s \tag{2.3}$$

where

ζ Modal damping ratio (recommended to 0.01), [-]

If the first eigenfrequency is lower than 8 Hz the floor is regarded as a low-frequency floor and a special investigation must be performed. There have been complains on floors designed according to Eurocode 5 and the Swedish National Annex (Brandin & Oscarsson, 2015). According to Brandin & Oscarsson (2015) other criteria need to be used and after comparing both old and recent studies they recommend the following criteria:

1. The first eigenfrequency must be over 8 Hz, same as Equation (2.1).

2. The instantaneous deflection must be under 1.0 mm when a concentrated load of 1 kN is applied in any point (taking load distribution into account)

$$w_{1kN} < 1.0\ mm \tag{2.4}$$

3. A limiting ratio between the first eigenfrequency and instantaneous deflection

$$18.7 < \frac{f_1}{{w_{1kN}}^{0.44}} \tag{2.5}$$

2.6 Deflection of timber floors

It is basically up to the structural engineer to determine, from case to case, the allowed deformation of timber structures. The decision should be based on the actual situation and the expectations of the client. Eurocode 5 gives recommendations which can be used in case more precise limits cannot be specified (Thelandersson, 1995). The recommendations in Eurocode 5 for beams on two supports are presented in the Table 2.1 (EN 1995-1-1, 2004).

Table 2.1: Deflection limitations for simply supported beams according to Eurocode 5.

	Type of deflection		
	w_{inst}	$w_{net,fin}$	w_{fin}
Maximum deflection [mm]	L/300 to L/500	L/250 to L/350	L/150 to L/300

Where w_{inst} is the instantaneous deflection, $w_{net,fin}$ is the net final deflection and w_{fin} is the final deflection. They are visualized in Figure 2.19. Note that the instantaneous deflection should be calculated with the characteristic combination of actions and the final deflection should be calculated with the quasi-permanent combination of actions.

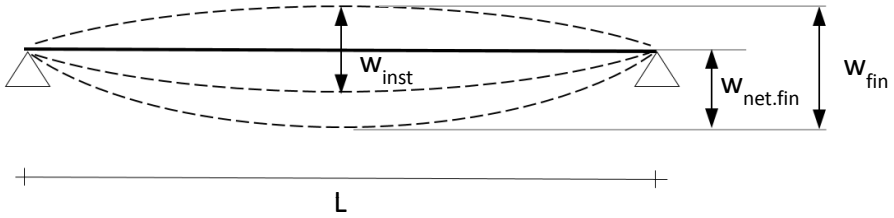

Figure 2.19: Different types of deflections are visualized.

The final deflection is calculated in the following way:

$$w_{fin} = w_{fin,G} + w_{fin,Q1} + \sum w_{fin,Qi} \tag{2.6}$$

where

$$w_{fin,G} = w_{inst,G}(1 + k_{def}) \tag{2.7}$$

$$w_{fin,Q1} = w_{inst,Q1}(1 + \psi_{2,1}k_{def}) \tag{2.8}$$

$$w_{fin,Qi} = w_{inst,Qi}(\psi_{0,i} + \psi_{2,i}k_{def}) \tag{2.9}$$

k_{def} Deformation factor, [-]
$\psi_{2,1}$ Factor for quasi-permanent value of leading variable action, [-]
$\psi_{2,i}$ Factor for quasi-permanent value of non-leading variable action, [-]
$w_{inst,G}$ Instantaneous deflection due to permanent action, [m]
$w_{inst,Q1}$ Instantaneous deflection due to leading variable load, [m]
$w_{inst,Qi}$ Instantaneous deflection due to non-leading variable loads, [m]

The net final deflection is calculated in the following way:

$$w_{net,fin} = w_{fin} - w_c \tag{2.10}$$

where
w_c Precambering, [m]

2.7 Static loading on floors

Actions on floors are given in EN 1991-1-1 (2002). A uniformly distributed load (q_k) and a concentrated load (Q_k) are given for floors as imposed load. The concentrated load is used for local verifications where it acts alone. The magnitude of the loads is dependent of the use of the floor. The magnitude of the loads with respect to category of use is presented in table 2.2 with an example of use from the category as well.

Table 2.2: Imposed loads on floors. For the categories of use an example from the categories is given.

	Category of use			
Load	A – residential	B – office	C – cinemas	D – shopping
q_k [kN/m^2]	2	3	3-5	5
Q_k [kN]	2	2	4-7	4-7

The concentrated load is acting on an area of a square with a width of 50 mm. Additional to these loads the self-weight of movable partitions should be added to the imposed load. If the self-weight of the movable partitions is smaller or equal to 1.0 kN/m wall length, hence the additional load is 0.5 kN/m^2.

Depending on the total area of the floor, the imposed load may be reduced for ULS calculations. The reduction factor is determined in the following way:

$$\alpha_A = 0.5 + \frac{10\ m^2}{A_f} \tag{2.11}$$

where
A_f Loaded area, [m^2]

3 Concept development

The first step in the concept development is an evaluation of different core configurations where a qualitative assessment is made in order to find a suitable core for further investigation. Different material possibilities are then elaborated. This is followed by a presentation of analytical analysis methods and further on how anisotropic timber properties are treated in FE-modelling. As all core configurations presented in Chapter 2.4 can provide high bending stiffness in two directions, the sandwich floor will be developed to have supports on four edges an allow for two-way action.

3.1 Alternative core configurations

The literature study reveals advantages and drawbacks of different core configurations and some concepts are eliminated in this phase of the study. Foam cores are rejected, as it is not a wood-based material. Balsa cores are also eliminated. Balsa wood does not grow in Nordic countries and the overall concept with solid wood as core material is considered material inefficient. The concept with bi-grid structures is rejected since studies have shown that it has lower shear resistance than iso-grid structures. The iso-grid structure with three intersections in one point is also rejected since it will be difficult to manufacture. However, kagome lattice grid configurations, honeycomb configurations and corrugated core configurations are regarded to have potential.

The shapes of the potential core configurations are illustrated in Figure 3.1 and 3.2. The corrugated cores can be made of veneers or wood fibres. Veneer layers can relatively easy be formed into curved shapes and it has been achieved in the work presented in Chapter 2.4.3. The corrugation gets rounded corners when it is made of veneers. The wood fibre-based core configuration can likely have sharper corners and shorter horizontal corrugation component. Literature indicates that it is advantageous to have a smaller horizontal corrugation component. The double corrugated core is also of interest, for larger structural heights the risk of buckling of the core is smaller with this shape. A honeycomb core can be shaped in a similar way as a corrugated core by pressing plywood and position it in vertical direction.

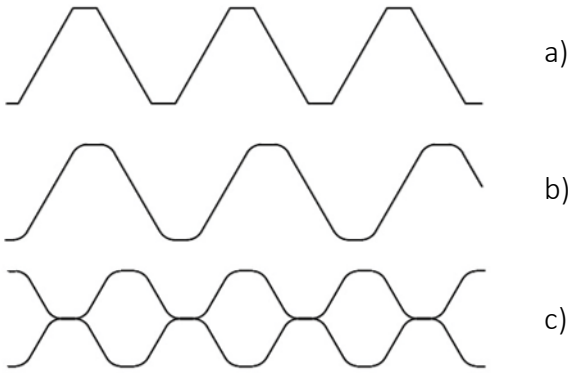

Figure 3.1: Cross-sections of corrugated core configurations. Figure a) with sharper corners can be produced with wood fibers and b) can be made of plywood due to its rounded corners. The double corrugation in figure c) can be made in order to decrease buckling lengths.

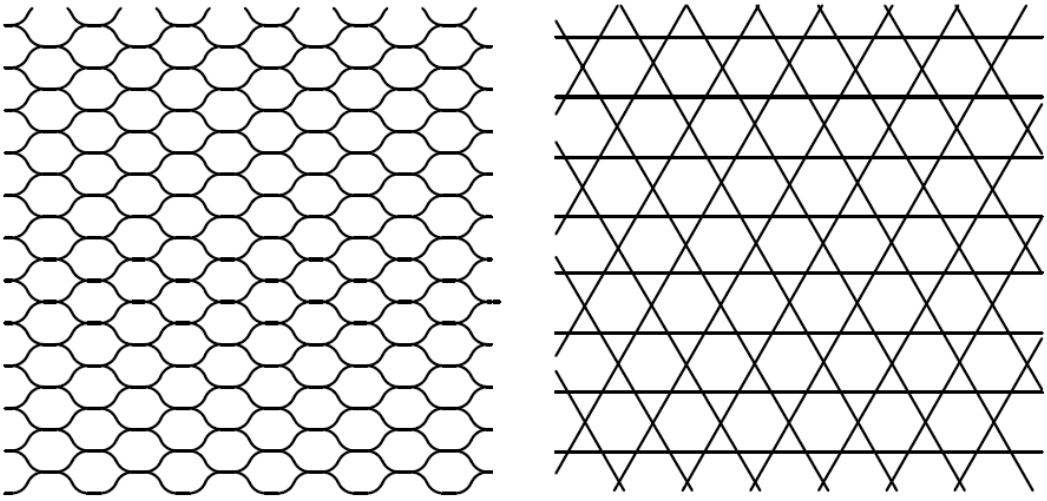

Figure 3.2: Visualisation of a) honeycomb and b) kagome lattice configurations in plan view.

3.2 Qualitative assessment of core configurations

The different core configurations proposed in Chapter 3.1 have different manufacturing methods. The kagome lattice core has the advantage that it consists only of straight parts. However the assembly of the different components is regarded as difficult and the nodes require precision in manufacturing. Both the corrugated core and the honeycomb core need to be pressed into curved shapes. The corrugated core configuration is assumed to have a superior design in this aspect compared to the honeycomb core since the shape of the configuration can be made in one solid part. The manufacturing of a pressed plywood core is estimated to be cheaper than processing wood fibres. Also, the corrugated core allows for easier gluing between core and faces than the kagome lattice and honeycomb core. On the other hand Chapter 2.4 indicates that the honeycomb core has better out-of-plane properties than the corrugated core and that the kagome lattice core performs similar or even somewhat better than the honeycomb core.

Despite potentially better out-of-plane properties the honeycomb and the kagome lattice cores are rejected. Timber floors are often governed by SLS criteria in design and the majority of the stiffness will be obtained by the faces. Due to the easier manufacturing the corrugated plywood core is chosen for further investigation.

3.3 Material possibilities for core and faces

The choice of material is limited to wood products from the Nordic countries. As mentioned in Chapter 3.2 the corrugation is preferably made of pressed veneer sheets. In order to achieve two-way action, faces that are strong and stiff in two directions are preferable. Panels made from boards or veneers are regarded as suitable. Common timber panels on the Swedish market are plywood, Kerto-Q and CLT. Plywood is considered a good option for the core, as smaller thicknesses are needed compared to

the faces. Plywood, Kerto-Q and CLT can all be used for the faces. The choice is dependent on desired dimensions.

Finnish plywood, from UPM, can be produced in either birch or conifer or a combination of them, called combi and combi mirror. A plywood sheet in birch is produced with a thickness of 4 mm up to 50 mm. Conifer plywood is produced in a thickness range of 4 mm up to 27 mm when using thin veneers (3-21 veneer layers). Finnish conifer plywood can also be made with thick veneers (3-13 veneer layers) (UPM, 2007). Swedish Vänerply, from Moelven, is made from spruce and pinewood and is produced within a thickness range of 12-27 mm (Moelven, 2013). Kerto-Q is produced by Metsä and has a thickness range of 21-69 mm (Moelven, 2016). In Sweden, CLT is made by Martinsons and they offer a thickness range of 60-300 mm (Martinsons, 2016). The different products and their thickness range are summarized in Table 3.1.

Table 3.1: Different thickness of different conventional wood panels. The dimensions are expressed in mm.

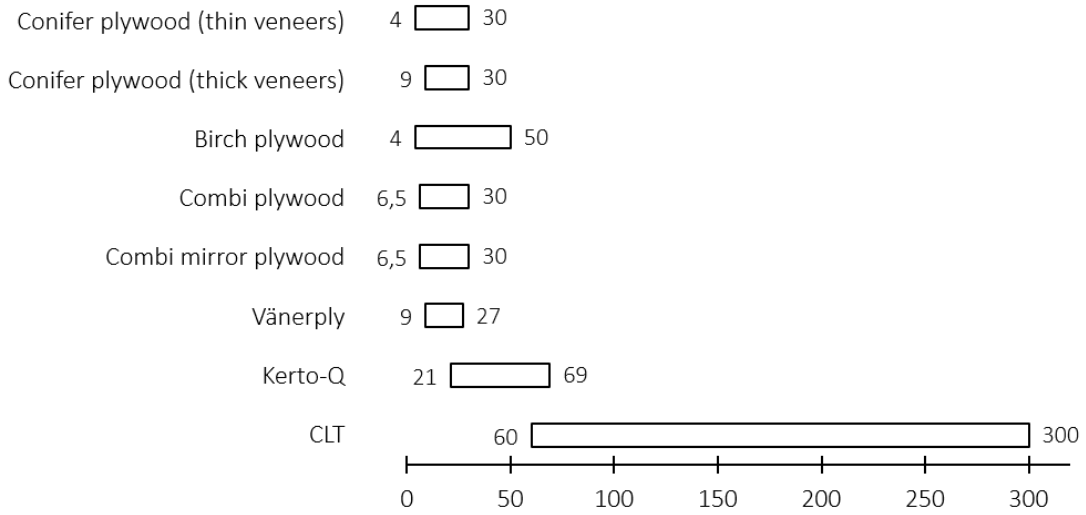

The strength and stiffness properties of birch and conifer plywood and Kerto-Q are presented in Table 3.2. CLT has lay-up of boards from strength-graded timber C14 and/or C24. For the thickness 60 mm CLT has 3 layers and for 300 mm it has 7 layers. The strength and stiffness are dependent on the lay-up of C14 and C24 timber.

Table 3.2: Mechanical properties of different thicknesses of Kerto-Q (Metsä, 2016), *Finnish conifer and birch plywood* (UPM, 2007)

Material	Thickness [mm]	Numbers of plies	Density	E_1 [GPa]	E_2 [GPa]	E_3 [GPa]	G_{12} [Gpa]	G_{13} [Gpa]	G_{23} [Gpa]
Conifer plywood	6.5	5	410	9.46	3.54	3.54	0.53	0.07	0.04
	30	25		7.07	5.93	5.93	0.53	0.07	0.06
Birch plywood	6.5	5	630	12.74	4.76	4.76	0.62	0.17	0.12
	50	35		9.20	8.30	8.30	0.62	0.20	0.20
Kerto-Q	21-24	7-8	480	10.00	2.40	2.40	0.60	0.15	0.05
	27-69	9-31		10.50	2.40	2.40	0.60	0.15	0.05

In Table 3.3 a cost estimation of the different materials is given. The prices are given per m^2 and are valid for sheets with a thickness of 24 mm. The price for Kerto-Q is

given by Metsä (Hed, 2016). They state that Kerto-Q is not a standard product in the same way as plywood. The sizes of the Kerto-Q sheets are often adapted to the project. They underline that the given prices for Kerto-Q is an estimation. The prices for Finnish conifer and birch plywood are given by CEOS (CEOS, 2016), the Swedish retailer of UPM plywood. The price for birch plywood is given for sheets with dimension 1525x1525 mm^2 and 17 veneer layers. The price for conifer plywood is given for sheets with dimension 2440x1220 mm^2 and 9 veneer layers, the so called conifer plywood with thick veneers. The price varies depending on glue and surface quality (allowance of knots and cracks). The prices for the birch plywood are given for quality BB and interior glue. The Finnish conifer plywood has the quality denotation III/III and weather and boil proof glue.

Table 3.3: Cost estimation of different veneer products. The square meter prices are given for sheets with thickness 24 mm.

Wood product (24 mm in thickness)	Price [SEK/m^2]
Kerto-Q	200
Conifer plywood	149
Birch plywood	164

3.4 Analysis methods of a corrugated sandwich plate

Analysis of sandwich plates is often performed in terms of effective properties used in conjunction with appropriate plate, composite or shell theory. The geometry of the sandwich plate is defined as Figure 3.3 illustrates.

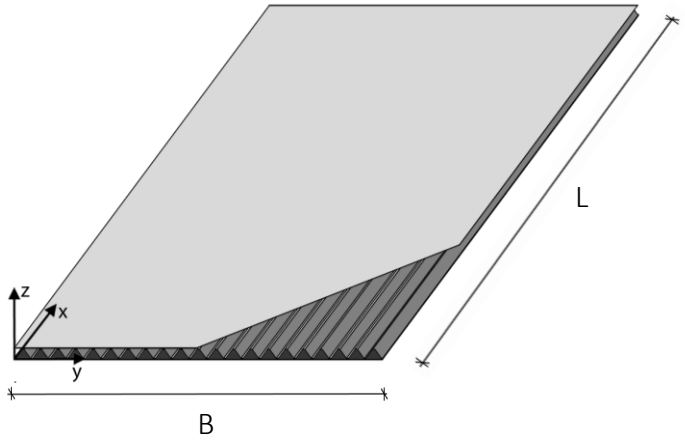

Figure 3.3: The definition of geometry of the sandwich plate where the area is notated L x B.

3.4.1 Effective properties of a sandwich plate

The effective properties of a sandwich plate can be determined analytically, numerically or by experimental methods. A classic study by Libove & Hubka (1951) presents effective properties for a corrugated core sandwich plate (Hohe & Becker, 2002). Libove & Hubka (1951) use a homogenization procedure to idealise the three dimensional sandwich plate as a homogeneous orthotropic plate and express the properties with eight elastic stiffness constants (see Figure 3.4). The constants consist of two bending stiffness constants (D_x and D_y), two axial stiffness constants (E_x and E_y), one torsional stiffness constant (D_{xy}), one horizontal stiffness constant (G_{xy}) and

two transverse shear stiffness constants (D_{Qx} and D_{Qy}).They also express two effective Poisson's ratios for stretching (ν'_x and ν'_y) and two for bending (ν_x and ν_y,).

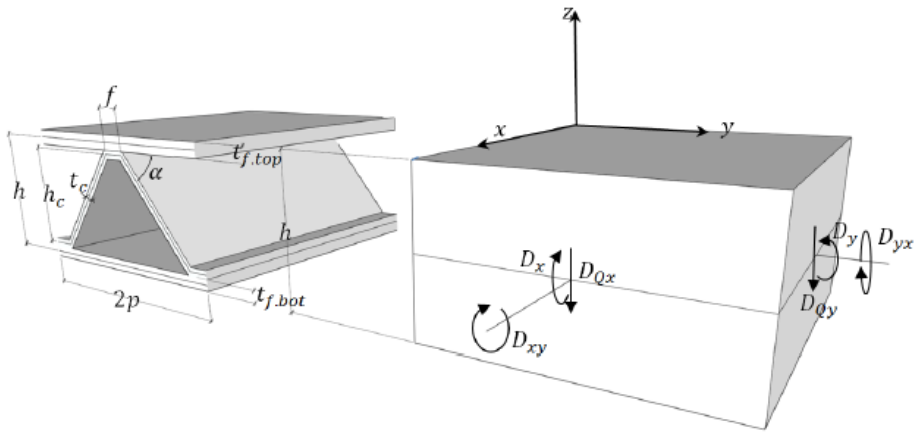

Figure 3.4: Transformation of corrugated sandwich plate to orthotropic homogeneous plate (Dackman & Ek, 2015).

The derivation of the elastic stiffness constants were made with following assumptions (Dackman & Ek, 2015):

- Straight lines normal to the mid-plane remain straight but not necessarily normal to the mid-plane.
- The modulus of elasticity in z-direction is infinite.
- The faces are connected to the corrugation with rigid joints.
- The thicknesses of the faces are thin compared to the height of the core.

According to Allen (1969) a sandwich plate is regarded to have thin faces if the criteria below are fulfilled.

$$100 > \frac{h_c}{t_{f.top}} > 5.77 \tag{3.1}$$

$$100 > \frac{h_c}{t_{f.bot}} > 5.77 \tag{3.2}$$

The elastic stiffness constants are derived for a sandwich plate where the faces and corrugation are made of isotropic materials, however necessarily not the same material. Tumino et al. (2014) have derived six elastic stiffness constants, excluding the transverse shear stiffness constants, for an orthotropic corrugated core sandwich plate in a similar fashion as Libove & Hubka (1951). However Tumino et al. (2014) further make assumptions that the core and faces are made of the same material and that the cross-section is symmetric, i.e. top and bottom faces have same thickness. The elastic stiffness constants defined by Libove & Hubka (1951) are presented below. They are presented for the case where the top and bottom faces are made of the same material (but not necessarily of the same thickness), when the corrugated core is symmetric and by setting the location of the stretching forces to the centroids of the transformed cross-sections. These simplified expressions as well as the full expressions are presented in Libove & Hubka (1951). All stiffness constants are defined per unit width.

Bending stiffness constants
The bending stiffness constants have the unit Nm. Note that the subscriptions denote along the axis and not around the axis.

$$D_x = E_f(I_{f.top} + I_{f.bot}) + E_c I_c \tag{3.3}$$

where

E_f	Modulus of elasticity of face material, [Pa]
$I_{f.top}$	Moment of inertia of top face per unit width, [m^4/m]
$I_{f.bot}$	Moment of inertia of bottom face per unit width, [m^4/m]
E_c	Modulus of elasticity of core material, [Pa]
I_c	Moment of inertia of core per unit width, [m^4/m]

$$D_y = \frac{E_f(I_{f.top} + I_{f.bot})}{1 - \nu_f{}^2\left(1 - \frac{E_f(I_{f.top} + I_{f.bot})}{D_x}\right)} \tag{3.4}$$

where

ν_f	Poisson's ratio of face material, [-]

Stretching stiffness constants
The stretching stiffness constants have the unit N/m.

$$E_x = E_f(A_{f.top} + A_{f.bot}) + E_c A_c \tag{3.5}$$

where

$A_{f.top}$	Area of top face per unit width, [m^2/m]
$A_{f.bot}$	Area of bottom face per unit width, [m^2/m]
A_c	Area of core per unit width, [m^2/m]

$$E_y = \frac{E_f(A_{f.top} + A_{f.bot})}{1 - \nu_f{}^2\left[1 - \frac{E_f\left(A_{f.top} + A_{f.bot}\right)}{E_x}\right]} \tag{3.6}$$

Torsional stiffness constant
The torsional stiffness constant has the unit Nm.

$$D_{xy} = 2GJ \tag{3.7}$$

where

$$GJ = \left[G_f t_{f.bot} k_{GJ} + \frac{G_c {t_c}^2}{A_c}\left(k_{GJ} - k_c\right)^2 + G_f t_{f.top}\left(1 - k_{GJ}\right)^2\right] h^2 \tag{3.8}$$

$$k_{GJ} = \frac{\frac{G_c {t_c}^2 k_c}{A_c} + G_f t_{f.top}}{GA} \tag{3.9}$$

$$k_c = \frac{1}{2}\left(1 + \frac{t_{f.bot} - t_{f.top}}{h}\right) \tag{3.10}$$

$$k_{GJ} = \frac{\frac{G_c {t_c}^2 k_c}{A_c} + G_f t_{f.top}}{GA} \tag{3.11}$$

$$GA = G_f t_{f.bot} + \frac{G_c {t_c}^2}{A_c} + G_f t_{f.top} \tag{3.12}$$

G_c Shear stiffness of core material, [Pa]
G_f Shear stiffness of face material, [Pa]
h Distance between centroid of top face and centroid of bottom face, [m]

Horizontal shear stiffness constant
The unit of the horizontal shear stiffness is N/m.

$$G_{xy} = GA \tag{3.13}$$

Transverse shear stiffness constants
The unit of the transverse shear stiffness constants is N/m. The expression for the transverse shear stiffness in x-direction is simplified by assuming that the corrugation carries no normal stress.

$$D_{Qx} = \frac{G_c {t_c}^2}{A_c}\left(\frac{h}{p}\right)^2 \tag{3.14}$$

where
p Half corrugation length, [m]

The shear stiffness in y-direction is expressed as follows:

$$D_{Qy} = Sh\left(\frac{E_c}{1 - {\nu_c}^2}\right)\left(\frac{t_c}{h_c}\right)^3 \tag{3.15}$$

where
S Factor based on the geometry of the corrugation (see Appendix A), [-]
ν_c Poisson's ratio of core material, [-]

Effective Poisson's ratios
Libove & Hubka (1951) also derived effective Poisson's ratios. Two related to bending and two related to stretching. The two Poisson's ratios related to stretching are denoted with a prime sign.

$$\nu_x = \nu_f \tag{3.16}$$

$$\nu_y = \nu_x \frac{D_y}{D_x} \tag{3.17}$$

$$\nu_x' = \nu_f \tag{3.18}$$

$$\nu_y' = \nu_x \frac{E_y}{E_x} \tag{3.19}$$

3.4.2 Plate theory

Reissner-Mindlin plate theory assumes that straight lines normal to the middle plane of the plate remain straight but not orthogonal to the middle plane when subjected to bending (Onate, 2013). This theory is more advanced than Kirchhoff theory, which does not include shear deformation. The shear deformation for a sandwich plate is important to consider. The Reissner-Mindlin theory is therefore more suitable, thus it is used in these calculations.

The constitutive relation for an orthotropic plate in plane stress state with symmetrical stiffness properties with regard to the middle plane can be defined in the following way (Dackman & Ek, 2015):

$$\begin{Bmatrix} N_{xx} \\ N_{yy} \\ N_{xy} \\ M_{xx} \\ M_{yy} \\ M_{xy} \end{Bmatrix} = \begin{bmatrix} D_{11} & D_{12} & 0 & 0 & 0 & 0 \\ D_{21} & D_{22} & 0 & 0 & 0 & 0 \\ 0 & 0 & D_{33} & 0 & 0 & 0 \\ 0 & 0 & 0 & D_{44} & D_{45} & 0 \\ 0 & 0 & 0 & D_{54} & D_{55} & 0 \\ 0 & 0 & 0 & 0 & 0 & D_{66} \end{bmatrix} \begin{Bmatrix} \varepsilon_{xx} \\ \varepsilon_{yy} \\ \gamma_{xy} \\ \kappa_{xx} \\ \kappa_{yy} \\ \kappa_{xy} \end{Bmatrix} \tag{3.20}$$

where

$$
\left.
\begin{aligned}
D_{11} &= \frac{E_x}{1-\nu'_x\nu'_y} \\
D_{12} = D_{21} &= \frac{\nu'_x E_y}{1-\nu'_x\nu'_y} = \frac{\nu'_y E_x}{1-\nu'_x\nu'_y} \\
D_{22} &= \frac{E_y}{1-\nu'_x\nu'_y} \\
D_{33} &= G_{xy} \\
D_{44} &= \frac{D_x}{1-\nu_x\nu_y} \\
D_{45} = D_{54} &= \frac{\nu_x D_x}{1-\nu_x\nu_y} = \frac{\nu_y D_y}{1-\nu_x\nu_y} \\
D_{55} &= \frac{D_y}{1-\nu_x\nu_y} \\
D_{66} &= \frac{D_{xy}}{2}
\end{aligned}
\right\} \quad (3.21)
$$

Deflection

The formula for deflection of an orthotropic plate with Reissner-Mindlin plate theory is presented in Dackman & Ek (2015) and originally obtained from Chang (2004). The solution converges for a sufficient number of terms in the double Fourier series. The expressions for deflection of the plate when subjected to a uniformly distributed load or a concentrated load are stated as follow:

$$w = \sum_j \sum_i w_{ij} q_{ij} \sin\left(\frac{i\pi x}{L}\right) \sin\left(\frac{j\pi y}{B}\right) \quad (3.22)$$

$$w = \sum_j \sum_i w_{ij} Q_{ij} \sin\left(\frac{i\pi x}{L}\right) \sin\left(\frac{j\pi y}{B}\right) \quad (3.23)$$

where

$$w_{ij} = \frac{L^2B^2\begin{pmatrix} D_{xy}\pi^2(D_{xx}\pi^2B^4i^4 + D_{yy}\pi^2L^4j^4 - D_{yy}\pi^2L^2B^2i^2j^2\nu_x + \\ D_{Qx}L^2B^4i^2) + D_{Qy}\pi^2L^2B^2(2D_{xx}B^2i^2 + D_{xy}L^2j^2) + \\ 2D_{Qx}L^4B^2(D_{yy}\pi^2j^2 + D_{Qy}B^2) + D_{xx}\pi^4L^2B^2i^2j^2(2D_{yy} + \\ -D_{xy}\nu_y - 2D_{yy}\nu_x\nu_y \end{pmatrix}}{\pi^2\begin{pmatrix} D_{Qx}\pi^2B^2(D_{xy}\pi^2D_{xx}B^4i^6 + 2D_{Qy}D_{xx}B^4L^2i^4 + 2D_{Qy}D_{yy}L^6j^4 + \\ 4D_{Qy}D_{xy}L^4B^2i^2j^2 + 2D_{xx}D_{yy}\pi^2L^2B^2i^4j^2 + 2D_{Qy}D_{xx}L^4B^2i^2j^2\nu_y + \\ 2D_{Qy}D_{yy}L^4B^2i^2j^2\nu_x + D_{xy}D_{yy}\pi^2L^2i^2j^4 - D_{xx}D_{xy}\pi^2L^2B^2i^4j^2\nu_y + \\ -D_{xy}D_{yy}\pi^2L^2B^2i^2j^2\nu_x - 2D_{xx}D_{yy}\pi^2L^2B^2i^4j^2\nu_x\nu_y) + \\ D_{Qy}\pi^4L^2(D_{xy}D_{yy}L^4j^6 + 2D_{yy}D_{xx}B^2L^2i^2j^4 + D_{xx}D_{xy}B^4i^4j^2 + \\ -D_{xy}D_{yy}B^2L^2i^2j^4\nu_x - D_{xx}D_{xy}B^2L^2i^2j^4\nu_y - 2D_{xx}D_{yy}B^2L^2i^2j^4\nu_x\nu_y) \end{pmatrix}} \tag{3.24}$$

$$D_{xx} = \frac{D_x}{1 - \nu_x\nu_y} \tag{3.25}$$

$$D_{yy} = \frac{D_y}{1 - \nu_x\nu_y} \tag{3.26}$$

$$q_{ij} = \frac{4q}{ij\pi^2}\left[1 - (-1)^i\right]\left[1 - (-1)^j\right] \tag{3.27}$$

$$Q_{ij} = \frac{4Q}{LB}\left[1 - (-1)^i\right]\left[1 - (-1)^j\right] \tag{3.28}$$

q Uniformly distributed load, [N/m^2]
Q Concentrated load, [N]

Eigenfrequency
The first eigenfrequency is calculated with Reissner-Mindlin plate theory. The formula for an orthotropic plate (omitting rotary inertia and in-plane inertia) is presented by Reddy (1997) and derived as:

$$f_1 = \frac{1}{2\pi}\sqrt{\frac{1}{\widehat{m}_{33}}}\sqrt{\bar{s}_{33} - \frac{\bar{s}_{13}\bar{s}_{22} - \bar{s}_{23}\bar{s}_{12}}{\bar{s}_{11}\bar{s}_{22} - \bar{s}_{12}\bar{s}_{12}}\bar{s}_{13} - \frac{\bar{s}_{11}\bar{s}_{23} - \bar{s}_{12}\bar{s}_{13}}{\bar{s}_{11}\bar{s}_{22} - \bar{s}_{12}\bar{s}_{12}}\bar{s}_{23}} \tag{3.29}$$

where

$$
\begin{aligned}
&\hat{m}_{33} = m_{freq} \\
&\bar{s}_{11} = \hat{s}_{11} - (\hat{s}_{14}\hat{s}_{55} - \hat{s}_{15}\hat{s}_{45})\hat{s}_{14}/\hat{s}_{00} - (\hat{s}_{15}\hat{s}_{44} - \hat{s}_{14}\hat{s}_{45})\hat{s}_{15}/\hat{s}_{00} \\
&\bar{s}_{12} = \hat{s}_{12} - (\hat{s}_{24}\hat{s}_{55} - \hat{s}_{25}\hat{s}_{45})\hat{s}_{14}/\hat{s}_{00} - (\hat{s}_{25}\hat{s}_{44} - \hat{s}_{24}\hat{s}_{45})\hat{s}_{15}/\hat{s}_{00} \\
&\bar{s}_{13} = -(\hat{s}_{34}\hat{s}_{55} - \hat{s}_{35}\hat{s}_{45})\hat{s}_{14}/\hat{s}_{00} - (\hat{s}_{35}\hat{s}_{44} - \hat{s}_{24}\hat{s}_{45})\hat{s}_{15}/\hat{s}_{00} \\
&\bar{s}_{22} = \hat{s}_{22} - (\hat{s}_{24}\hat{s}_{55} - \hat{s}_{25}\hat{s}_{45})\hat{s}_{24}/\hat{s}_{00} - (\hat{s}_{25}\hat{s}_{44} - \hat{s}_{24}\hat{s}_{45})\hat{s}_{25}/\hat{s}_{00} \\
&\bar{s}_{23} = \hat{s}_{23} - (\hat{s}_{34}\hat{s}_{55} - \hat{s}_{35}\hat{s}_{45})\hat{s}_{24}/\hat{s}_{00} - (\hat{s}_{35}\hat{s}_{44} - \hat{s}_{34}\hat{s}_{45})\hat{s}_{25}/\hat{s}_{00} \\
&\bar{s}_{33} = \hat{s}_{33} - (\hat{s}_{34}\hat{s}_{55} - \hat{s}_{35}\hat{s}_{45})\hat{s}_{34}/\hat{s}_{00} - (\hat{s}_{35}\hat{s}_{44} - \hat{s}_{34}\hat{s}_{45})\hat{s}_{35}/\hat{s}_{00} \\
&\hat{s}_{00} = \hat{s}_{44}\hat{s}_{55} - \hat{s}_{45}\hat{s}_{45} \\
&\hat{s}_{11} = A_{11}\alpha^2 + A_{66}\beta^2 \\
&\hat{s}_{12} = (A_{12} + A_{66})\alpha\beta \\
&\hat{s}_{14} = B_{11}\alpha^2 + B_{66}\beta^2 \\
&\hat{s}_{15} = (B_{12} + B_{66})\alpha\beta \\
&\hat{s}_{22} = A_{66}\alpha^2 + A_{22}\beta^2 \\
&\hat{s}_{24} = \hat{s}_{15} \\
&\hat{s}_{25} = B_{66}\alpha^2 + B_{22}\beta^2 \\
&\hat{s}_{33} = K(A_{55}\alpha^2 + A_{44}\beta^2) \\
&\hat{s}_{34} = KA_{55}\alpha \\
&\hat{s}_{35} = KA_{44}\beta \\
&\hat{s}_{44} = D_{s.11}\alpha^2 + D_{s.66}\beta^2 + KA_{55} \\
&\hat{s}_{45} = (D_{s.12} + D_{s.66})\alpha\beta \\
&\hat{s}_{55} = D_{s.66}\alpha^2 + D_{s.22}\beta^2 + KA_{44} \\
&\alpha = \frac{m\pi}{L} \\
&\beta = \frac{n\pi}{B}
\end{aligned}
\qquad (3.30)
$$

m_{freq} Mass per unit area, [kg/m^2]
K Shear correction factor, [-]

The variables *m* and *n* are set to 1 to obtain the first eigenfrequency. The shear correction factor is used to correct the difference between the actual and the constant shear stress state. It is set to 5/6 in Dackman & Ek (2015).

The plate is assumed to be a specially orthotropic single-layered plate. This means that the principal material coordinates coincide with those of the plate. The A_{ij}-coefficients are related to in-plane stiffness and the $D_{s.ij}$-coefficients are related to bending stiffness. The B_{ij}-coefficients are due to bending-stretching coupling, they are equal to zero for specially orthotropic plates. A_{16}, A_{26}, $D_{s.16}$ and $D_{s.26}$ are also zero while the other coefficients are found in the plate constitutive equations:

$$\begin{Bmatrix} N_{xx} \\ N_{yy} \\ N_{xy} \end{Bmatrix} = \begin{bmatrix} A_{11} & A_{12} & 0 \\ A_{12} & A_{22} & 0 \\ 0 & 0 & A_{66} \end{bmatrix} \begin{Bmatrix} \varepsilon_{xx} \\ \varepsilon_{yy} \\ \gamma_{xy} \end{Bmatrix} \tag{3.31}$$

$$\begin{Bmatrix} M_{xx} \\ M_{yy} \\ M_{xy} \end{Bmatrix} = \begin{bmatrix} D_{s.11} & D_{s.12} & 0 \\ D_{s.12} & D_{s.22} & 0 \\ 0 & 0 & D_{s.66} \end{bmatrix} \begin{Bmatrix} \kappa_{xx} \\ \kappa_{yy} \\ \kappa_{xy} \end{Bmatrix} \tag{3.32}$$

$$\begin{Bmatrix} Q_y \\ Q_x \end{Bmatrix} = \begin{bmatrix} A_{44} & 0 \\ 0 & A_{55} \end{bmatrix} \begin{Bmatrix} \gamma_{yz} \\ \gamma_{xz} \end{Bmatrix} \tag{3.33}$$

where

$$\left.\begin{aligned} A_{11} &= D_{11} \\ A_{12} &= D_{12} \\ A_{22} &= D_{22} \\ A_{44} &= KD_{Qy} \\ A_{55} &= KD_{Qx} \\ A_{66} &= D_{33} \\ D_{s.11} &= D_{44} \\ D_{s.12} &= D_{45} \\ D_{s.22} &= D_{55} \\ D_{s.66} &= D_{66} \end{aligned}\right\} \tag{3.34}$$

When taking into account all zero values the formula for the first eigenfrequency can be simplified to:

$$f_1 = \frac{1}{2\pi}\sqrt{\frac{\bar{s}_{33}}{\hat{m}_{33}}} \tag{3.35}$$

The full expression containing both rotary and in-plane inertia is presented in Reddy (1997). The full expression needs to be used if in-plane vibrations are of interest or if the plate consists of antisymmetric laminates. Therefore the simplified expression can be used for a sandwich floor, where frequencies of flexural vibration are of interest.

Shear force

A way to calculate the shear force for an orthotropic sandwich plate supported on four edges is presented by Zenkert (2007). Origin of the plate is placed in the top left corner hence maximum shear force regarding shear stress flow in x-direction occur in the middle of the short side at *x=0* and *y=b/2*. The shear force is stated as:

$$T = \sum_i \sum_j \frac{X_{ij} q_{ij}}{Z_{ij}} \cos\left(\frac{i\pi x}{L}\right) sin\left(\frac{j\pi y}{B}\right) \tag{3.36}$$

where

$$Z_{ij} = \left(\frac{i\pi}{L}\right) X_{ij} - \left(\frac{j\pi}{B}\right) Y_{ij} \tag{3.37}$$

$$X_{ij} = \frac{\begin{array}{c} \frac{1}{2}\left(\frac{i\pi}{L}\right)^5 \frac{D_x D_{xy}}{1-\nu_x\nu_y} + \left(\frac{i\pi}{L}\right)^3\left(\frac{j\pi}{B}\right)^2\left[\frac{D_x D_y}{1-\nu_x\nu_y} - \frac{D_{xy}\left(\nu_x D_y + \nu_y D_x\right)}{2\left(1-\nu_x\nu_y\right)}\right] \\ + \frac{1}{2}\left(\frac{i\pi}{L}\right)\left(\frac{j\pi}{B}\right)^4 \frac{D_y D_{xy}}{1-\nu_x\nu_y} \\ + D_{Qy}\left(\frac{i\pi}{L}\right)\left[\left(\frac{j\pi}{L}\right)^2 \frac{D_x}{1-\nu_x\nu_y} + \left(\frac{j\pi}{B}\right)^2\left(D_{xy} + \frac{\nu_y D_x}{1-\nu_x\nu_y}\right)\right] \end{array}}{D_{Qy}} \tag{3.38}$$

$$Y_{ij} = \frac{\begin{array}{c} -\frac{1}{2}\left(\frac{j\pi}{B}\right)^5 \frac{D_y D_{xy}}{1-\nu_x\nu_y} - \left(\frac{i\pi}{L}\right)^2\left(\frac{j\pi}{B}\right)^3\left[\frac{D_x D_y}{1-\nu_x\nu_y} - \frac{D_{xy}\left(\nu_x D_y + \nu_y D_x\right)}{2\left(1-\nu_x\nu_y\right)}\right] \\ - \frac{1}{2}\left(\frac{i\pi}{L}\right)^4\left(\frac{j\pi}{B}\right)\frac{D_x D_{xy}}{1-\nu_x\nu_y} \\ + D_{Qx}\left(\frac{j\pi}{B}\right)\left[\left(\frac{j\pi}{B}\right)^2 \frac{D_y}{1-\nu_x\nu_y} + \left(\frac{i\pi}{L}\right)^2\left(D_{xy} + \frac{\nu_x D_y}{1-\nu_x\nu_y}\right)\right] \end{array}}{D_{Qx}} \tag{3.39}$$

q_{ij} is calculated in the same way as for Equation (3.22).

3.4.3 Local bending of sandwich plate

Euler-Bernoulli beam theory is used to analyse the local bending in a cell. The upper face is analysed as a clamped-clamped beam with a length of l_c-f_c which is illustrated in Figure 3.5. Note that the homogenised stiffness properties defined by Libove & Hubka (1951) are not used when analysing the local bending. The width of the beam is 50 mm as the concentrated imposed load is recommended to act on an area of 50x50 mm^2 (see Chapter 2.7). The maximum local bending moment and local bending resistance is calculated as stated below. This approach is conservative and underestimates the moment resistance of the top face.

$$M_{Ed.local} = \frac{Q(l_c - f_c)}{8} \tag{3.40}$$

$$M_{Rd.local} = \frac{(50\ mm){t_{f.top}}^2}{6} f_m \tag{3.41}$$

where

f_m Bending strength of top face material, [Pa]

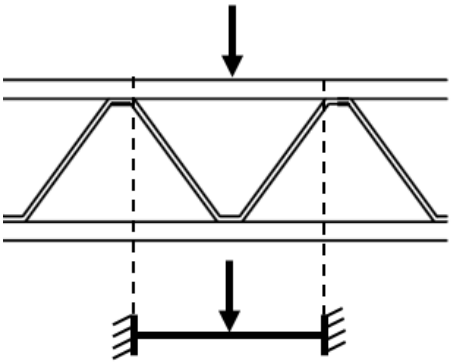

Figure 3.5: Visualisation of structural model used when calculating local deflection.

3.4.4 Strength analysis of timber

Conventionally, strength analysis of timber is made with a linear elastic stress analysis in combination with a stressed-based failure criterion. Timber is assumed to have ideal brittle performance, i.e. the timber element breaks when the stress state is equal to the failure criterion. A commonly used failure criterion is the Norris stress criterion (Gustafsson, 2003). The Norris criterion for a 3D state of stress with considerations for the three different planes of the orthotropic material is expressed as follows

$$\begin{cases} \left(\frac{\sigma_{11}}{f_{11}}\right)^2 + \left(\frac{\sigma_{22}}{f_{22}}\right)^2 + \left(\frac{\tau_{12}}{f_{12}}\right)^2 - \left(\frac{\sigma_{11}}{f_{11}}\right)\left(\frac{\sigma_{22}}{f_{22}}\right) = 1 \\ \left(\frac{\sigma_{11}}{f_{11}}\right)^2 + \left(\frac{\sigma_{33}}{f_{33}}\right)^2 + \left(\frac{\tau_{13}}{f_{13}}\right)^2 - \left(\frac{\sigma_{11}}{f_{11}}\right)\left(\frac{\sigma_{33}}{f_{33}}\right) = 1 \\ \left(\frac{\sigma_{22}}{f_{22}}\right)^2 + \left(\frac{\sigma_{33}}{f_{33}}\right)^2 + \left(\frac{\tau_{23}}{f_{23}}\right)^2 - \left(\frac{\sigma_{22}}{f_{22}}\right)\left(\frac{\sigma_{33}}{f_{33}}\right) = 1 \end{cases} \tag{3.42}$$

where

σ_{11}	Normal stress in first direction, [Pa]
f_{11}	Compression/tension strength in first direction, [Pa]
σ_{22}	Normal stress in second direction, [Pa]
f_{22}	Compression/tension strength in second direction, [Pa]
τ_{12}	Shear stress in the plane of first and second axis, [Pa]
f_{12}	Shear strength in the plane of first and second axis, [Pa]
σ_{33}	Normal stress in third direction, [Pa]
f_{33}	Compression/tension strength in third direction, [Pa]
τ_{13}	Shear stress in the plane of first and third axis, [Pa]
f_{13}	Shear strength in the plane of first and third axis, [Pa]
τ_{23}	Shear stress in the plane of second and third axis, [Pa]
f_{23}	Shear strength in the plane of second and third axis, [Pa]

Timber is also checked with regard to ULS-criteria in EN 1995-1-1 (2004). The following expressions should be satisfied for normal and shear stress.

$$\sigma_{t.0.d} \leq f_{t.0.d} \tag{3.43}$$

where

$\sigma_{t.0.d}$	Tensile stress parallel to the grain [Pa]
$f_{t.0.d}$	Tensile strength parallel to the grain [Pa]

$$\sigma_{c.0.d} \leq f_{c.0.d} \tag{3.44}$$

where

$\sigma_{c.0.d}$	Compressive stress parallel to the grain [Pa]
$f_{c.0.d}$	Compressive strength parallel to the grain [Pa]

Tension perpendicular to grain:

$$\sigma_{t.90.d} \leq f_{t.90.d} \tag{3.45}$$

where

$\sigma_{t.90.d}$	Tensile stress perpendicular to the grain [Pa]
$f_{t.90.d}$	Tensile strength perpendicular to the grain [Pa]

$$\sigma_{c.90.d} \leq k_{c.90} f_{c.0.d} \tag{3.46}$$

where

$\sigma_{c.90.d}$	Compressive stress perpendicular to the grain [Pa]
$f_{c.90.d}$	Compressive strength perpendicular to the grain [Pa]
$k_{c.90}$	Factor taking account the load configuration, possibility of splitting and degree of compressive deformation [-]

$$\tau_d \leq f_{v.d} \tag{3.47}$$

where

τ_d	Shear stress [Pa]
$f_{v.d}$	Shear strength [Pa]

3.4.5 Verification of analytical calculations

The analytical plate theory formula presented in Chapter 3.4.2 can be verified by modelling the sandwich floor as a single layer shell in Abaqus/CAE. The properties of the plate are obtained by defining a general shell stiffness matrix as section in Abaqus/CAE. The general shell stiffness matrix is displayed in Figure 3.6.

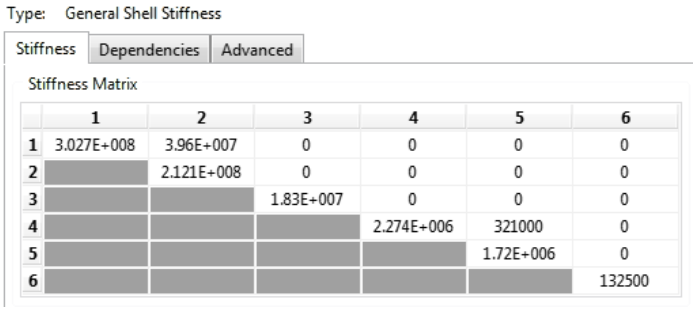

	1	2	3	4	5	6
1	3.027E+008	3.96E+007	0	0	0	0
2		2.121E+008	0	0	0	0
3			1.83E+007	0	0	0
4				2.274E+006	321000	0
5					1.72E+006	0
6						132500

Figure 3.6: Implementation of general shell stiffness matrix in Abaqus/CAE.

The 6x6 matrix is the same as the constitutive matrix presented in Equation (3.20). The transverse stiffness of the shell is defined as the so-called "K-values" under the tab "Advanced". These constants are the same as D_{Qx} (K11) and D_{Qy} (K22). The density is defined as the mass per unit area. The implementation in Abaqus/CAE is illustrated in Figure 3.7.

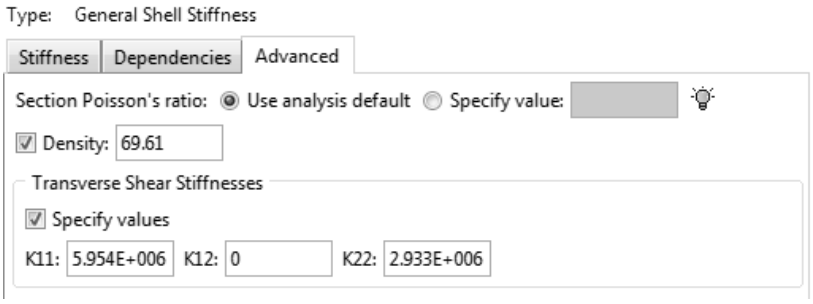

Figure 3.7: Implementation of transverse stiffness and density in Abaqus/CAE.

3.4.6 Method to obtain preliminary dimensions

The preliminary design of the corrugated core is being developed using an optimisation code in Mathcad originally developed by Beneus & Koc (2014) and modified by Dackman & Ek (2015). The code is created for steel sandwich plates with isotropic material to reduce material volume in sandwich bridge decks. The material volume is minimized by optimising six independent variables. Constrains are defined to assure sufficient structural performance and valid geometry. The plate is being optimised with regard to:

h_c Height of corrugation
t_c Thickness of core
$t_{f.top}$ Thickness of top face
$t_{f.bot}$ Thickness of bottom face
α_c Angle of corrugation
f_c Length of horizontal corrugation segment

The geometrical notations are visualised in Figure 3.8.

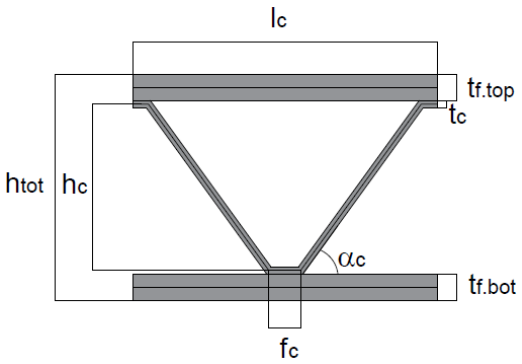

Figure 3.8: Geometrical notations for the corrugated sandwich panel.

The code must be modified to be suitable for sandwich timber floors. Both material input values and constrains have to be changed. Also, the corrugated core in plywood will have rounded corrugation corners due to manufacturing. The rounded corners are not included in the defined geometry in the Mathcad code by Dackman & Ek (2015). The sandwich theory in the Mathcad code is based on the elastic stiffness constants derived by Libove & Hubka (1951) which assumes isotropic material. Therefore the orthotropic timber material must in some way be interpreted as an isotropic material. The interpretation will be more or less correct depending on the anisotropy of the timber material, for example plywood with high nominal thickness, with low anisotropy, will be more suitable for isotropic theory than Kerto-Q, with high anisotropy. The rough treatment of the timber anisotropy is an evident simplification to reality and the Mathcad code is only used to obtain preliminary dimensions for the sandwich plate. To analyse the behaviour and confirm the structural performance of the timber sandwich plate, numerical calculations are necessary.

Choice of material properties

The material properties in the code are based on plywood material properties of Finnish conifer plywood with thin veneers and a nominal thickness of 24 mm. The values are obtained from UPM (2007). However they do not give any values for Poisson's ratios, these values are instead taken from Swedish Vänerply stated in Kliger (2015).

The simplifications in the Mathcad file include the E-modulus as an average value of $E_{m.0.mean}$ and $E_{m.90.mean}$ and the shear stiffness is considered as the panel shear stiffness, $G_{v.mean}$. The Poisson's ratio is an average value between v_{12}, v_{13} and v_{23}. The bending strength is an average of $f_{m.0.k}$ and $f_{m.90.k}$ while the shear strength is given as the panel shear $f_{v.k}$. The following equations describe the simplified material treatment for the material used in the Mathcad code.

$$E = \frac{E_{m.0.mean} + E_{m.90.mean}}{2} = \frac{7.218\ GPa + 5.782\ GPa}{2} = 6.5\ GPa \tag{3.48}$$

$$G = G_{v.mean} = 0.53\ GPa \tag{3.49}$$

$$\nu = \frac{\nu_{12} + \nu_{13} + \nu_{23}}{3} = \frac{0.5 + 0.05 + 0.01}{2} = 0.187 \tag{3.50}$$

$$f_m = \frac{f_{m.0.k} + f_{m.90.k}}{2} = \frac{22.2\ MPa + 19.7\ MPa}{2} = 20.95\ MPa \tag{3.51}$$

$$f_v = f_{v.k} = 7\ MPa \tag{3.52}$$

The choice of shear stiffness parameters and Poisson's ratio are elaborated in Chapter 4.1.5.

Geometric constrains
The thickness of the core and the bottom face should be equal or larger than 6.5 mm. It is considered rare to produce structural plywood with a smaller thickness.

$$t_{f.bot} \geq 6.5\ mm \tag{3.53}$$

$$t_{f.top} \geq 6.5\ mm \tag{3.54}$$

$$t_c \geq 6.5\ mm \tag{3.55}$$

Also, due to manufacturing reasons the bond length between the core and the top and bottom faces is assumed to be at least 30 mm long.

$$f_c \geq 30\ mm \tag{3.56}$$

The corrugation angle is restrained to be minimum 5° and maximum 85°. A larger or smaller angle is regarded difficult to manufacture.

$$5° \leq \alpha_c \leq 85° \tag{3.57}$$

The constrains regarding thin faces of a sandwich plate, Equation (3.1) and Equation (3.2), are also implemented in the Mathcad code.

Structural constrains
Regarding deflection, the stricter beam deflection requirement in Eurocode 5 is chosen. Only instantaneous deflection is considered.

$$w_{inst} \leq \frac{min(B, L)}{500} \tag{3.53}$$

The deflection is calculated with Equation (3.22).

The local bending strength of the sandwich plate when subjected to an imposed concentrated load is included in the optimisation. The local bending resistance should be equal or larger than the acting bending moment.

$$M_{Rd.local} \geq M_{Ed.local} \tag{3.54}$$

The moment resistance and the bending moment is approximated with Equation (3.40) and Equation (3.41).

A constrain regarding maximum shear stress parallel to the corrugation at the core-face intersection is used to obtain a minimum value for the bond line. The adhesive used for the connection is assumed to have superior shear strength than the plywood.

$$\tau_{x.top} \leq f_{vd} \tag{3.55}$$

where

$$\tau_{x.top} = \frac{TS_{top}}{I_x b_{top}} \tag{3.56}$$

$$\tau_{x.bot} \leq f_{vd} \tag{3.57}$$

The three vibration requirements proposed by Brandin & Oscarsson (2015), presented in Chapter 2.5.3, are used as constrains. The first eigenfrequency of the floor should be above 8 Hz, the deflection when subjected to a 1 kN concentrated load should be less than 1 mm and the frequency/deflection ratio should be larger or equal to 18.7. The requirements are presented in Equations (2.1), (2.4) and (2.5).

3.5 Modelling of timber in Abaqus/CAE

Timber has different properties in mainly three directions, longitudinal, radial and tangential direction. Timber can therefore be modelled as an orthotropic material. For linear elasticity of the orthotropic material the constitutive relationship is the following (Sandhaas & Van de Kuilen, 2013)

$$\begin{Bmatrix} \varepsilon_{11} \\ \varepsilon_{22} \\ \varepsilon_{33} \\ \gamma_{12} \\ \gamma_{13} \\ \gamma_{23} \end{Bmatrix} = \begin{bmatrix} 1/E_1 & -\nu_{21}/E_2 & -\nu_{31}/E_3 & 0 & 0 & 0 \\ -\nu_{12}/E_1 & 1/E_2 & -\nu_{32}/E_3 & 0 & 0 & 0 \\ -\nu_{13}/E_1 & -\nu_{23}/E_2 & 1/E_3 & 0 & 0 & 0 \\ 0 & 0 & 0 & 1/G_{12} & 0 & 0 \\ 0 & 0 & 0 & 0 & 1/G_{13} & 0 \\ 0 & 0 & 0 & 0 & 0 & 1/G_{23} \end{bmatrix} \begin{Bmatrix} \sigma_{11} \\ \sigma_{22} \\ \sigma_{33} \\ \sigma_{12} \\ \sigma_{13} \\ \sigma_{23} \end{Bmatrix} \tag{3.58}$$

This elastic behaviour is modelled in Abaqus/CAE by choosing the elastic type "engineering constants" (D Systèmes, 2012). If the floor is modelled with shell elements and is not loaded in-plane and out-of-plane at the same time, the lamina material model can be used. The lamina model considers orthotropic materials under plane stress conditions (Dackman & Ek, 2015).

The material can be assigned a local coordinate system in Abaqus/CAE in order to keep track of the different directions. The local coordinate system of veneer products such as plywood and Kerto-Q is defined as in Figure 3.9.

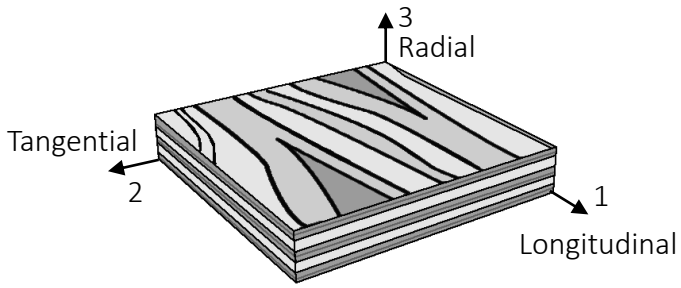

Figure 3.9: The definition of the wood fiber orientation in veneer products.

4 Investigation of the structural behaviour of the sandwich floor

The structural behaviour of the sandwich floor is mainly analysed with finite element calculations in Abaqus/CAE. Three different aspect ratios of the floor are chosen for investigation; $\sqrt{98}$x$\sqrt{98}$ m^2, 14x7 m^2 and 7x14 m^2. All three floors have the same area and the difference between the rectangular floors is the positioning of the corrugation. They are defined with the objective to identify which design considerations should be made for different aspect ratios. The floors have simply supported boundaries with no flexibility along all four edges. The aspect ratios are visualised in Figure 4.1 and are referred to as plate 1:1, 2:1 and 1:2 further on in the text.

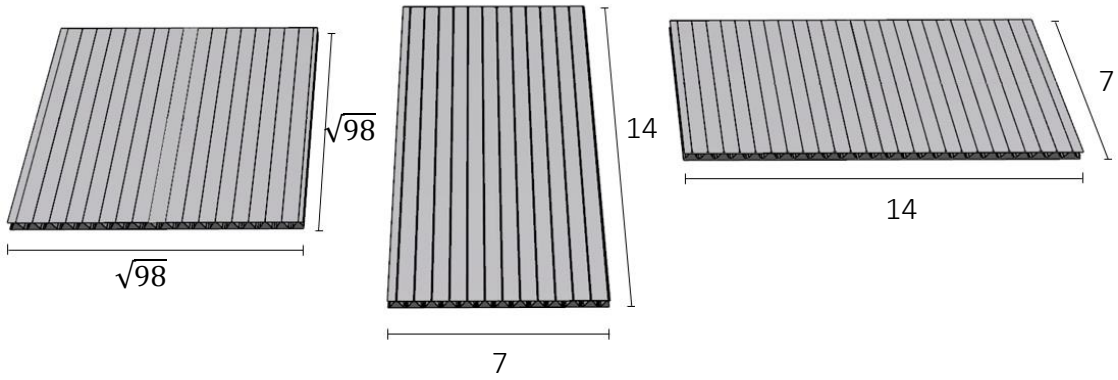

Figure 4.1: Dimensions of the three different plates with the same area but different aspect ratio (from left), 1:1, 2:1 and 1:2.

The influence of aspect ratio, shape of corrugation and different type of materials are being investigated. The main fibre direction can either be placed perpendicular (⊥) or parallel (//) to the corrugation as illustrated in Figure 4.2. The fibres are oriented in different manners for different types of engineered wood products but commonly for all are that the outer layers indicate the main fibre orientation. The highest modulus of elasticity also indicates the main fibre orientation.

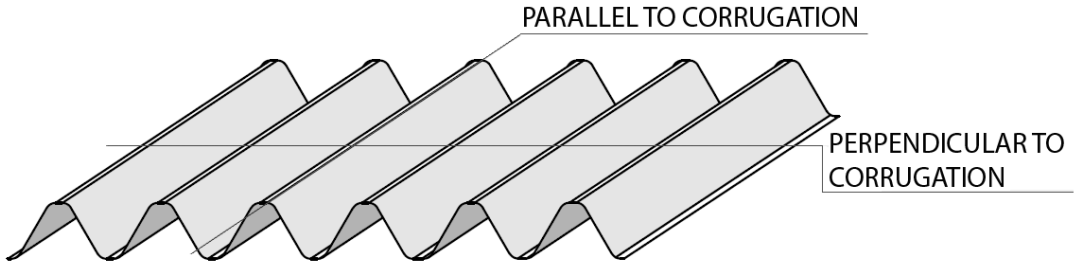

Figure 4.2: Definition of corrugation directions.

In the behaviour analysis the maximum instantaneous deflection when subjected to the uniformly distributed imposed load, dead weight and self-weight is used as indicator of the performance regarding the global behaviour. The performance

regarding instantaneous deflection and eigenfrequency are influenced by the same parameters, high bending and shear stiffness and low self-weight yield better performance.

For the behaviour analysis a cross-section is generated for plate 1:1 with the Mathcad code, introduced in Chapter 3.4.6 and presented in Appendix B. The floor is loaded with an imposed load of 2 kN/m^2, the self-weight of the structure and an additional dead weight of 50 kg/m^2 from installation and extra-added material. A height constrain is added to restrain the height of the plate to 410 mm. The corrugation has no curved corners. The horizontal component of the corrugation, f_c, is given a minimum constrain of 100 mm. It is likely more than needed for manufacturing but the influence of including the curved corners can be investigated later on. When performing the optimisation, local bending as stated in Equation (3.54) and the deflection/eigenfrequency-ratio stated in Equation (2.5) are the governing structural criteria. The dimensions of the cross-section are presented in Table 4.1 and visualised in Figure 4.3. The cross-section is referred to as cross-section 1 and these are the basic dimensions also for other cross-sections used later on in this chapter.

Table 4.1: Dimensions obtained for cross-section 1 from the Mathcad code.

h_c [mm]	341.1
t_c [mm]	13.3
$t_{f.top}$ [mm]	38.4
$t_{f.bot}$ [mm]	17.2
α_c [°]	62.4
f_c [mm]	100.0
l_c [mm]	556.7
h_{tot} [mm]	410

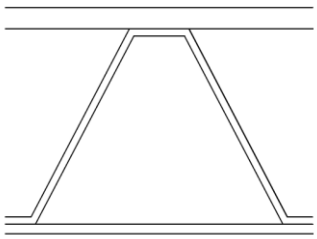

Figure 4.3: Illustration of cross-section 1 with dimensions relative to each other.

4.1 Verification and elaboration of analytical calculations

This chapter has the main objective to investigate if the analytical calculations in the Mathcad code are in close agreement with the numerical calculations to ensure that the analytical calculations can be used when generating preliminary dimensions of the cross-section.

4.1.1 Verification of analytical deflection and eigenfrequency formula

An analytical eigenfrequency formula has been implemented in the Mathcad code. The formula is verified by creating an equivalent 2D shell plate in Abaqus/CAE in same way as described in Chapter 3.4.4. The validity of the deflection formula is also controlled as it will be the performance indicator in the behaviour analysis. The verification is performed for plate 1:1 with cross-section 1.

When making the verification it is important to include sufficient number of terms in the Fourier series in the analytical expression of the deflection, presented in Equation (3.22). When considering a solution expressed in mm and with three decimals the analytical solution for the deflection converges when the Fourier series have 37 terms in the first summation and 37 terms in the second summation. The shear correction factor, *K*, is set equal to 1 in the analytical calculation of the eigenfrequency; otherwise it has to be implemented in the general shell stiffness matrix. How the equivalent 2D shell model is created in Abaqus/CAE is presented in Appendix C. Table 4.2 presents the result obtained with analytical and numerical calculations.

Table 4.2: The results from the analytical and numerical 2D model regarding deflection and first eigenfrequency and the difference between analytical and numerical calculations.

	w_{inst} [mm]	f_1 [Hz]
Analytical	17.151	8.783
Numerical	17.128	8.817
Difference	0.134 %	0.387 %

The difference is smaller than 0.4 % for both deflection and eigenfrequency which is considered acceptable.

4.1.2 Influence of curved corrugation

The shape of the corners of the corrugation will be curved due to manufacturing. In Chapter 2.1.2, literature indicates that the minimum ratio between the corrugation radius and veneer thickness must be 6 or larger. This means that the length l_c will increase and consequently decrease the number of corrugation cells if the radius is included while all additional dimensions, stated in Table 4.1, are kept the same. The Mathcad code by Dackman & Ek (2015) does not include the radius of the corners but Libove & Hubka (1951) present additional formulas where the radius is included. The Mathcad code is therefore improved, by implementing the corrugation radius. The expressions are verified with numerical results presented in Libove & Hubka (1951) and show to be in close agreement. The changes made in the Mathcad code are presented in Appendix B and the new cross-section with its notations is visualised in Figure 4.4.

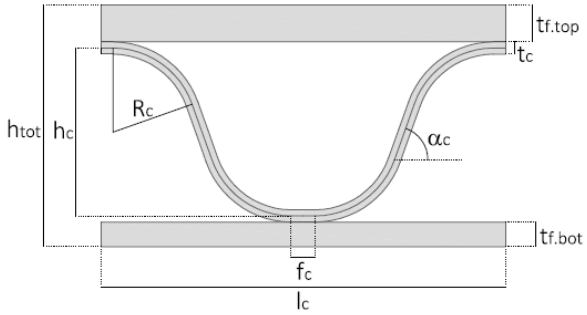

Figure 4.4: Geometrical definitions and notations of the sandwich floor with the included corrugation radius.

The deflection is investigated in the analytical calculations for plate 1:1 with different radiuses to see its influence and importance of implementing the radius in the analytical calculations. Table 4.3 illustrates that when all other dimensions in cross-section 1 are kept the same, except the l_c, and the corrugation radius is included the deflection increases from 14.5 mm to 19.3 mm. When adding the corrugation radius in this way the number of corrugation cells consequently decreases.

Table 4.3: The deflection when including different corrugation radius when keeping the distance f_c constant.

Radius	$0t_c$	$1t_c$	$2t_c$	$3t_c$	$4t_c$	$5t_c$	$6t_c$
l_c [mm]	417	449	481	513	546	578	610
w_{inst} [mm]	14.5	14.9	15.5	16.3	17.2	18.3	19.3
Number of corrugation cells	23.8	22.1	20.6	19.3	18.1	17.1	16.2

The deflection of the plate, when adding the radius, is also investigated when the number of corrugation cells is kept constant. This means that the distance of f_c is changed depending on the radius. This is visualised for four cross-sections with different corrugation radiuses in Figure 4.5 named cross section 1-4 further on in the text.

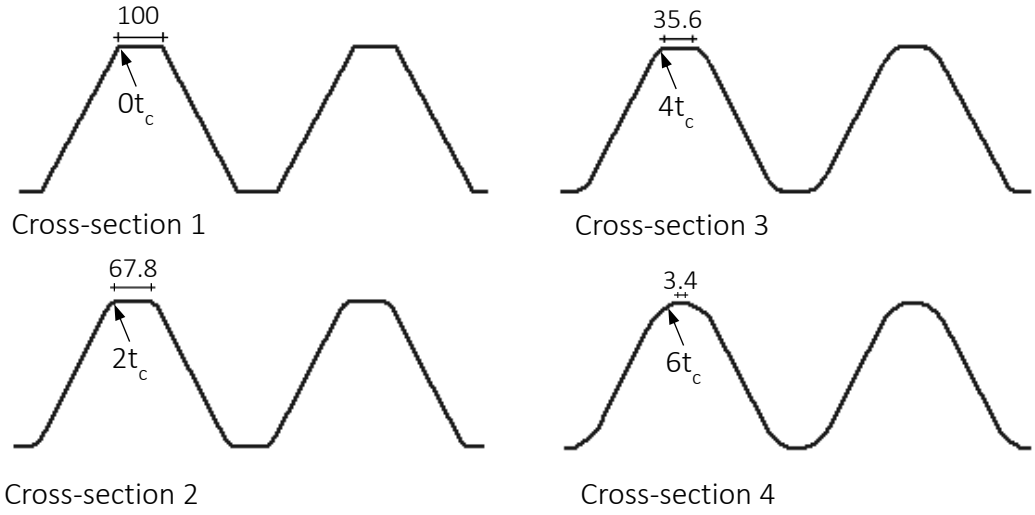

Figure 4.5: Different core configurations named cross-section 1-4 represented by their center lines with different corrugation radius and length of f_c.

As can be seen Table 4.4, the deflection changes marginally for the different cross-sections.

Table 4.4: The deflection when including different corrugation radius and the number of corrugation cells is kept constant.

Radius	$0t_c$	$1t_c$	$2t_c$	$3t_c$	$4t_c$	$5t_c$	$6t_c$
f_c [mm]	100	89.9	67.8	51.7	35.6	19.5	3.4
w_{inst} [mm]	17.9	17.8	17.8	17.7	17.6	17.5	17.4
Number of corrugation cells	17.8	17.8	17.8	17.8	17.8	17.8	17.8

The results indicate that the deflection is dependent on the number of corrugation cells and not the corrugation radius itself. So, the modification of the analytical calculations shows to suit a plywood core better than adding the radius to the sharp corners after the calculations are performed since the number of corrugation cells is an important factor.

4.1.3 Comparison between analytical calculations and 3D FE-models

Cross-section 1, 2, 3 and 4 are modelled for plate 1:1, 2:1 and 1:2 in Abaqus/CAE to compare the analytical calculations with FE-models with 3D geometry. The FE-models are built up with shell elements. The models are assigned the same average isotropic material properties as used in the Mathcad code and presented in Chapter 3.4.6. The material properties are referred to as Mathcad isotropic further on in the text and the mechanical properties are presented in Table 4.5.

Table 4.5: Mechanical properties for Mathcad isotropic material.

Material	Density [kg/m^2]	E_1 [GPa]	E_2 [GPa]	E_3 [GPa]	ν_{12} [-]	ν_{13} [-]	ν_{23} [-]	G_{12} [GPa]	G_{13} [GPa]	G_{23} [GPa]
Mathcad isotiopic	410	6.5	6.5	6.5	0.187	0.187	0.187	0.53	0.53	0.53

The analytical calculations are based on theory from Libove & Hubka (1951) which only assumes one "interaction-line" between the core and faces at its troughs and crests. This type of interaction is modelled in the 3D shell models in Abaqus/CAE to get a correct comparison with the analytical calculations. However, the interaction between the face and core will be designed in a different way in reality and the length f_c is assumed to be the bond length where the face and core are agglutinated. This type of interaction and behaviour of the plate will also be investigated in Abaqus/CAE in Chapter 4.1.4. The two different types of interactions are illustrated in Figure 4.6. They are referred to as Libove and Hubka interaction and full interaction further on in the text.

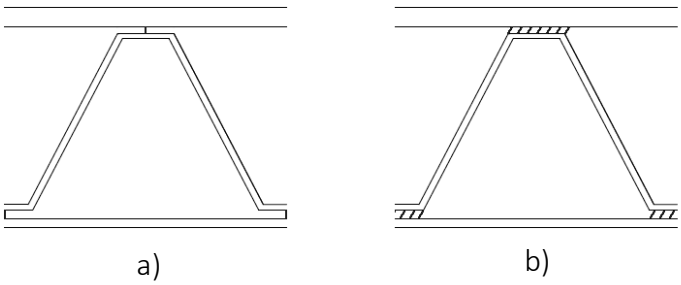

Figure 4.6: Different types of interaction where figure a) illustrates the interaction that Libove and Hubka (1951) assume and figure b) illustrates a full interaction over the length f_c.

A convergence study for the FE-models is presented in Appendix D. The comparison between the analytical Mathcad result and the numerical Abaqus/CAE result is illustrated in Figure 4.7-4.9 for plate 1:1, 2:1 and 1:2.

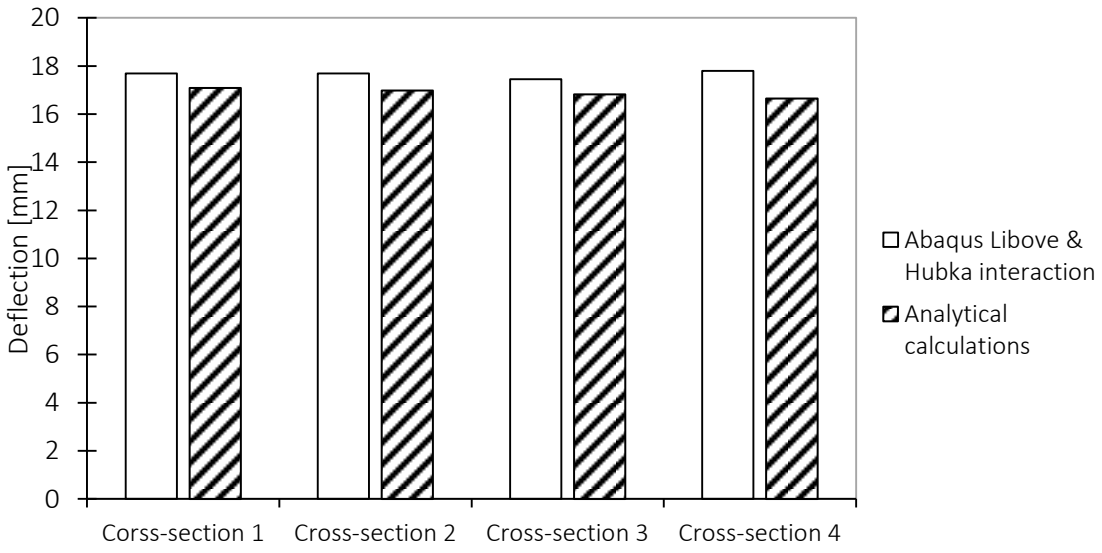

Figure 4.7: The deflection for plate 1:1 with numerical Libove & Hubka interaction and analytical calculations for cross-section 1-4.

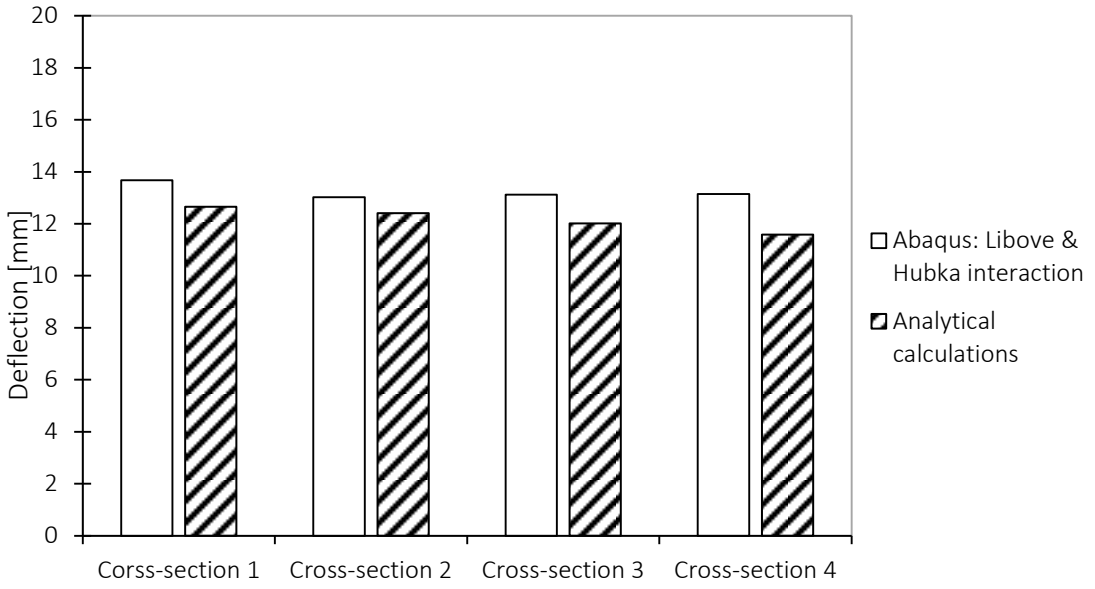

Figure 4.8: The deflection for plate 2:1 with numerical Libove & Hubka interaction and analytical calculations for cross-section 1-4.

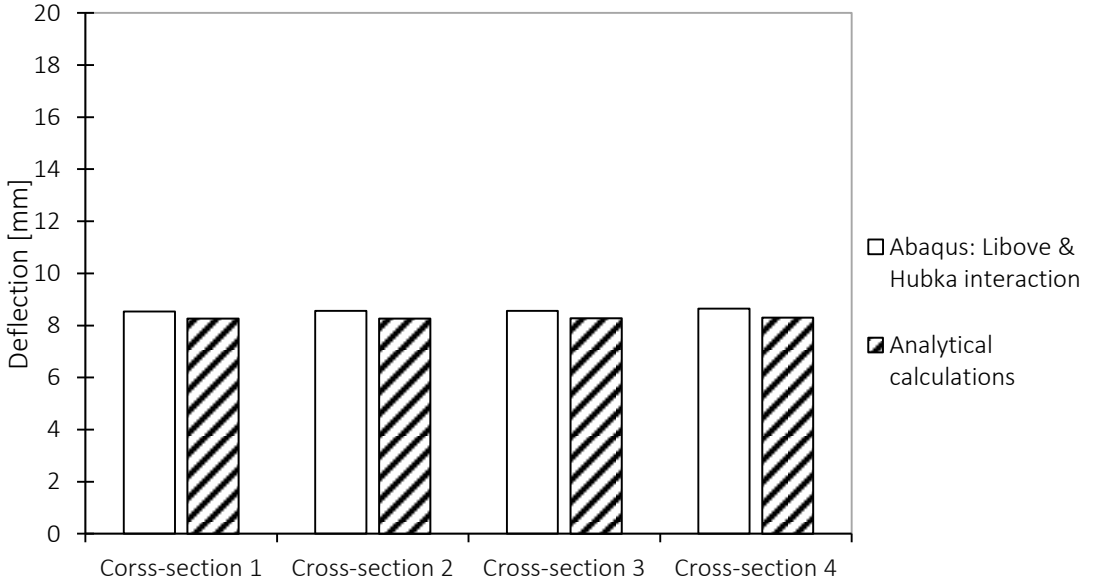

Figure 4.9: The deflection for plate 1:2 with numerical Libove & Hubka interaction and analytical calculations for cross-section 1-4.

The results illustrate that the difference in deflection is less than 7% between the analytical and numerical results for plate 1:1 and 1:2. The difference is considered acceptable. However, the deflections differ between 5-13.5% for plate 2:1. This greater difference should be investigated further and the difference should be kept in mind when performing the following investigations. For all cases the analytical result is lower than the numerical result.

4.1.4 Influence of full interaction

Cross-section 1, 2, 3 and 4 are also modelled for plate 1:1, 2:1 and 1:2 in Abaqus/CAE with full interaction to understand how the bond line affects the

stiffness. The FE-models are still assigned Mathcad isotropic material. These results are furthermore compared with the analytical calculations to see how well these calculations will correspond to the numerical result and if the numerical deflection will be lower than the analytical.

The deflections in the analytical calculations compared to the deflections in Abaqus/CAE differ depending on the length of f_c. Figure 4.10-4.12 illustrate the difference between the analytical calculations and the numerical models with full interaction for plate 1:1, 2:1 and 1:2.

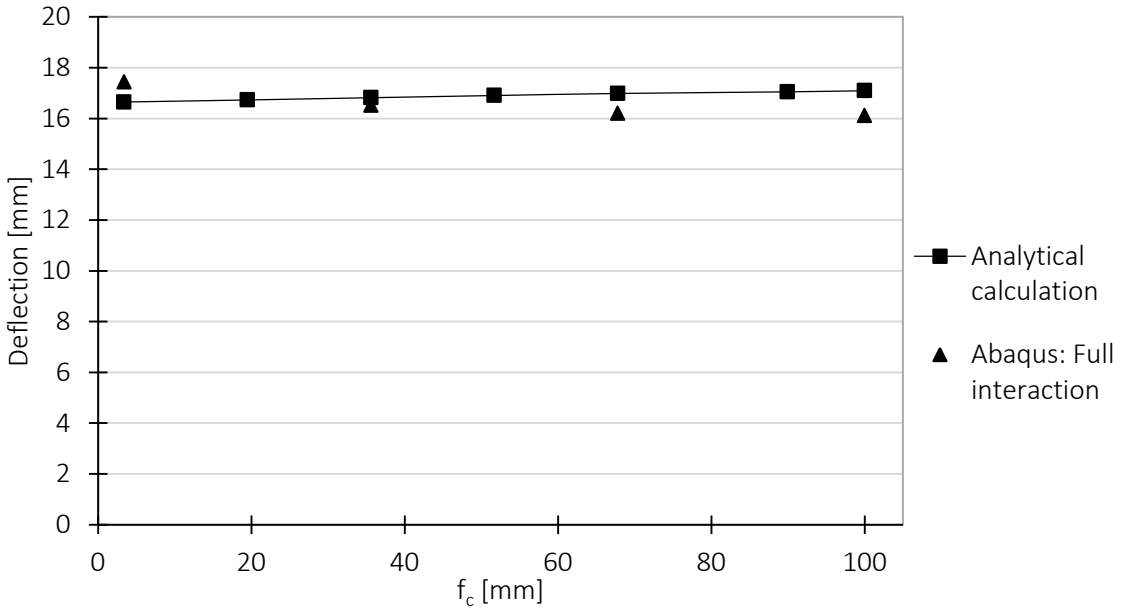

Figure 4.10: Deflection for plate 1:1 with different length of f_c and radius.

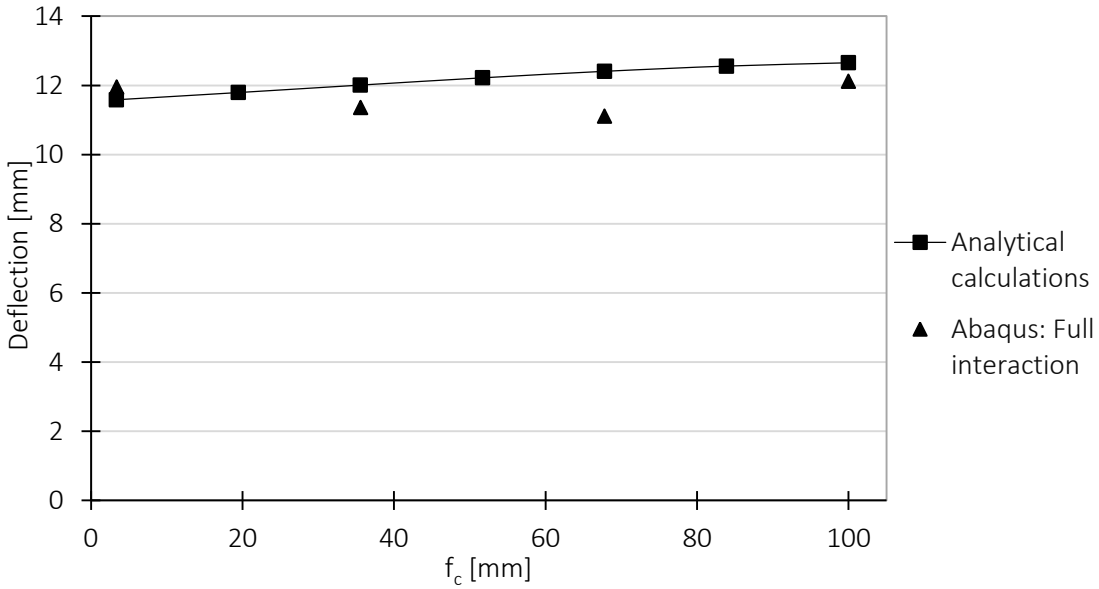

Figure 4.11: Deflection for plate 2:1 with different length of f_c and radius.

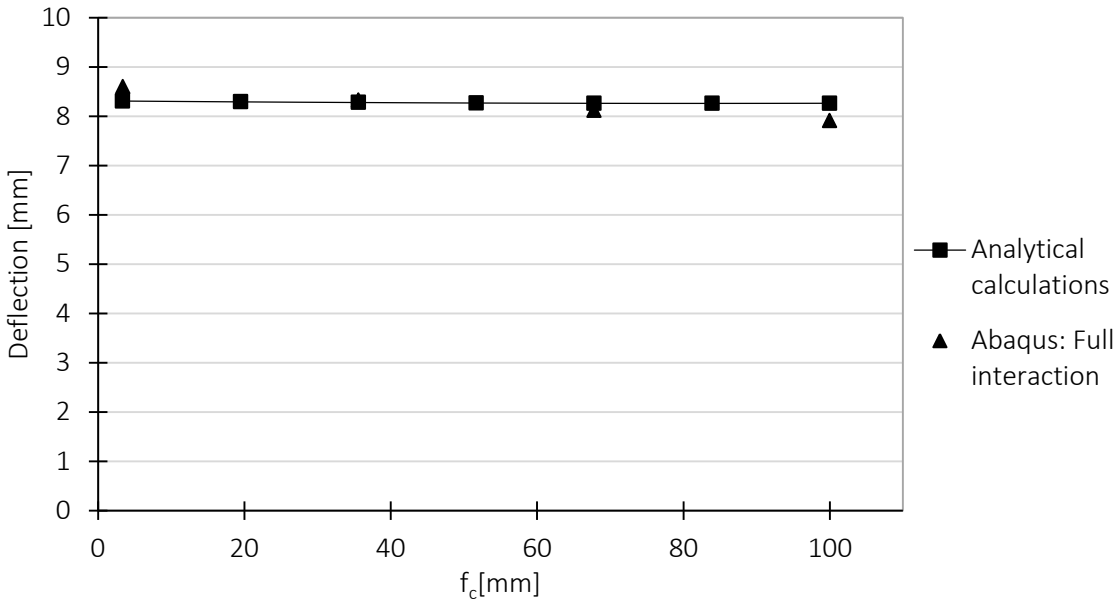

Figure 4.12: Deflection for plate 1:2 with different length of f_c and radius.

The results for plate 1:1, 2:1 and 1:2 with full interaction show, for cross-section 1-3, to yield less deflection than the analytical calculations. This means that the plate gains stiffness when changing from Libove and Hubka to full interaction as the numerical calculations with Libove and Hubka interaction were always lower than the analytical calculations. The numerical deflection for cross-section 4 shows to be higher than the analytical calculations. This can most probably be explained by the small length of f_c for this case that will have almost no influence on the stiffness. As was seen in the investigations in Chapter 4.1.3 the analytical calculations gave lower deflection than the numerical with Libove and Hubka interaction.

The difference between the numerical full interaction and the analytical calculation for plate 2:1 are illustrated in Figure 4.15 and shows to be less precise than the results for plate 1:1 and 1:2. The deflection vary and is lower for cross-section 2 compared to cross-section 1.This should be investigated further since the results from plate 1:1 and 1:2 have indicated that stiffness will increase with increasing length of f_c.

4.1.5 Choice of material transformation in analytical calculations

As presented in Chapter 3.4.4 the orthotropic mechanical properties of timber is treated as isotropic material in the analytical calculations due to the fact that the elastic stiffness constants derived by Libove & Hubka (1951) assume isotropic material. When Libove & Hubka (1951) derive the constants D_x, D_y, E_x, E_y and the bending and stretching Poisson's ratios v_x, v_y, v'_x and v'_y they assume plane stress. The constitutive relationship for an orthotropic material when assuming plane stress is stated as follows (Roylance, 2000):

$$\begin{Bmatrix} \varepsilon_{11} \\ \varepsilon_{22} \\ \gamma_{12} \end{Bmatrix} = \begin{bmatrix} 1/E_1 & -\nu_{21}/E_1 & 0 \\ -\nu_{12}/E_1 & 1/E_2 & 0 \\ 0 & 0 & 1/G_{12} \end{bmatrix} \begin{Bmatrix} \sigma_{11} \\ \sigma_{22} \\ \sigma_{12} \end{Bmatrix} \tag{4.1}$$

where

$$\nu_{21} = \frac{E_2}{E_1}\nu_{12} \tag{4.2}$$

Therefore one could argue that the shear stiffness should be treated as in Equation (3.49) while the Poisson's ratio should be treated as:

$$\nu = \frac{\nu_{12} + \nu_{21}}{2} = \frac{0.5 + 0.40}{2} = 0.45 \tag{4.3}$$

However for the other stiffness constants plane stress is not the case. So, one could also argue that the shear stiffness should be treated as:

$$G = \frac{G_{v.mean} + G_{r.0.mean} + G_{r.90.mean}}{3} = \frac{0.53\ GPa + 0.069\ GPa + 0.063\ GPa}{3} = 0.221\ GPa \tag{4.4}$$

The modulus of elasticity is assumed to be equal in radial direction as in tangential direction, $E_2 = E_3$, hence the modulus of elasticity is not affected by plane stress or not. In order to get a picture of how the treatment of shear stiffness and Poisson's ratio influence the analytical calculations four cases are investigated with the Mathcad code:

- Material transformation 1 (Mt1): Equations (4.4) and (3.50)
- Material transformation 2 (Mt2): Equations (3.49) and (3.50)
- Material transformation 3 (Mt3): Equations (4.4) and (4.3)
- Material transformation 4 (Mt4): Equations (3.49) and (4.3)

Mt2 represents the way of treating material properties as described in Chapter 3.4.4 and was used when generating cross-section 1. The FE-models for cross-section 1 with Libove and Hubka interaction from Chapter 4.1.3 are used again but the material properties are changed. The sandwich floor is given properties for conifer plywood with thickness 24 mm. It is the basis for the Mathcad isotropic material properties. To clarify, the top face has the thickness 38.4 mm but is given the material properties for plywood with thickness 24 mm. Orthotropic orientations are taken into account in the FE-models. The models are evaluated for four cases as it can be given different main fibre directions:

- Core: Main fibre direction parallel (//) to corrugation, Faces: Main fibre direction parallel to corrugation
- Core: Main fibre direction parallel to corrugation, Faces: Main fibre direction perpendicular (⊥) to corrugation
- Core: Main fibre direction perpendicular to corrugation, Faces: Main fibre direction parallel to corrugation
- Core: Main fibre direction perpendicular to corrugation, Faces: Main fibre direction perpendicular to corrugation

The deflections obtained with the FE-models for the different main fibre directions are presented as columns in Figure 4.13 for plate 1:1, in Figure 4.14 for plate 2:1 and in Figure 4.15 for plate 1:2. The lines represent the deflections obtained with the

analytical calculation in Mathcad using the four different ways of treating the material properties.

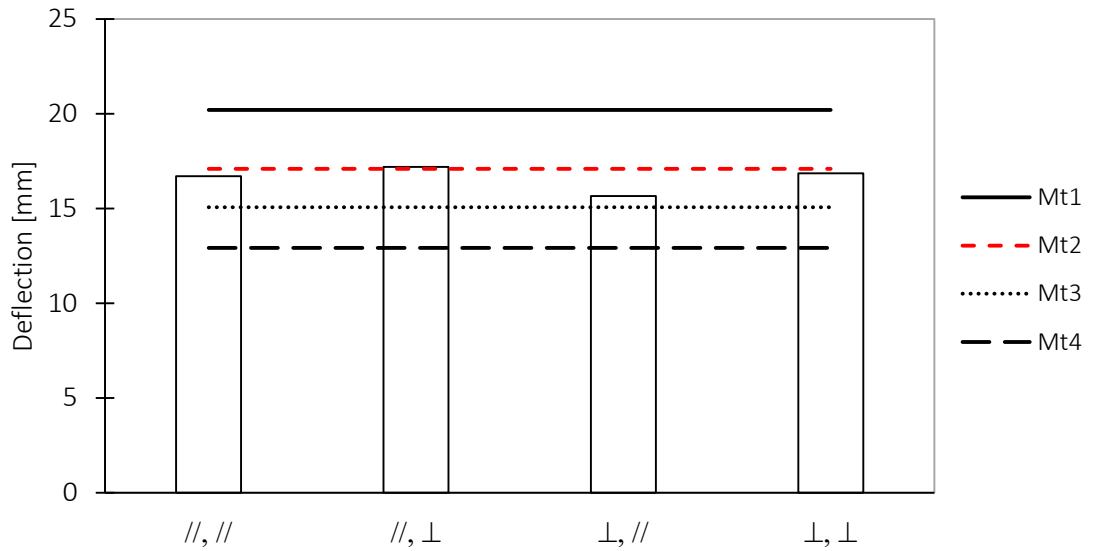

Figure 4.13: Numerical and analytical calculations of deflection for plate 1:1. The numerical results are presented with columns, where the four different columns represent different fibre orientations. The first sign under the column represent main fibre direction for core and the second sign is for the faces. The analytical deflections are presented with the lines. The four different lines represent four different ways of interpreting the material properties from orthotropic to isotropic material.

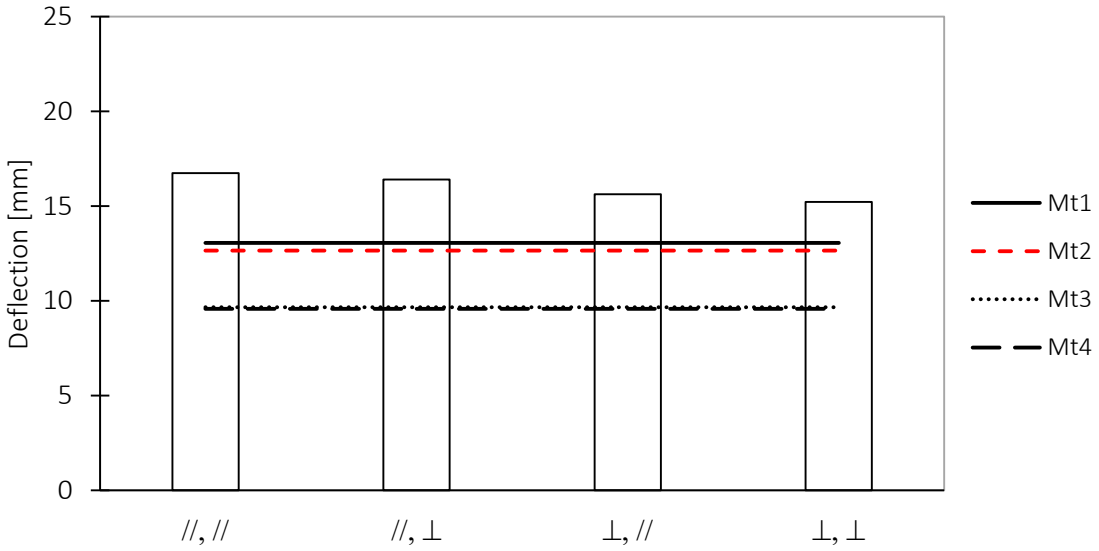

Figure 4.14: Numerical and analytical calculations of deflection for plate 2:1. The numerical results are presented with columns, where the four different columns represent different fibre orientations. The first sign under the column represent main fibre direction for core and the second sign is for the faces. The analytical deflections are presented with the lines. The four different lines represent four different ways of interpreting the material properties from orthotropic to isotropic material.

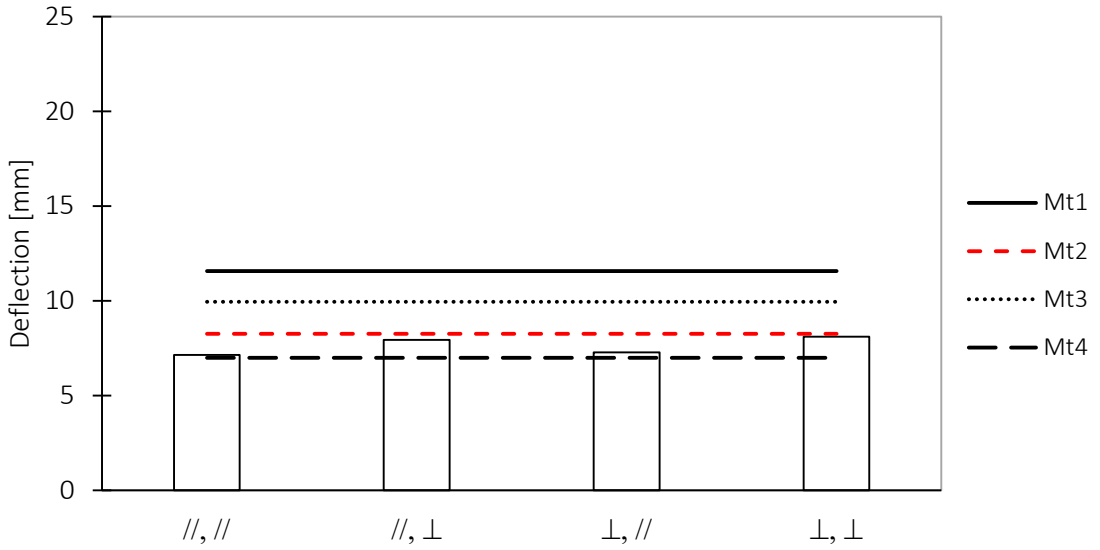

Figure 4.15: Numerical and analytical calculations of deflection for plate 1:2. The numerical results are presented with columns, where the four different columns represent different fibre orientations. The first sign under the column represent main fibre direction for core and the second sign is for the faces. The analytical deflections are presented with the lines. The four different lines represent four different ways of interpreting the material properties from orthotropic to isotropic material.

As can be seen in Figure 4.8-4.10 Mt2 yields a good approximation of plywood for plate 1:1 and 1:2. None of the material transformations give close result for plate 2:1 but Mt1 is somewhat better than Mt2. As mounted in Chapter 4.1.3 there is a significant difference between the analytical and numerical result for plate 2:1 even when Mathcad isotropic material is defined in the Abaqus/CAE model.

From the result, it cannot be said that the treatment of the shear stiffness and Poisson's ration in the Mathcad code (Mt2) is good. However none of the other investigated possibilities are better when taking into account all three aspect ratios.

4.1.6 Elaboration of the influence of modulus of elasticity and shear modulus on the positioning of the corrugation

The stiffness in a certain direction is dependent on both the bending stiffness and the transverse shear stiffness. The bending stiffness parallel to the corrugation is always higher than the bending stiffness perpendicular to the corrugation. However it cannot be said directly if the transverse shear stiffness is higher in x-direction than in y-direction.

According to Equation (3.22) the deflection is dependent of the stiffness constants D_x, D_y, D_{xy}, D_{Qx} and D_{Qy}. By observing the Libove & Hubka (1951) formulas for the stiffness constants one can tell that there is a direct linear relationship between the modulus of elasticity and D_x, D_y and D_{Qy}, while there is a direct linear relationship between the shear modulus and D_{xy} and D_{Qy}.

The Mathcad code is used to investigate the influence of the modulus of elasticity and shear modulus on the positioning of the corrugation. The study is performed for plate 2:1 and 1:2 with cross-section 1 and Mathcad isotropic is used as material. First the

shear modulus is fixed at start value 0.53 GPa and the modulus of elasticity is multiplied times two and times four from the standard value 6.5 GPa for Mathcad isotropic as well as divided with two and four. The result is displayed in Figure 4.16. The procedure is repeated but now the modulus of elasticity is fixed and the shear modulus is increased and decreased. The result is displayed in Figure 4.17.

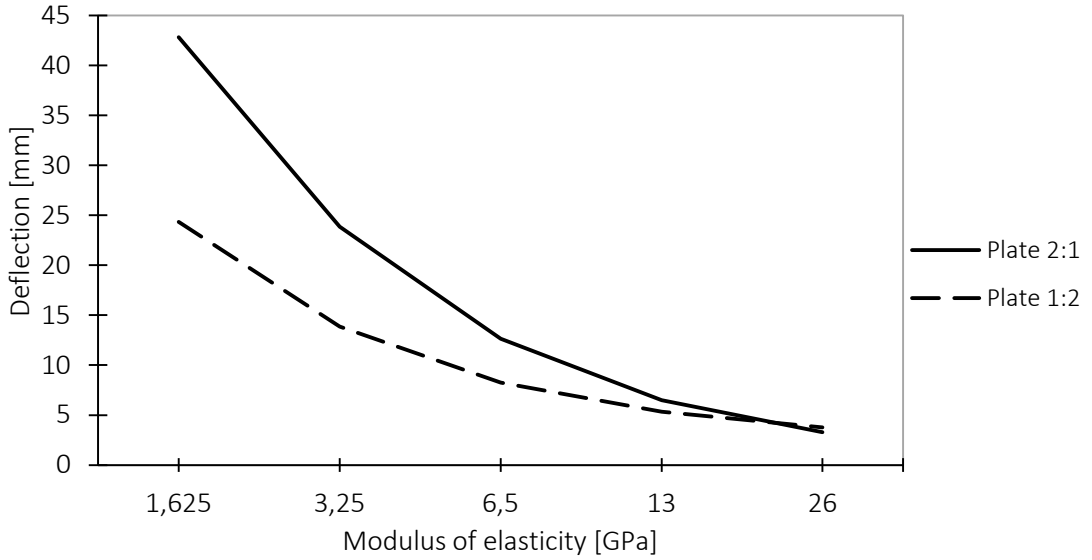

Figure 4.16: Deflection as a function of modulus of elasticity for plate 1:2 and 2:1.

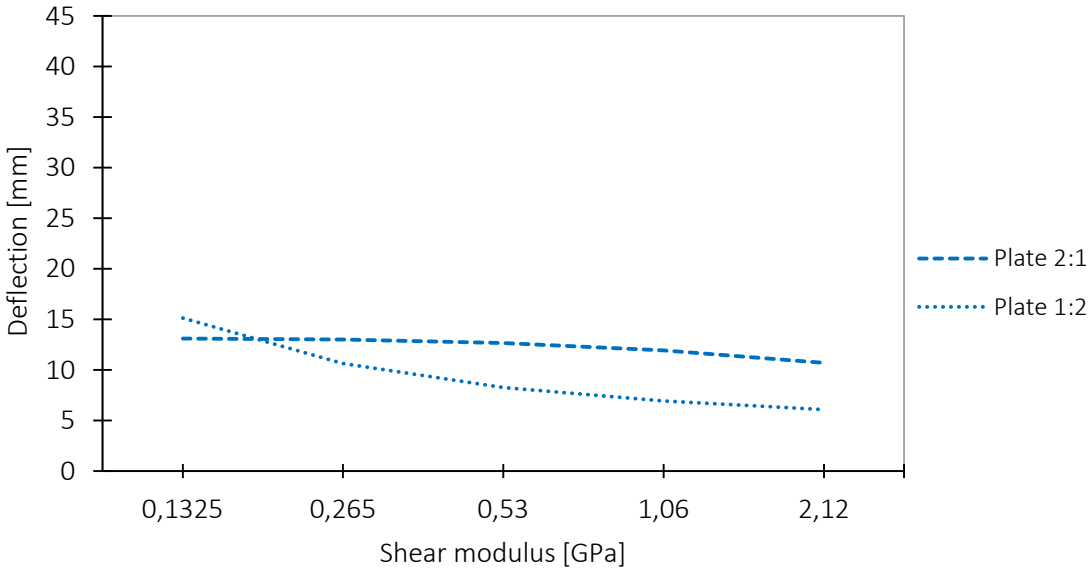

Figure 4.17: Deflection as a function of shear modulus for plate 1:2 and 2:1.

As can be seen in Figure 4.16 and 4.17, plate 1:2 with corrugation along short span, gives for most part of the interval lower deflection than plate 2:1, corrugation along long span, but for high modulus of elasticity or low shear modulus it can be seen that it is more efficient to place the corrugation along the long span. In Figure 4.18 the deflection is plotted as a function of the ratio between modulus of elasticity and shear modulus for the total four cases (plate 2:1 or 1:2 and fixed shear modulus or fixed modulus of elasticity).

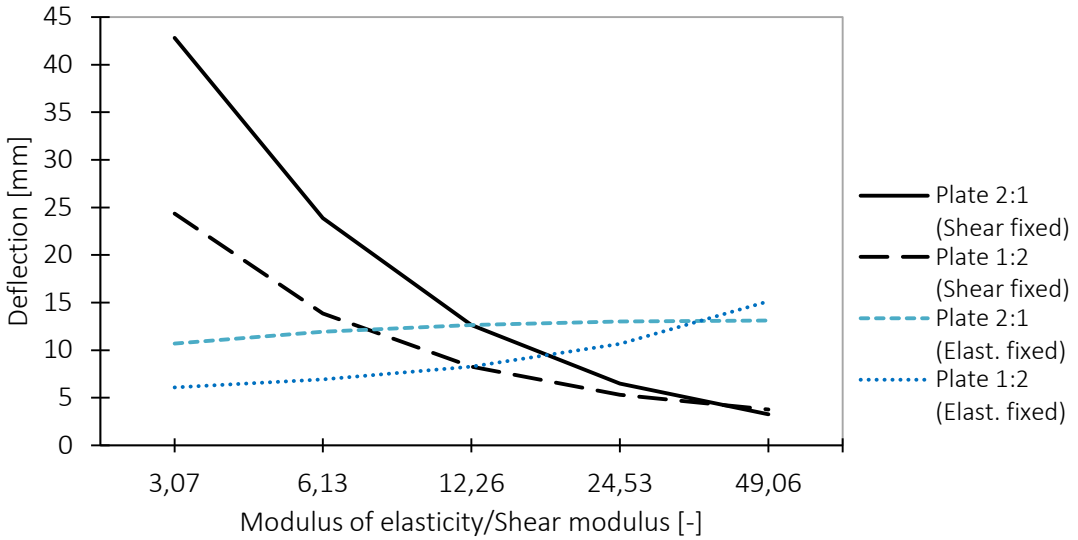

Figure 4.18: Deflection plotted as a function of the ratio between modulus of elasticity and shear modulus for four different cases. Cross-section 1 is used for all cases.

As can be seen in Figure 4.7 it is at a certain ratio between modulus of elasticity and shear modulus that plate 2:1 gives lower deflection than plate 1:2. It can be said that if the length and width of the plate, cross-sectional geometry and Poisson's ratio are fixed, it is the ratio between the modulus of elasticity and the shear modulus that determine the positioning of the corrugation with regard to deflection. However for the materials used in this study it is likely that plate 1:2 will provide higher stiffness than plate 2:1.

4.2 Design choices influence on the structural performance

This chapter is performed with the objective to investigate how different design choices of the floor influence the performance. The investigations are performed in Abaqus/CAE with 3D shell models.

4.2.1 Influence of material and main fibre orientation

The selection of material and main fibre orientation are being investigated in the numerical analysis by comparing the deflection for different cases. Cross section 4, with a corrugation radius of $6t_c$, is used for plate 1:1, 2:1 and 1:2.
In this study the main fibre direction is either placed parallel or perpendicular to the corrugation for both faces and core material. This yields four different combinations illustrated in Figure 4.19.

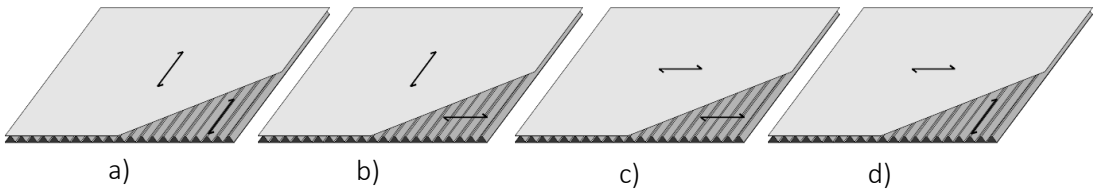

Figure 4.19: Illustration of different combinations of main fiber orientation in face and core where fibers are placed a) parallel to corrugation for faces and core, b) parallel to corrugation for faces and perpendicular to corrugation for core, c) perpendicular to corrugation for faces and core and d) perpendicular to corrugation for faces and parallel to corrugation for core

Different types of material and main fibre directions are accordingly investigated and the mechanical properties used for each material and thicknesses for top, bottom faces and core are presented in Table 4.6.

Table 4.6: Mechanical properties of conifer and birch plywood and Kerto-Q with different thicknesses suitable for each part of the plate.

Material	Thickness [mm]	Density [kg/m^2]	E_1 [GPa]	E_2 [GPa]	E_3 [GPa]	ν_{12} [-]	ν_{13} [-]	ν_{23} [-]	G_{12} [GPa]	G_{13} [GPa]	G_{23} [GPa]
Conifer plywood	12	410	7.96	5.04	5.04	0.5	0.05	0.01	0.53	0.069	0.057
	18		7.46	5.54	5.54					0.069	0.062
	30		7.07	5.93	5.93					0.068	0.064
Birch plywood	12	630	10.72	6.78	6.78	0.5	0.05	0.01	0.62	0.21	0.16
	18		10.05	7.45	7.45					0.21	0.17
	35		9.39	8.11	8.11					0.20	0.20
Kerto-Q	21-24	480	10	2.4	2.4	0.02	0.02	0.5	0.60	0.15	0.15
	27-69		13.8	11.6	11.6						

The combination between the materials and main fibre orientation are presented in Table 4.7.

Table 4.7: Definition of cases a-p with altered combinations between materials and main fibre orientation for both top and bottom face and core. The parentheses clarify which mechanical properties, presented in Table 4.7, are used for each part. Note that the geometric dimensions for cross-section 4 are still used in the models, so the top face has a thickness of 38.4 mm and the bottom face a thickness of 17.2 mm idenpendent of material combination.

Case	Bottom face	Core (12 mm)	Top face
a	⊥ Birch plywood (18 mm)	⊥ Birch plywood	⊥ Birch plywood (35 mm)
b	// Birch plywood (18 mm)	⊥ Birch plywood	// Birch plywood (35 mm)
c	// Birch plywood (18 mm)	// Birch plywood	// Birch plywood (35 mm)
d	⊥ Birch plywood (18 mm)	// Birch plywood	⊥ Birch plywood (35 mm)
e	⊥ Conifer plywood (18 mm)	⊥ Conifer plywood	⊥ Conifer plywood (30 mm)
f	// Conifer plywood (18 mm)	⊥ Conifer plywood	// Conifer plywood (30 mm)
g	// Conifer plywood (18 mm)	// Conifer plywood	// Conifer plywood (30 mm)
h	⊥ Conifer plywood (18 mm)	// Conifer plywood	⊥ Conifer plywood (30 mm)
i	⊥ Kerto-Q (21-24 mm)	⊥ Birch plywood	⊥ Kerto-Q (27-69 mm)
j	// Kerto-Q (21-24 mm)	⊥ Birch plywood	// Kerto-Q (27-69 mm)
k	// Kerto-Q (21-24 mm)	// Birch plywood	// Kerto-Q (27-69 mm)
l	⊥ Kerto-Q (21-24 mm)	// Birch plywood	⊥ Kerto-Q (27-69 mm)
m	⊥ Kerto-Q (21-24 mm)	⊥ Conifer plywood	⊥ Kerto-Q (27-69 mm)
n	// Kerto-Q (21-24 mm)	⊥ Conifer plywood	// Kerto-Q (27-69 mm)
o	// Kerto-Q (21-24 mm)	// Conifer plywood	// Kerto-Q (27-69 mm)
p	⊥ Kerto-Q (21-24 mm)	// Conifer plywood	⊥ Kerto-Q (27-69 mm)

Result of material and main fibre orientation

The results from the material and main fibre orientation are presented in Figure 4.20-4.22 for plate 1:1, 2:1 and 1:2.

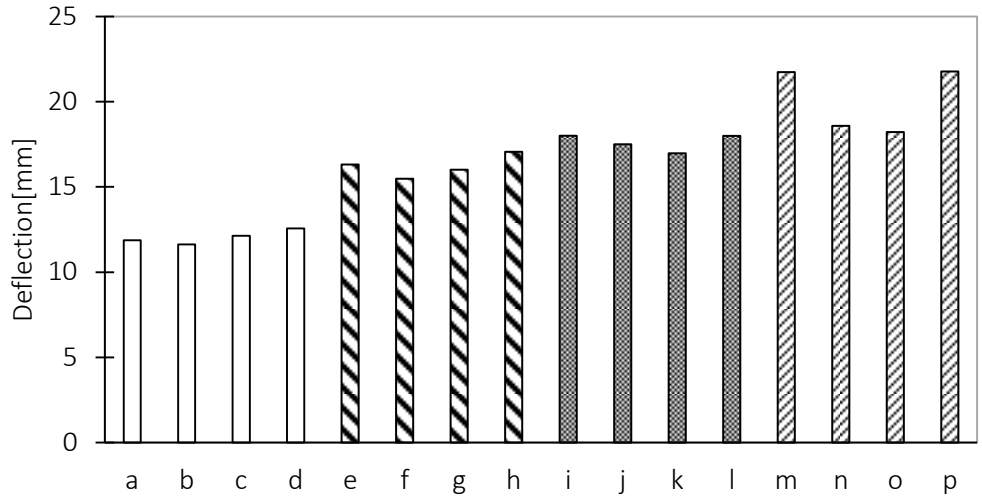

Figure 4.20: The deflection for case a-p for plate 1:1 where case b shows to yield the lowest deflection.

Plate 1:1 has lowest deflection, as Figure 4.17 illustrates, when the birch plywood is placed with fibres as case *b*. Plate 1:1 has largest deflection when Kerto-Q is placed perpendicular to corrugation in the faces and conifer plywood is used in the core. Kerto-Q has higher difference between E_1 and E_2 compared to conifer and birch plywood which explains the larger difference between the deflections when the fibres are placed parallel to corrugation compared to perpendicular to corrugation.

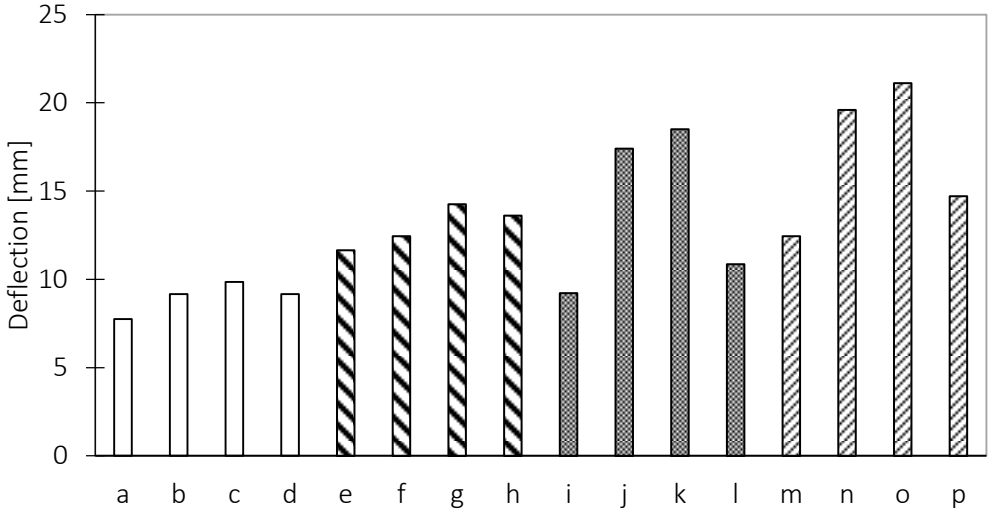

Figure 4.21: The deflection for case a-p for the plate 2:1 where case a shows to yield the lowest deflection.

Plate 2:1 has lowest deflection, as Figure 4.19 illustrates, for case *a*, when the main fibre direction of birch plywood is placed perpendicular to corrugation. The plate also has low deflection when the fibres are placed as in case *i*, with Kerto-Q perpendicular to corrugation. The plate has highest deflection when the fibres of Kerto-Q are placed as case *o*, parallel corrugation. The result indicates that plate 2:1 performs better when the stiff material direction of both core and faces is positioned perpendicular to the corrugation.

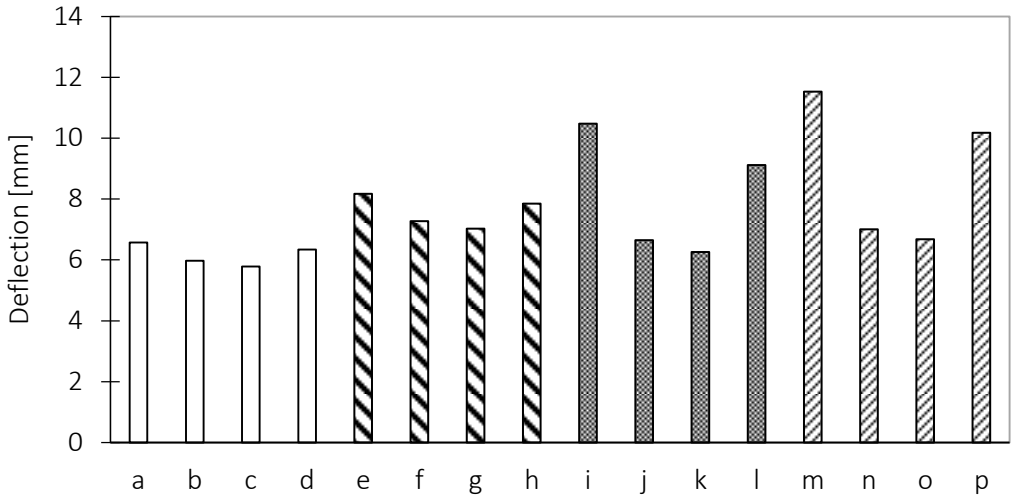

Figure 4.22: The deflection for case a-p for plate 1:2 where case c shows to yield lowest deflection.

Plate 1:2 has lowest deflection as Figure 4.18 illustrates when the main fibres are placed as case *c*, where all fibres are placed parallel to corrugation. The deflection is low for case *b* and also for case *k* where Kerto-Q is placed parallel to corrugation. The result indicates that plate 1:2 performs better when the stiff material direction of both core and faces is positioned parallel to corrugation.

The results for plate 1:1, 2:1 and 1:2 indicate that birch plywood has the best mechanical properties over conifer plywood and Kerto-Q for all three plates. The main fibre direction of the core does not influence the stiffness as much as the main fibre direction of the faces. In Chapter 2.4.4, literature indicates that it is beneficial to place the main fibre direction of the corrugated core perpendicular to corrugation due to manufacturing. This should therefore be the essential parameter. The placement of the main fibre direction of the faces should according to the analysis always be positioned along the short span. How to place the main fibres in the faces are more important for more anisotropic materials like Kerto-Q since the stiffness vary to a greater extent in different directions than for plywood material.

When comparing the result for plate 1:2 with 2:1, plate 1:2 has less deflection for all cases. It can be said that a higher performance is reached when positioning the parallel direction of the corrugation along the short span for the materials investigated here.

4.2.2 Influence of four edges support

In order to investigate the need for supports on four edges, an analysis is performed where the plates are only supported on two edges. Plate 1:1, 2:1 and 1:2 with cross-section 4 are investigated in Abaqus/CAE. The supports and the fibres are placed in a beneficial way for the plates supported on two edges. The supports are placed along the long edges for plate 1:2 and 2:1. For the square plate the supports are placed on the edges perpendicular to the corrugation. Conifer plywood is used as material in the analysis where the main fibre direction for both faces and core is oriented perpendicular to the supporting edge.

The maximum deflection of the plates supported on two edges is presented in Figure 4.23. The figure also contains the deflection for the corresponding plates with the same cross-section and material properties supported on four edges.

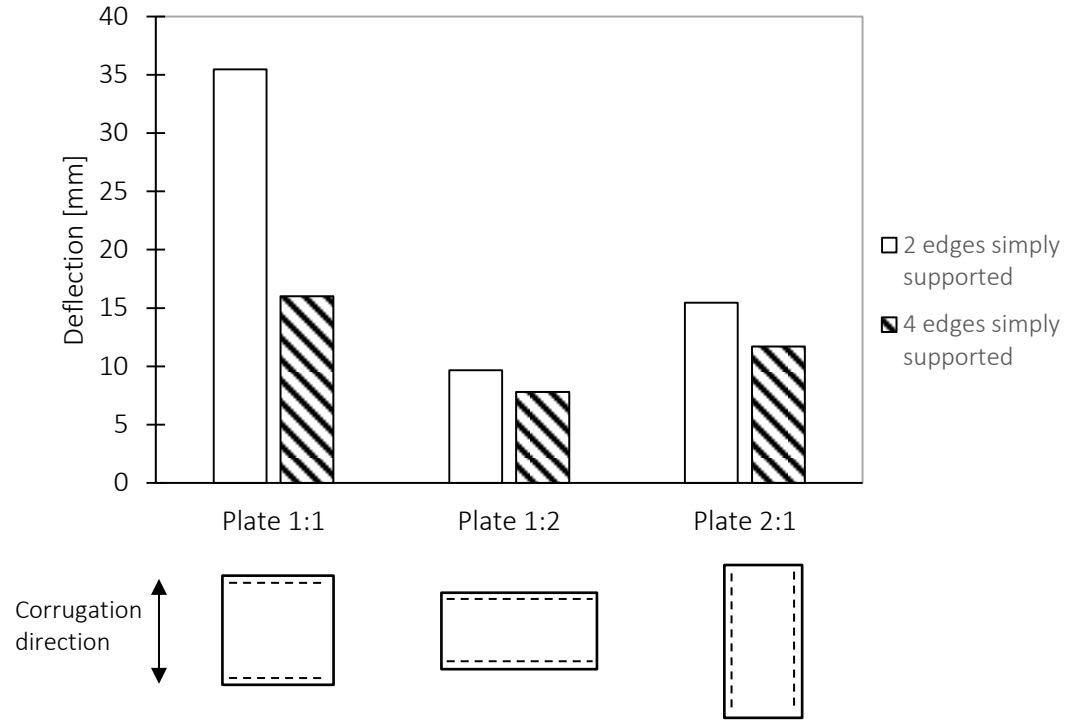

Figure 4.23: The white columns represent the deflection of the plates on two edges support while the patterned columns represent the deflection of the plates on four edges support. The corrugation direction for each plate is visualised in the figures below the graph.

It can be seen in Figure 4.23 that the influence of four edges support is dependent on the aspect ratio. For plate 1:1 the maximum deflection is more than doubled when only supported on two edges. For plate 1:2 and 2:1 the difference in deflection is small, especially for plate 1:2. The result indicates the benefits of supports on four edges for a square plate since the two directional stiffness of the plate will be used more efficiently.

4.2.3 Influence of core configuration

As mentioned in Chapter 2.4.2, literature indicates that the out-of-plane properties of the sandwich plate are better with a honeycomb core than a corrugated core. Therefore a comparable honeycomb sandwich plate is modelled in Abaqus/CAE and the deflection is obtained in order to get a picture of the performance of a honeycomb core in serviceability limit state. The honeycomb sandwich is compared to plate 1:1 with cross-section 4. The dimension of the plate is illustrated in Figure 4.24. It will be given the same top and bottom faces, same height of the core and same material volume. The total material volume for plate 1:1 with cross-section 4 is 7.628 m^3.

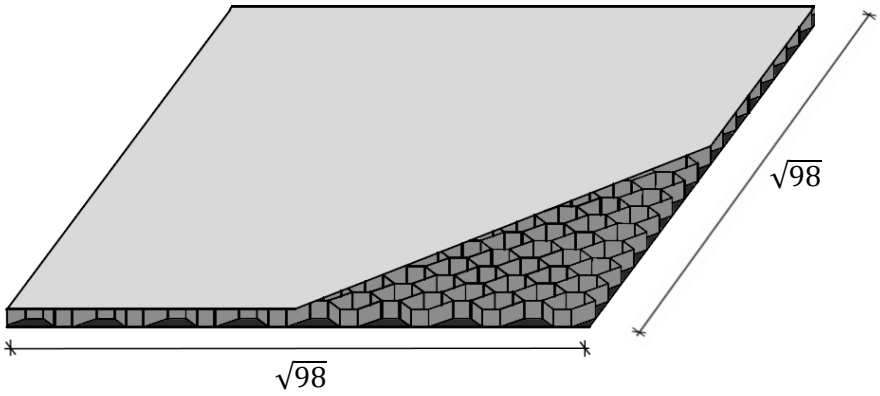

Figure 4.24: Illustration of a plate with honeycomb core, aspect ratio 1:1 and same area as plate 1:1.

Shape of honeycomb

The honeycomb is assumed to be made of corrugated parts glued to each other. As mentioned in Chapter 2.4.2 most honeycombs have hexagonal shapes. Therefore a hexagonal-similar shape is chosen for the honeycomb here. A hexagon has a corrugation angle equal to 60° and the straight sides, f_c and l_α, should be equal to each other. The notations are visualised in Figure 4.25.

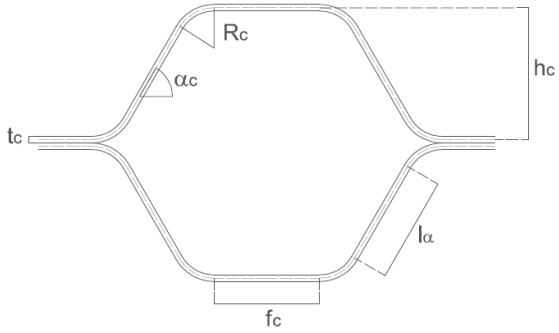

Figure 4.25: Notations used for the dimensions of the honeycomb core.

A Mathcad file is written where a cross-section with dimensions fulfilling the requirements, regarding hexagon shape and material volume, is generated (see Appendix E). Same as for the corrugated core t_c should be equal or larger than 6.5 mm and R_c should be equal or larger than $6t_c$. A local bending constrain, similar as for the corrugation, is also implemented. The generated geometry is stated in Table 4.14. Honeycomb height, h_h, refers to the height of the core in z-direction (same as h_c plus t_c for the corrugated core). Note that the honeycomb cross-section is not structurally optimised as the corrugated core, it is just a honeycomb fulfilling the geometric and material volume constrains and the local bending constrain.

Table 4.8: Dimensions of the honeycomb sandwich floor.

h_c [mm]	130.1
t_c [mm]	6.5
$t_{f.top}$ [mm]	38.4
$t_{f.bot}$ [mm]	17.6
α_c [°]	60.0
f_c [mm]	104.3
R_c [mm]	39.8
h_h [mm]	354.4

In the middle of the honeycomb cells, the thickness t_c will be double due to manufacturing, as illustrated in Figure 4.26. The double thickness is not included in the FE-model. The honeycomb core is modelled as a single shell therefore the thickness is preferably constant in the whole cross-section. The influence on the result by neglecting the double thickness is assumed to be small.

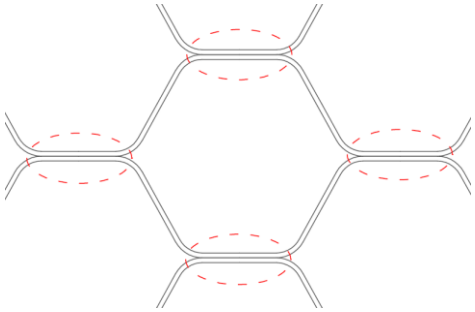

Figure 4.26: The red dashed lines indicate the double thickness not included in the FE-model. It is modelled as t_c instead of $2t_c$.

The FE-model is given full interaction between core and faces. The honeycomb sandwich plate is loaded with 2 kN/m^2 imposed load, self-weight and 50 kg/m^2 additional dead weight, same as for the corrugated plates.

The honeycomb sandwich is modelled with birch plywood. The core is given the properties for birch plywood 6.5 mm. The top face is modelled with birch plywood 35 mm properties and the bottom face with 18 mm properties. The main fibres of the honeycomb core can either be placed parallel to the corrugation or perpendicular to the corrugation (in global z-direction). The main fibres of the faces can be positioned in global x-direction or global y-directions. All combinations are tried in Abaqus/CAE.

Result from comparison with honeycomb

The obtained deflections from the FE-model of the honeycomb sandwich with main fibres positioned in different directions are presented in Table 4.14.

Table 4.9: Deflection of honeycomb sandwich plate when the main fibres are oriented in different directions.

	Face fibres: // corrugation	Face fibres: ⊥ corrugation
Core fibres: //	13.81 mm	14.75 mm
Core fibres: ⊥	14.45 mm	15.65 mm

The honeycomb with best performance in Table 4.14 is compared with the corrugated birch sandwich that had best performance in Chapter 4.2.1, referred to as case *b* for plate 1:1. The result is presented in Table 4.10.

Table 4.10: Comparison between corrugated core sandwich and honeycomb core sandwich. Both sandwiches have birch plywood as material and the main fibre direction of the core and faces are oriented in best way for each case.

	Corrugated core	Honeycomb core
Deflection [mm]	11.6	13.8

The results are close to each other but the sandwich plate with corrugated core has slightly lower deflection than the sandwich plate with honeycomb core. The geometry of the honeycomb core is not structurally optimised for out-of-plane behaviour in the same way as the corrugated core which could explain the difference in performance. However it can be said that the honeycomb core is not a "superior" structure than the corrugated core with regard to deflection in SLS.

4.3 Ultimate limit state (ULS) analysis of sandwich plates

The sandwich plate is checked in ULS regarding principal stresses and buckling. These controls are performed to give an indication if the plate is close to failure in ULS. The same loads are applied as in Chapter 4.1 and 4.2 but the ULS load combination is used in the analysis. The same material combination is used for all ULS calculations where the faces have conifer plywood with main fibre direction parallel to corrugation and the core has conifer plywood with main fibre direction perpendicular to corrugation. Conifer is chosen for the ULS analysis as it has lower strength properties than birch plywood.

4.3.1 Principal stresses

The principal stresses are checked with the Norris criteria presented in Equation (3.42). The stresses are obtained with FE-models in Abaqus/CAE. What is considered to be the most critical element is identified by studying where the highest Von Mises stress is located; edge elements are neglected as singularity can occur there. The principal stresses are checked both with the imposed uniformly distributed load and the imposed concentrated load. The concentrated load is placed in the middle of l_c.

Principal stresses due to uniformly distributed load
For the uniformly distributed load, checks are performed for plate 1:1, 1:2 and 2:1 with cross-section 4. Plate 1:1 is also checked with cross-section 1 in order to see if the curved shape of the corrugation corners has an influence on the ULS stresses. The critical stress locations are for all cases located in the core close to the middle part of the edge which is parallel to the corrugation. The critical stress positions are visualized in Figure 4.27-4.30. The obtained stresses are presented in Table 4.11.

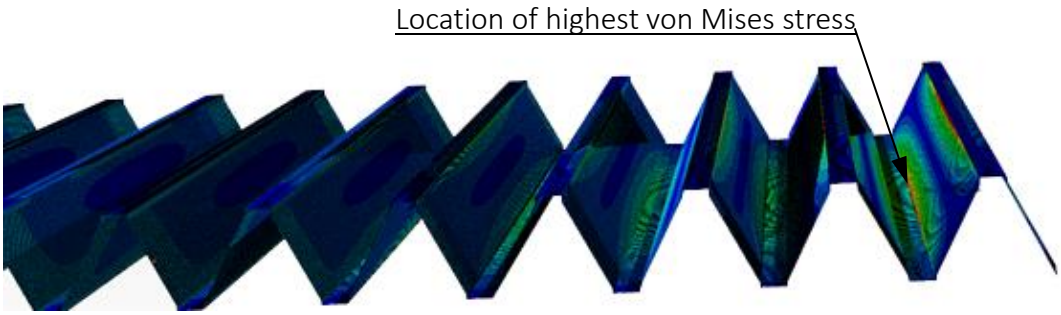

Figure 4.27: Most stressed region for plate 1:1 with cross section 1.

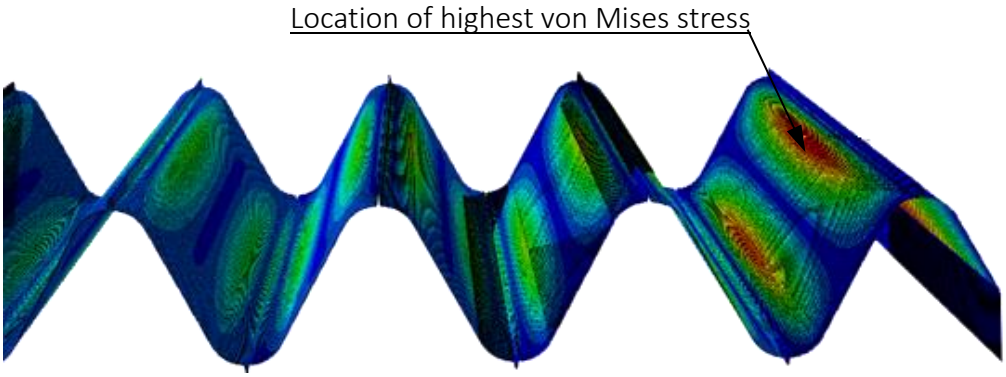

Figure 4.28: Most stressed region for plate 1:1 with cross section 4.

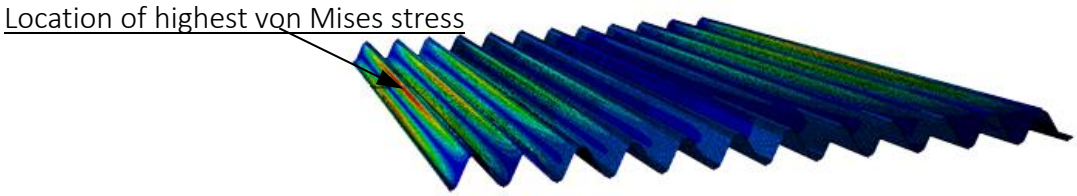

Figure 4.29: Most stressed region for plate 2:1 with cross section 4.

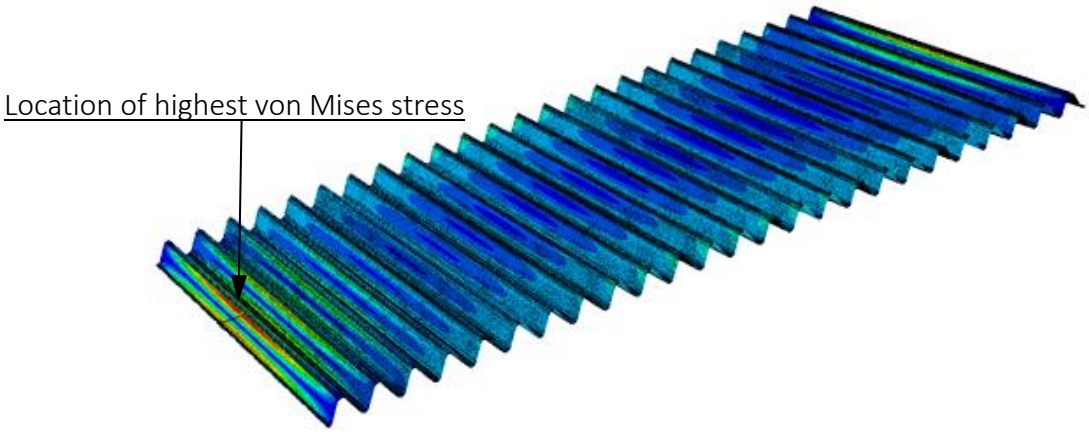

Figure 4.30: Most stressed region for plate 1:2 with cross section 4.

Table 4.11: Normal and shear stresses for plate 1:1, 2:1 and 1:2 when loaded with a uniformly distributed load in ULS. Abaqus/CAE is used to calculate the stresses. The stresses are obtained in the element with highest Von Mises stress.

	Cross-section 1	Cross-section 4		
	Plate 1:1	Plate 1:1	Plate 2:1	Plate 1:2
σ_{11} [MPa]	-5.533	6.910	-7.64	-4.147
σ_{22} [MPa]	-1.523	2.177	-2.453	-1.368
σ_{33} [MPa]	$-1.454 \cdot 10^{-12}$	$7.443 \cdot 10^{-12}$	0	$-5.215 \cdot 10^{-14}$
τ_{12} [MPa]	$6.169 \cdot 10^{-4}$	$2.393 \cdot 10^{-5}$	$4.245 \cdot 10^{-4}$	$1.092 \cdot 10^{-3}$
τ_{13} [MPa]	0	0	0	0
τ_{23} [MPa]	0	0	0	0

As τ_{13} and τ_{23} are equal to zero and σ_{33} is almost equal to zero for all cases, only the first part of Equation (3.42) is used. The characteristic strength of conifer plywood is divided with the material partial factor, for plywood it is 1.20, and multiplied with the modification factor, k_{mod}, which is set to 0.8. As the critical stresses occur in the corrugation, the strength values for conifer plywood 12 mm are used.

$$f_{c.0.d} = k_{mod}\frac{f_{c.0.k}}{\gamma_M} = 0.8\frac{19.2\ MPa}{1.2} = 12.8\ MPa \tag{4.5}$$

$$f_{c.90.d} = k_{mod}\frac{f_{c.90.k}}{\gamma_M} = 0.8\frac{16.8\ MPa}{1.2} = 11.2\ MPa \tag{4.6}$$

$$f_{t.0.d} = k_{mod}\frac{f_{t.0.k}}{\gamma_M} = 0.8\frac{14.9\ MPa}{1.2} = 9.9\ MPa \tag{4.7}$$

$$f_{t.90.d} = k_{mod}\frac{f_{t.90.k}}{\gamma_M} = 0.8\frac{13.1\ MPa}{1.2} = 8.7\ MPa \tag{4.8}$$

$$f_{v.d} = k_{mod}\frac{f_{v.d}}{\gamma_M} = 0.8\frac{7\ MPa}{1.2} = 4.6\ MPa \tag{4.9}$$

When implementing the design strength and excluding the zero values in the Norris failure criterion it is stated as:

$$\left(\frac{\sigma_{11}}{f_{0.d}}\right)^2 + \left(\frac{\sigma_{22}}{f_{90.d}}\right)^2 + \left(\frac{\tau_{12}}{f_{v.d}}\right)^2 - \left(\frac{\sigma_{11}}{f_{0.d}}\right)\left(\frac{\sigma_{22}}{f_{90.d}}\right) = 1 \tag{4.10}$$

The strength values for compression or tension are used based on the sign of the stress. The 3D state of stress for the different plates and cross-sections are presented in Table 4.12.

Table 4.12: Performance of plate 1:1, 2:1 and 1:2 with the Norris criterion. A value of one indicates failure.

	Cross-section 1 Plate 1:1	Cross-section 4 Plate 1:1	Plate 2:1	Plate 1:2
Norris criterion	0.147	0.375	0.274	0.080

As can be seen in Table 4.10 none of the plates are close to failure. The principal stresses are higher in plate 1:1 with curved corners (cross-section 4) than with sharp corners (cross-section 1).

Principal stresses due to concentrated load

Plate 1:2 with cross-section 4 is analysed when subjected to a concentrated load in ULS. The Norris criterion is used as stress-based failure criterion. The design load is equal to 3 kN which is spread on a surface of 50 x 50 mm^2 as recommended in Eurocode 1. The load is positioned in a corrugation cell. Only one plate is checked since the behaviour will be the same for all plates as l_c does not differ. The plate is also subjected to self-weight and the added dead weight. The highest Von Mises stress occurs in the top plate under the concentrated load, this is visualised in Figure 4.31. The obtained stresses from the analysis are presented in Table 4.13.

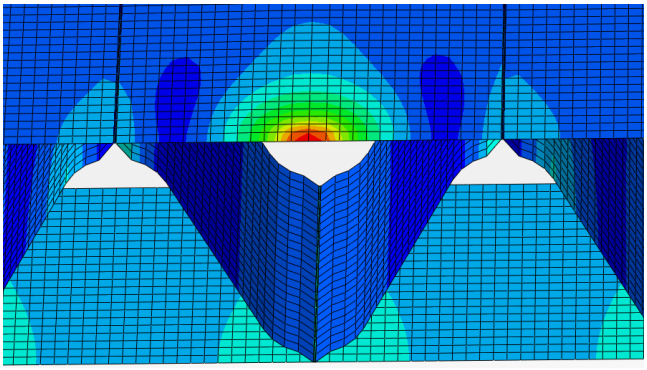

Figure 4.31: The contour plot indicates Von Mises stress. Note that the figure is cropped and only the region with highest stress is included in the figure.

Table 4.13: Normal and shear stresses for plate 1:2 when loaded with a concentrated load in ULS. Abaqus/CAE is used to calculate the stresses. The stresses are obtained in the element with highest Von Mises stress.

	Cross-section 4 Plate 1:2
σ_{11} [MPa]	3.693
σ_{22} [MPa]	3.836
σ_{33} [MPa]	0
τ_{12} [MPa]	0.043
τ_{13} [MPa]	0
τ_{23} [MPa]	0

As τ_{13}, τ_{23} and σ_{33} are equal to zero, only the first part of Equation (3.42) is used. For the top plate, mechanical properties from plywood 30 mm are used. As can be seen in

Table 4.13 the element is in tension hence only the tension strength and shear strength are of interest. The design strength values are:

$$f_{t.0.d} = k_{mod}\frac{f_{t.0.k}}{\gamma_M} = 0.8\frac{14.4\ MPa}{1.2} = 9.6\ MPa \tag{4.11}$$

$$f_{t.90.d} = k_{mod}\frac{f_{t.90.k}}{\gamma_M} = 0.8\frac{13.6\ MPa}{1.2} = 9.0\ MPa \tag{4.12}$$

$$f_{v.d} = k_{mod}\frac{f_{v.d}}{\gamma_M} = 0.8\frac{7\ MPa}{1.2} = 4.6\ MPa \tag{4.13}$$

The Norris failure criterion is calculated to be 0.166 which indicates that the plate will not fail in ULS when subjected to the imposed concentrated load.

4.3.2 Buckling analysis

A linear buckling analysis is performed in Abaqus/CEA with the Lanczos eigensolver. The load factor λ and the buckling mode are obtained from the analysis. The buckling mode indicates where the plate will buckle. The load factor indicates the ratio between applied load and buckling load. The plate is loaded with a uniformly distributed imposed load, self-weight and extra dead weight, same as for the principal stress analysis. The analysis is performed for plate 1:1 with cross-section class 4. Conifer plywood is used as material with main fibre direction parallel to corrugation in faces and perpendicular to corrugation in the core. The three first mode shapes are visualised in Figure 4.32 and 4.33 and the corresponding load factors are presented in Table 4.14.

Table 4.14: The three buckling modes for plate 1:1.

	Plate 1:1
λ – mode 1	19.533
λ – mode 2	20.148
λ – mode 3	20.170

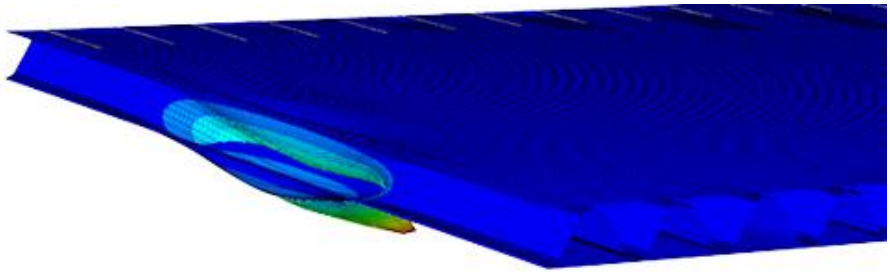

Figure 4.32: Illustration of the first buckling mode. Buckling occur in the corrugation close to the edge

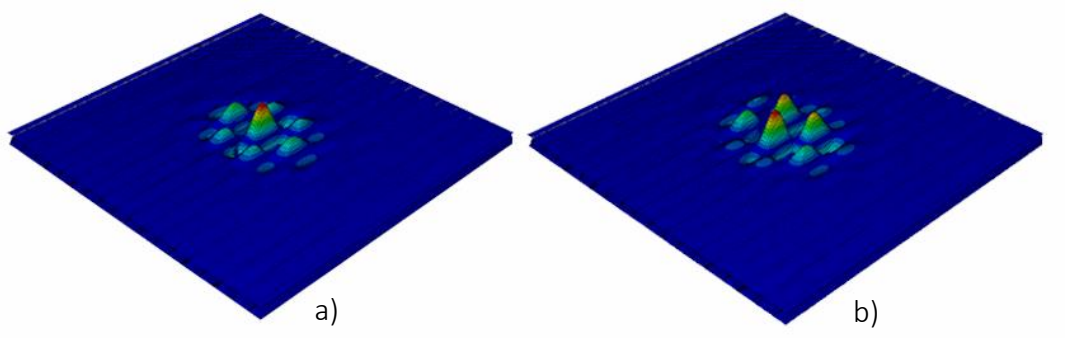

Figure 4.33: Illustration of a) the second buckling mode and b) the third buckling mode, both occurring in the top face.

According to the linear buckling analysis, the load can be almost 20 times as high before the plate will buckle. In reality material imperfections will influence the buckling behaviour however as the linear buckling load is so much higher than the acting load the plate can be regarded as safe from buckling.

5 Case studies

This chapter treats two case studies for two different situations. The first case study aims to illustrate the performance of the sandwich timber floor in comparison to an existing timber floor system on the market. This first case study treats loads for a normal situation in a residential building.

The second case study aims to illustrate the performance of the sandwich timber floor for a different situation where the loads are considerably higher. The added dead weight due to installations and extra material give a permanent load of 2 kN/m^2 and the distributed imposed load acting on the floor is 5 kN/ m^2. This rare situation challenges the capacity of the timber sandwich floor. Existing timber floors solutions on the Swedish market will likely have problems to fulfil the SLS-requirements for this situation.

The outcome from these case studies will help to increase the understanding of the performance in a common timber floor case and in a more rare case where there is prospect to gain market in a new area for timber floors.

Following assumptions are made regarding the sandwich floors in the case studies:

- The floor is regarded as one single member therefore joints and connections are neglected. In reality the floor would likely be produced in several members due to transportation and manufacturing restrains.
- The supporting edges are assumed to be stiff and do not contribute to extra deflection or lower eigenfrequency of the floor.
- The face-core connection is regarded as rigid and has higher shear strength than the material. The connection has full interaction between face and core.

5.1 Case study 1 – comparison with existing floor system

A case study is performed where the sandwich floor is compared with an existing timber floor system.

5.1.1 Introduction to case study 1

The sandwich floor system with a corrugated plywood core is compared with one of Martinsons floor systems, *MBK-12-02*, which is introduced in Chapter 2.2.3. It spans 8.5 m and has a width of 1.202 m per prefabricated member. Martinsons floor system is supported on two edges and utilizes one way action while the sandwich floor system uses two-way action i.e. supported on four edges. To compare the sandwich floor with the existing floor system a span of 8.5 m and width of 9.616 m (8x1.202 m^2) is considered which is illustrated in Figure 5.1. The dimensions are regarded as realistic for a room surrounded with load-bearing walls and it is logic to use 8.5 m long floor elements if the width is larger than the span i.e. the load is carried in the short span.

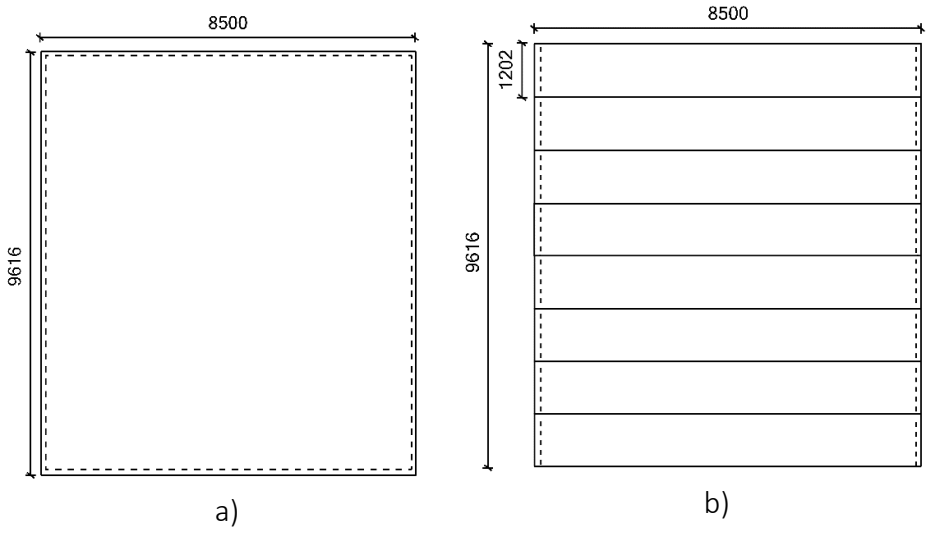

Figure 5.1: Illustration of the length and width of a) the sandwich floor system supported on four edges and b) the Martinsons floor system supported on two edges.

The Martinsons *MBK 12-02* floor has a structural height of 410 mm. The floor system is illustrated in Figure 5.2 where the grey part illustrates the structural part. Only the structural part is regarded in the case study. The performance of MBK 12-02 is presented in Table 5.1. The numbers are collected from the information sheet of the floor which can be found in Appendix F.

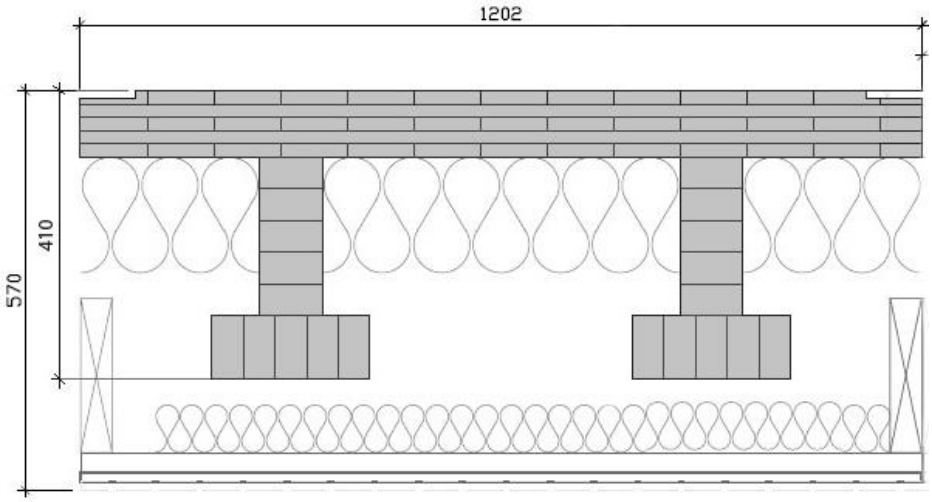

Figure 5.2: Illustation of the Martinsons MBK 12-02 system with a structural height of 410 mm and a width of 1202 mm

Table 5.1: Performance of MBK 12-02 in the case study. The frequency is for the self-weight of the structure and 50 kg/m^2 added dead weight. The material volume is specified for the 8.5 x 9.616 m^2 case.

w_{1kN} [mm]	0.45
f_1 [Hz]	9.2
Structural height [mm]	410
Material volume of floor [m^3]	13.273

The Mathcad optimisation code is used to obtain a material volume optimised and height optimised cross-section. It is presented in Appendix B how the Mathcad code is rewritten to perform height optimisations. The optimisation is performed with similar constrains as before but the structural height is limited to 410 mm and the material volume to 13.273 m^3 (same as MBK 12-02). The lowest eigenfrequency allowed is changed from 8 Hz to 9.2 Hz to be comparable with MBK 12-02. The corrugation angle is restricted to the range 40° to 70°. The influence on the structural behaviour of other angles is regarded as unpredictable, as it is far from the geometry in the behaviour analysis in Chapter 4.

5.1.2 Choice of direction of corrugation and material

The behaviour study in Chapter 4.2.1 indicates that it is more beneficial to place the corrugation along the short span and it is therefore done in this case study (see Figure 5.3). Birch plywood will be used for both faces and core as it is the best material choice for plate 1:2 and 1:1 according to Chapter 4.2.1. The main fibre direction of the faces will be placed parallel to the corrugation as it yields highest performance. Plate 1:1 has higher performance when the main fibres of the core are placed perpendicular to the corrugation while plate 1:2 has the best performance when the main fibre direction of the core is parallel to the corrugation. In this case the core fibres will be placed perpendicular to the corrugation, as the aspect ratio is closer to 1:1 than 1:2.

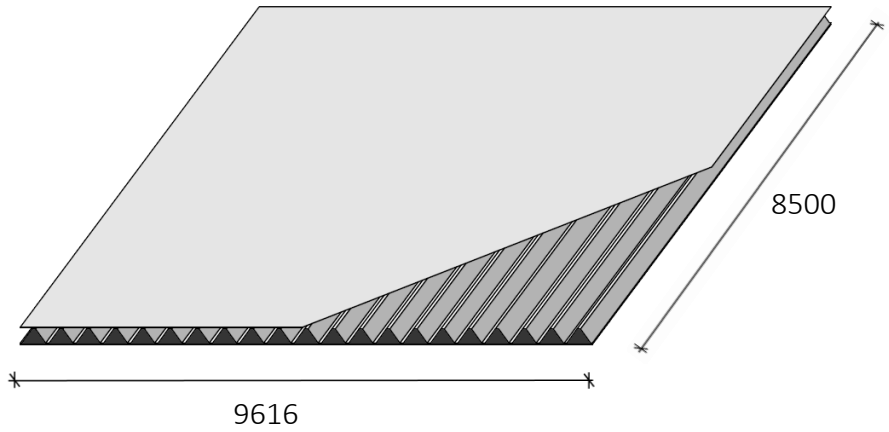

Figure 5.3: Positioning of the corrugation of the floor system (dimensions in mm).

5.1.3 Generating cross-sections for case study 1

The geometrical definitions of the sandwich floor cross-section are presented in Figure 5.4.

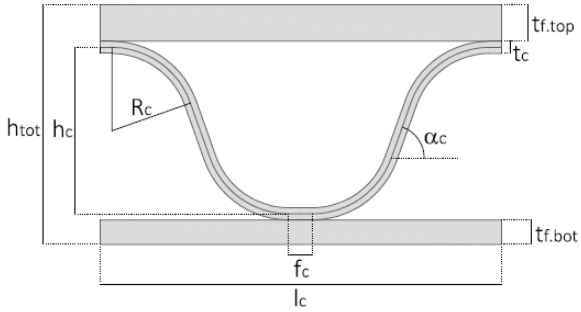

Figure 5.4: Geometrical definitions and notations of the sandwich floor.

The dimensions obtained when performing the material volume and height optimisations are presented in Table 3.2 and visualised in Figure 5.5.

Table 5.2: Dimension, material volume and material volume ratio of height and material volume optimised sandwich floors.

	Material volume optimised	Height optimised
h_c [mm]	353.9	206.3
t_c [mm]	8.7	17.2
$t_{f.top}$ [mm]	32.9	46.8
$t_{f.bot}$ [mm]	14.5	46.8
α_c [°]	58.1	70.0
f_c [mm]	30.0	30.0
R_c [mm]	52.4	103.1
l_c [mm]	617.1	499.0
h_{tot} [mm]	410.0	317.1
Material volume [m^3]	5.017	9.669
Material volume ratio to MBK 12-02 [-]	0.378	0.728

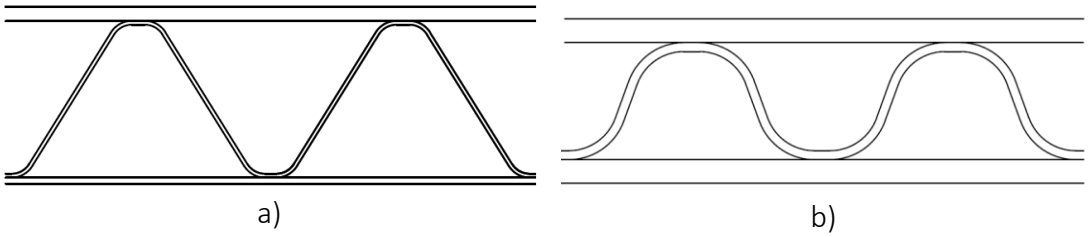

Figure 5.5: Illustration of cross-section for a) material volume optimised and b) height optimised sandwich floor in relation to each other.

The limiting criterion when optimising with regard to material volume is first eigenfrequency, Equation (2.1), and local bending, Equation (3.54). For the height optimisation the limiting criteria are first eigenfrequency and the lower thin face criteria, Equation (3.1).

In Figure 5.6 the material volume of the sandwich floor is plotted as a function of the structural height, where a material volume optimisation has been performed for each height. The point most to the left is the height optimised floor and the point most to

the right is the material volume optimised floor. The structural behaviour of a sandwich plate is clearly seen in the figure, when separating the faces more by increasing the structural height, the structure becomes more efficient and lower material volume is needed. In order to decrease the structural height (from the material volume optimised point) more material needs to be added.

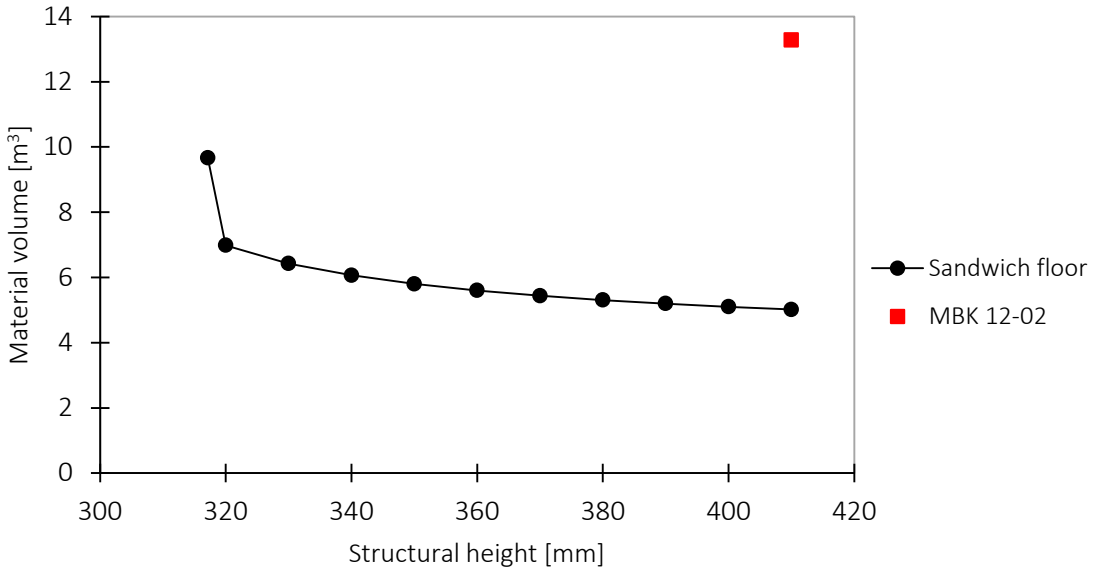

Figure 5.6: Illustration of how the material volume of the sandwich floor changes with the structural height. The red square indicates the material volume and structural height for MBK 12-02.

It can be stated that the choice of dimensions of the cross-section is dependent of interest, it should be evaluated what is most prioritised, minimum structural height or material volume. In this case study structural height is of interest and the performance of the height optimised cross-section will be verified with a FE-model. The dimensions of the height optimised floor is somewhat modified, the thickness of top and bottom plate and thickness of corrugation are adjusted to existing dimensions of birch plywood sheets. The other cross-section values are rounded down to whole numbers. The dimensions can be rounded down as extra stiffness is added to the structure when the main fibre direction and full interaction are included in the FE-model, as demonstrated in Chapter 4.1.4 and 4.2.1. In Table 5.3 the chosen cross-section dimensions are presented.

Table 5.3: Dimension, material volume and material volume ratio of sandwich floor with modified dimensions.

h_c [mm]	200
t_c [mm]	15
$t_{f.top}$ [mm]	35
$t_{f.bot}$ [mm]	35
α_c [°]	70
f_c [mm]	30
R_c [mm]	90
h_{tot} [mm]	285
Material volume [m^3]	7.526
Material volume ratio to MBK 12-02 [-]	0.567

5.1.4 Result from case study 1

The 1 kN concentrated load deflection and the first eigenfrequency are verified with a FE-model in Abaqus/CAE. The model is created in the same way as the models in Chapter 4. For the deflection analysis the floor is loaded with 1 kN on a surface of 50x50 mm^2. The eigenfrequency analysis is performed with the self-weight and extra dead weight of 50 kg/m^2. Birch plywood with thickness 35 mm is used for both top and bottom faces and birch plywood with thickness 15 mm is used for the corrugation. The result obtained from the FE-model is presented in Table 5.4 as well as the performance of MBK 12-02.

Table 5.4: Performance of MBK 12-02 and the sandwich floor in the case study.

	MBK 12-02	Sandwich floor
First eigenfrequency [Hz]	9.2	9.5
w_{1kN} [mm]	0.45	0.18
$\frac{f_1}{{w_{1kN}}^{0.44}}$	13.1	20.2
Structural height [mm]	410	285
Material volume [m^3]	13.3	7.5

As can be seen in Table 5.4 the sandwich floor has a structural height 125 mm lower than MBK 12-02. It uses a material volume of 56.7 % of the MBK 12-02 floor. Note that the MBK 12-02 is an open floor system which could be an advantage regarding positioning of technical installations. The criterion in Equation (2.5) is fulfilled for the sandwich floor but not fullfilled for MBK 12-02. The deflection of the sandwich floor is lower and the frequency/deflection-ratio and the first eigenfrequency is higher compared to MBK 12-02 and the recommended criteria in Chapter 2.5.3. Hence further optimisation can be done on the sandwich floor in order to decrease structural height and/or material volume.

5.2 Case study 2 – Landvetter airport

A new floor system will be built in the domestic terminal at Landvetter airport where the space during construction is limited. The activity at the airport should be able to continue during the construction time and it is therefore preferable if the floor system is easy and fast to erect. The visitors should not feel any difference when walking from the existing concrete floor on to the new floor. Therefore the new floor system should not be prone to vibrations. The new floor system will be placed as Figure 5.7b illustrates and one segment has a long span of 16 m and main beams are placed on columns with a spacing of 9.6 m.

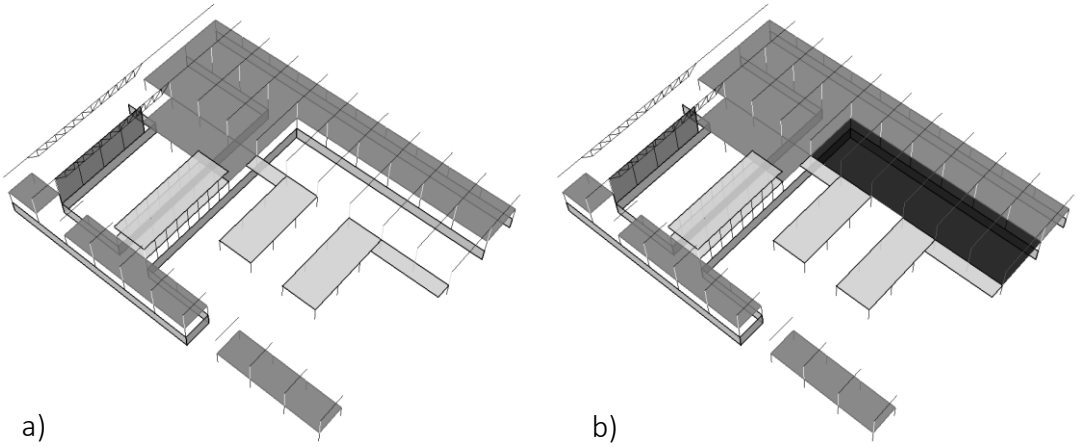

Figure 5.7: a) Illustrates the existing area of the domestic terminal and the darker part in figure b) illustrates where the new floor system should be placed.

The floor system should have a maximum structural height of 1.2 m including underlying beams. The uniformly distributed imposed load acting on the floor system is 5 kN/m^2. The weight due to installations is 1 kN/m^2 and extra dead weight from material is also 1 kN/m^2.

Ramböll was asked to investigate what type of floor system that could be used for this case. Ramböll proposed four different alternatives of floor systems with a solution of beam systems for each proposal (Johansson N. , 2016).

Alternative 1: Hollow core slab (HD/F) 120/27 that has a self-weight of 4.6 kN/m^2 and will span 9.6 m. This alternative will be difficult to assemble on site since one element is 9.6 m and weights approximately 5.5 tons. The steel beams for this alternative will span 16 m and have a height of 1000 mm, a flange width of 400 mm, a flange thickness of 35 mm and web thickness of 15 mm. These dimensions of the beam will result in a self-weight of 330 kg/m.

Alternative 2: Plate cast in situ on a trapezoidal steel plate placed on secondary beams, which are placed 2 m from each other. This alternative gives a heavier floor system than Alternative 1 but is easier to assemble on site. The weight of the floor system could be adjusted by adding foam inside the element.

Alternative 3: Concrete plate cast in situ in the same manner as Alternative 2. The difference between Alternative 2 and 3 is that Alternative 2 uses a steel plate while alternative 3 does not. However, this will make the cast in situ more complicated.

Alternative 4: This system uses glulam beams with a spacing of 1.2 m and a plate of CLT with a thickness of approximately 70 mm that is placed on top of the beams. The dimension of the beams will be about 165x1035 mm^2. The main problem with this light weighted alternative is the vibrations.

The main problem for this case is as mentioned that the structure should be easy to erect and therefore preferably be lightweight but at the same time it should be stiff enough to reach the vibration criteria. The lightweight alternative, Alternative 4, has most likely problems to reach the vibration criteria. The demands on the new floor system are high. A sandwich floor system made out of timber could be suitable for this case and is therefore investigated further.

5.2.1 Generating cross-sections for case study 2

The sandwich timber floor will be supported on four edges. Main beams with the length of 16 m and end beams with the length of 9.6 m are therefore needed. The floor system can either serve as one plate with the dimension of 16x9.6 m^2 or be divided into several parts by introducing secondary beams. Different possibilities are evaluated by generating different cross-sections with the Mathcad code. The floor systems should reach the SLS criteria for vibration presented in Equations (2.1), (2.4) and (2.5) and the deflection criteria $w_{inst}/500$. The material that is used in the Mathcad code is an average of birch plywood properties (similar as Mathcad isotropic). The imposed concentrated load is set to 5 kN. Imposed loads are usually 7 kN for this type of floors however the Mathcad code clearly underestimates the local bending strength of the sandwich structure, as shown in Chapter 4.3.1. The total material volume and the structural height of the alternative sandwich solutions are being compared with each other and visualised in Figure 5.8.

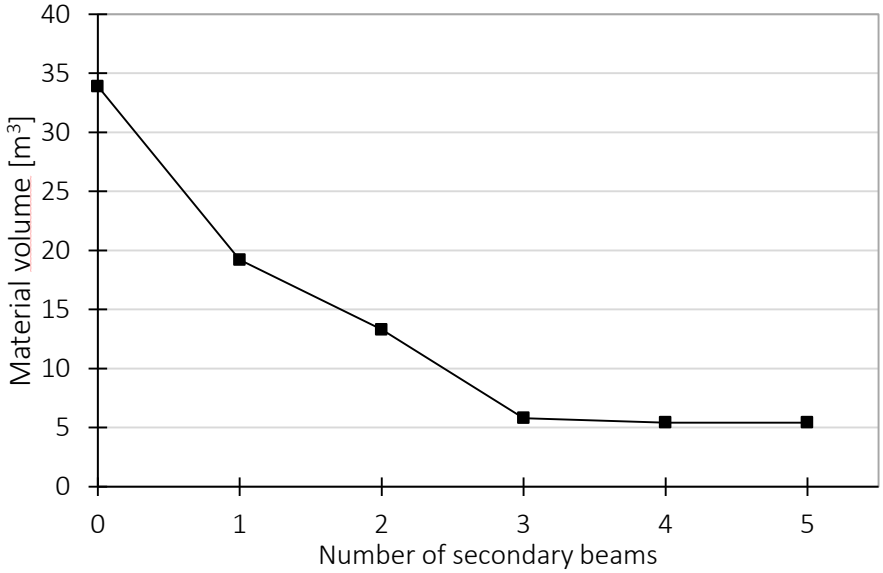

Figure 5.8: Illustration of the material volume as a function of number of secondary beam where zero secondary beams corresponds to one plate with dimensions 16 x

9.6 m^2, one secondary beam to two plates with dimension 8 x 9.6 m^2 and so on.

A low self-weight is considered as preferable since it will be easier to assemble at site and at the same time decrease the height of the main beams. The structural height of the floor should be low as it will be supported on at least two main beams and two end beams and need to fulfil the height requirement on 1.2 m including the height of the beams. But minimizing the number of secondary beams is also considered as desirable. Finding the best solution for this floor system is therefore evaluated with regard to these different aspects.

Concepts with zero, one and two secondary beams are further investigated. The dimensions of the concepts are 16x9.6 m^2, two times 8x9.6 m^2 and three times 5.33x9.6 m^2 and they are named concept 1, 2 and 3 respectively further on in the text. The sandwich floor is simply supported and not continuous over secondary beams. Figure 5.9 visualises the concepts with support conditions. Cross-sectional dimensions and material volume of the concepts are presented in Table 5.5.

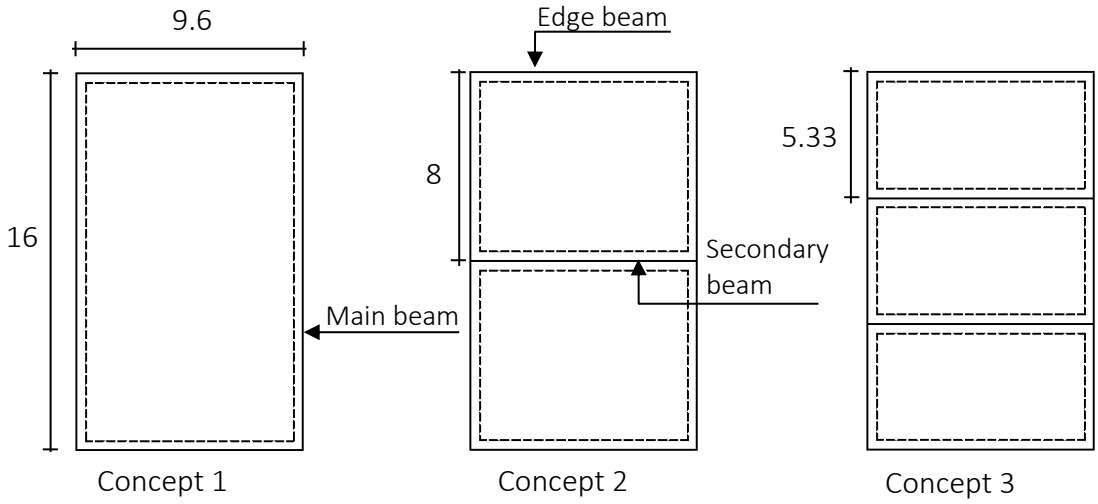

Figure 5.9: Visualisation of the dimensions (in m) and support conditions of concept 1, 2 and 3.

Table 5.5: The generated dimensions in the Mathcad code for each concept.

	Concept 1	Concept 2	Concept 3
h_c [mm]	404.4	272.3	210.0
t_c [mm]	33.7	22.7	10.3
$t_{f.top}$ [mm]	85.8	56.9	40.5
$t_{f.bot}$ [mm]	86.0	38.0	29.1
α_c [°]	70.0	54.0	70.0
f_c [mm]	30.0	30.0	30.0
R_c [mm]	202.3	136.2	62.0
h_{tot} [mm]	610	390	290
Material volume for one floor area [m^3]	33.9	9.6	4.4
Total material volume [m^3]	33.9	19.2	13.3

The generated values have to be modified to fit existing dimensions of plywood, Kerto-Q or CLT. The generated values in the Mathcad code are by experience an overestimation which enable a slightly decrease of the thicknesses to suit existing dimensions.

5.2.2 Result from case study 2

Each concept is modelled in Abaqus/CAE with the modified dimensions as Table 5.6 illustrates.

Table 5.6: The modified dimensions for each concept to suit existing dimensions.

	Concept 1	Concept 2	Concept 3
h_c [mm]	405	275	210
t_c [mm]	30	21	9
$t_{f.top}$ [mm]	80	50	40
$t_{f.bot}$ [mm]	80	40	27
α_c [°]	70	54	70
f_c [mm]	30	30	30
R_c [mm]	200	135	60
h_{tot} [mm]	595	386	286
Material volume for one floor part [m^3]	31.3	9.05	4.2
Total material volume [m^3]	31.3	18.1	12.6
Self-weight [kN/ m^2]	0.99	0.73	0.51

The core for each concept is made out of birch plywood with the main fibre orientation placed perpendicular to corrugation due to manufacturing benefits as stated in Chapter 2.1.2. The faces are made out of Kerto-Q for concept 1 and birch plywood for concept 2 and 3 where the main fibre orientation is placed parallel to corrugation for each case. The maximum standard thickness of Kerto-Q is 69 mm but according to Metsä (2016) other sizes are available on request. The cross-section for each concept is illustrated in Figure 5.10.

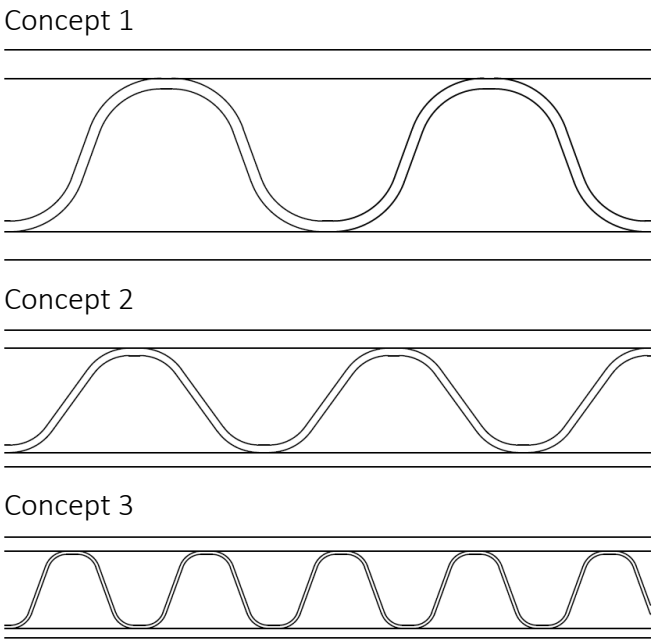

Figure 5.10: Illustration of the cross section for each concept in relation to each other.

The performance of each concept in serviceability limit and ultimate limit state are checked and presented in Table 5.7-5.9. $k_{c.90}$ is set to 1 for compression perpendicular to fibre direction.

Table 5.7: The performance and utilization ratio of concept 1.

Criterion	Performance	Limit	Utilization
	SLS		
$w_{inst} \leq L/500$	12.56 mm	19 mm	0.66
$f_1 > 8\ Hz$	8.75 Hz	8 Hz	0.91
$w_{1kN} < 1\ mm$	0.05 mm	1.00 mm	0.05
$\frac{f_1}{{w_{1kN}}^{0.44}} > 18.7$	32.52	18.7	0.58
	ULS		
Norris criterion	0.29	1.00	0.29
$\sigma_{t.0.d} \leq f_{t.0.d}$	9.15 MPa	25.66 MPa	0.36
$\sigma_{c.0.d} \leq f_{c.0.d}$	9.63 MPa	17.80 MPa	0.54
$\sigma_{t.90.d} \leq f_{t.90.d}$	3.84 MPa	24.34 MPa	0.16
$\sigma_{c.90.d} \leq f_{c.90.d}$	4.16 MPa	16.86 MPa	0.25
$\tau_{v.d} \leq f_{v.d}$	1.63 MPa	6.34 MPa	0.26

Table 5.8: The performance and utilization ratio of concept 2.

Criterion	Performance	Limit	Utilization
	SLS		
$w_{inst} \leq L/500$	13.59 mm	16.00 mm	0.85
$f_1 > 8\ Hz$	8.78 Hz	8 Hz	0.91
$w_{1kN} < 1\ mm$	0.10 mm	1.00 mm	0.1
$\frac{f_1}{{w_{1kN}}^{0.44}} > 18.7$	24.18	18.7	0.77
	ULS		
Norris criterion	0.26	1.00	0.26
$\sigma_{t.0.d} \leq f_{t.0.d}$	8.20 MPa	26 MPa	0.32
$\sigma_{c.0.d} \leq f_{c.0.d}$	9.59 MPa	18 MPa	0.53
$\sigma_{t.90.d} \leq f_{t.90.d}$	4.29 MPa	24 MPa	0.18
$\sigma_{c.90.d} \leq f_{c.90.d}$	3.87 MPa	16.66MPa	0.23
$\tau_{v.d} \leq f_{v.d}$	1.39 MPa	6.34 MPa	0.22

Table 5.9: The performance and utilization ratio of concept 3.

Criterion	Performance	Limit	Utilization
	SLS		
$w_{inst} \leq L/500$	10.00 mm	10.67 mm	0.94
$f_1 > 8\ Hz$	10.27 Hz	8 Hz	0.78
$w_{1kN} < 1\ mm$	0.16 mm	1.00 mm	0.16
$\frac{f_1}{{w_{1kN}}^{0.44}} > 18.7$	23.00	18.7	0.81
	ULS		
Norris criterion	0.66	1.00	0.66
$\sigma_{t.0.d} \leq f_{t.0.d}$	16.55 MPa	27.20 MPa	0.61
$\sigma_{c.0.d} \leq f_{c.0.d}$	16.20 MPa	18.86 MPa	0.86
$\sigma_{t.90.d} \leq f_{t.90.d}$	4.43 MPa	22.8 MPa	0.19
$\sigma_{c.90.d} \leq f_{c.90.d}$	4.48 MPa	15.8MPa	0.28
$\tau_{v.d} \leq f_{v.d}$	1.86 MPa	6.34 MPa	0.29

5.2.3 Concept proposal

All three concepts are verified in Abaqus/CAE and show to fulfil the design requirements in SLS and ULS. The Table 5.6 illustrates that the self-weight will decrease by approximately 30 % when adding one secondary beam and an additional 20 % when adding another secondary beam. This indicates that the profit in decrease of material volume is higher in the beginning and decreases with the increased number of secondary beams.

It is considered as beneficial to have a low material volume but at the same time limit the number of secondary beams. After discussing each concept, concept 2 was chosen to be the most suitable concept for this case due to its low self-weight and few secondary beams. The long span of 16 m is divided into two parts by a secondary beam for this case which enables the activity at the airport to continue on one part and obstruct the other part for construction. The plate dimensions of concept 2 are almost

square which is preferable for utilization of the four edges support. If choosing concept 1 the self-weight would be unnecessarily high compared to concept 2.

The result shows that the first eigenfrequency of 8 Hz is the leading criterion for concept 1 and 2 and will influence the dimensions of the cross-sections for each concept. Why the frequency criterion is the leading criterion can be explained by the high load from added material dead-weight and installations. This load was for example 0.5 kN/m^2 in case study 1 but in this case study it is four times higher, 2 kN/m^2. The requirements on this timber floor are considered as high and a structural height of 386 mm and self-weight of 0.7 kN/m^2 are therefore considered as good. The self-weight is approximately 15 % of a hollow core concrete slab which will decrease the height of the main and secondary beams and at the same time simplify the assembly on site. The higher structural height of the floor system compared to a hollow core slab would therefore likely not be a problem for this case.

5.2.4 Performance of an existing timber floor

As mentioned in the introduction to Chapter 5 timber solutions are regarded as rare for this situation as both the imposed load and the added dead weight are high. In order to see if an existing timber floor system can be used; Martinsons MBK 12-02 is studied again. Of the identified timber floor systems on the Swedish market, MBK 12-02 is regarded to have highest potential for this case. Same conditions as for concept 2 is regarded where one secondary beam in the middle is used, hence MBK 12-02 has to span 8 m. No acoustic ceiling is assumed to be needed; therefore it is not included in the self-weight. When calculating the first eigenfrequency, the floor system is regarded as a beam simply supported on two edges with no flexural supports. The eigenfrequency is calculated with Euler-Bernoulli theory and stated as follows:

$$f_1 = \frac{\pi}{2L^2}\sqrt{\frac{EI_x}{m_{freq}}} \tag{5.1}$$

The needed input data and the calculations are presented in Appendix F. The obtained frequency is 7.59 Hz which is lower than 8 Hz as required according to Equation (2.1). A comparison between the proposed concept and MBK 12-02 for the case is presented in Table 5.10.

Table 5.10: Comparison between proposed concept and MBK 12-02.

	Proposed concept	MBK 12-02
h_{tot} [mm]	386	410
Self-weight [kN/m^2]	0.73	0.65
f_1 [Hz]	8.78	7.59

As can be seen in Table 5.10 the proposed concept has somewhat lower structural height but a little bit higher self-weight than MBK 12-02. The proposed concept fulfils the first eigenfrequency requirement while MBK 12-02 does not.

6 Highlighted details

The sandwich floor has different details that need to be developed to retain the structural performance and to implement installations. This chapter highlights some of these details, visualized in Figure 6.1, and discusses possible solutions.

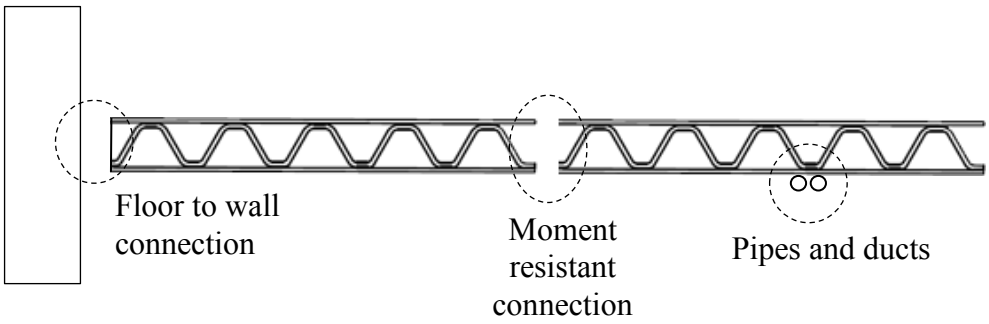

Figure 6.1. Visualisation of the highlighted details that need to be developed.

The floor connection to a load bearing wall can have different arrangements as Chapter 2.2.2 explains and the common attribute is that floor systems have to be stiff at the ends. If the floor is laid on top of the wall it must resist large compression forces. The screw must also be able to tie into something within the floor. This detail could also be used when lifting the elements on site. These aspects should be considered when developing the connection to wall detail. It is likely needed to place a stiffener at the ends of the sandwich floor system.

Due to transportation constrains, it is often needed to divide a floor system into smaller parts. The structural performance of the whole system has to be remained when several elements are assembled. The floor needs to have a moment resistant connection to ensure that the floor utilize two-way action. This connection should not influence the structural height of the sandwich floor and will therefore preferably be included under the top face.

The connections between the core and faces are assumed to be rigid which could be achieved by gluing and nailing the face to the core. The minimum length of f_c has to be sufficient to allow for a stiff and strong connection. These connections are preferably carried out at the factory to minimize the work on site and to ensure the quality of the connection. This will imply that the floor systems will be closed when arriving at the construction site and there will be no possibilities of including pipes and horizontal ducts inside the structural part of the floor. The possibilities for inspection and maintenance should also be considered when planning where and how the ducts and pipes are placed.

The total height of the floor system including the structural and acoustic part should, if possible, not be influenced by the ducts and pipes. The pipes and ducts could be placed in between the acoustic part and the structural part. The ducts can be suspended with round or rectangular rods which could be anchorage in the lower face. This will increase the load on the bottom face and the solution has to be investigated further. One additional investigation is also to ensure that the acoustic performance is kept when this part is utilized for pipes and ducts.

7 Discussion

In the report, the performance in the behaviour analysis of the sandwich floor has been defined as maximum instantaneous deflection. For timber design SLS criteria are often governing and especially for timber floors deflection and first eigenfrequency are often governing. It was seen in Chapter 4 that ULS criteria were not a problem for the investigated sandwich plates and the idea of defining deflection as performance is considered appropriate. It is to some extent more difficult to compare performance based on SLS criteria than ULS criteria. The ULS criteria are strict requirements while SLS criteria are more or less recommendations. The SLS criteria are based on perception and the limit of the criteria can always be discussed.

The behaviour analysis in Chapter 4 gave an increased understanding of the influence of aspect ratios and cross-section geometry on the performance of the timber sandwich floor. The rounded corners themselves does not decrease the performance of the sandwich floor, it is the number of corrugation cells that influence the performance. Therefore one can see an advantage with a small corrugation radius, R_c, as more corrugation cells can be included on a fixed length. The length of the horizontal part of the corrugation, f_c, has influence on the performance of the floor in both a positive and negative way. It is located far from the neutral axis hence the material contribute efficiently to the bending stiffness, however a longer f_c decreases the number of corrugation cells. If the corrugation thickness, t_c, is small f_c should likely be kept as short as possible for best performance. Nevertheless the length of f_c should be such that a sufficient adhesive layer can be placed on it to allow for a strong interaction between core and face. The length can also be affected by manufacturing restrains. Manufacturing restrains and shape stability of the corrugation should be further investigated in order to see if additional dimensional restrains are necessary. The corrugated core is chosen mainly because it is regarded as easier to manufacture, if the corrugation tend to have manufacturing problems in the future a corrugated core made of wood fibres or a kagome lattice core can be interesting to further investigate. An advantage with the kagome lattice core is that it does not contain any curved parts. According to Chapter 4.8 the performance of the corrugated and the honeycomb core were close to each other which supports the idea of choosing core configuration based on manufacturing possibilities.

The imposed concentrated load on floors has a significant influence on the choice of cross-section for a sandwich floor. It influences both the thickness of the top face as well as the length of the corrugation, l_c, and therefore also the corrugation angle, α_c, as well as f_c and R_c. In the Mathcad code the action of the concentrated load in the top face was analysed as a clamped-clamped beam loaded with a concentrated load in middle span. This is an underestimation of the strength of the sandwich floor as the load distribution is disregarded. Also the concentrated load will not act in a single point as it should be distributed on an area of 50x50 mm^2. A more accurate structural model should be implemented in the Mathcad optimisation code in order to generate more efficient cross-sections.

According to Chapter 4.2 there is a notable difference between analytical and numerical calculations when calculating deflection of plate 2:1. A reason for the difference could be an overestimation of the shear stiffness in y-direction in the analytical calculations. For aspect ratio 2:1 the shear forces related to y-direction are

larger than for aspect ratio 1:1 and 1:2 and an overestimation would be more prominent.

As the calculations in the Mathcad code assume Libove and Hubka interaction the sandwich plate will always gain some stiffness in a physical model or when modelled in Abaqus/CAE with full interaction. Therefore the analytical calculations will in a greater extent underestimate the stiffness for cross-sections with long f_c as it in reality provides longer bond length. Further stiffness is gained by positioning the fibres of faces and core in an advantageous way in a FE-model or a physical model.

To further analyse timber sandwich structures a great value is seen in deriving Libove & Hubka stiffness constants for orthotropic material. This has been proved possible by Tumino et al. (2014) however formulas should be derived that allows different thickness of top and bottom faces as well as different material properties of faces and core. With stiffness constants for orthotropic material the structural behaviour could be further analysed, especially the influence of changes in the cross-section geometry.

In the study boundaries with no flexibility were assumed. This is a simplification of reality especially if the floor system is supported on beams. When the floor system is supported on beams a full system analysis should be done when calculating deflection and eigenfrequency, hence taken into account the deflection and eigenfrequency of the beams. The positioning of the corrugation and main fibre direction could be influenced by boundaries with flexibility. If the boundaries are modelled as springs it could be beneficial to distribute the load more evenly to the edges in order to achieve as low deflection as possible for the whole system. This could be done by placing the main fibre direction of the faces perpendicular to the corrugation.

It is not common that prefabricated timber floors are supported on four edges and utilises two-way action. As was seen in Chapter 4.6 it is clearly beneficial to use two-way action for aspect ratios about 1:1. However the idea of using two-way action for prefabricated members could be met with disbelief from the building industry as it brings an unconventional way of assembling prefabricated members.

Timber sandwich elements could be used for other structural components than floors in a building. With their high bending stiffness they could also be prominent as load-bearing walls and roof structures.

8 Conclusion

Based on the study in this report conclusions can be made regarding possibilities and benefits of a timber sandwich floor. The structural behaviour analysis mount the possibilities of influencing the performance by design choices while the two case studies place the timber sandwich floor in a content which exhibit benefits of the new floor.

The investigation of the timber sandwich floor shows that the corrugation has its stiff direction parallel to corrugation. This indicates that the corrugation should be placed along the shorter span to yield highest performance of the floor.

The placements of the main fibre direction of the faces have a great influence on the deflection. However, the choice of main fibre direction in the core will have a smaller influence on the global behaviour. Birch plywood is identified as an attractive material for the faces as it has high stiffness in two-directions.

The four edges support significantly increases the performance for an aspect ratio of 1:1. It provides some increase in performance for aspect ratio 2:1 but only little increase for aspect ratio 1:2.

The sandwich timber floor system can yield higher performance, regarding vibration, with lower structural height and material volume, than a conventional timber floor system. Due to the lower structural height, the new floor system is competitive to conventional timber floors for multi-storey buildings.

Further on, the timber sandwich floor offers a new market for timber floors where loads are high as it does not need to compromise with SLS criteria. The timber sandwich floor can compete with concrete floors for these applications as the self-weight is only about 15 % of a hollow core slab.

9 Recommendations for further research

This thesis has been focused on the development of the structural part of a new timber floor system and several limitations were made in the study. Further investigations are needed before the timber sandwich floor system can be established on the market.

An estimation of material and manufacturing costs of the sandwich floor system has to be performed to see if it is competitive to other floor systems when it comes to price and to evaluate if design choices can be made to decrease the cost.

Furthermore, manufacturing of the corrugation has to be investigated further. Dimensional restrains need to be established from form-pressing of veneers and plywood. It should be evaluated if a corrugation made of wood fibres, with acceptable mechanical properties, is cheaper to manufacture.

Chapter 6 highlights important details that need to be developed. These details are important for the performance of the floor system. Based on how the floor to wall connection is designed other boundary conditions can be introduced. The structural behaviour of a timber sandwich floor should be evaluated for other types of boundary conditions, for example clamped supports, to see how the supports influence the behaviour and if the connection can be designed to increase the performance of the floor system.

The fire resistance and the acoustic part of the timber floor have to be developed and investigated. Acoustics are often an important factor for floor systems. It should be evaluated if the acoustics can be improved by filling the corrugation with sound insulation.

Moreover should a more detailed investigation of the structural behaviour be performed to increase the understanding and possibilities of timber sandwich floors. The gained knowledge and technique of using timber sandwich elements could also lead to a possible market for timber sandwich elements as roof and wall structures.

10 References

Allen, H. G. (1969). *Analysis and design of structural sandwich panels* (1:st ed.). Oxford: Pergamon Press.

Alwan, U., & Järve, D. (2012). *New concept for industrial bridge construction.* Gothenburg : Chalmers University of Technology.

Banerjee, S., & Bhattacharyya, D. (2011). Optimal design of sandwich panels made of wood veneer hollow cores. *Composites science and technology, 71,* 425-432.

Beneus, E., & Koc, I. (2014). *Innovative road bridges with steel sandwich decks.* Göteborg: Chalmers University of Technology.

Brandin, J., & Oscarsson, A. (2015). *Dynamic response of timber floors - criteria, performance and design for acceptability.* Gothenburg: Chalmers University of Technology.

CEOS. (2016). *Prislista.*

Chang, W.-S. (2004). *Elasto-plastic analysis of crrugated sandwich steel panels.* The Pennsylvania State University .

Chang, W.-S., Ventsel, E., Krauthammer, T., & John, J. (2005). Bending behaviour of corrugated-core sandwich plate. *Composite Structures 70,* pp. 80-89.

Colling, F. (1995). Glued laminated timber - production and strength classes. In H. Blass, P. Aune, B. Choo, R. Görlacher, D. Griffiths, B. Hilson, . . . G. Steck (Eds.), *Timber engineering STEP1* (pp. A8/1-A8/8). Almere: Centrum Hout.

D Systèmes. (2012). *Abaqus Analysis User's Manual.* Retrieved 03 16, 2016, from https://things.maths.cam.ac.uk/computing/software/abaqus_docs/docs/v6.12/books/usb/default.htm

Dackman, D., & Ek, W. (2015). *Steel sandwich decks in medium span.* Gothenburg: Chalmers University of Technology.

Dendrolight Latvija. (2016). *Building systems.* Retrieved 02 03, 2016, from http://dendrolight.lv/en/products/building-systems/

EN 1995-1-1. (2004). *Eurocode 5: Design of timber structures - Part 1-1: Common rules and rules for buildings.*

Fan, H. L., Meng, F. H., & Yang, W. (2006). *Sandwich panels with Kagome lattice cores reinforced by carbon fibers.* Beijing: Tsinghua University.

Feldmann, M., Heinemeyer, C., & Völling, B. (n.d.). *Design guide for floor vibrations.* Luxemburg: ArcelorMittel.

Frolovs, G., Rocens, K., & Sliseris, J. (2014). Numerical investigations of waved ribs shape's influence on specific stiffness of a plate. Riga: Riga Technical University .

Gard, W. (2015). *CIE5124 Timber structures 2 - engineered timber products.* Delft.

Grenestedt, J. L., & Bekisli, B. (2003). Analyses and preliminary tests of a balsa sandwich core with improved shear properties. *International Journal of Mechanical Sciences 45*, pp. 1327-1346.

Griffiths, D. (1995). Wood-based panels - fibreboard, particleboard and OSB. In H. Blass, P. Aune, B. Choo, R. Görlacher, D. Griffiths, B. Hilson, . . . G. Steck (Eds.), *Timber engineering STEP1* (pp. A11/1-A11/12). Almere: Centrum Hout.

Gustafsson, P. (2003). Fracture perpendicular to grain - structural applications. In S. Thelandersson, & H. J. Larsen (Eds.), *Timber Engineering* (pp. 103-130). Wst Sussex: John Wiley & Sons Ltd.

Hed, K. (2016, 03 22). Prisskillnad mellan plywood och Kerto Q.

Hisgett, T. (2012, 09 18). *Mosquito Fuselage.* Retrieved 05 26, 2016, from https://www.flickr.com/photos/hisgett/8048040982/in/photolist-dgbjch-e8U6xi-aSCo2R-eQmq4x-2r7rdv-5pmNys-nXX6Zk-cC5FKQ-ehjpkL-pEPhf2-gFLWjT-efJUw5-eaSkQe-cdbh8d-ehjpkA-efK6j9-cjf2Mw-q6ReP4-ehdE5n-q9H3Ds-qk2Aim-cC5EMW-qk2ACE-cdaWPQ-r1MMFG-cdbfmW-qJhKwS-qYzs

Hohe , J., & Becker, W. (2002). *Effective stress-strain relations for two-dimensional cellular sandwich cores: Homogenization, material models, and properties.* Siegen: Universität Siegen .

Hunt, J. F. (2004). 3D structural panels: a literature review. *Pasific rim bio-based composite syposium, II*(7), 272-281.

Johansson, M. (2011). Structural properties of sawn timber and engineered wood products. In P. Bergkvist (Ed.), *Design of timber structures* (pp. 2.1-2.39). Stockholm: Swedish Wood.

Johansson, N. (2016, 05 16). Meeting with Niklas Johansson, Civil Engineer at Byggteknik, Ramböll Göteborg.

Johansson, T. (2016, 04 13). E-mail to Thomas Johansson, Head of Structural Engineering, Moelven Töreboda.

Johnsson, H. (2011). Timber building systems for housing. In P. Bergkvist (Ed.), *Design of timber structures* (1st ed., pp. 8.1-8.33). Stockholm: Swedish Wood.

Kavermann, S. W. (2013). *Mechanical properties of lightweight sandwich panels with corrugated plywood core.* Auckland: University of Auckland.

Kielsteg. (2015). *Workbook for architects and planners* (- ed.). Graz: Kielsteg.

Kliger, R. (2015). *Extracts from Eurocode 5 - Timber Engineering VSM 196.* Gothenburg : Chalmers University och Technology.

Klimek, P., Wimmer, R., Brabec, M., & Sebera, V. (2015). *Novel sandwich panel with interlocking plywood Kagome lattice core and grooved particleboard facings.* Brno: Mendel University in Brno.

Labans, E., & Kalnins, K. (2011). *Numerical versus experimental investigation of plywood sandwich panels with corrugated core.* Riga: Riga Technical University.

Li, J., Hunt, J. F., Gong, S., & Cai, Z. (2014). *Wood-based tri-axial sandwich composite materials: design, fabrication, testing, modeling and application.* Madison: University of Wisconsin.

Libove, C., & Hubka, R. E. (1951). *Elastic constants for corrugated-core sandwich plates.* Washington: Langley Aeronautical Laboratory.

Lignatur. (2014). *Lignatur workbook* (7th ed.). Waldstatt: Lignatur AG. Retrieved from http://www.lignatur.ch/fileadmin/ablage/downloads/workbook_a4_en/2014-06-04_workbook_a4_en.pdf

Magnevik, Å. (2006). *Numerical simulation of moulding and distortion in hot-pressed veneer products.* Göteborg: Chalmers University of Technology.

Markwardt, L., & Wood, L. (1959). *Case studies of four sandwich panel houses.* Madison: U.S. Forest Product Laboratory.

Martinsons. (2006). Massivträ. Handboken. Martinsons.

Martinsons. (2012, 09 19). *Produktblad för MBK-03-02.*

Martinsons. (2012, 12 07). *Produktblad för MBK-12-02.*

Martinsons. (2016). *Martinsons handbok i KL-trä.* Bygdsiljum.

Masonite Beams AB. (2010). *MFB handbok.* Byggma Group.

Metsä. (2016). *Kerto Q cross-bonded panels*. Retrieved 05 20, 2016, from http://www.metsawood.com/uk/Products/Kerto/Kerto-Q/Pages/default.aspx

Metsä Wood. (2013, 10 15). *Prestandadeklaration MW/LVL/311-001/CPR/DOP*. Retrieved 05 26, 2016, from http://www.metsawood.com/global/Tools/DoP/DOPOpenDocuments/DoP_Kerto-S_2013-10-15_se.pdf

Metsä Wood. (2016). *Kerto-Ripa LVL floor elements*. Retrieved 02 02, 2016, from http://www.metsawood.com/uk/Applications/Building-and-Construction/Flooring-Solutions/Kerto-Ripa

Moelven. (2013, 06 27). *Prestandadeklaration Konstruktionsplywood.* Retrieved 05 11, 2016, from https://www.moelven.com/PageFiles/311157/Plywood_P30.PDF

Moelven. (2016). *Kerto-q*. Retrieved 05 11, 2016, from https://www.moelven.com/se/Produkter-och-tjanster/Limtra-Massivtra-och-Kerto/Kerto/Kerto-q/

Moelven. (2016). *Trä8.* Retrieved 02 02, 2016, from https://www.moelven.com/Documents/Toreboda/Broschyren/TRÄ8.pdf

Nordic Wood. (2001). *Glulam handbook.* Stockholm: Swedish Wood.

Ohlsson, S. (1988). *Springiness and human-induced floor vibrations - a design guide.* Gothenburg: Swedish Council for Building Research.

Onate, E. (2013). *Structural analysis with finit element method.* Barcelona: CIMNE.

Ranta-Maunus, A. (1995). Laminated veneer lumber and other structural sections. In H. Blass, P. Aune, B. Choo, R. Görlacher, D. Griffiths, B. Hilson, . . . G. Steck (Eds.), *Timber engineering STEP1* (pp. A9/1-A9/7). Almere: Centrum Hout.

Ricker, C. S. (2005). *Design analysis no 6: DeHavilland Mosquito.* Retrieved 01 28, 2016, from http://legendsintheirowntime.com/Mosquito/Mosquito_Av_4405-06_DA.html

Risberg, H. (2016, 04 08). E-mail to Håkan Risberg, Head of Structural Engineering, Martinsons.

Roylance, D. (2000). *Constitutive Equations.* Cambridge : Massachusetts Instituite of Technology .

Sandhaas, C., & Van de Kuilen, J. (2013). Material model for wood. *Heron*(58).

Sliseris, J., & Rocens, K. (2011). Rational structure of panel with curved plywood ribs. *International journal of civil, environmental, structural, construction & architectural engineering, 5*(3), 150-156.

Smith, A., Hicks, S., & Devine, P. (2009). *Design of floors for vibration - A new approach.* Berkshire : The Steel Construction Institute .

Srinivasan, N., Bhattacharyya, D., & Jayaraman, K. (2007). Termoforming of wood veneer composite sheets. *Holzforschung, 61*, 558-562.

Steck, G. (1995). Wood-based panels - plywood. In H. Blass, P. Aune, B. Choo, R. Görlacher, D. Griffiths, B. Hilson, . . . G. Steck (Eds.), *Timber engineering STEP1* (pp. A10/1-A10/9). Almere: Centrum Hout.

Thelandersson, S. (1995). Serviceability limit states - deformations. In H. Blass, P. Aune, B. Choo, R. Görlacher, D. Griffiths, B. Hilson, . . . G. Steck (Eds.), *Timber engineering STEP 1* (pp. A17/1-A17/8). Centrum Hout: Delft University of Technology.

Träguiden. (2014). *Träguiden*. Retrieved February 1, 2016, from http://www.traguiden.se/konstruktion/dimensionering/dimensioneringsgang/massivtra/platt--och-kassettbjalklag/

Tumino, D., Ingrassia, T., Nigrelli, V., Pitarresi, G., & Urso Miano, V. (2014). Mechanical behavior of a sandwich with corrugated GRP core: numerical modeling and experimental validation. *Frattura ed Integrita Strutturale*(30), 317-326.

UPM. (2007). *Handbook of Finnish plywood.* Lahti: Finnish forest industries federation.

UPM. (2014, August). *UPM Grada 2000.* Retrieved 05 24, 2016, from http://www.upmgrada.com/userData/upmgrada/pdf/UPM_Grada2000_EN_0814_LR_53583.pdf

Vinson, J. (2001). Sandwich structures. *Applied Mechanics Reviews, 54*(3), 201-214.

Vinson, J. R. (2005). Sandwich structures: past, present and future. In O. e. Thomsen (Ed.), *Sandwich structures 7: advancing with sandwich structures and materials* (pp. 3-12). Aalborg: Springer.

Zenkert, D. (1997). *The handbook of sandwich construction* (1:st ed.). West Midlands: EMAS Publishing.

Zhang, J., Supernak, P., Mueller-Alander, S., & Wang, C. H. (2013). Improving the bending strength & energy absorption of corrugated sandwich composite structure. *Materials & Design* (52), 767-773.

Appendix A – Calculation of S-factor

This appendix presents the expression for the non-dimensional S-factor used when calculating the transverse shear stiffness in y-direction, D_{Qy}, for a corrugated sandwich plate. The expression is obtained from Libove & Hubka (1951). The factor is based on the geometry of the corrugation. The S-factor is given for the simplified case where the corrugation is symmetric, the corrugation consists of straight lines and circular arcs, the origin is chosen at the midpoint of the corrugation leg and the top and bottom faces are made of the same material. Further simplifications can be made if the whole sandwich is symmetric, i.e. the thickness of top and bottom faces are equal.

$$S = \frac{3\frac{h_c}{p}C_7\left(C_2{}^2 - C_1C_3\right) - C_3 + \frac{p}{h_c}\left(2C_2 - \frac{p}{h_c}C_1\right)}{12\left\{\begin{array}{c} 2\frac{p}{h_c}\left[\frac{p}{h_c}(C_1C_4 - C_2C_5) - (C_2C_4 - C_3C_5)\right] + \\ \frac{h_c}{h}\left\{\begin{array}{c} 3C_7\left[C_4(C_1C_4 - 2C_2C_5) + C_3C_5{}^2 - C_6\left(C_1C_3 - C_2{}^2\right)\right] + \\ \frac{p}{h_c}\left(C_4{}^2 - C_3C_6\right) + 2\left(\frac{p}{h_c}\right)^2(C_2C_6 - C_4C_5) + \left(\frac{p}{h_c}\right)^3 C_5{}^2 - C_1C_6 \end{array}\right\} \\ \frac{h_c}{h}\frac{p}{h_c}\left(C_2{}^2 - C_1C_3\right) \end{array}\right\}} \quad \text{(C.1)}$$

where

$$\left.\begin{aligned} C_1 &= K_L + \frac{1}{3}\frac{E_c\left(1-\nu_f{}^2\right)}{E_f\left(1-\nu_c{}^2\right)}\left(\frac{t_c}{t_{f.top}}\right)^3\frac{p}{h_c} \\ C_2 &= \frac{1}{2}\frac{p}{h_c}K_L \\ C_3 &= K_{I.z} + \frac{p}{h_c}\left(\frac{1}{4}\frac{p}{h_c}K_L\right) + \frac{1}{12}\left(\frac{t_c}{h_c}\right)^2 K_{L.z} \\ C_4 &= K_{I.yz} + \frac{1}{2}\left[1 + \left(1 + \frac{t_{f.top}}{t_c}\right)\left(\frac{t_c}{h_c}\right)\right]\left(\frac{1}{2}\frac{p}{h_c}K_L\right) - \frac{1}{12}\left(\frac{t_c}{h_c}\right)^2 K_{L.yz} \\ C_5 &= \frac{1}{2}\left[1 + \left(1 + \frac{t_{f.top}}{t_c}\right)\frac{t_c}{h_c}\right]K_L \\ C_6 &= K_{I.y} + \frac{1}{4}\left[1 + \left(1 + \frac{t_{f.top}}{t_c}\right)\frac{t_c}{h_c}\right]\left[1 + \left(1 + \frac{t_{f.top}}{t_c}\right)\frac{t_c}{h_c}\right]K_L \\ &\quad + \frac{1}{12}\left(\frac{t_c}{h_c}\right)^2 K_{L.y} \\ C_7 &= \frac{E_f}{E_c}\left(\frac{1-\nu_c{}^2}{1-\nu_f{}^2}\right)\left(\frac{t_{f.bot}}{t_c}\right)^3 \end{aligned}\right\} \quad \text{(C.2)}$$

and

$$
\left.
\begin{aligned}
K_L &= 2\frac{d_1}{h_c} + 2\theta\frac{R_{C1}}{h_c} + \frac{f_c}{h_c} \\
K_{I.z} &= \frac{2}{3}\left(\frac{k_1}{h_c}\right)^2\frac{d_1}{h_c} + \frac{2}{3}\left[\frac{1}{8}\left(\frac{p}{h_c}\right)^3 - \left(\frac{b_1}{h_c}\right)^3\right] + \\
&\quad +2\frac{R_{C1}}{h_c}\left\{\frac{b_1}{h_c}\left[\theta\frac{b_1}{h_c} - 2\left(\frac{R_{C1}}{h_c} - \frac{e_1}{h_c}\right)\right] + \frac{1}{2}\left[\theta\left(\frac{R_{C1}}{h_c}\right)^2 - \frac{g_1}{h_c}\frac{e_1}{h_c}\right]\right\} \\
K_{L.z} &= 2\frac{d_1}{h_c}\sin^2\theta + \frac{R_{C1}}{h_c}(\theta - \sin\theta\cos\theta) \\
K_{I.yz} &= \frac{2}{3}\frac{j_1}{h_c}\frac{k_1}{h_c}\frac{d_1}{h_c} + \frac{1}{2}\left[\frac{1}{4}\left(\frac{p}{h_c}\right)^2 - \left(\frac{b_1}{h_c}\right)^2\right] + \\
&\quad +2\frac{R_{C1}}{h_c}\left[\frac{a_1}{h_c}\left(\theta\frac{b_1}{h_c} + \frac{e_1}{h_c} - \frac{R_{C1}}{h_c}\right) + \frac{g_1}{h_c}\left(\frac{b_1}{h_c} - \frac{1}{2}\frac{g_1}{h_c}\right)\right] \\
K_{L.yz} &= 2\frac{d_1}{h_c}\sin\theta\cos\theta + \frac{R_{C1}}{h_c}\sin^2\theta \\
K_{I.y} &= \frac{2}{3}\left(\frac{j_1}{h_c}\right)^2\frac{d_1}{h_c} + \frac{1}{4}\frac{f_c}{h_c} + \\
&\quad +2\frac{R_{C1}}{h_c}\left\{\frac{a_1}{h_c}\left(\theta\frac{a_1}{h_c} + 2\frac{g_1}{h_c}\right) + \frac{1}{2}\left[\theta\left(\frac{R_{C1}}{h_c}\right)^2 + \frac{g_1}{h_c}\frac{e_1}{h_c}\right]\right\} \\
K_{L.y} &= \frac{f_c}{h_c} + 2\frac{d_1}{h_c}\cos^2 + \frac{R_{C1}}{h_c}(\theta + \sin\theta\cos\theta)
\end{aligned}
\right\} \quad \text{(C.3)}
$$

and remaining expressions are based on the geometry of the cross-section. They are visualised in figure C1.

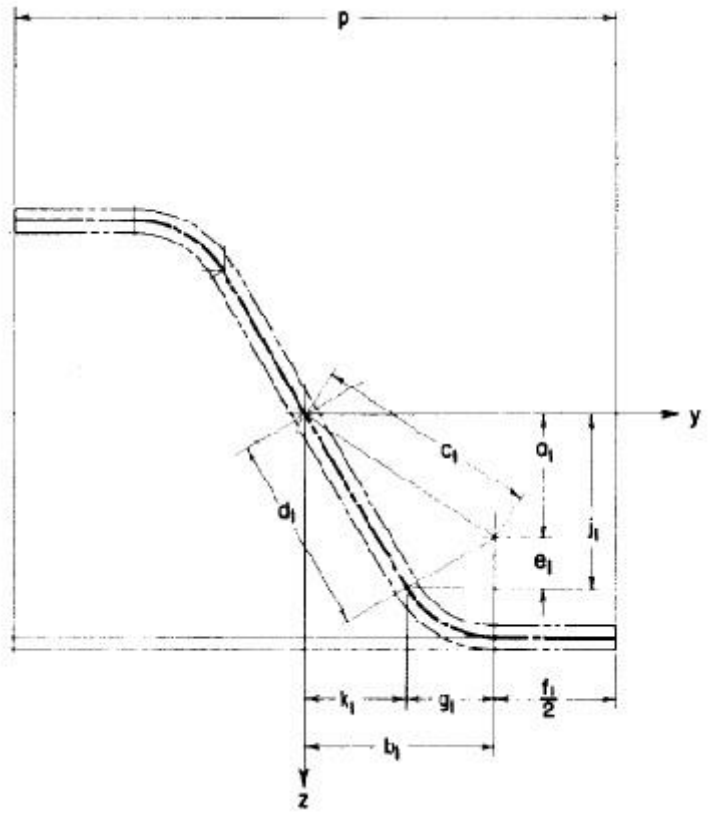

Figure C1. Geometrical definitions of constants.

If the corrugation length, p, is unknown the constants can be obtained in the following way

$$\left.\begin{aligned}
\theta &= \alpha_c \\
a_1 &= \frac{h_c}{2} - R_c \\
e_1 &= R_c \cos\theta \\
g_1 &= R_c \sin\theta \\
j_1 &= a_1 + e_1 \\
p &= f_c + 2g_1 + 2j_1 \cot\theta \\
b_1 &= \frac{p - f_c}{2} \\
c_1 &= \sqrt{{a_1}^2 + {b_1}^2} \\
d_1 &= \sqrt{{c_1}^2 - {R_c}^2} \\
k_1 &= b_1 - g_1
\end{aligned}\right\} \quad \text{(C.4)}$$

Appendix B - Analytical volume optimisation of a timber sandwich floor

The optimisation was originally made by Beneus & Koc (2014) and modified by Dackman & Ek (2015) for a sandwich steel deck in a bridge. The code was therefore further modified to suit a sandwich timber floor. This code is for corrugation with rounded corners.

Changes are made in the code to implement the roundning of the corners. R_{C1} (denoted R_c in the report) is the radius of the corner curvature. It is now regarded as an unknown variable. Half the corrugation length, p, and the length of the inclined corrugation leg, α_c, is then unknown. They are now defined from the geometrical variables a_1 to k_1, which in turn are rearranged as p and l_α are unknown. When these geometrical definitions are defined, the curved part is included in the area and moment of inertia calculations.

Contents

1. Input data

1. Input data

1.1. Floor geometry

$L := 14m$ Length of floor

$B := 7m$ Width of floor

1.2. Material properties

Only isotropic materials can be used in the calculation. Therefore averaged mechanical properties of timber is used in order to "translate" the anistropy of timber to isotropic properties.

Poisson's ratio

$\nu_{12} := 0.5$

$\nu_{13} := 0.05$

$\nu_{23} := 0.01$

$$\nu := \frac{(\nu_{12} + \nu_{13} + \nu_{23})}{3} = 0.187$$

Density

$$\rho := 410 \frac{kg}{m^3}$$

Modulus of elasticity

$E_1 := 7.218GPa$

$E_2 := 5.782GPa$

$$E := \left[\frac{(E_1 + E_2)}{2}\right] = 6.5 \cdot GPa$$

Shear modulus (panel shear)

$G := 0.53GPa$

Bending stress

$f_{m.0.k} := 22.2MPa$

$f_{m.90.k} := 19.7MPa$

$$f_m := \left[\frac{(f_{m.0.k} + f_{m.90.k})}{2}\right] = 20.95 \cdot MPa$$

Shear strength (panel shear)

$f_{vk} := 7MPa$

Material partial factor

$\gamma_M := 1.2$

Creep deformation factor

$k_{def} := 0.8$

1.3. Loads

Partial coefficients

For SLS

$\gamma_{G.SLS} := 1$

$\gamma_{Q.SLS} := 1$

For ULS

$\gamma_{G.ULS} := 1.35$

$\gamma_{Q.ULS} := 1.5$

Combination factors

$\psi_0 := 0.7$

$\psi_2 := 0.3$

Variable loads

$q_k := 2\frac{kN}{m^2}$	Imposed load for floors
$Q_k := 2kN$	Point load for local effects (imposed load)
$q_{dw} := 50\frac{kg}{m^2}\cdot g = 0.49\cdot\frac{kN}{m^2}$	Added dead weight (ceiling, flooring etc.)
$Q_{1kN} := 1kN$	Point load (for dynamic requirement)
$k_{mod} := 0.8$	Load-duration: Medium
$\alpha_A := \min\left(1, 0.5 + \frac{10m^2}{L\cdot B}\right)$	Area reduction factor (in ULS)

1. Input data

2. Sandwich panel

2.1. Geometry

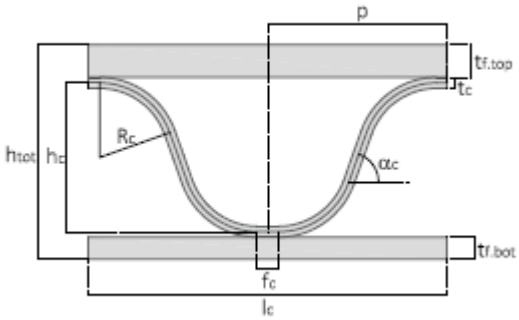

Height of the cross-section
Measured from centreline of top plate to centreline of bottom plate

$$h\left(h_c, t_{f.top}, t_{f.bot}, t_c\right) := h_c + \frac{t_{f.top}}{2} + \frac{t_{f.bot}}{2} + t_c$$

Measured from top to bottom of sanwich panel

$$h_{tot}\left(h_c, t_{f.top}, t_{f.bot}, t_c\right) := h_c + t_{f.top} + t_{f.bot} + t_c$$

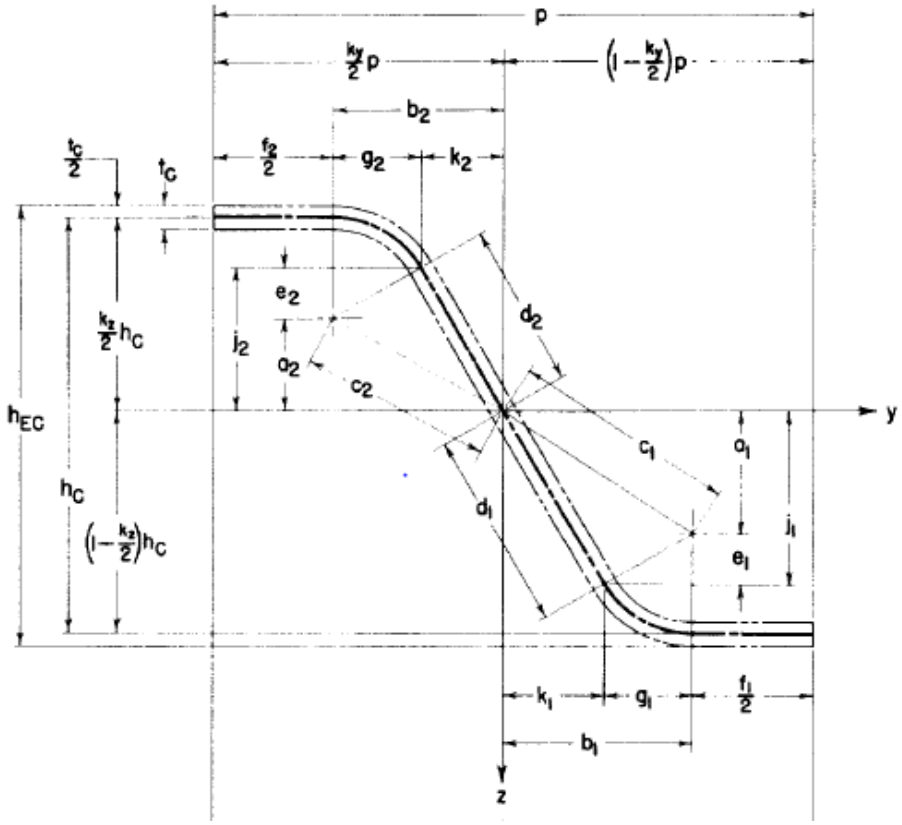

Symmetrical corrugation k.y=k.z --> K.Ay and K.Az vanish

$k_y := 1 \qquad k_z := 1 \qquad K_{Ay} := 0 \qquad K_{Az} := 0$

$e_1\left(\alpha_c, R_{C1}\right) := R_{C1} \cdot \cos\left(\alpha_c\right)$

$g_1\left(\alpha_c, R_{C1}\right) := R_{C1} \cdot \sin\left(\alpha_c\right)$

$$a_1(h_c, R_{C1}) := \left(1 - \frac{k_z}{2}\right) \cdot h_c - R_{C1}$$

$$j_1(h_c, \alpha_c, R_{C1}) := a_1(h_c, R_{C1}) + e_1(\alpha_c, R_{C1})$$

$$p(h_c, \alpha_c, f_c, R_{C1}) := f_c + 2 \cdot g_1(\alpha_c, R_{C1}) + 2 \cdot j_1(h_c, \alpha_c, R_{C1}) \cdot \frac{\sin\left(\frac{\pi}{2} - \alpha_c\right)}{\cos\left(\frac{\pi}{2} - \alpha_c\right)}$$

$$b_1(h_c, \alpha_c, f_c, R_{C1}) := \left(1 - \frac{k_y}{2}\right) \cdot p(h_c, \alpha_c, f_c, R_{C1}) - \frac{f_c}{2}$$

$$c_1(h_c, \alpha_c, f_c, R_{C1}) := \left(a_1(h_c, R_{C1})^2 + b_1(h_c, \alpha_c, f_c, R_{C1})^2\right)^{\frac{1}{2}}$$

$$\alpha_1(h_c, \alpha_c, f_c, R_{C1}) := \operatorname{atan}\left(\frac{a_1(h_c, R_{C1})}{b_1(h_c, \alpha_c, f_c, R_{C1})}\right)$$

$$\beta_1(h_c, \alpha_c, f_c, R_{C1}) := \operatorname{asin}\left(\frac{R_{C1}}{c_1(h_c, \alpha_c, f_c, R_{C1})}\right)$$

$$\theta(h_c, \alpha_c, f_c, R_{C1}) := \alpha_1(h_c, \alpha_c, f_c, R_{C1}) + \beta_1(h_c, \alpha_c, f_c, R_{C1})$$

$$d_1(h_c, \alpha_c, f_c, R_{C1}) := \left(c_1(h_c, \alpha_c, f_c, R_{C1})^2 - {R_{C1}}^2\right)^{\frac{1}{2}}$$

$$k_1(h_c, \alpha_c, f_c, R_{C1}) := b_1(h_c, \alpha_c, f_c, R_{C1}) - g_1(\alpha_c, R_{C1})$$

Height of radius (z-direction)

$$l_1(h_c, \alpha_c, f_c, R_{C1}) := \frac{h_c}{2} - j_1(h_c, \alpha_c, R_{C1})$$

Length of one corrugation leg

$$l_s(h_c, \alpha_c, f_c, R_{C1}) := f_c + 2.R_{C1} \cdot \theta(h_c, \alpha_c, f_c, R_{C1}) + 2 \cdot d_1(h_c, \alpha_c, f_c, R_{C1})$$

Area, per unit width, of the corrugation cross-section, [m^2/m]

$$A_C(h_c, t_c, \alpha_c, f_c, R_{C1}) := \frac{l_s(h_c, \alpha_c, f_c, R_{C1}) \cdot t_c}{p(h_c, \alpha_c, f_c, R_{C1})}$$

Length of the inclined corrrugation leg

$$l_\alpha(h_c, \alpha_c, f_c, R_{C1}) := 2\, d_1(h_c, \alpha_c, f_c, R_{C1})$$

Length of cross-section

$$l_c(h_c, \alpha_c, f_c, R_{C1}) := 2 \cdot p(h_c, \alpha_c, f_c, R_{C1})$$

2.2. Cross-sectional constants

Area

Area of top face

$$A_{f.top}(h_c, t_{f.top}, \alpha_c, f_c, R_{C1}) := t_{f.top} \cdot l_c(h_c, \alpha_c, f_c, R_{C1})$$

Area of bottom face

$$A_{f.bot}(h_c, t_{f.bot}, \alpha_c, f_c, R_{C1}) := t_{f.bot} \cdot l_c(h_c, \alpha_c, f_c, R_{C1})$$

Area of one curved part

$$A_R(t_c, \alpha_c, R_{C1}) := R_{C1} \cdot \alpha_c \cdot t_c$$

Area of core

$$A_c(h_c, t_c, \alpha_c, f_c, R_{C1}) := 2 \cdot l_s(h_c, \alpha_c, f_c, R_{C1}) \cdot t_c$$

Total Area

$$\begin{aligned} A_{tot}(h_c, t_{f.top}, t_{f.bot}, t_c, \alpha_c, f_c, R_{C1}) := {} & A_{f.top}(h_c, t_{f.top}, \alpha_c, f_c, R_{C1}) \dots \\ & + A_{f.bot}(h_c, t_{f.bot}, \alpha_c, f_c, R_{C1}) \dots \\ & + A_c(h_c, t_c, \alpha_c, f_c, R_{C1}) \end{aligned}$$

Total area per unit width:

$$A(h_c, t_{f.top}, t_{f.bot}, t_c, \alpha_c, f_c, R_{C1}) := \frac{A_{tot}(h_c, t_{f.top}, t_{f.bot}, t_c, \alpha_c, f_c, R_{C1})}{l_c(h_c, \alpha_c, f_c, R_{C1})}$$

$$z_{na}(h_c, t_{f.top}, t_{f.bot}, t_c, \alpha_c, f_c, R_{C1}) := \frac{\left[\begin{array}{l} t_c \cdot f_c \cdot \left(\frac{t_{f.top}}{2} + \frac{t_c}{2}\right) \dots \\ + 2 \cdot t_c \cdot l_\alpha(h_c, \alpha_c, f_c, R_{C1}) \cdot \left(\frac{h_c}{2} + \frac{t_{f.top}}{2} + \frac{t_c}{2}\right) \dots \\ + 2\, A_R(t_c, \alpha_c, R_{C1}) \cdot \left(\frac{l_1(h_c, \alpha_c, f_c, R_{C1})}{2} + \frac{t_c}{2} + \frac{t_{f.top}}{2}\right) \dots \\ + 2\, A_R(t_c, \alpha_c, R_{C1}) \cdot \left[\begin{array}{l} \left(-\frac{l_1(h_c, \alpha_c, f_c, R_{C1})}{2} - \frac{t_c}{2}\right) \dots \\ + -\frac{t_{f.bot}}{2} + h(h_c, t_{f.top}, t_{f.bot}, t_c) \end{array}\right] \dots \\ + t_c \cdot f_c \cdot \left(\frac{t_{f.top}}{2} + \frac{t_c}{2} + h_c\right) \dots \\ + A_{f.bot}(h_c, t_{f.bot}, \alpha_c, f_c, R_{C1}) \cdot h(h_c, t_{f.top}, t_{f.bot}, t_c) \end{array}\right]}{A_{tot}(h_c, t_{f.top}, t_{f.bot}, t_c, \alpha_c, f_c, R_{C1})}$$

Moment of inertia

X-direction

Moment of inertia of the top face:

$$I_{f.top.x}(h_c, t_{f.top}, t_{f.bot}, t_c, \alpha_c, f_c, R_{C1}) := \frac{l_c(h_c, \alpha_c, f_c, R_{C1}) \cdot t_{f.top}^{\,3}}{12} \ldots + l_c(h_c, \alpha_c, f_c, R_{C1}) \cdot t_{f.top} \cdot \left(z_{na}(h_c, t_{f.top}, t_{f.bot}, t_c, \alpha_c, f_c, R_{C1})\right)^2$$

Moment of inertia of the top horisontal part of the core:

$$I_{c.top.x}(h_c, t_{f.top}, t_{f.bot}, t_c, \alpha_c, f_c, R_{C1}) := \frac{f_c \cdot t_c^{\,3}}{12} \ldots + f_c \cdot t_c \cdot \left[z_{na}(h_c, t_{f.top}, t_{f.bot}, t_c, \alpha_c, f_c, R_{C1}) + \left(-\frac{t_{f.top}}{2} - \frac{t_c}{2} \right) \right]^2$$

Moment of inertia of the inclined part of the core:

$$I_{inc.x}(h_c, t_{f.top}, t_{f.bot}, t_c, \alpha_c, f_c, R_{C1}) := 2 \cdot \frac{t_c \cdot l_\alpha(h_c, \alpha_c, f_c, R_{C1})^3}{12} \cdot \sin(\alpha_c)^2 \ldots + 2 t_c \cdot l_\alpha(h_c, \alpha_c, f_c, R_{C1}) \cdot \left[\begin{array}{l} \left(\frac{t_{f.top}}{2} + \frac{t_c}{2} + \frac{h_c}{2} \right) \ldots \\ + -z_{na}(h_c, t_{f.top}, t_{f.bot}, t_c, \alpha_c, f_c, R_{C1}) \end{array} \right]^2$$

Moment of inertia of the bottom horisontal part of the core:

$$I_{c.bot.x}(h_c, t_{f.top}, t_{f.bot}, t_c, \alpha_c, f_c, R_{C1}) := \frac{f_c \cdot t_c^{\,3}}{12} \ldots + f_c \cdot t_c \cdot \left(\frac{t_{f.top}}{2} + \frac{t_c}{2} + h_c - z_{na}(h_c, t_{f.top}, t_{f.bot}, t_c, \alpha_c, f_c, R_{C1}) \right)^2$$

Moment of inertia of upper curved parts:

$$I_{c.R.top}(h_c, t_{f.top}, t_{f.bot}, t_c, \alpha_c, f_c, R_{C1}) := 2 \cdot A_R(t_c, \alpha_c, R_{C1}) \cdot \left[\begin{array}{l} z_{na}(h_c, t_{f.top}, t_{f.bot}, t_c, \alpha_c, f_c, R_{C1}) \ldots \\ + -\left(\frac{l_1(h_c, \alpha_c, f_c, R_{C1})}{2} + \frac{t_c}{2} + \frac{t_{f.top}}{2} \right) \end{array} \right]^2$$

Moment of inertia of lower curved parts:

$$I_{c.R.bot}(h_c, t_{f.top}, t_{f.bot}, t_c, \alpha_c, f_c, R_{C1}) := 2 \cdot A_R(t_c, \alpha_c, R_{C1}) \cdot \left[\begin{array}{l} \left[\left(-\frac{l_1(h_c, \alpha_c, f_c, R_{C1})}{2} - \frac{t_c}{2} \right) - \frac{t_{f.bot}}{2} \ldots \right] \ldots \\ + h(h_c, t_{f.top}, t_{f.bot}, t_c) \\ + -z_{na}(h_c, t_{f.top}, t_{f.bot}, t_c, \alpha_c, f_c, R_{C1}) \end{array} \right]^2$$

Moment of inertia of the bottom flange:

$$I_{f.bot.x}(h_c, t_{f.top}, t_{f.bot}, t_c, \alpha_c, f_c, R_{C1}) := \frac{l_c(h_c, \alpha_c, f_c, R_{C1}) \cdot t_{f.bot}^{\,3}}{12} \ldots + l_c(h_c, \alpha_c, f_c, R_{C1}) \cdot t_{f.bot} \cdot \left(\begin{array}{l} h(h_c, t_{f.top}, t_{f.bot}, t_c) \ldots \\ + -z_{na}(h_c, t_{f.top}, t_{f.bot}, t_c, \alpha_c, f_c, R_{C1}) \end{array} \right)^2$$

Total moment of inertia of sandwich panel in x-direction:

$$I_{tot.x}(h_c, t_{f.top}, t_{f.bot}, t_c, \alpha_c, f_c, R_{C1}) := I_{f.top.x}(h_c, t_{f.top}, t_{f.bot}, t_c, \alpha_c, f_c, R_{C1}) \ldots + I_{c.top.x}(h_c, t_{f.top}, t_{f.bot}, t_c, \alpha_c, f_c, R_{C1}) \ldots + I_{inc.x}(h_c, t_{f.top}, t_{f.bot}, t_c, \alpha_c, f_c, R_{C1}) \ldots + I_{c.bot.x}(h_c, t_{f.top}, t_{f.bot}, t_c, \alpha_c, f_c, R_{C1}) \ldots + I_{f.bot.x}(h_c, t_{f.top}, t_{f.bot}, t_c, \alpha_c, f_c, R_{C1}) \ldots + I_{c.R.top}(h_c, t_{f.top}, t_{f.bot}, t_c, \alpha_c, f_c, R_{C1}) \ldots + I_{c.R.bot}(h_c, t_{f.top}, t_{f.bot}, t_c, \alpha_c, f_c, R_{C1})$$

Y-direction

Moment of inertia of the top face:

$$I_{f.top.y}(h_c, t_{f.top}, t_{f.bot}, t_c, \alpha_c, f_c, R_{C1}) := \frac{l_c(h_c, \alpha_c, f_c, R_{C1}) \cdot t_{f.top}^{3}}{12} \ldots + l_c(h_c, \alpha_c, f_c, R_{C1}) \cdot t_{f.top} \cdot z_{na}(h_c, t_{f.top}, t_{f.bot}, t_c, \alpha_c, f_c, R_{C1})^2$$

Moment of inertia of the bottom flange:

$$I_{f.bot.y}(h_c, t_{f.top}, t_{f.bot}, t_c, \alpha_c, f_c, R_{C1}) := \frac{l_c(h_c, \alpha_c, f_c, R_{C1}) \cdot t_{f.bot}^{3}}{12} \ldots + l_c(h_c, \alpha_c, f_c, R_{C1}) \cdot t_{f.bot} \cdot \left(h(h_c, t_{f.top}, t_{f.bot}, t_c) \ldots + -z_{na}(h_c, t_{f.top}, t_{f.bot}, t_c, \alpha_c, f_c, R_{C1}) \right)^2$$

Total moment of inertia of sanwich panel in y-direction:

$$I_{tot.y}(h_c, t_{f.top}, t_{f.bot}, t_c, \alpha_c, f_c, R_{C1}) := I_{f.top.y}(h_c, t_{f.top}, t_{f.bot}, t_c, \alpha_c, f_c, R_{C1}) \ldots + I_{f.bot.y}(h_c, t_{f.top}, t_{f.bot}, t_c, \alpha_c, f_c, R_{C1})$$

Moment of inertia in x- and y-direction per unit width [m^4/m]

$$I_x(h_c, t_{f.top}, t_{f.bot}, t_c, \alpha_c, f_c, R_{C1}) := \frac{I_{tot.x}(h_c, t_{f.top}, t_{f.bot}, t_c, \alpha_c, f_c, R_{C1})}{l_c(h_c, \alpha_c, f_c, R_{C1})}$$

$$I_y(h_c, t_{f.top}, t_{f.bot}, t_c, \alpha_c, f_c, R_{C1}) := \frac{I_{tot.y}(h_c, t_{f.top}, t_{f.bot}, t_c, \alpha_c, f_c, R_{C1})}{l_c(h_c, \alpha_c, f_c, R_{C1})}$$

2.3. Elastic stiffness constants

The elastic constants are calculated according to "*Elastic constants for corrugated-core*" by C.Libove & R.Hubka. All constants are calculated per unit width of the plate.

2.3.1. Axial Stiffness, Ex & Ey

Axial stiffness in the stiff direction per unit width:

$$E_x\left(h_c, t_{f.top}, t_{f.bot}, t_c, \alpha_c, f_c, R_{C1}\right) := E \cdot A\left(h_c, t_{f.top}, t_{f.bot}, t_c, \alpha_c, f_c, R_{C1}\right)$$

Axial stiffness in the weak direction per unit width:

$$E_y\left(h_c, t_{f.top}, t_{f.bot}, t_c, \alpha_c, f_c, R_{C1}\right) := \frac{E \cdot \left(t_{f.top} + t_{f.bot}\right)}{1 - \nu^2 \left[1 - \frac{E \cdot \left(t_{f.top} + t_{f.bot}\right)}{E_x\left(h_c, t_{f.top}, t_{f.bot}, t_c, \alpha_c, f_c, R_{C1}\right)}\right]}$$

2.3.2. Horizontal shear stiffness, Gxy

$$GA\left(h_c, t_{f.top}, t_{f.bot}, t_c, \alpha_c, f_c, R_{C1}\right) := G \cdot t_{f.top} + \frac{G \cdot {t_c}^2}{A_C\left(h_c, t_c, \alpha_c, f_c, R_{C1}\right)} + G \cdot t_{f.bot}$$

Horizontal shear stiffness per unit width:

$$G_{xy}\left(h_c, t_{f.top}, t_{f.bot}, t_c, \alpha_c, f_c, R_{C1}\right) := GA\left(h_c, t_{f.top}, t_{f.bot}, t_c, \alpha_c, f_c, R_{C1}\right)$$

2.3.3. Bending Stiffness, Dx & Dy

Bending stiffness in the stiff direction per unit width

$$D_x\left(h_c, t_{f.top}, t_{f.bot}, t_c, \alpha_c, f_c, R_{C1}\right) := E \cdot I_x\left(h_c, t_{f.top}, t_{f.bot}, t_c, \alpha_c, f_c, R_{C1}\right)$$

Bending stiffness in the weak direction per unit width

$$D_y\left(h_c, t_{f.top}, t_{f.bot}, t_c, \alpha_c, f_c, R_{C1}\right) := \frac{E \cdot I_y\left(h_c, t_{f.top}, t_{f.bot}, t_c, \alpha_c, f_c, R_{C1}\right)}{1 - \nu^2 \left(1 - \frac{E \cdot I_y\left(h_c, t_{f.top}, t_{f.bot}, t_c, \alpha_c, f_c, R_{C1}\right)}{D_x\left(h_c, t_{f.top}, t_{f.bot}, t_c, \alpha_c, f_c, R_{C1}\right)}\right)}$$

2.3.4. Torsional stiffness, Dxy

$$k_c = \frac{1}{2}\cdot\left(1 + \frac{A_1 - A_2}{2\cdot p\cdot h}\right)$$

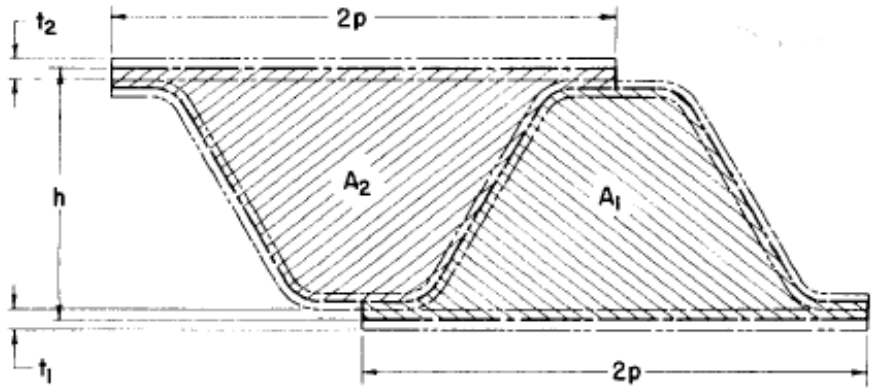

$$k_c\left(h_c, t_{f.top}, t_{f.bot}, t_c\right) := \frac{1}{2}\left(1 + \frac{t_{f.bot} - t_{f.top}}{2\cdot h\left(h_c, t_{f.top}, t_{f.bot}, t_c\right)}\right)$$

$$k_{GJ}\left(h_c, t_{f.top}, t_{f.bot}, t_c, \alpha_c, f_c, R_{C1}\right) := \frac{\frac{G\cdot {t_c}^2\cdot k_c\left(h_c, t_{f.top}, t_{f.bot}, t_c\right)}{A_C\left(h_c, t_c, \alpha_c, f_c, R_{C1}\right)} + G\cdot t_{f.bot}}{GA\left(h_c, t_{f.top}, t_{f.bot}, t_c, \alpha_c, f_c, R_{C1}\right)}$$

$$GJ\left(h_c, t_{f.top}, t_{f.bot}, t_c, \alpha_c, f_c, R_{C1}\right) := \left[\begin{array}{l} G\cdot t_{f.top}\cdot k_{GJ}\left(h_c, t_{f.top}, t_{f.bot}, t_c, \alpha_c, f_c, R_{C1}\right)^2 \ldots \\ + \frac{G\cdot {t_c}^2}{A_C\left(h_c, t_c, \alpha_c, f_c, R_{C1}\right)}\cdot\left(\begin{array}{l} k_{GJ}\left(h_c, t_{f.top}, t_{f.bot}, t_c, \alpha_c, f_c, R_{C1}\right) \ldots \\ + -k_c\left(h_c, t_{f.top}, t_{f.bot}, t_c\right) \end{array}\right)^2 \ldots \\ + G\cdot t_{f.bot}\cdot\left(1 - k_{GJ}\left(h_c, t_{f.top}, t_{f.bot}, t_c, \alpha_c, f_c, R_{C1}\right)\right)^2 \end{array}\right]\cdot h\left(h_c, t_{f.top}, t_{f.bot}, t_c\right)^2$$

Torsional stiffness per unit width:

$$D_{xy}\left(h_c, t_{f.top}, t_{f.bot}, t_c, \alpha_c, f_c, R_{C1}\right) := 2\cdot GJ\left(h_c, t_{f.top}, t_{f.bot}, t_c, \alpha_c, f_c, R_{C1}\right)$$

2.3.5. Transverse shear stiffness parallel to the corrugation, DQx

Area, per unit width, of the corrugation cross-section, [m^2/m]

$$A_{c.x}\left(h_c, t_c, \alpha_c, f_c, R_{C1}\right) := \frac{l_s\left(h_c, \alpha_c, f_c, R_{C1}\right) \cdot t_c}{p\left(h_c, \alpha_c, f_c, R_{C1}\right)}$$

Transverse shear stiffness parallel to the corrugation per unit width

$$D_{Qx}\left(h_c, t_{f.top}, t_{f.bot}, t_c, \alpha_c, f_c, R_{C1}\right) := \frac{G \cdot {t_c}^2}{A_{c.x}\left(h_c, t_c, \alpha_c, f_c, R_{C1}\right)} \cdot \left(\frac{h\left(h_c, t_{f.top}, t_{f.bot}, t_c\right)}{p\left(h_c, \alpha_c, f_c, R_{C1}\right)} \right)^2$$

2.3.6. Transverse shear stiffness perpendicular to the corrugation, DQy

The tranverse shear stiffness perpendicular to the corrugation per unit width is calculated as

$$D_{Qy} = S \cdot h \left(\frac{E}{1 - {\nu_c}^2} \right) \left(\frac{t_c}{h_c} \right)^3$$

where S is a non-dimensional cofieceint.

Nondimensional coefficient S

The non-dimensional coefficient S is calculated for symmetrical corrugation of the sandwich panel but allows for different thicknesses of the top and bottom plate.

K values

The K values are non-dimensional functions of the corrugation shape

$$K_{Iz}(h_c,\alpha_c,f_c,R_{C1}) := \frac{2}{3}\cdot\left(\frac{k_1(h_c,\alpha_c,f_c,R_{C1})}{h_c}\right)^2\cdot\frac{d_1(h_c,\alpha_c,f_c,R_{C1})}{h_c}\ \ldots$$
$$+\frac{2}{3}\cdot\left[\frac{1}{8}\cdot\left(\frac{p(h_c,\alpha_c,f_c,R_{C1})}{h_c}\right)^3-\left(\frac{b_1(h_c,\alpha_c,f_c,R_{C1})}{h_c}\right)^3\right]\ \ldots$$
$$+2\cdot\frac{R_{C1}}{h_c}\cdot\left[\frac{b_1(h_c,\alpha_c,f_c,R_{C1})}{h_c}\cdot\left[\begin{array}{l}\theta(h_c,\alpha_c,f_c,R_{C1})\cdot\dfrac{b_1(h_c,\alpha_c,f_c,R_{C1})}{h_c}\ \ldots\\ +-2\cdot\left(\dfrac{R_{C1}}{h_c}-\dfrac{e_1(\alpha_c,R_{C1})}{h_c}\right)\end{array}\right]\ \ldots\right.$$
$$\left.+\frac{1}{2}\cdot\left[\begin{array}{l}\theta(h_c,\alpha_c,f_c,R_{C1})\cdot\left(\dfrac{R_{C1}}{h_c}\right)^2\ \ldots\\ +-\dfrac{g_1(\alpha_c,R_{C1})}{h_c}\cdot\dfrac{e_1(\alpha_c,R_{C1})}{h_c}\end{array}\right]\right]$$

$$K_{Iyz}(h_c,\alpha_c,f_c,R_{C1}) := \frac{2}{3}\cdot\frac{j_1(h_c,\alpha_c,R_{C1})}{h_c}\cdot\frac{k_1(h_c,\alpha_c,f_c,R_{C1})}{h_c}\cdot\frac{d_1(h_c,\alpha_c,f_c,R_{C1})}{h_c}\ \ldots$$
$$+\frac{1}{2}\cdot\left[\frac{1}{4}\cdot\left(\frac{p(h_c,\alpha_c,f_c,R_{C1})}{h_c}\right)^2-\left(\frac{b_1(h_c,\alpha_c,f_c,R_{C1})}{h_c}\right)^2\right]\ \ldots$$
$$+2\cdot\frac{R_{C1}}{h_c}\cdot\left[\frac{a_1(h_c,R_{C1})}{h_c}\cdot\left[\begin{array}{l}\theta(h_c,\alpha_c,f_c,R_{C1})\cdot\dfrac{b_1(h_c,\alpha_c,f_c,R_{C1})}{h_c}\ \ldots\\ +\dfrac{e_1(\alpha_c,R_{C1})}{h_c}-\dfrac{R_{C1}}{h_c}\end{array}\right]\ \ldots\right.$$
$$\left.+\frac{g_1(\alpha_c,R_{C1})}{h_c}\cdot\left[\begin{array}{l}\dfrac{b_1(h_c,\alpha_c,f_c,R_{C1})}{h_c}\ \ldots\\ +-\dfrac{1}{2}\cdot\dfrac{g_1(\alpha_c,R_{C1})}{h_c}\end{array}\right]\right]$$

$$K_{Iy}(h_c,\alpha_c,f_c,R_{C1}) := \frac{2}{3}\cdot\left(\frac{j_1(h_c,\alpha_c,R_{C1})}{h_c}\right)^2\cdot\frac{d_1(h_c,\alpha_c,f_c,R_{C1})}{h_c}+\frac{1}{4}\cdot\frac{f_c}{h_c}\ \ldots$$
$$+2\cdot\frac{R_{C1}}{h_c}\cdot\left[\frac{a_1(h_c,R_{C1})}{h_c}\cdot\left[\begin{array}{l}\theta(h_c,\alpha_c,f_c,R_{C1})\cdot\dfrac{a_1(h_c,R_{C1})}{h_c}\ \ldots\\ +2\cdot\dfrac{g_1(\alpha_c,R_{C1})}{h_c}\end{array}\right]\ \ldots\right.$$
$$\left.+\frac{1}{2}\cdot\left[\begin{array}{l}\theta(h_c,\alpha_c,f_c,R_{C1})\cdot\left(\dfrac{R_{C1}}{h_c}\right)^2\ \ldots\\ +\dfrac{g_1(\alpha_c,R_{C1})}{h_c}\cdot\dfrac{e_1(\alpha_c,R_{C1})}{h_c}\end{array}\right]\right]$$

$$K_L(h_c,\alpha_c,f_c,R_{C1}) := 2\cdot\frac{d_1(h_c,\alpha_c,f_c,R_{C1})}{h_c} + 2\cdot\theta(h_c,\alpha_c,f_c,R_{C1})\cdot\frac{R_{C1}}{h_c} + \frac{f_c}{h_c}$$

$$K_{Ly}(h_c,\alpha_c,f_c,R_{C1}) := \frac{f_c}{h_c} + 2\cdot\frac{d_1(h_c,\alpha_c,f_c,R_{C1})}{h_c}\cdot\cos(\theta(h_c,\alpha_c,f_c,R_{C1}))^2 \ldots + \frac{R_{C1}}{h_c}\cdot\begin{pmatrix}\theta(h_c,\alpha_c,f_c,R_{C1}) \ldots \\ +\sin(\theta(h_c,\alpha_c,f_c,R_{C1}))\cdot\cos(\theta(h_c,\alpha_c,f_c,R_{C1}))\end{pmatrix}$$

$$K_{Lyz}(h_c,\alpha_c,f_c,R_{C1}) := 2\cdot\frac{d_1(h_c,\alpha_c,f_c,R_{C1})}{h_c}\cdot\sin(\theta(h_c,\alpha_c,f_c,R_{C1}))\cdot\cos(\theta(h_c,\alpha_c,f_c,R_{C1})) \ldots + \frac{R_{C1}}{h_c}\cdot\sin(\theta(h_c,\alpha_c,f_c,R_{C1}))^2$$

$$K_{Lz}(h_c,\alpha_c,f_c,R_{C1}) := 2\cdot\frac{d_1(h_c,\alpha_c,f_c,R_{C1})}{h_c}\cdot\sin(\theta(h_c,\alpha_c,f_c,R_{C1}))^2 \ldots + \frac{R_{C1}}{h_c}\cdot\begin{pmatrix}\theta(h_c,\alpha_c,f_c,R_{C1}) \ldots \\ +-\sin(\theta(h_c,\alpha_c,f_c,R_{C1}))\cdot\cos(\theta(h_c,\alpha_c,f_c,R_{C1}))\end{pmatrix}$$

C values

$$C_1(h_c, t_{f.top}, t_c, \alpha_c, f_c, R_{C1}) := K_L(h_c, \alpha_c, f_c, R_{C1}) + \frac{1}{3}\cdot\left(\frac{t_c}{t_{f.top}}\right)^3\cdot\frac{p(h_c, \alpha_c, f_c, R_{C1})}{h_c}$$

$$C_2(h_c, \alpha_c, f_c, R_{C1}) := \frac{k_y}{2}\cdot\frac{p(h_c, \alpha_c, f_c, R_{C1})}{h_c}\cdot K_L(h_c, \alpha_c, f_c, R_{C1})$$

$$\begin{aligned} C_3(h_c, t_c, \alpha_c, f_c, R_{C1}) := {} & K_{Iz}(h_c, \alpha_c, f_c, R_{C1}) \ldots \\ & + k_y\cdot\frac{p(h_c, \alpha_c, f_c, R_{C1})}{h_c}\cdot\left(\frac{k_y}{4}\cdot\frac{p(h_c, \alpha_c, f_c, R_{C1})}{h_c}\cdot K_L(h_c, \alpha_c, f_c, R_{C1})\right) \ldots \\ & + \frac{1}{12}\cdot\left(\frac{t_c}{h_c}\right)^2\cdot K_{Lz}(h_c, \alpha_c, f_c, R_{C1}) \end{aligned}$$

$$\begin{aligned} C_4(h_c, t_{f.top}, t_c, \alpha_c, f_c, R_{C1}) := {} & K_{Iyz}(h_c, \alpha_c, f_c, R_{C1}) \ldots \\ & + \frac{1}{2}\cdot\left[k_z + \left(1 + \frac{t_{f.top}}{t_c}\right)\cdot\frac{t_c}{h_c}\right]\cdot\left(\frac{k_y}{2}\cdot\frac{p(h_c, \alpha_c, f_c, R_{C1})}{h_c}\cdot K_L(h_c, \alpha_c, f_c, R_{C1})\right) \ldots \\ & + -\frac{1}{12}\cdot\left(\frac{t_c}{h_c}\right)^2\cdot K_{Lyz}(h_c, \alpha_c, f_c, R_{C1}) \end{aligned}$$

$$C_5(h_c, t_{f.top}, t_c, \alpha_c, f_c, R_{C1}) := \frac{1}{2}\cdot\left[k_z + \left(1 + \frac{t_{f.top}}{t_c}\right)\cdot\frac{t_c}{h_c}\right]\cdot K_L(h_c, \alpha_c, f_c, R_{C1})$$

$$\begin{aligned} C_6(h_c, t_{f.top}, t_c, \alpha_c, f_c, R_{C1}) := {} & K_{Iy}(h_c, \alpha_c, f_c, R_{C1}) \ldots \\ & + \left[k_z + \left(1 + \frac{t_{f.top}}{t_c}\right)\cdot\frac{t_c}{h_c}\right]\cdot\left[\frac{1}{4}\cdot\left[k_z + \left(1 + \frac{t_{f.top}}{t_c}\right)\cdot\frac{t_c}{h_c}\right]\cdot K_L(h_c, \alpha_c, f_c, R_{C1})\right] \ldots \\ & + \frac{1}{12}\cdot\left(\frac{t_c}{h_c}\right)^2\cdot K_{Ly}(h_c, \alpha_c, f_c, R_{C1}) \end{aligned}$$

$$C_7(t_{f.bot}, t_c) := \left(\frac{t_{f.bot}}{t_c}\right)^3$$

Non-dimensional cofficient S

$$S(h_c, t_{f.top}, t_{f.bot}, t_c, \alpha_c, f_c, R_{C1}) :=$$

$$\frac{\begin{aligned}&3\cdot\frac{h_c}{p(h_c,\alpha_c,f_c,R_{C1})}\cdot C_7(t_{f.bot},t_c)\cdot\left(C_2(h_c,\alpha_c,f_c,R_{C1})^2 - C_1(h_c,t_{f.top},t_c,\alpha_c,f_c,R_{C1})\cdot C_3(h_c,t_c,\alpha_c,f_c,R_{C1})\right)\dots\\&+-C_3(h_c,t_c,\alpha_c,f_c,R_{C1}) + \frac{p(h_c,\alpha_c,f_c,R_{C1})}{h_c}\cdot\left(2\cdot C_2(h_c,\alpha_c,f_c,R_{C1}) - \frac{p(h_c,\alpha_c,f_c,R_{C1})}{h_c}\cdot C_1(h_c,t_{f.top},t_c,\alpha_c,f_c,R_{C1})\right)\end{aligned}}{\begin{aligned}&12\cdot\left[2\cdot\frac{p(h_c,\alpha_c,f_c,R_{C1})}{h_c}\cdot\left[\frac{p(h_c,\alpha_c,f_c,R_{C1})}{h_c}\cdot\begin{pmatrix}C_1(h_c,t_{f.top},t_c,\alpha_c,f_c,R_{C1})\cdot C_4(h_c,t_{f.top},t_c,\alpha_c,f_c,R_{C1})\dots\\+-C_2(h_c,\alpha_c,f_c,R_{C1})\cdot C_5(h_c,t_{f.top},t_c,\alpha_c,f_c,R_{C1})\end{pmatrix}\dots\right]\dots\right.\\&+-\begin{pmatrix}C_2(h_c,\alpha_c,f_c,R_{C1})\cdot C_4(h_c,t_{f.top},t_c,\alpha_c,f_c,R_{C1})\dots\\+-C_3(h_c,t_c,\alpha_c,f_c,R_{C1})\cdot C_5(h_c,t_{f.top},t_c,\alpha_c,f_c,R_{C1})\end{pmatrix}\\&+\frac{h_c}{h(h_c,t_{f.top},t_{f.bot},t_c)}\cdot\left[3\cdot C_7(t_{f.bot},t_c)\cdot\left[C_4(h_c,t_{f.top},t_c,\alpha_c,f_c,R_{C1})\cdot\begin{pmatrix}C_1(h_c,t_{f.top},t_c,\alpha_c,f_c,R_{C1})\cdot C_4(h_c,t_{f.top},t_c,\alpha_c,f_c,R_{C1})\dots\\+-2\cdot C_2(h_c,\alpha_c,f_c,R_{C1})\cdot C_5(h_c,t_{f.top},t_c,\alpha_c,f_c,R_{C1})\end{pmatrix}\dots\right]\dots\right.\\&\quad+C_3(h_c,t_c,\alpha_c,f_c,R_{C1})\cdot C_5(h_c,t_{f.top},t_c,\alpha_c,f_c,R_{C1})^2\dots\\&\quad+-C_6(h_c,t_{f.top},t_c,\alpha_c,f_c,R_{C1})\cdot\begin{pmatrix}C_1(h_c,t_{f.top},t_c,\alpha_c,f_c,R_{C1})\cdot C_3(h_c,t_c,\alpha_c,f_c,R_{C1})\dots\\+-C_2(h_c,\alpha_c,f_c,R_{C1})^2\end{pmatrix}\\&\quad+\frac{p(h_c,\alpha_c,f_c,R_{C1})}{h_c}\cdot\left(C_4(h_c,t_{f.top},t_c,\alpha_c,f_c,R_{C1})^2 - C_3(h_c,t_c,\alpha_c,f_c,R_{C1})\cdot C_6(h_c,t_{f.top},t_c,\alpha_c,f_c,R_{C1})\right)\dots\\&\quad+2\cdot\left(\frac{p(h_c,\alpha_c,f_c,R_{C1})}{h_c}\right)^2\cdot\begin{pmatrix}C_2(h_c,\alpha_c,f_c,R_{C1})\cdot C_6(h_c,t_{f.top},t_c,\alpha_c,f_c,R_{C1})\dots\\+-C_4(h_c,t_{f.top},t_c,\alpha_c,f_c,R_{C1})\cdot C_5(h_c,t_{f.top},t_c,\alpha_c,f_c,R_{C1})\end{pmatrix}\dots\\&\quad+\left(\frac{p(h_c,\alpha_c,f_c,R_{C1})}{h_c}\right)^3\cdot\begin{pmatrix}C_5(h_c,t_{f.top},t_c,\alpha_c,f_c,R_{C1})^2\dots\\+-C_1(h_c,t_{f.top},t_c,\alpha_c,f_c,R_{C1})\cdot C_6(h_c,t_{f.top},t_c,\alpha_c,f_c,R_{C1})\end{pmatrix}\\&\left.+\frac{h(h_c,t_{f.top},t_{f.bot},t_c)}{h_c}\cdot\frac{p(h_c,\alpha_c,f_c,R_{C1})}{h_c}\cdot\left(C_2(h_c,\alpha_c,f_c,R_{C1})^2 - C_1(h_c,t_{f.top},t_c,\alpha_c,f_c,R_{C1})\cdot C_3(h_c,t_c,\alpha_c,f_c,R_{C1})\right)\right]\end{aligned}}$$

Transverse shear stiffness perpendicular to the corrugation per unit width

$$D_{Qy}(h_c, t_{f.top}, t_{f.bot}, t_c, \alpha_c, f_c, R_{C1}) := S(h_c, t_{f.top}, t_{f.bot}, t_c, \alpha_c, f_c, R_{C1})\cdot h(h_c, t_{f.top}, t_{f.bot}, t_c)\cdot\left(\frac{E}{1-\nu^2}\right)\left(\frac{t_c}{h_c}\right)^3$$

2.4 Poisson's ratios

$$\nu_{xy} := \nu = 0.187$$

$$\nu_{yx}(h_c, t_{f.top}, t_{f.bot}, t_c, \alpha_c, f_c, R_{C1}) := \nu_{xy}\cdot\frac{D_y(h_c, t_{f.top}, t_{f.bot}, t_c, \alpha_c, f_c, R_{C1})}{D_x(h_c, t_{f.top}, t_{f.bot}, t_c, \alpha_c, f_c, R_{C1})}$$

$$\nu_{xp} := \nu_{xy}$$

$$\nu_{yp}(h_c, t_{f.top}, t_{f.bot}, t_c, \alpha_c, f_c, R_{C1}) := \nu_{xp}\cdot\frac{E_y(h_c, t_{f.top}, t_{f.bot}, t_c, \alpha_c, f_c, R_{C1})}{E_x(h_c, t_{f.top}, t_{f.bot}, t_c, \alpha_c, f_c, R_{C1})}$$

2.5 Stiffness constants (general shell stiffness matrix)

First the stiffness constants are calculated, these are the same as the abaqus constants (chapter 9).

In-plane constants

$$D_{11}(h_c, t_{f.top}, t_{f.bot}, t_c, \alpha_c, f_c, R_{C1}) := \frac{E_x(h_c, t_{f.top}, t_{f.bot}, t_c, \alpha_c, f_c, R_{C1})}{1 - \nu_{xp} \cdot \nu_{yp}(h_c, t_{f.top}, t_{f.bot}, t_c, \alpha_c, f_c, R_{C1})}$$

$$D_{12}(h_c, t_{f.top}, t_{f.bot}, t_c, \alpha_c, f_c, R_{C1}) := \frac{\nu_{xp} \cdot E_y(h_c, t_{f.top}, t_{f.bot}, t_c, \alpha_c, f_c, R_{C1})}{1 - \nu_{xp} \cdot \nu_{yp}(h_c, t_{f.top}, t_{f.bot}, t_c, \alpha_c, f_c, R_{C1})}$$

$$D_{21}(h_c, t_{f.top}, t_{f.bot}, t_c, \alpha_c, f_c, R_{C1}) := \frac{\nu_{yp}(h_c, t_{f.top}, t_{f.bot}, t_c, \alpha_c, f_c, R_{C1}) \cdot E_x(h_c, t_{f.top}, t_{f.bot}, t_c, \alpha_c, f_c, R_{C1})}{1 - \nu_{xp} \cdot \nu_{yp}(h_c, t_{f.top}, t_{f.bot}, t_c, \alpha_c, f_c, R_{C1})}$$

$$D_{22}(h_c, t_{f.top}, t_{f.bot}, t_c, \alpha_c, f_c, R_{C1}) := \frac{E_y(h_c, t_{f.top}, t_{f.bot}, t_c, \alpha_c, f_c, R_{C1})}{1 - \nu_{xp} \cdot \nu_{yp}(h_c, t_{f.top}, t_{f.bot}, t_c, \alpha_c, f_c, R_{C1})}$$

$$D_{33}(h_c, t_{f.top}, t_{f.bot}, t_c, \alpha_c, f_c, R_{C1}) := G_{xy}(h_c, t_{f.top}, t_{f.bot}, t_c, \alpha_c, f_c, R_{C1})$$

Out-of-plane constants

$$D_{44}(h_c, t_{f.top}, t_{f.bot}, t_c, \alpha_c, f_c, R_{C1}) := \frac{D_x(h_c, t_{f.top}, t_{f.bot}, t_c, \alpha_c, f_c, R_{C1})}{1 - \nu_{xy} \cdot \nu_{yx}(h_c, t_{f.top}, t_{f.bot}, t_c, \alpha_c, f_c, R_{C1})}$$

$$D_{45}(h_c, t_{f.top}, t_{f.bot}, t_c, \alpha_c, f_c, R_{C1}) := \frac{\nu_{xy} \cdot D_y(h_c, t_{f.top}, t_{f.bot}, t_c, \alpha_c, f_c, R_{C1})}{1 - \nu_{xy} \cdot \nu_{yx}(h_c, t_{f.top}, t_{f.bot}, t_c, \alpha_c, f_c, R_{C1})}$$

$$D_{54}(h_c, t_{f.top}, t_{f.bot}, t_c, \alpha_c, f_c, R_{C1}) := \frac{\nu_{yx}(h_c, t_{f.top}, t_{f.bot}, t_c, \alpha_c, f_c, R_{C1}) \cdot D_x(h_c, t_{f.top}, t_{f.bot}, t_c, \alpha_c, f_c, R_{C1})}{1 - \nu_{xy} \cdot \nu_{yx}(h_c, t_{f.top}, t_{f.bot}, t_c, \alpha_c, f_c, R_{C1})}$$

$$D_{55}(h_c, t_{f.top}, t_{f.bot}, t_c, \alpha_c, f_c, R_{C1}) := \frac{D_y(h_c, t_{f.top}, t_{f.bot}, t_c, \alpha_c, f_c, R_{C1})}{1 - \nu_{xy} \cdot \nu_{yx}(h_c, t_{f.top}, t_{f.bot}, t_c, \alpha_c, f_c, R_{C1})}$$

$$D_{66}(h_c, t_{f.top}, t_{f.bot}, t_c, \alpha_c, f_c, R_{C1}) := \frac{D_{xy}(h_c, t_{f.top}, t_{f.bot}, t_c, \alpha_c, f_c, R_{C1})}{2}$$

$$K_{11}(h_c, t_{f.top}, t_{f.bot}, t_c, \alpha_c, f_c, R_{C1}) := D_{Qx}(h_c, t_{f.top}, t_{f.bot}, t_c, \alpha_c, f_c, R_{C1})$$

$$K_{22}(h_c, t_{f.top}, t_{f.bot}, t_c, \alpha_c, f_c, R_{C1}) := D_{Qy}(h_c, t_{f.top}, t_{f.bot}, t_c, \alpha_c, f_c, R_{C1})$$

2.6 Total material volume in sandwich panel

$$V(h_c, t_{f.top}, t_{f.bot}, t_c, \alpha_c, f_c, R_{C1}) := A(h_c, t_{f.top}, t_{f.bot}, t_c, \alpha_c, f_c, R_{C1}) \cdot B \cdot L$$

2. Sandwich panel

3. Local bending

3. Local bending

The local bending of the top plate is calulated by treating the top plate as a fixed beam with 50 mm width and the length equal to the free span between two corrugations. An imposed point load is applied in the middle of the beam. The load is given in Eurocode as an imposed local load for floors. Self-weight is neglected.

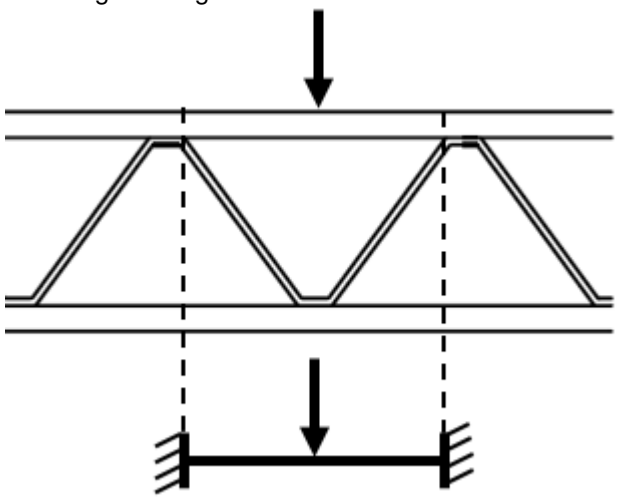

$$Q_{local} := \gamma_{Q.ULS} \cdot Q_k = 3 \cdot kN$$

Local moment:

$$M_{Ed.local}(h_c, t_{f.top}, \alpha_c, f_c, R_{C1}) := \frac{Q_{local} \cdot (l_c(h_c, \alpha_c, f_c, R_{C1}) - f_c)}{8}$$

Local moment capacity

$$W_{top}(t_{f.top}) := \frac{50mm \cdot t_{f.top}^{2}}{6}$$

$$M_{Rd.local}(t_{f.top}) := W_{top}(t_{f.top}) \cdot k_{mod} \cdot \frac{f_m}{\gamma_M}$$

3. Local bending

4. Deflection of sandwich panel

The deflection of the sandwich panel is calculated with the analytical solution for deflection of a simply supported plate. The analytical solution was obtained from " *Elasto-plasto analysis of corrugated sandwich steel panels*" W.Chang.

Loads

Total weight of the section:

$$G_{ssp}(h_c, t_{f.top}, t_{f.bot}, t_c, \alpha_c, f_c, R_{C1}) := A(h_c, t_{f.top}, t_{f.bot}, t_c, \alpha_c, f_c, R_{C1}) \cdot \rho$$

Self-weight per unit width:

$$q_{self}(h_c, t_{f.top}, t_{f.bot}, t_c, \alpha_c, f_c, R_{C1}) := G_{ssp}(h_c, t_{f.top}, t_{f.bot}, t_c, \alpha_c, f_c, R_{C1}) \cdot g$$

Distributed load

$$q_d(h_c, t_{f.top}, t_{f.bot}, t_c, \alpha_c, f_c, R_{C1}) := \gamma_{Q.SLS} \cdot q_k + \gamma_{G.SLS} \cdot (q_{self}(h_c, t_{f.top}, t_{f.bot}, t_c, \alpha_c, f_c, R_{C1}) + q_{dw})$$

Uniformly distributed load

Load used in the optimisation:

$$q_{ijC}(i, j, h_c, t_{f.top}, t_{f.bot}, t_c, \alpha_c, f_c, R_{C1}) := \frac{4 \cdot q_d(h_c, t_{f.top}, t_{f.bot}, t_c, \alpha_c, f_c, R_{C1})}{i \cdot j \, \pi^2} \cdot \left[1 - (-1)^i\right] \cdot \left[1 - (-1)^j\right]$$

Point load

$$x_1 := \frac{L}{2} = 7\,\text{m} \qquad y_1 := \frac{B}{2} = 3.5\,\text{m}$$

$$Q_1(i, j) := \frac{4 \cdot Q_{1kN}}{L \cdot B} \cdot \sin\left(\frac{i \cdot \pi \cdot x_1}{L}\right) \cdot \sin\left(\frac{j \cdot \pi \cdot y_1}{B}\right)$$

Deflection

Coefficients used in deflection formula

$$D_{xx}(h_c, t_{f.top}, t_{f.bot}, t_c, \alpha_c, f_c, R_{C1}) := \frac{D_x(h_c, t_{f.top}, t_{f.bot}, t_c, \alpha_c, f_c, R_{C1})}{1 - \nu_{xy} \cdot \nu_{yx}(h_c, t_{f.top}, t_{f.bot}, t_c, \alpha_c, f_c, R_{C1})}$$

$$D_{yy}(h_c, t_{f.top}, t_{f.bot}, t_c, \alpha_c, f_c, R_{C1}) := \frac{D_y(h_c, t_{f.top}, t_{f.bot}, t_c, \alpha_c, f_c, R_{C1})}{1 - \nu_{xy} \cdot \nu_{yx}(h_c, t_{f.top}, t_{f.bot}, t_c, \alpha_c, f_c, R_{C1})}$$

$$w_{ij}\left(h_c, t_{f.top}, t_{f.bot}, t_c, \alpha_c, f_c, R_{C1}, i, j\right) :=$$

$$\frac{L^2 B^2 \cdot \left(\begin{array}{l}
2 \cdot D_{Qx}(h_c, t_{f.top}, t_{f.bot}, t_c, \alpha_c, f_c, R_{C1}) \cdot D_{Qy}(h_c, t_{f.top}, t_{f.bot}, t_c, \alpha_c, f_c, R_{C1}) \cdot L^4 \cdot B^4 \ldots \\
+ D_{xx}(h_c, t_{f.top}, t_{f.bot}, t_c, \alpha_c, f_c, R_{C1}) \cdot D_{xy}(h_c, t_{f.top}, t_{f.bot}, t_c, \alpha_c, f_c, R_{C1}) \cdot \pi^4 \cdot B^4 \cdot i^4 \ldots \\
+ D_{xy}(h_c, t_{f.top}, t_{f.bot}, t_c, \alpha_c, f_c, R_{C1}) \cdot D_{yy}(h_c, t_{f.top}, t_{f.bot}, t_c, \alpha_c, f_c, R_{C1}) \cdot \pi^4 \cdot L^4 \cdot j^4 \ldots \\
+ D_{Qx}(h_c, t_{f.top}, t_{f.bot}, t_c, \alpha_c, f_c, R_{C1}) \cdot D_{xy}(h_c, t_{f.top}, t_{f.bot}, t_c, \alpha_c, f_c, R_{C1}) \cdot \pi^2 \cdot L^2 \cdot B^4 \cdot i^2 \ldots \\
+ 2 \cdot D_{Qy}(h_c, t_{f.top}, t_{f.bot}, t_c, \alpha_c, f_c, R_{C1}) \cdot D_{xx}(h_c, t_{f.top}, t_{f.bot}, t_c, \alpha_c, f_c, R_{C1}) \cdot \pi^2 \cdot L^2 \cdot B^4 \cdot i^2 \ldots \\
+ D_{Qy}(h_c, t_{f.top}, t_{f.bot}, t_c, \alpha_c, f_c, R_{C1}) \cdot D_{xy}(h_c, t_{f.top}, t_{f.bot}, t_c, \alpha_c, f_c, R_{C1}) \cdot \pi^2 \cdot L^4 \cdot B^2 \cdot j^2 \ldots \\
+ 2 \cdot D_{Qx}(h_c, t_{f.top}, t_{f.bot}, t_c, \alpha_c, f_c, R_{C1}) \cdot D_{yy}(h_c, t_{f.top}, t_{f.bot}, t_c, \alpha_c, f_c, R_{C1}) \cdot \pi^2 \cdot L^4 \cdot B^2 \cdot j^2 \ldots \\
+ 2 \cdot D_{xx}(h_c, t_{f.top}, t_{f.bot}, t_c, \alpha_c, f_c, R_{C1}) \cdot D_{yy}(h_c, t_{f.top}, t_{f.bot}, t_c, \alpha_c, f_c, R_{C1}) \cdot \pi^4 \cdot L^2 \cdot B^2 \cdot i^2 \cdot j^2 \ldots \\
+ -D_{xx}(h_c, t_{f.top}, t_{f.bot}, t_c, \alpha_c, f_c, R_{C1}) \cdot D_{xy}(h_c, t_{f.top}, t_{f.bot}, t_c, \alpha_c, f_c, R_{C1}) \cdot \pi^4 \cdot L^2 \cdot B^2 \cdot i^2 \cdot j^2 \cdot \nu_{yx}(h_c, t_{f.top}, t_{f.bot}, t_c, \alpha_c, f_c, R_{C1}) \ldots \\
+ -D_{xy}(h_c, t_{f.top}, t_{f.bot}, t_c, \alpha_c, f_c, R_{C1}) \cdot D_{yy}(h_c, t_{f.top}, t_{f.bot}, t_c, \alpha_c, f_c, R_{C1}) \cdot \pi^4 \cdot L^2 \cdot B^2 \cdot i^2 \cdot j^2 \cdot \nu_{xy} \ldots \\
+ -2 \cdot D_{xx}(h_c, t_{f.top}, t_{f.bot}, t_c, \alpha_c, f_c, R_{C1}) \cdot D_{yy}(h_c, t_{f.top}, t_{f.bot}, t_c, \alpha_c, f_c, R_{C1}) \cdot \pi^4 \cdot L^2 \cdot B^2 \cdot i^2 \cdot j^2 \cdot \nu_{xy} \cdot \nu_{yx}(h_c, t_{f.top}, t_{f.bot}, t_c, \alpha_c, f_c, R_{C1})
\end{array}\right)}{\pi^2 \cdot \left(\begin{array}{l}
D_{Qx}(h_c, t_{f.top}, t_{f.bot}, t_c, \alpha_c, f_c, R_{C1}) \cdot D_{xx}(h_c, t_{f.top}, t_{f.bot}, t_c, \alpha_c, f_c, R_{C1}) \cdot D_{xy}(h_c, t_{f.top}, t_{f.bot}, t_c, \alpha_c, f_c, R_{C1}) \cdot \pi^4 \cdot B^6 \cdot i^6 \ldots \\
+ D_{Qy}(h_c, t_{f.top}, t_{f.bot}, t_c, \alpha_c, f_c, R_{C1}) \cdot D_{xy}(h_c, t_{f.top}, t_{f.bot}, t_c, \alpha_c, f_c, R_{C1}) \cdot D_{yy}(h_c, t_{f.top}, t_{f.bot}, t_c, \alpha_c, f_c, R_{C1}) \cdot \pi^4 L^6 \cdot j^6 \ldots \\
+ 2 \cdot D_{Qx}(h_c, t_{f.top}, t_{f.bot}, t_c, \alpha_c, f_c, R_{C1}) \cdot D_{Qy}(h_c, t_{f.top}, t_{f.bot}, t_c, \alpha_c, f_c, R_{C1}) \cdot D_{xx}(h_c, t_{f.top}, t_{f.bot}, t_c, \alpha_c, f_c, R_{C1}) \cdot \pi^2 \cdot L^2 \cdot B^6 \cdot i^4 \ldots \\
+ 2 \cdot D_{Qx}(h_c, t_{f.top}, t_{f.bot}, t_c, \alpha_c, f_c, R_{C1}) \cdot D_{Qy}(h_c, t_{f.top}, t_{f.bot}, t_c, \alpha_c, f_c, R_{C1}) \cdot D_{yy}(h_c, t_{f.top}, t_{f.bot}, t_c, \alpha_c, f_c, R_{C1}) \pi^2 \cdot L^6 \cdot B^2 \cdot j^4 \ldots \\
+ 4 \cdot D_{Qx}(h_c, t_{f.top}, t_{f.bot}, t_c, \alpha_c, f_c, R_{C1}) \cdot D_{Qy}(h_c, t_{f.top}, t_{f.bot}, t_c, \alpha_c, f_c, R_{C1}) \cdot D_{xy}(h_c, t_{f.top}, t_{f.bot}, t_c, \alpha_c, f_c, R_{C1}) \cdot \pi^2 L^4 B^4 \cdot i^2 \cdot j^2 \ldots \\
+ D_{Qy}(h_c, t_{f.top}, t_{f.bot}, t_c, \alpha_c, f_c, R_{C1}) \cdot D_{xx}(h_c, t_{f.top}, t_{f.bot}, t_c, \alpha_c, f_c, R_{C1}) \cdot D_{xy}(h_c, t_{f.top}, t_{f.bot}, t_c, \alpha_c, f_c, R_{C1}) \cdot \pi^4 \cdot L^2 \cdot B^4 \cdot i^4 \cdot j^2 \ldots \\
+ 2 \cdot D_{Qx}(h_c, t_{f.top}, t_{f.bot}, t_c, \alpha_c, f_c, R_{C1}) \cdot D_{xx}(h_c, t_{f.top}, t_{f.bot}, t_c, \alpha_c, f_c, R_{C1}) \cdot D_{yy}(h_c, t_{f.top}, t_{f.bot}, t_c, \alpha_c, f_c, R_{C1}) \cdot \pi^4 \cdot L^2 \cdot B^4 \cdot i^4 \cdot j^2 \ldots \\
+ D_{Qx}(h_c, t_{f.top}, t_{f.bot}, t_c, \alpha_c, f_c, R_{C1}) \cdot D_{xy}(h_c, t_{f.top}, t_{f.bot}, t_c, \alpha_c, f_c, R_{C1}) \cdot D_{yy}(h_c, t_{f.top}, t_{f.bot}, t_c, \alpha_c, f_c, R_{C1}) \cdot \pi^4 \cdot L^4 \cdot B^2 \cdot i^2 \cdot j^4 \ldots \\
+ 2 \cdot D_{Qy}(h_c, t_{f.top}, t_{f.bot}, t_c, \alpha_c, f_c, R_{C1}) \cdot D_{xx}(h_c, t_{f.top}, t_{f.bot}, t_c, \alpha_c, f_c, R_{C1}) \cdot D_{yy}(h_c, t_{f.top}, t_{f.bot}, t_c, \alpha_c, f_c, R_{C1}) \cdot \pi^4 \cdot L^4 \cdot B^2 \cdot i^2 \cdot j^4 \ldots \\
+ 2 D_{Qx}(h_c, t_{f.top}, t_{f.bot}, t_c, \alpha_c, f_c, R_{C1}) \cdot D_{Qy}(h_c, t_{f.top}, t_{f.bot}, t_c, \alpha_c, f_c, R_{C1}) \cdot D_{xx}(h_c, t_{f.top}, t_{f.bot}, t_c, \alpha_c, f_c, R_{C1}) \cdot \pi^2 \cdot L^4 \cdot B^4 \cdot i^2 \cdot j^2 \cdot \nu_{yx}(h_c, t_{f.top}, t_{f.bot}, t_c, \alpha_c, f_c, R_{C1}) \ldots \\
+ 2 D_{Qx}(h_c, t_{f.top}, t_{f.bot}, t_c, \alpha_c, f_c, R_{C1}) \cdot D_{Qy}(h_c, t_{f.top}, t_{f.bot}, t_c, \alpha_c, f_c, R_{C1}) \cdot D_{yy}(h_c, t_{f.top}, t_{f.bot}, t_c, \alpha_c, f_c, R_{C1}) \cdot \pi^2 \cdot L^4 \cdot B^4 \cdot i^2 \cdot j^2 \cdot \nu_{xy} \ldots \\
+ -D_{Qx}(h_c, t_{f.top}, t_{f.bot}, t_c, \alpha_c, f_c, R_{C1}) \cdot D_{xx}(h_c, t_{f.top}, t_{f.bot}, t_c, \alpha_c, f_c, R_{C1}) \cdot D_{xy}(h_c, t_{f.top}, t_{f.bot}, t_c, \alpha_c, f_c, R_{C1}) \cdot \pi^4 \cdot L^2 \cdot B^4 \cdot i^4 \cdot j^2 \cdot \nu_{yx}(h_c, t_{f.top}, t_{f.bot}, t_c, \alpha_c, f_c, R_{C1}) \ldots \\
+ -D_{Qx}(h_c, t_{f.top}, t_{f.bot}, t_c, \alpha_c, f_c, R_{C1}) \cdot D_{xy}(h_c, t_{f.top}, t_{f.bot}, t_c, \alpha_c, f_c, R_{C1}) \cdot D_{yy}(h_c, t_{f.top}, t_{f.bot}, t_c, \alpha_c, f_c, R_{C1}) \cdot \pi^4 \cdot L^2 \cdot B^4 \cdot i^4 \cdot j^2 \cdot \nu_{xy} \ldots \\
+ -D_{Qy}(h_c, t_{f.top}, t_{f.bot}, t_c, \alpha_c, f_c, R_{C1}) \cdot D_{xx}(h_c, t_{f.top}, t_{f.bot}, t_c, \alpha_c, f_c, R_{C1}) \cdot D_{xy}(h_c, t_{f.top}, t_{f.bot}, t_c, \alpha_c, f_c, R_{C1}) \cdot \pi^4 \cdot L^4 \cdot B^2 \cdot i^2 \cdot j^4 \cdot \nu_{yx}(h_c, t_{f.top}, t_{f.bot}, t_c, \alpha_c, f_c, R_{C1}) \ldots \\
+ -D_{Qy}(h_c, t_{f.top}, t_{f.bot}, t_c, \alpha_c, f_c, R_{C1}) \cdot D_{xy}(h_c, t_{f.top}, t_{f.bot}, t_c, \alpha_c, f_c, R_{C1}) \cdot D_{yy}(h_c, t_{f.top}, t_{f.bot}, t_c, \alpha_c, f_c, R_{C1}) \cdot \pi^4 \cdot L^4 \cdot B^2 \cdot i^2 \cdot j^4 \cdot \nu_{xy} \ldots \\
+ -2 D_{Qx}(h_c, t_{f.top}, t_{f.bot}, t_c, \alpha_c, f_c, R_{C1}) \cdot D_{xx}(h_c, t_{f.top}, t_{f.bot}, t_c, \alpha_c, f_c, R_{C1}) \cdot D_{yy}(h_c, t_{f.top}, t_{f.bot}, t_c, \alpha_c, f_c, R_{C1}) \cdot \pi^4 \cdot L^4 \cdot B^4 \cdot i^2 \cdot j^2 \cdot \nu_{xy} \cdot \nu_{yx}(h_c, t_{f.top}, t_{f.bot}, t_c, \alpha_c, f_c, R_{C1}) \ldots \\
+ -2 D_{Qy}(h_c, t_{f.top}, t_{f.bot}, t_c, \alpha_c, f_c, R_{C1}) \cdot D_{xx}(h_c, t_{f.top}, t_{f.bot}, t_c, \alpha_c, f_c, R_{C1}) \cdot D_{yy}(h_c, t_{f.top}, t_{f.bot}, t_c, \alpha_c, f_c, R_{C1}) \cdot \pi^4 \cdot L^4 \cdot B^2 \cdot i^2 \cdot j^4 \cdot \nu_{xy} \cdot \nu_{yx}(h_c, t_{f.top}, t_{f.bot}, t_c, \alpha_c, f_c, R_{C1})
\end{array}\right)}$$

Deflection

The deflection in the middle of the plate is considered

$$X := \frac{L}{2} = 7\,m \qquad Y := \frac{B}{2} = 3.5\,m$$

Number of terms in the Fourier seris used in the deflection solution. Here both i and j are choosen to 1 since using more terms is more computationally demanding in the optimisation analysis.

$$i := 1..1 \qquad j := 1..1$$

Distributed load

$$w_{inst}(h_c, t_{f.top}, t_{f.bot}, t_c, \alpha_c, f_c, R_{C1}) := \sum_j \left[\sum_i \left(w_{ij}(h_c, t_{f.top}, t_{f.bot}, t_c, \alpha_c, f_c, R_{C1}, i, j) \cdot q_{ijC}(i, j, h_c, t_{f.top}, t_{f.bot}, t_c, \alpha_c, f_c, R_{C1}) \cdot \sin\left(\frac{i \cdot \pi \cdot X}{L}\right) \cdot \sin\left(\frac{j \cdot \pi \cdot Y}{B}\right) \right) \right]$$

Deflection due to point load (dynamic requirement)

$$w_{1kN}(h_c, t_{f.top}, t_{f.bot}, t_c, \alpha_c, f_c, R_{C1}) := \sum_j \left[\sum_i \left(w_{ij}(h_c, t_{f.top}, t_{f.bot}, t_c, \alpha_c, R_{C1}, f_c, i, j) \cdot Q_1(i, j) \cdot \sin\left(\frac{i \cdot \pi \cdot X}{L}\right) \cdot \sin\left(\frac{j \cdot \pi \cdot Y}{B}\right) \right) \right]$$

4. Deflection of sandwich panel

5. Shear stress at flange-core connection

5. Shear stress at face-core connection

Only shear stress parallel to corrugation is evaluated

Shear force at support

$$q_{d.ULS}(h_c, t_{f.top}, t_{f.bot}, t_c, \alpha_c, f_c, R_{C1}) := \alpha_A \cdot \gamma_{Q.ULS} \cdot q_k \cdots + \gamma_{G.ULS} \cdot \begin{pmatrix} q_{self}(h_c, t_{f.top}, t_{f.bot}, t_c, \alpha_c, f_c, R_{C1}) \cdots \\ + q_{dw} \end{pmatrix}$$

$$q_{mn}(h_c, t_{f.top}, t_{f.bot}, t_c, \alpha_c, f_c, R_{C1}, m_{shear}, n_{shear}) := \frac{\left(16 \cdot q_{d.ULS}(h_c, t_{f.top}, t_{f.bot}, t_c, \alpha_c, f_c, R_{C1})\right)}{m_{shear} \cdot n_{shear} \cdot \pi^2}$$

$$X_{mn}\left(h_c, t_{f.top}, t_{f.bot}, t_c, \alpha_c, f_c, R_{C1}, m_{shear}, n_{shear}\right) :=$$

$$\left[\left(\frac{1}{2}\right)\cdot\left(m_{shear}\cdot\frac{\pi}{L}\right)^5\cdot\left[\frac{\left(D_x\left(h_c, t_{f.top}, t_{f.bot}, t_c, \alpha_c, f_c, R_{C1}\right)\right)\cdot D_{xy}\left(h_c, t_{f.top}, t_{f.bot}, t_c, \alpha_c, f_c, R_{C1}\right)\right)}{\left(1-\nu_{xy}\cdot\nu_{yx}\left(h_c, t_{f.top}, t_{f.bot}, t_c, \alpha_c, f_c, R_{C1}\right)\right)}\right]\cdots\right.$$
$$+\left(m_{shear}\cdot\frac{\pi}{L}\right)^3\cdot\left(n_{shear}\cdot\frac{\pi}{B}\right)^2\cdot\left[\frac{\left(D_x\left(h_c, t_{f.top}, t_{f.bot}, t_c, \alpha_c, f_c, R_{C1}\right)\right)\cdot D_y\left(h_c, t_{f.top}, t_{f.bot}, t_c, \alpha_c, f_c, R_{C1}\right)\right)}{\left(1-\nu_{xy}\cdot\nu_{yx}\left(h_c, t_{f.top}, t_{f.bot}, t_c, \alpha_c, f_c, R_{C1}\right)\right)}\cdots\right.$$
$$\left.+\frac{\left[D_{xy}\left(h_c, t_{f.top}, t_{f.bot}, t_c, \alpha_c, f_c, R_{C1}\right)\cdot\left(\begin{matrix}\nu_{xy}\cdot D_y\left(h_c, t_{f.top}, t_{f.bot}, t_c, \alpha_c, f_c, R_{C1}\right)\cdots\\+\nu_{yx}\left(h_c, t_{f.top}, t_{f.bot}, t_c, \alpha_c, f_c, R_{C1}\right)\cdot D_x\left(h_c, t_{f.top}, t_{f.bot}, t_c, \alpha_c, f_c, R_{C1}\right)\end{matrix}\right)\right]}{\left[2\cdot\left(1-\nu_{xy}\cdot\nu_{yx}\left(h_c, t_{f.top}, t_{f.bot}, t_c, \alpha_c, f_c, R_{C1}\right)\right)\right]}\right]\cdots$$
$$+\left(\frac{1}{2}\right)\cdot\left(m_{shear}\cdot\frac{\pi}{L}\right)\cdot\left(n_{shear}\cdot\frac{\pi}{B}\right)^4\cdot\left[\frac{\left(D_y\left(h_c, t_{f.top}, t_{f.bot}, t_c, \alpha_c, f_c, R_{C1}\right)\right)\cdot D_{xy}\left(h_c, t_{f.top}, t_{f.bot}, t_c, \alpha_c, f_c, R_{C1}\right)\right)}{\left(1-\nu_{xy}\cdot\nu_{yx}\left(h_c, t_{f.top}, t_{f.bot}, t_c, \alpha_c, f_c, R_{C1}\right)\right)}\right]\cdots$$
$$\left.+D_{Qy}\left(h_c, t_{f.top}, t_{f.bot}, t_c, \alpha_c, f_c, R_{C1}\right)\cdot\left(m_{shear}\cdot\frac{\pi}{L}\right)\cdot\left[\left(m_{shear}\cdot\frac{\pi}{L}\right)^2\cdot\frac{\left(D_x\left(h_c, t_{f.top}, t_{f.bot}, t_c, \alpha_c, f_c, R_{C1}\right)\right)}{\left(1-\nu_{xy}\cdot\nu_{yx}\left(h_c, t_{f.top}, t_{f.bot}, t_c, \alpha_c, f_c, R_{C1}\right)\right)}\cdots\right.\right.$$
$$\left.\left.+\left(n_{shear}\cdot\frac{\pi}{B}\right)^2\cdot\left(\begin{matrix}D_{xy}\left(h_c, t_{f.top}, t_{f.bot}, t_c, \alpha_c, f_c, R_{C1}\right)\cdots\\+\dfrac{\nu_{yx}\left(h_c, t_{f.top}, t_{f.bot}, t_c, \alpha_c, f_c, R_{C1}\right)\cdot D_x\left(h_c, t_{f.top}, t_{f.bot}, t_c, \alpha_c, f_c, R_{C1}\right)}{1-\nu_{xy}\cdot\nu_{yx}\left(h_c, t_{f.top}, t_{f.bot}, t_c, \alpha_c, f_c, R_{C1}\right)}\end{matrix}\right)\right]\right]$$
$$D_{Qy}\left(h_c, t_{f.top}, t_{f.bot}, t_c, \alpha_c, f_c, R_{C1}\right)$$

$$Y_{mn}\left(h_c, t_{f.top}, t_{f.bot}, t_c, \alpha_c, f_c, R_{C1}, m_{shear}, n_{shear}\right) :=$$

$$\left[-\left(\frac{1}{2}\right)\cdot\left(n_{shear}\cdot\frac{\pi}{B}\right)^5\cdot\left[\frac{\left(D_y\left(h_c, t_{f.top}, t_{f.bot}, t_c, \alpha_c, f_c, R_{C1}\right)\right)\cdot D_{xy}\left(h_c, t_{f.top}, t_{f.bot}, t_c, \alpha_c, f_c, R_{C1}\right)\right)}{\left(1-\nu_{xy}\cdot\nu_{yx}\left(h_c, t_{f.top}, t_{f.bot}, t_c, \alpha_c, f_c, R_{C1}\right)\right)}\right]\cdots\right.$$
$$+\left(m_{shear}\cdot\frac{\pi}{L}\right)^2\cdot\left(n_{shear}\cdot\frac{\pi}{B}\right)^3\cdot\left[\frac{\left(D_x\left(h_c, t_{f.top}, t_{f.bot}, t_c, \alpha_c, f_c, R_{C1}\right)\right)\cdot D_y\left(h_c, t_{f.top}, t_{f.bot}, t_c, \alpha_c, f_c, R_{C1}\right)\right)}{\left(1-\nu_{xy}\cdot\nu_{yx}\left(h_c, t_{f.top}, t_{f.bot}, t_c, \alpha_c, f_c, R_{C1}\right)\right)}\cdots\right.$$
$$\left.+\frac{\left[D_{xy}\left(h_c, t_{f.top}, t_{f.bot}, t_c, \alpha_c, f_c, R_{C1}\right)\cdot\left(\begin{matrix}\nu_{xy}\cdot D_y\left(h_c, t_{f.top}, t_{f.bot}, t_c, \alpha_c, f_c, R_{C1}\right)\cdots\\+\nu_{yx}\left(h_c, t_{f.top}, t_{f.bot}, t_c, \alpha_c, f_c, R_{C1}\right)\cdot D_x\left(h_c, t_{f.top}, t_{f.bot}, t_c, \alpha_c, f_c, R_{C1}\right)\end{matrix}\right)\right]}{\left[2\cdot\left(1-\nu_{xy}\cdot\nu_{yx}\left(h_c, t_{f.top}, t_{f.bot}, t_c, \alpha_c, f_c, R_{C1}\right)\right)\right]}\right]\cdots$$
$$\left.+-\left(\frac{1}{2}\right)\cdot\left(m_{shear}\cdot\frac{\pi}{L}\right)^4\cdot\left(n_{shear}\cdot\frac{\pi}{B}\right)\cdot\frac{\left(D_x\left(h_c, t_{f.top}, t_{f.bot}, t_c, \alpha_c, f_c, R_{C1}\right)\right)\cdot D_{xy}\left(h_c, t_{f.top}, t_{f.bot}, t_c, \alpha_c, f_c, R_{C1}\right)\right)}{\left(1-\nu_{xy}\cdot\nu_{yx}\left(h_c, t_{f.top}, t_{f.bot}, t_c, \alpha_c, f_c, R_{C1}\right)\right)}\right]\cdots$$
$$\left.+-D_{Qx}\left(h_c, t_{f.top}, t_{f.bot}, t_c, \alpha_c, f_c, R_{C1}\right)\cdot\left(n_{shear}\cdot\frac{\pi}{B}\right)\cdot\left[\left(n_{shear}\cdot\frac{\pi}{B}\right)^2\cdot\frac{\left(D_y\left(h_c, t_{f.top}, t_{f.bot}, t_c, \alpha_c, f_c, R_{C1}\right)\right)}{\left(1-\nu_{xy}\cdot\nu_{yx}\left(h_c, t_{f.top}, t_{f.bot}, t_c, \alpha_c, f_c, R_{C1}\right)\right)}\cdots\right.\right.$$
$$\left.\left.+\left(m_{shear}\cdot\frac{\pi}{L}\right)^2\cdot\left(\begin{matrix}D_{xy}\left(h_c, t_{f.top}, t_{f.bot}, t_c, \alpha_c, f_c, R_{C1}\right)\cdots\\+\dfrac{\nu_{xy}\cdot D_y\left(h_c, t_{f.top}, t_{f.bot}, t_c, \alpha_c, f_c, R_{C1}\right)}{1-\nu_{xy}\cdot\nu_{yx}\left(h_c, t_{f.top}, t_{f.bot}, t_c, \alpha_c, f_c, R_{C1}\right)}\end{matrix}\right)\right]\right]$$
$$D_{Qx}\left(h_c, t_{f.top}, t_{f.bot}, t_c, \alpha_c, f_c, R_{C1}\right)$$

$$Z_{mn}(h_c, t_{f.top}, t_{f.bot}, t_c, \alpha_c, f_c, R_{C1}, m_{shear}, n_{shear}) :=$$

$$\left(m_{shear} \cdot \frac{\pi}{L}\right) \cdot X_{mn}(h_c, t_{f.top}, t_{f.bot}, t_c, \alpha_c, f_c, R_{C1}, m_{shear}, n_{shear}) \ldots$$
$$+ -\left(n_{shear} \cdot \frac{\pi}{B}\right) \cdot Y_{mn}(h_c, t_{f.top}, t_{f.bot}, t_c, \alpha_c, f_c, R_{C1}, m_{shear}, n_{shear})$$

Only one variable in the Fourier series is used. More terms are computionally demanding.

$m_{shear} := 1 .. 1$ $\quad$ $n_{shear} := 1 .. 1$

The highest shear force in x-direction occur in the middle of the short side

$x_{shear} := 0$ $\quad$ $y_{shear} := \frac{B}{2}$

The absolute value is used as the force is regarded as positive in the optimisation criteria

$$T(h_c, t_{f.top}, t_{f.bot}, t_c, \alpha_c, f_c, R_{C1}) :=$$

$$\left| \sum_{n_{shear}} \left[\sum_{m_{shear}} \left[\left(\frac{X_{mn}(h_c, t_{f.top}, t_{f.bot}, t_c, \alpha_c, f_c, R_{C1}, m_{shear}, n_{shear}) \cdot q_{mn}(h_c, t_{f.top}, t_{f.bot}, t_c, \alpha_c, f_c, R_{C1}, m_{shear}, n_{shear})}{Z_{mn}(h_c, t_{f.top}, t_{f.bot}, t_c, \alpha_c, f_c, R_{C1}, m_{shear}, n_{shear})} \right) \cdot \cos\left[\frac{(m_{shear} \cdot \pi \cdot x_{shear})}{L} \right] \cdot \sin\left[\frac{(n_{shear} \cdot \pi \cdot y_{shear})}{B} \right] \right] \right] \right|$$

Upper face

$$nr_{fc}(h_c, \alpha_c, f_c, R_{C1}) := \left(\frac{1}{l_c(h_c, \alpha_c, f_c, R_{C1})} \right)$$

$$S_{top}(h_c, t_{f.top}, t_{f.bot}, t_c, \alpha_c, f_c, R_{C1}) := t_{f.top} \cdot (z_{na}(h_c, t_{f.top}, t_{f.bot}, t_c, \alpha_c, f_c, R_{C1}))$$

$$b_{top}(h_c, \alpha_c, f_c, R_{C1}) := nr_{fc}(h_c, \alpha_c, f_c, R_{C1}) \cdot f_c$$

$$\tau_{x.top}(h_c, t_{f.top}, t_{f.bot}, t_c, \alpha_c, f_c, R_{C1}) := \frac{(T(h_c, t_{f.top}, t_{f.bot}, t_c, \alpha_c, f_c, R_{C1}) \cdot S_{top}(h_c, t_{f.top}, t_{f.bot}, t_c, \alpha_c, f_c, R_{C1}))}{(I_x(h_c, t_{f.top}, t_{f.bot}, t_c, \alpha_c, f_c, R_{C1}) \cdot b_{top}(h_c, \alpha_c, f_c, R_{C1}))}$$

Lower face

$$S_{bot}(h_c, t_{f.top}, t_{f.bot}, t_c, \alpha_c, f_c, R_{C1}) := t_{f.bot} \cdot (h(h_c, t_{f.top}, t_{f.bot}, t_c) - z_{na}(h_c, t_{f.top}, t_{f.bot}, t_c, \alpha_c, f_c, R_{C1}))$$

$$b_{bot}(h_c, \alpha_c, f_c, R_{C1}) := nr_{fc}(h_c, \alpha_c, f_c, R_{C1}) \cdot f_c$$

$$\tau_{x.bot}(h_c, t_{f.top}, t_{f.bot}, t_c, \alpha_c, f_c, R_{C1}) := \frac{(T(h_c, t_{f.top}, t_{f.bot}, t_c, \alpha_c, f_c, R_{C1}) \cdot S_{bot}(h_c, t_{f.top}, t_{f.bot}, t_c, \alpha_c, f_c, R_{C1}))}{(I_x(h_c, t_{f.top}, t_{f.bot}, t_c, \alpha_c, f_c, R_{C1}) \cdot b_{bot}(h_c, \alpha_c, f_c, R_{C1}))}$$

5. Shear stress at flange-core connection

6. Eigenfrequency

First order plate theory is used. Formulas are from *Mechanics of Laminated Composite Plates* (Reddy, 1997). Rotary inertia and in-plane vibration are neglected. Same notations as in the book are used.

Mass per square meter

$$m_{freq}(h_c, t_{f.top}, t_{f.bot}, t_c, \alpha_c, f_c, R_{C1}) := \frac{(q_{self}(h_c, t_{f.top}, t_{f.bot}, t_c, \alpha_c, f_c, R_{C1}) + q_{dw})}{g}$$

Variables related to mass matrix

$$I_{s.0}(h_c, t_{f.top}, t_{f.bot}, t_c, \alpha_c, f_c, R_{C1}) := m_{freq}(h_c, t_{f.top}, t_{f.bot}, t_c, \alpha_c, f_c, R_{C1})$$

$$m_{33}(h_c, t_{f.top}, t_{f.bot}, t_c, \alpha_c, f_c, R_{C1}) := I_{s.0}(h_c, t_{f.top}, t_{f.bot}, t_c, \alpha_c, f_c, R_{C1})$$

Shear correction factor

$$K := \frac{5}{6}$$

Frequency modes

$$m_s := 1$$

$$n_s := 1$$

$$\alpha_s := m_s \cdot \frac{\pi}{L}$$

$$\beta_s := n_s \cdot \frac{\pi}{B}$$

Definition of Q-functions

$$Q_{s.11}(h_c, t_{f.top}, t_{f.bot}, t_c, \alpha_c, f_c, R_{C1}) := D_{11}(h_c, t_{f.top}, t_{f.bot}, t_c, \alpha_c, f_c, R_{C1})$$

$$Q_{s.12}(h_c, t_{f.top}, t_{f.bot}, t_c, \alpha_c, f_c, R_{C1}) := D_{12}(h_c, t_{f.top}, t_{f.bot}, t_c, \alpha_c, f_c, R_{C1})$$

$$Q_{s.22}(h_c, t_{f.top}, t_{f.bot}, t_c, \alpha_c, f_c, R_{C1}) := D_{22}(h_c, t_{f.top}, t_{f.bot}, t_c, \alpha_c, f_c, R_{C1})$$

$$Q_{s.44}(h_c, t_{f.top}, t_{f.bot}, t_c, \alpha_c, f_c, R_{C1}) := D_{Qy}(h_c, t_{f.top}, t_{f.bot}, t_c, \alpha_c, f_c, R_{C1})$$

$$Q_{s.55}(h_c, t_{f.top}, t_{f.bot}, t_c, \alpha_c, f_c, R_{C1}) := D_{Qx}(h_c, t_{f.top}, t_{f.bot}, t_c, \alpha_c, f_c, R_{C1})$$

$$Q_{s.66}(h_c, t_{f.top}, t_{f.bot}, t_c, \alpha_c, f_c, R_{C1}) := D_{33}(h_c, t_{f.top}, t_{f.bot}, t_c, \alpha_c, f_c, R_{C1})$$

In-plane constants

$$A_{11}(h_c, t_{f.top}, t_{f.bot}, t_c, \alpha_c, f_c, R_{C1}) := Q_{s.11}(h_c, t_{f.top}, t_{f.bot}, t_c, \alpha_c, f_c, R_{C1})$$

$$A_{12}(h_c, t_{f.top}, t_{f.bot}, t_c, \alpha_c, f_c, R_{C1}) := Q_{s.12}(h_c, t_{f.top}, t_{f.bot}, t_c, \alpha_c, f_c, R_{C1})$$

$$A_{22}(h_c, t_{f.top}, t_{f.bot}, t_c, \alpha_c, f_c, R_{C1}) := Q_{s.22}(h_c, t_{f.top}, t_{f.bot}, t_c, \alpha_c, f_c, R_{C1})$$

$$A_{44}(h_c, t_{f.top}, t_{f.bot}, t_c, \alpha_c, f_c, R_{C1}) := K \cdot Q_{s.44}(h_c, t_{f.top}, t_{f.bot}, t_c, \alpha_c, f_c, R_{C1})$$

$$A_{55}(h_c, t_{f.top}, t_{f.bot}, t_c, \alpha_c, f_c, R_{C1}) := K \cdot Q_{s.55}(h_c, t_{f.top}, t_{f.bot}, t_c, \alpha_c, f_c, R_{C1})$$

$$A_{66}(h_c, t_{f.top}, t_{f.bot}, t_c, \alpha_c, f_c, R_{C1}) := Q_{s.66}(h_c, t_{f.top}, t_{f.bot}, t_c, \alpha_c, f_c, R_{C1})$$

Out-of-plane constants

$$D_{s.11}(h_c, t_{f.top}, t_{f.bot}, t_c, \alpha_c, f_c, R_{C1}) := D_{44}(h_c, t_{f.top}, t_{f.bot}, t_c, \alpha_c, f_c, R_{C1})$$

$$D_{s.12}(h_c, t_{f.top}, t_{f.bot}, t_c, \alpha_c, f_c, R_{C1}) := D_{45}(h_c, t_{f.top}, t_{f.bot}, t_c, \alpha_c, f_c, R_{C1})$$

$$D_{s.22}(h_c, t_{f.top}, t_{f.bot}, t_c, \alpha_c, f_c, R_{C1}) := D_{55}(h_c, t_{f.top}, t_{f.bot}, t_c, \alpha_c, f_c, R_{C1})$$

$$D_{s.66}(h_c, t_{f.top}, t_{f.bot}, t_c, \alpha_c, f_c, R_{C1}) := D_{66}(h_c, t_{f.top}, t_{f.bot}, t_c, \alpha_c, f_c, R_{C1})$$

s-functions related to the S-matrix

$$s_{11}(h_c, t_{f.top}, t_{f.bot}, t_c, \alpha_c, f_c, R_{C1}) := \begin{pmatrix} A_{11}(h_c, t_{f.top}, t_{f.bot}, t_c, \alpha_c, f_c, R_{C1}) \cdot \alpha_s^{\,2} \ldots \\ + A_{66}(h_c, t_{f.top}, t_{f.bot}, t_c, \alpha_c, f_c, R_{C1}) \cdot \beta_s^{\,2} \end{pmatrix}$$

$$s_{12}(h_c, t_{f.top}, t_{f.bot}, t_c, \alpha_c, f_c, R_{C1}) := \begin{pmatrix} A_{12}(h_c, t_{f.top}, t_{f.bot}, t_c, \alpha_c, f_c, R_{C1}) \ldots \\ + A_{66}(h_c, t_{f.top}, t_{f.bot}, t_c, \alpha_c, f_c, R_{C1}) \end{pmatrix} \cdot \alpha_s \cdot \beta_s$$

$$s_{14} := 0$$

$$s_{15} := 0$$

$$s_{22}(h_c, t_{f.top}, t_{f.bot}, t_c, \alpha_c, f_c, R_{C1}) := \begin{pmatrix} A_{66}(h_c, t_{f.top}, t_{f.bot}, t_c, \alpha_c, f_c, R_{C1}) \cdot \alpha_s^{\,2} \ldots \\ + A_{22}(h_c, t_{f.top}, t_{f.bot}, t_c, \alpha_c, f_c, R_{C1}) \cdot \beta_s^{\,2} \end{pmatrix}$$

$$s_{23} := 0$$

$$s_{24} := s_{15}$$

$$s_{25} := 0$$

$$s_{33}(h_c, t_{f.top}, t_{f.bot}, t_c, \alpha_c, f_c, R_{C1}) := K \cdot \begin{pmatrix} A_{55}(h_c, t_{f.top}, t_{f.bot}, t_c, \alpha_c, f_c, R_{C1}) \cdot \alpha_s^{\,2} \ldots \\ + A_{44}(h_c, t_{f.top}, t_{f.bot}, t_c, \alpha_c, f_c, R_{C1}) \cdot \beta_s^{\,2} \end{pmatrix}$$

$$s_{34}(h_c, t_{f.top}, t_{f.bot}, t_c, \alpha_c, f_c, R_{C1}) := K \cdot A_{55}(h_c, t_{f.top}, t_{f.bot}, t_c, \alpha_c, f_c, R_{C1}) \cdot \alpha_s$$

$$s_{35}(h_c, t_{f.top}, t_{f.bot}, t_c, \alpha_c, f_c, R_{C1}) := K \cdot A_{44}(h_c, t_{f.top}, t_{f.bot}, t_c, \alpha_c, f_c, R_{C1}) \cdot \beta_s$$

$$s_{44}(h_c, t_{f.top}, t_{f.bot}, t_c, \alpha_c, f_c, R_{C1}) := \begin{pmatrix} D_{s.11}(h_c, t_{f.top}, t_{f.bot}, t_c, \alpha_c, f_c, R_{C1}) \cdot \alpha_s^{\,2} \ldots \\ + D_{s.66}(h_c, t_{f.top}, t_{f.bot}, t_c, \alpha_c, f_c, R_{C1}) \cdot \beta_s^{\,2} \ldots \\ + K \cdot A_{55}(h_c, t_{f.top}, t_{f.bot}, t_c, \alpha_c, f_c, R_{C1}) \end{pmatrix}$$

$$s_{45}(h_c, t_{f.top}, t_{f.bot}, t_c, \alpha_c, f_c, R_{C1}) := \begin{pmatrix} D_{s.12}(h_c, t_{f.top}, t_{f.bot}, t_c, \alpha_c, f_c, R_{C1}) \ldots \\ + D_{s.66}(h_c, t_{f.top}, t_{f.bot}, t_c, \alpha_c, f_c, R_{C1}) \end{pmatrix} \cdot (\alpha_s \cdot \beta_s)$$

$$s_{55}(h_c, t_{f.top}, t_{f.bot}, t_c, \alpha_c, f_c, R_{C1}) := \begin{pmatrix} D_{s.66}(h_c, t_{f.top}, t_{f.bot}, t_c, \alpha_c, f_c, R_{C1}) \cdot \alpha_s^{\,2} \ldots \\ + D_{s.22}(h_c, t_{f.top}, t_{f.bot}, t_c, \alpha_c, f_c, R_{C1}) \cdot \beta_s^{\,2} \ldots \\ + K \cdot A_{44}(h_c, t_{f.top}, t_{f.bot}, t_c, \alpha_c, f_c, R_{C1}) \end{pmatrix}$$

s-functions for the simplified formula

$$s_{00}(h_c, t_{f.top}, t_{f.bot}, t_c, \alpha_c, f_c, R_{C1}) :=$$

$$s_{44}(h_c, t_{f.top}, t_{f.bot}, t_c, \alpha_c, f_c, R_{C1}) \cdot s_{55}(h_c, t_{f.top}, t_{f.bot}, t_c, \alpha_c, f_c, R_{C1}) \ldots$$
$$+ -s_{45}(h_c, t_{f.top}, t_{f.bot}, t_c, \alpha_c, f_c, R_{C1}) \cdot s_{45}(h_c, t_{f.top}, t_{f.bot}, t_c, \alpha_c, f_c, R_{C1})$$

$$s_{I.11}(h_c, t_{f.top}, t_{f.bot}, t_c, \alpha_c, f_c, R_{C1}) := s_{11}(h_c, t_{f.top}, t_{f.bot}, t_c, \alpha_c, f_c, R_{C1})$$

$$s_{I.12}(h_c, t_{f.top}, t_{f.bot}, t_c, \alpha_c, f_c, R_{C1}) := s_{12}(h_c, t_{f.top}, t_{f.bot}, t_c, \alpha_c, f_c, R_{C1})$$

$$s_{I.13}(h_c, t_{f.top}, t_{f.bot}, t_c, \alpha_c, f_c, R_{C1}) := 0$$

$$s_{I.22}(h_c, t_{f.top}, t_{f.bot}, t_c, \alpha_c, f_c, R_{C1}) := s_{22}(h_c, t_{f.top}, t_{f.bot}, t_c, \alpha_c, f_c, R_{C1})$$

$$s_{I.23}(h_c, t_{f.top}, t_{f.bot}, t_c, \alpha_c, f_c, R_{C1}) := 0$$

$$s_{I.33}(h_c, t_{f.top}, t_{f.bot}, t_c, \alpha_c, f_c, R_{C1}) :=$$

$$s_{33}(h_c, t_{f.top}, t_{f.bot}, t_c, \alpha_c, f_c, R_{C1}) \ldots$$
$$+ -\left(\begin{matrix} s_{34}(h_c, t_{f.top}, t_{f.bot}, t_c, \alpha_c, f_c, R_{C1}) \cdot s_{55}(h_c, t_{f.top}, t_{f.bot}, t_c, \alpha_c, f_c, R_{C1}) \ldots \\ + -s_{35}(h_c, t_{f.top}, t_{f.bot}, t_c, \alpha_c, f_c, R_{C1}) \cdot s_{45}(h_c, t_{f.top}, t_{f.bot}, t_c, \alpha_c, f_c, R_{C1}) \end{matrix}\right) \cdot \frac{s_{34}(h_c, t_{f.top}, t_{f.bot}, t_c, \alpha_c, f_c, R_{C1})}{s_{00}(h_c, t_{f.top}, t_{f.bot}, t_c, \alpha_c, f_c, R_{C1})} \ldots$$
$$+ -\left(\begin{matrix} s_{35}(h_c, t_{f.top}, t_{f.bot}, t_c, \alpha_c, f_c, R_{C1}) \cdot s_{44}(h_c, t_{f.top}, t_{f.bot}, t_c, \alpha_c, f_c, R_{C1}) \ldots \\ + -s_{34}(h_c, t_{f.top}, t_{f.bot}, t_c, \alpha_c, f_c, R_{C1}) \cdot s_{45}(h_c, t_{f.top}, t_{f.bot}, t_c, \alpha_c, f_c, R_{C1}) \end{matrix}\right) \cdot \left(\frac{s_{35}(h_c, t_{f.top}, t_{f.bot}, t_c, \alpha_c, f_c, R_{C1})}{s_{00}(h_c, t_{f.top}, t_{f.bot}, t_c, \alpha_c, f_c, R_{C1})}\right)$$

Eigenfrequency

$$f_1(h_c, t_{f.top}, t_{f.bot}, t_c, \alpha_c, f_c, R_{C1}) :=$$

$$\frac{1}{2 \cdot \pi} \cdot \left(\sqrt{\frac{1}{m_{33}(h_c, t_{f.top}, t_{f.bot}, t_c, \alpha_c, f_c, R_{C1})}}\right) \cdot \sqrt{s_{I.33}(h_c, t_{f.top}, t_{f.bot}, t_c, \alpha_c, f_c, R_{C1})}$$

6. Eigenfrequency

7. Optimisation

In the optimisation the cross-secional area of the sandwich panel was minimised within given constraints.

$CTOL := 1 \cdot 10^{-3}$ Tolerance the minimising iteration

Minimising sandwich panel area

Predefined values

$h_c := 200mm$ $t_{f.top} := 18mm$ $\alpha_c := 70 \cdot deg$ $R_{C1} := 42mm$

$t_c := 6.5mm$ $t_{f.bot} := 7mm$ $f_c := 30mm$

Constraints

Given

Geometric constrains

$0deg \le \alpha_c \le 85deg$

$f_c \ge 30mm$

$18mm \le t_{f.top}$

$6.5mm \le t_{f.bot}$

$6.5mm \le t_c$

$0mm \le h_{tot}(h_c, t_{f.top}, t_{f.bot}, t_c) \le 410mm$

$6 \cdot t_c \le R_{C1}$

$l_1(h_c, \alpha_c, f_c, R_{C1}) \le \frac{h_c}{2}$

Constrain to take into account the assumption of thin faces in the sandwich theory

$5.77 < \frac{h(h_c, t_{f.top}, t_{f.bot}, t_c)}{\max(t_{f.top}, t_{f.bot})}$

$\frac{h(h_c, t_{f.top}, t_{f.bot}, t_c)}{\min(t_{f.top}, t_{f.bot})} < 100$

Deflection constrains

$w_{inst}(h_c, t_{f.top}, t_{f.bot}, t_c, \alpha_c, f_c, R_{C1}) \le \frac{\max(B, L)}{500}$

Bending constrains

$$M_{Ed.local}\left(h_c, t_{f.top}, \alpha_c, f_c, R_{C1}\right) \le M_{Rd.local}\left(t_{f.top}\right)$$

Shear stress constrains

$$\tau_{x.top}\left(h_c, t_{f.top}, t_{f.bot}, t_c, \alpha_c, f_c, R_{C1}\right) \le k_{mod} \cdot \frac{f_{vk}}{\gamma_M}$$

$$\tau_{x.bot}\left(h_c, t_{f.top}, t_{f.bot}, t_c, \alpha_c, f_c, R_{C1}\right) \le k_{mod} \cdot \frac{f_{vk}}{\gamma_M}$$

Vibration constrains

$$w_{1kN}\left(h_c, t_{f.top}, t_{f.bot}, t_c, \alpha_c, f_c, R_{C1}\right) < 1\,mm$$

$$f_1\left(h_c, t_{f.top}, t_{f.bot}, t_c, \alpha_c, f_c, R_{C1}\right) > 8\,Hz$$

$$\frac{f_1\left(h_c, t_{f.top}, t_{f.bot}, t_c, \alpha_c, f_c, R_{C1}\right)}{\left(w_{1kN}\left(h_c, t_{f.top}, t_{f.bot}, t_c, \alpha_c, f_c, R_{C1}\right)\right)^{0.44}} \ge 18.7 \cdot \frac{Hz}{(mm)^{0.44}}$$

Minimising sandwich panel area

$$\begin{pmatrix} h_{c.A} \\ t_{f.topA} \\ t_{f.botA} \\ t_{c.A} \\ \alpha_{c.A} \\ f_{c.A} \\ R_{C1.A} \end{pmatrix} := \text{Minimize}\left(V, h_c, t_{f.top}, t_{f.bot}, t_c, \alpha_c, f_c, R_{C1}\right)$$

7. Optimisation

8. Material volume and efficency grades

The total volume of the floor is calculated as well as the efficency grades related to the optimisation requirements.

8.1 Material volume of sandwich panel

$$V\left(h_{c.A}, t_{f.topA}, t_{f.botA}, t_{c.A}, \alpha_{c.A}, f_{c.A}, R_{C1.A}\right) = 6.895 \cdot m^3$$

8.2 Efficency grades

Thin face/thick face criteria

$$\frac{5.77}{\left(\frac{h\left(h_{c.A}, t_{f.topA}, t_{f.botA}, t_{c.A}\right)}{\max\left(t_{f.topA}, t_{f.botA}\right)}\right)} = 0.733$$

$$\frac{\left(\frac{h\left(h_{c.A}, t_{f.topA}, t_{f.botA}, t_{c.A}\right)}{\min\left(t_{f.topA}, t_{f.botA}\right)}\right)}{100} = 0.291$$

Instantaneuous deflection

$$\frac{w_{inst}\left(h_{c.A}, t_{f.topA}, t_{f.botA}, t_{c.A}, \alpha_{c.A}, f_{c.A}, R_{C1.A}\right)}{\frac{\max(B, L)}{500}} = 0.613$$

Local bending

$$\frac{M_{Ed.local}\left(h_c, t_{f.top}, \alpha_c, f_c, R_{C1}\right)}{M_{Rd.local}\left(t_{f.topA}\right)} = 0.407$$

Shear stress top face

$$\frac{\tau_{x.top}\left(h_{c.A}, t_{f.topA}, t_{f.botA}, t_{c.A}, \alpha_{c.A}, f_{c.A}, R_{C1.A}\right)}{\left(k_{mod} \cdot \frac{f_{vk}}{\gamma_M}\right)} = 0.045$$

Shear stress bottom face

$$\frac{\tau_{x.bot}\left(h_{c.A}, t_{f.topA}, t_{f.botA}, t_{c.A}, \alpha_{c.A}, f_{c.A}, R_{C1.A}\right)}{\left(k_{mod} \cdot \frac{f_{vk}}{\gamma_M}\right)} = 0.036$$

Deflection with 1kN point load

$$\frac{w_{1kN}\left(h_{c.A}, t_{f.topA}, t_{f.botA}, t_{c.A}, \alpha_{c.A}, f_{c.A}, R_{C1.A}\right)}{1mm} = 0.159$$

Eigenfrequency

$$\frac{(8Hz)}{f_1\left(h_{c.A}, t_{f.topA}, t_{f.botA}, t_{c.A}, \alpha_{c.A}, f_{c.A}, R_{C1.A}\right)} = 0.96$$

$$\frac{\left[18.7 \cdot \frac{Hz}{(mm)^{0.44}}\right]}{\left[\frac{f_1\left(h_{c.A}, t_{f.topA}, t_{f.botA}, t_{c.A}, \alpha_{c.A}, f_{c.A}, R_{C1.A}\right)}{\left(w_{1kN}\left(h_{c.A}, t_{f.topA}, t_{f.botA}, t_{c.A}, \alpha_{c.A}, f_{c.A}, R_{C1.A}\right)\right)^{0.44}}\right]} = 1$$

8. Material volume and efficency grades

9. Result

Dimensions of corrugated sandwich plate

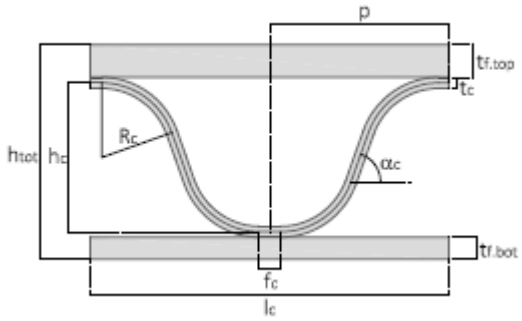

$h_{c.A} = 342.229 \cdot mm$

$t_{f.topA} = 48.174 \cdot mm$

$t_{f.botA} = 13.016 \cdot mm$

$t_{c.A} = 6.582 \cdot mm$

$\alpha_{c.A} = 47.818 \cdot deg$

$f_{c.A} = 30 \cdot mm$

$R_{C1.A} = 39.49 \cdot mm$

Outer interesting output

Total height of sandwich

$h_{tot}\left(h_{c.A}, t_{f.topA}, t_{f.botA}, t_{c.A}\right) = 410 \cdot mm$

Length between corrugation

$l_c\left(h_{c.A}, \alpha_{c.A}, f_{c.A}, R_{C1.A}\right) = 750.275 \cdot mm$

Total volume

$V\left(h_{c.A}, t_{f.topA}, t_{f.botA}, t_{c.A}, \alpha_{c.A}, f_{c.A}, R_{C1.A}\right) = 6.895 \cdot m^3$

Eigenfrequency

$f_1\left(h_{c.A}, t_{f.topA}, t_{f.botA}, t_{c.A}, \alpha_{c.A}, f_{c.A}, R_{C1}\right) = 8.16 \cdot Hz$

Deflection (instantaneous)

$w_{inst}\left(h_{c.A}, t_{f.topA}, t_{f.botA}, t_{c.A}, \alpha_{c.A}, f_{c.A}, R_{C1.A}\right) = 17.168 \cdot mm$

Stiffnesses imported to Abaqus (general shell stiffness)

$$D_{11}\left(h_{c.A}, t_{f.topA}, t_{f.botA}, t_{c.A}, \alpha_{c.A}, f_{c.A}, R_{C1}\right) = 4.716 \times 10^{8} \frac{kg}{s^2}$$

$$D_{12}\left(h_{c.A}, t_{f.topA}, t_{f.botA}, t_{c.A}, \alpha_{c.A}, f_{c.A}, R_{C1}\right) = 7.692 \times 10^{7} \frac{kg}{s^2}$$

$$D_{22}\left(h_{c.A}, t_{f.topA}, t_{f.botA}, t_{c.A}, \alpha_{c.A}, f_{c.A}, R_{C1}\right) = 4.121 \times 10^{8} \frac{kg}{s^2}$$

$$D_{33}\left(h_{c.A}, t_{f.topA}, t_{f.botA}, t_{c.A}, \alpha_{c.A}, f_{c.A}, R_{C1}\right) = 3.494 \times 10^{7} \frac{kg}{s^2}$$

$$D_{44}\left(h_{c.A}, t_{f.topA}, t_{f.botA}, t_{c.A}, \alpha_{c.A}, f_{c.A}, R_{C1}\right) = 1.143 \times 10^{7}\,J$$

$$D_{45}\left(h_{c.A}, t_{f.topA}, t_{f.botA}, t_{c.A}, \alpha_{c.A}, f_{c.A}, R_{C1}\right) = 1.884 \times 10^{6}\,J$$

$$D_{55}\left(h_{c.A}, t_{f.topA}, t_{f.botA}, t_{c.A}, \alpha_{c.A}, f_{c.A}, R_{C1}\right) = 1.009 \times 10^{7}\,J$$

$$D_{66}\left(h_{c.A}, t_{f.topA}, t_{f.botA}, t_{c.A}, \alpha_{c.A}, f_{c.A}, R_{C1}\right) = 8.052 \times 10^{5}\,J$$

$$K_{11}\left(h_{c.A}, t_{f.topA}, t_{f.botA}, t_{c.A}, \alpha_{c.A}, f_{c.A}, R_{C1}\right) = 2.536 \times 10^{6} \frac{kg}{s^2}$$

$$K_{22}\left(h_{c.A}, t_{f.topA}, t_{f.botA}, t_{c.A}, \alpha_{c.A}, f_{c.A}, R_{C1}\right) = 1.99 \times 10^{6} \frac{kg}{s^2}$$

Engineering constants

The engineering constants are used when the sandwich panel is modelled with the lamina model in Abaqus/CAE

$$E_{xeN}\left(h_{c.A}, t_{f.topA}, t_{f.botA}, t_{c.A}, \alpha_{c.A}, f_{c.A}, R_{C1}\right) := \frac{12 \cdot D_x\left(h_{c.A}, t_{f.topA}, t_{f.botA}, t_{c.A}, \alpha_{c.A}, f_{c.A}, R_{C1}\right)}{h\left(h_{c.A}, t_{f.topA}, t_{f.botA}, t_{c.A}\right)^3}$$

$$E_{yeN}\left(h_{c.A}, t_{f.topA}, t_{f.botA}, t_{c.A}, \alpha_{c.A}, f_{c.A}, R_{C1}\right) := \frac{12 \cdot D_y\left(h_{c.A}, t_{f.topA}, t_{f.botA}, t_{c.A}, \alpha_{c.A}, f_{c.A}, R_{C1}\right)}{h\left(h_{c.A}, t_{f.topA}, t_{f.botA}, t_{c.A}\right)^3}$$

$$G_{xyeN}\left(h_{c.A}, t_{f.topA}, t_{f.botA}, t_{c.A}, \alpha_{c.A}, f_{c.A}, R_{C1}\right) := \frac{6 \cdot D_{xy}\left(h_{c.A}, t_{f.topA}, t_{f.botA}, t_{c.A}, \alpha_{c.A}, f_{c.A}, R_{C1}\right)}{h\left(h_{c.A}, t_{f.topA}, t_{f.botA}, t_{c.A}\right)^3}$$

$$G_{xzeN}\left(h_{c.A}, t_{f.topA}, t_{f.botA}, t_{c.A}, \alpha_{c.A}, f_{c.A}, R_{C1}\right) := \frac{D_{Qx}\left(h_{c.A}, t_{f.topA}, t_{f.botA}, t_{c.A}, \alpha_{c.A}, f_{c.A}, R_{C1}\right)}{\left(\frac{5}{6}\right) \cdot h\left(h_{c.A}, t_{f.topA}, t_{f.botA}, t_{c.A}\right)}$$

$$G_{yzeN}\left(h_{c.A}, t_{f.topA}, t_{f.botA}, t_{c.A}, \alpha_{c.A}, f_{c.A}, R_{C1}\right) := \frac{D_{Qy}\left(h_{c.A}, t_{f.topA}, t_{f.botA}, t_{c.A}, \alpha_{c.A}, f_{c.A}, R_{C1}\right)}{\left(\frac{5}{6}\right) \cdot h\left(h_{c.A}, t_{f.topA}, t_{f.botA}, t_{c.A}\right)}$$

$$E_{xeN}\left(h_{c.A}, t_{f.topA}, t_{f.botA}, t_{c.A}, \alpha_{c.A}, f_{c.A}, R_{C1}\right) = 2.434 \times 10^9\ \text{Pa}$$

$$E_{yeN}\left(h_{c.A}, t_{f.topA}, t_{f.botA}, t_{c.A}, \alpha_{c.A}, f_{c.A}, R_{C1}\right) = 2.15 \times 10^9\ \text{Pa}$$

$$G_{xyeN}\left(h_{c.A}, t_{f.topA}, t_{f.botA}, t_{c.A}, \alpha_{c.A}, f_{c.A}, R_{C1}\right) = 1.769 \times 10^8\ \text{Pa}$$

$$G_{xzeN}\left(h_{c.A}, t_{f.topA}, t_{f.botA}, t_{c.A}, \alpha_{c.A}, f_{c.A}, R_{C1}\right) = 8.021 \times 10^6\ \text{Pa}$$

$$G_{yzeN}\left(h_{c.A}, t_{f.topA}, t_{f.botA}, t_{c.A}, \alpha_{c.A}, f_{c.A}, R_{C1}\right) = 6.295 \times 10^6\ \text{Pa}$$

9. Result

How to change of the volume optimisation to a height optimisation code

The volume optimisation code can quite easily be rewritten to a height optimisation code. First a height expression must be defined where all unknown variables are included. For example the expression for the neutral axis could be used in order to define the new height expression:

$$\text{height}\left(h_c, t_{f.top}, t_{f.bot}, t_c, \alpha_c, f_c, R_{C1}\right) :=$$

$$\frac{\left[\begin{array}{l} z_{na}\left(h_c, t_{f.top}, t_{f.bot}, t_c, \alpha_c, f_c, R_{C1}\right) \cdot A_{tot}\left(h_c, t_{f.top}, t_{f.bot}, t_c, \alpha_c, f_c, R_{C1}\right) \ldots \\ + -\left[\begin{array}{l} t_c \cdot f_c \cdot \left(\frac{t_{f.top}}{2} + \frac{t_c}{2}\right) + 2 \cdot t_c \cdot l_\alpha\left(h_c, \alpha_c, f_c, R_{C1}\right) \cdot \left(\frac{h_c}{2} + \frac{t_{f.top}}{2} + \frac{t_c}{2}\right) \ldots \\ + 2\, A_R\left(t_c, \alpha_c, R_{C1}\right) \cdot \left(\frac{l_1\left(h_c, \alpha_c, f_c, R_{C1}\right)}{2} + \frac{t_c}{2} + \frac{t_{f.top}}{2}\right) \ldots \\ + 2\, A_R\left(t_c, \alpha_c, R_{C1}\right) \cdot \left[\begin{array}{l} \left(-\frac{l_1\left(h_c, \alpha_c, f_c, R_{C1}\right)}{2} - \frac{t_c}{2}\right) \ldots \\ + -\frac{t_{f.bot}}{2} + h\left(h_c, t_{f.top}, t_{f.bot}, t_c\right) \end{array}\right] \ldots \\ + t_c \cdot f_c \cdot \left(\frac{t_{f.top}}{2} + \frac{t_c}{2} + h_c\right) \end{array}\right] \end{array}\right]}{A_{f.bot}\left(h_c, t_{f.bot}, \alpha_c, f_c, R_{C1}\right)}$$

Appendix C – Modelling of equivalent 2D shell plate in Abaqus/CAE

To verify the analytical calculations of deflection and first eigenfrequency a single layer shell is modeled in Abaqus/CAE. Two almost identical models are created, one for the deflection and one for the eigenfrequency. The differences are the definition of the steps and that a uniformly distributed load is defined for the deflection model.

Parts
The plate is modeled as a deformable planar shell defined in the 3D-space. The length and width are the set to $\sqrt{98}$ m in the Mathcad calculation, it is rounded to 9.899495 m. The large number of decimals is chosen in order avoid impact on the result based on the round off error.

Property
The properties of the plate are defined with the general shell stiffness matrix which is found under "create section" and under category "shell". In the stiffness matrix D_{11}, D_{12}, D_{22}, D_{33}, D_{44}, D_{45}, D_{55}, D_{66} are implemented (see figure A1). They are specified in the Mathcad code under "Abaqus constants".

Type: General Shell Stiffness

Stiffness | Dependencies | Advanced

Stiffness Matrix

	1	2	3	4	5	6
1	5.25063E+008	6.98969E+007	0	0	0	0
2		3.74447E+008	0	0	0	0
3			3.3514E+007	0	0	0
4				1.44406E+007	2.22489E+006	0
5					1.1919E+007	0
6						935932

Figure A1. Implementation of stiffness constants related to stretching, bending, torsion and horizontal shear in the general shell stiffness matrix.

Under "advanced", the density and the shear stiffness values, K_{11} and K_{22}, are implemented (see figure A2). The density should be expressed in kg/m2 and is the same as the variable m_{freq} in the Mathcad code. It is needed for the eigenfrequency calculation.

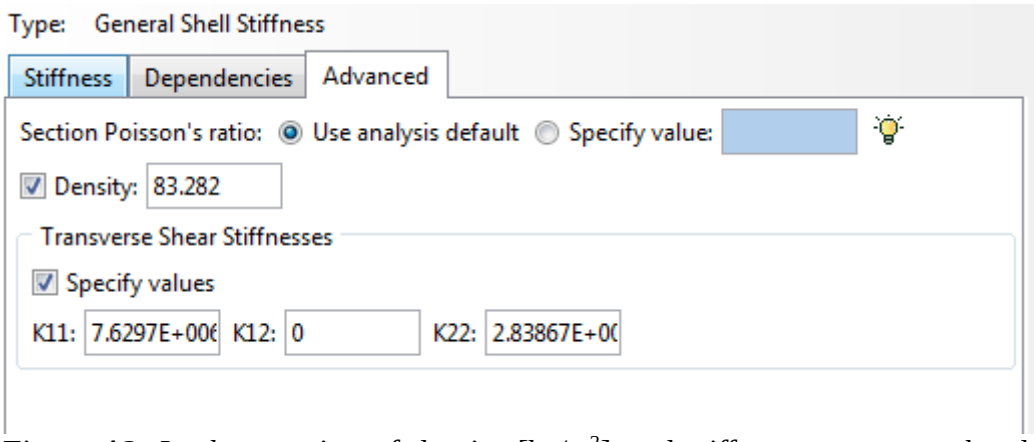

Figure A2. Implementation of density [kg/m^2] and stiffness constants related to transverse shear.

Load and boundary conditions

A uniformly distributed pressure load is defined for the deflection model. The load contains both the imposed load and the self-weight, the value of the load is found with the variable q_d in the Mathcad code, in this case it is equal to 2816.72 N/m2.

The plate should be modelled with hard type simply supported boundaries. The plate is sensitive to the choice of boundary conditions and if the result should be compared to analytical calculations it is important to define the boundaries equivalent to the mathematical expression in the analytical formulation. For hard type simply supported boundaries the displacement in vertical direction is locked along all edges. Further on the edges are locked for displacements in parallel direction and for rotation around the axis perpendicular to the edge. How the boundaries are defined is visualised in figure A3 and figure A4.

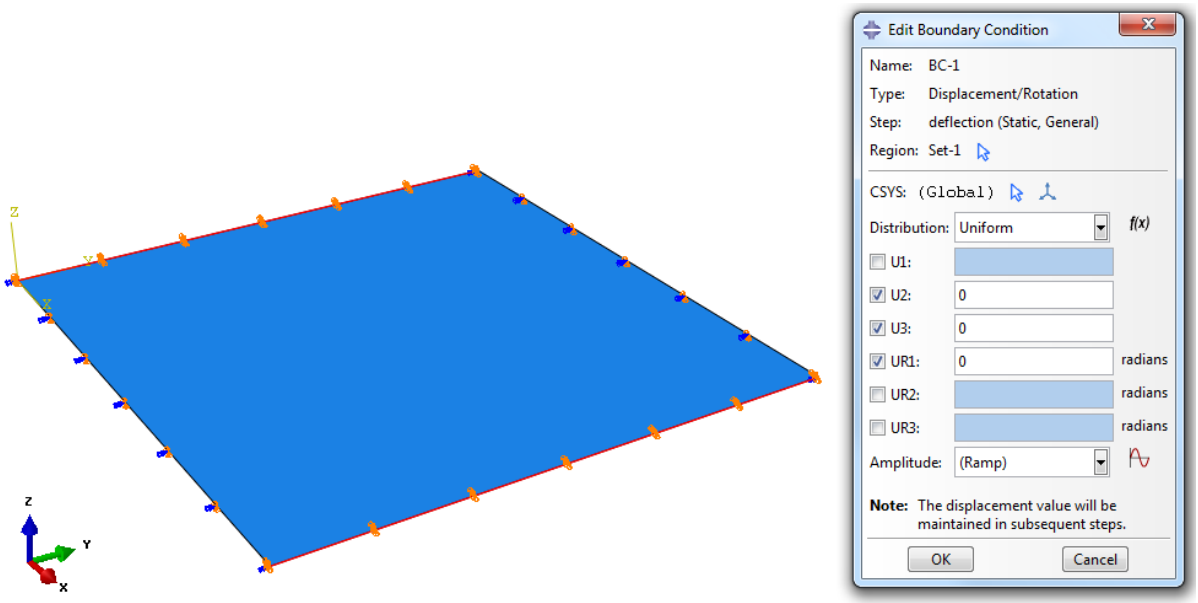

Figure A3. Definition of boundaries along edge parallel to y-axis. The displacements are locked in vertical direction (z-axis) and in y-direction. Rotations around the x-axis are prescribed to zero.

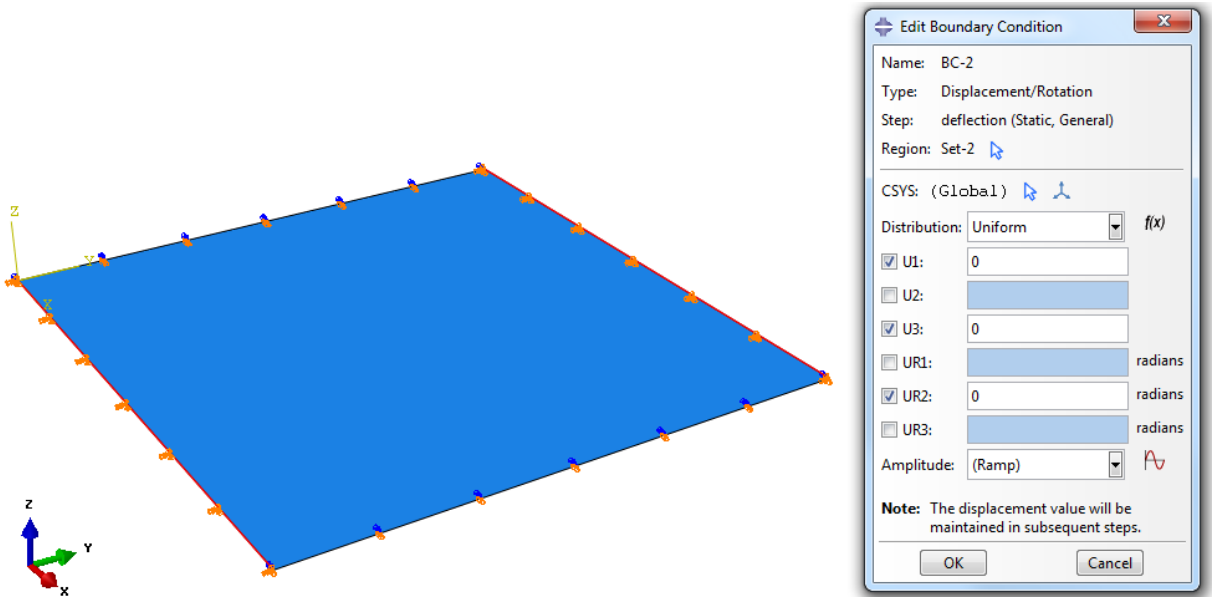

Figure A4. Definition of boundaries along edge parallel to x-axis. The displacements are locked in vertical direction (z-axis) and in x-direction. Rotations around the y-axis are prescribed to zero.

Mesh

The plate is meshed with triangular elements of the type STRI65 containing six nodes and five degrees of freedom per node. Convergence is reached with a seed size of 0.08. The number of elements is 30752.

Appendix D – Convergence studies of FE-model

Two convergence studies are presented for the FE-models. One study is performed for the plate when considering global deflection and the second study is performed when stresses are studied. A finer mesh is needed when studying stresses. For both studies plate 1:1 with cross-section 4 is used. The elements are of type S4R, hence they are quadratic shell elements with four nodes per element.

Convergence study for global deflection analysis
The deflection is presented in figure D1 as a function of the total number of elements and the model shows to converge with two decimals at 500 000 elements. Convergence studies were performed in the same manner for the other plates and dimensions to ensure that convergence was reached.

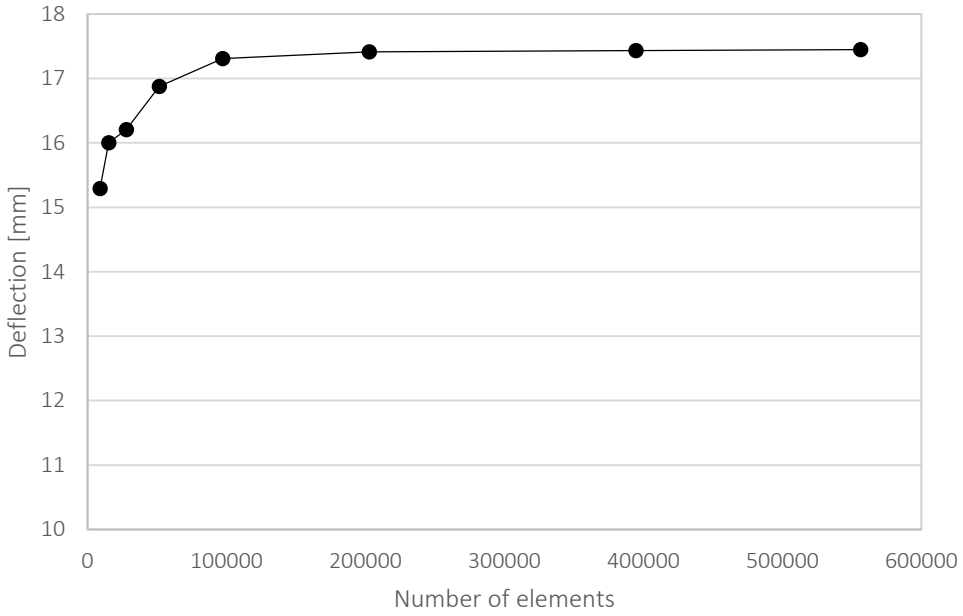

Figure D1. Convergence for global deflection analysis

Convergence study for stress analysis
The maximum Von Mises stresses are assumed to be located in the core, therefore a point in the core is chosen for the convergence study. The point investigated for the convergence is located at x=4.950 and y=4.314. The position is located close to the middle of the plate and close to the middle of a corrugation where no stress concentrations are likely to occur. The convergence is based on minimizing the difference between the maximum Von Mises stress and minimum Von Mises stress in the element. The convergence is presented in figure D2. As can be seen the convergence is rather good at when using about 1.2 million elements. A finer mesh would be computational demanding, hence the convergence is regarded as acceptable.

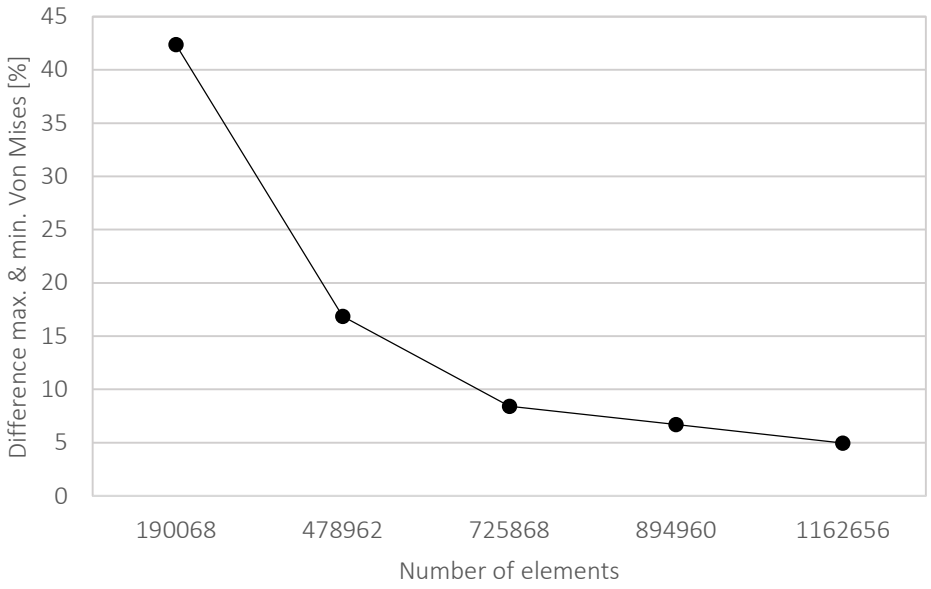

Figure D2. Convergence for stress analysis

Appendix E- Generating dimensions for hexagonal honeycomb

Following appendix presents how the dimensions for the honeycomb core is generated based on a given material volume. The honeycomb core has the same material volume as the corrugated.

Contents

1. Input data

Geometric input

$B := \sqrt{98}\,m$ — Witdh of floor, perpendicular to corrugation

$L := \sqrt{98}\,m$ — Length of floor, parallel to corrugation

$h_h := (341.1 + 13.3)mm$ — Height of core (equal to h_c+t_c for corrugated core)

$t_{f.top} := 38.4mm$ — Thickness of top plate (same as corrugated sandwich)

$t_{f.bot} := 17.6mm$ — Thickness of bottom plate (same as corrugated sandwich)

$V_{corr.tot} := 7.628 \cdot m^3$ — Reference volume (volume of sandwich with corrugated core)

Bending strength

$f_{m.0.k} := 22.2MPa$ — Bending strength in main fibre direction

$f_{m.90.k} := 19.7MPa$ — Bending strength perpendicular to main fibre direction

$f_m := \left[\frac{(f_{m.0.k} + f_{m.90.k})}{2}\right] = 20.95 \cdot MPa$ — Average bending strength

$\gamma_M := 1.2$ — Material partial factor (plywood)

Imposed loads

$Q_k := 2kN$ — Point load for local effects (imposed load)

$\gamma_{Q.ULS} := 1.5$ — ULS load partial factor

$k_{mod} := 0.8$ — Load-duration: Medium

2. Geometry of corrugation/honeycomb

Height of the cross-section (measured from centreline of top plate to centreline of bottom plate)

$$h(h_c, t_{f.top}, t_{f.bot}, t_c) := h_c + \frac{t_{f.top}}{2} + \frac{t_{f.bot}}{2} + t_c$$

Height of the cross-section (measured from top to bottom of SSP)

$$h_{tot}(h_c, t_{f.top}, t_{f.bot}, t_c) := h_c + t_{f.top} + t_{f.bot} + t_c$$

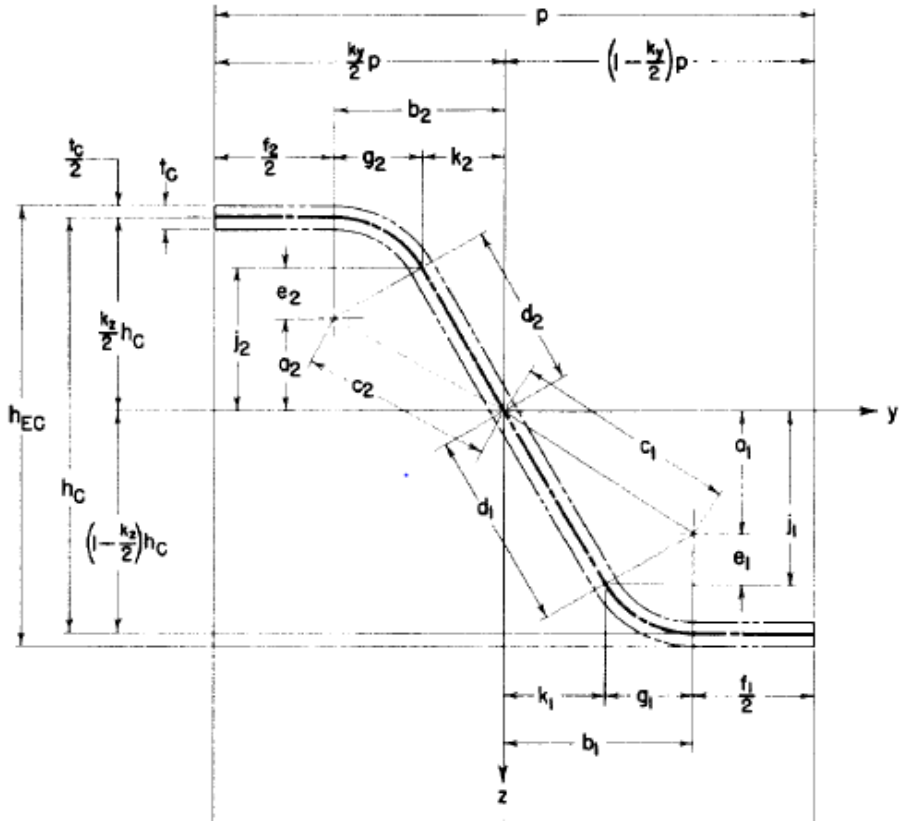

Symmetrical corrugation k.y=k.z --> K.Ay and K.Az vanish

$$k_y := 1 \qquad k_z := 1 \qquad K_{Ay} := 0 \qquad K_{Az} := 0$$

$$e_1(\alpha_c, R_{C1}) := R_{C1} \cdot \cos(\alpha_c)$$

$$g_1(\alpha_c, R_{C1}) := R_{C1} \cdot \sin(\alpha_c)$$

$$a_1(h_c, R_{C1}) := \left(1 - \frac{k_z}{2}\right) \cdot h_c - R_{C1}$$

$$j_1(h_c, \alpha_c, R_{C1}) := a_1(h_c, R_{C1}) + e_1(\alpha_c, R_{C1})$$

$$p(h_c, \alpha_c, f_c, R_{C1}) := f_c + 2 \cdot g_1(\alpha_c, R_{C1}) + 2 \cdot j_1(h_c, \alpha_c, R_{C1}) \cdot \frac{\sin\left(\frac{\pi}{2} - \alpha_c\right)}{\cos\left(\frac{\pi}{2} - \alpha_c\right)}$$

$$b_1(h_c, \alpha_c, f_c, R_{C1}) := \left(1 - \frac{k_y}{2}\right) \cdot p(h_c, \alpha_c, f_c, R_{C1}) - \frac{f_c}{2}$$

$$c_1(h_c, \alpha_c, f_c, R_{C1}) := \left(a_1(h_c, R_{C1})^2 + b_1(h_c, \alpha_c, f_c, R_{C1})^2\right)^{\frac{1}{2}}$$

$$\alpha_1(h_c, \alpha_c, f_c, R_{C1}) := \operatorname{atan}\left(\frac{a_1(h_c, R_{C1})}{b_1(h_c, \alpha_c, f_c, R_{C1})}\right)$$

$$\beta_1(h_c, \alpha_c, f_c, R_{C1}) := \operatorname{asin}\left(\frac{R_{C1}}{c_1(h_c, \alpha_c, f_c, R_{C1})}\right)$$

$$\theta(h_c, \alpha_c, f_c, R_{C1}) := \alpha_1(h_c, \alpha_c, f_c, R_{C1}) + \beta_1(h_c, \alpha_c, f_c, R_{C1})$$

$$d_1(h_c, \alpha_c, f_c, R_{C1}) := \left(c_1(h_c, \alpha_c, f_c, R_{C1})^2 - {R_{C1}}^2\right)^{\frac{1}{2}}$$

$$k_1(h_c, \alpha_c, f_c, R_{C1}) := b_1(h_c, \alpha_c, f_c, R_{C1}) - g_1(\alpha_c, R_{C1})$$

Height of radius (z-direction)

$$l_1(h_c, \alpha_c, f_c, R_{C1}) := \frac{h_c}{2} - j_1(h_c, \alpha_c, R_{C1})$$

Length of one corrugation leg

$$l_s(h_c, \alpha_c, f_c, R_{C1}) := f_c + 2.R_{C1} \cdot \theta(h_c, \alpha_c, f_c, R_{C1}) + 2 \cdot d_1(h_c, \alpha_c, f_c, R_{C1})$$

Area, per unit width, of the corrugation cross-section, [m^2/m]

$$A_C(h_c, t_c, \alpha_c, f_c, R_{C1}) := \frac{l_s(h_c, \alpha_c, f_c, R_{C1}) \cdot t_c}{p(h_c, \alpha_c, f_c, R_{C1})}$$

Length of the inclined corrrugation leg

$$l_{\alpha}(h_c, \alpha_c, f_c, R_{C1}) := 2\, d_1(h_c, \alpha_c, f_c, R_{C1})$$

Length of cross-section

$$l_c(h_c, \alpha_c, f_c, R_{C1}) := 2 \cdot p(h_c, \alpha_c, f_c, R_{C1})$$

Area of top flange

$$A_{f.top}(h_c, t_{f.top}, \alpha_c, f_c, R_{C1}) := t_{f.top} \cdot l_c(h_c, \alpha_c, f_c, R_{C1})$$

Area of bottom flange

$$A_{f.bot}(h_c, t_{f.bot}, \alpha_c, f_c, R_{C1}) := t_{f.bot} \cdot l_c(h_c, \alpha_c, f_c, R_{C1})$$

Area of one curved part

$$A_R(t_c, \alpha_c, R_{C1}) := R_{C1} \cdot \alpha_c \cdot t_c$$

Area of core

$$A_c(h_c, t_c, \alpha_c, f_c, R_{C1}) := 2 \cdot l_s(h_c, \alpha_c, f_c, R_{C1}) \cdot t_c$$

Total Area

$$A_{tot}(h_c, t_{f.top}, t_{f.bot}, t_c, \alpha_c, f_c, R_{C1}) := A_{f.top}(h_c, t_{f.top}, \alpha_c, f_c, R_{C1}) + A_{f.bot}(h_c, t_{f.bot}, \alpha_c, f_c, R_{C1}) \ldots + A_c(h_c, t_c, \alpha_c, f_c, R_{C1})$$

Total area per unit width

$$A(h_c, t_{f.top}, t_{f.bot}, t_c, \alpha_c, f_c, R_{C1}) := \frac{A_{tot}(h_c, t_{f.top}, t_{f.bot}, t_c, \alpha_c, f_c, R_{C1})}{l_c(h_c, \alpha_c, f_c, R_{C1})}$$

Area of the core per unit width

$$A_C(h_c, t_c, \alpha_c, f_c, R_{C1}) := \frac{A_c(h_c, t_c, \alpha_c, f_c, R_{C1})}{l_c(h_c, \alpha_c, f_c, R_{C1})}$$

Volume of honeycomb per unit width

$$V_C(h_c, t_c, \alpha_c, f_c, R_{C1}) := 2\, A_C(h_c, t_c, \alpha_c, f_c, R_{C1}) \cdot h_h$$

Width of one honeycomb

$$b_h(h_c, t_c) := (h_c + t_c) \cdot 2$$

Number of corrugations in width

$$nr_h(h_c, t_c) := \frac{B}{b_h(h_c, t_c)}$$

Total honeycomb core volume

$$V_{C.tot}(h_c, t_c, \alpha_c, f_c, R_{C1}) := V_C(h_c, t_c, \alpha_c, f_c, R_{C1}) \cdot L \cdot nr_h(h_c, t_c)$$

Total material volume of honeycomb floor

$$V_{tot}(h_c, t_c, \alpha_c, f_c, R_{C1}) := V_{C.tot}(h_c, t_c, \alpha_c, f_c, R_{C1}) + (t_{f.top} + t_{f.bot}) \cdot B \cdot L$$

3. Local bending

The local bending of the top plate is calculated by treating the top plate as a fixed beam with 50 mm width and the length equal to the free span in a cell. An imposed point load is applied in the middle of the beam. The load is given in Eurocode as an imposed local load for floors. Self-weight is neglected. The structural model underestimates the real capacity of the top plate as no transversal load distribution is taken into account.

Point load

$$Q_{local} := \gamma_{Q.ULS} \cdot Q_k = 3 \cdot kN$$

Local moment

$$M_{Ed.local}(h_c) := \frac{Q_{local} \cdot (2 \cdot h_c)}{8}$$

Local moment capacity

$$W_{top}(t_{f.top}) := \frac{50mm \cdot t_{f.top}^{2}}{6}$$

$$M_{Rd.local}(t_{f.top}) := W_{top}(t_{f.top}) \cdot k_{mod} \cdot \frac{f_m}{\gamma_M}$$

4. Optimisation

Tolerance in the minimising iteration

$CTOL := 1 \cdot 10^{-3}$

Predefined values

$h_c := 200mm$ $\alpha_c := 60 \cdot deg$

$t_c := 6.5mm$ $f_c := 30mm$

Given

Constrains

Minimum dimensions

$f_c \geq 30mm$

$t_c \geq 6.5mm$

$R_{C1} := 6 \cdot t_c$

Corrugation angle (60 degrees in a hexagonal)

$\alpha_c = 60deg$

Length of corrugation equal to horizontal part in a hexagonal

$l_\alpha(h_c, \alpha_c, f_c, R_{C1}) = f_c$

Structural constrain regarding local bending

$M_{Ed.local}(h_c) \leq M_{Rd.local}(t_{f.top})$

Volume larger or equal to reference volume (becomes equal when minimising)

$V_{tot}(h_c, t_c, \alpha_c, f_c, R_{C1}) \geq V_{corr.tot}$

Minimising volume

$$\begin{pmatrix} h_{c.A} \\ t_{c.A} \\ \alpha_{c.A} \\ f_{c.A} \\ R_{C1.A} \end{pmatrix} := Minimize(V_{tot}, h_c, t_c, \alpha_c, f_c, R_{C1})$$

5. Output

Dimensions

$h_{c.A} = 130.149 \cdot mm$

$t_{c.A} = 6.5 \cdot mm$

$\alpha_{c.A} = 60 \cdot deg$

$f_{c.A} = 104.299 \cdot mm$

$R_{C1.A} = 39.824 \cdot mm$

$h_h = 354.4 \cdot mm$

Appendix F – Martinsons MBK 12-02 floor system

This appendix contains information about Martinsons MBK 12-02 floor system. The structural performance is presented with a span of 8.5 m for type 1 in the information sheet. Additional calculations are included to re-calculate the first eigenfrequency for different loads and span. The bending stiffness used in these calculations is obtained from Martinsons.

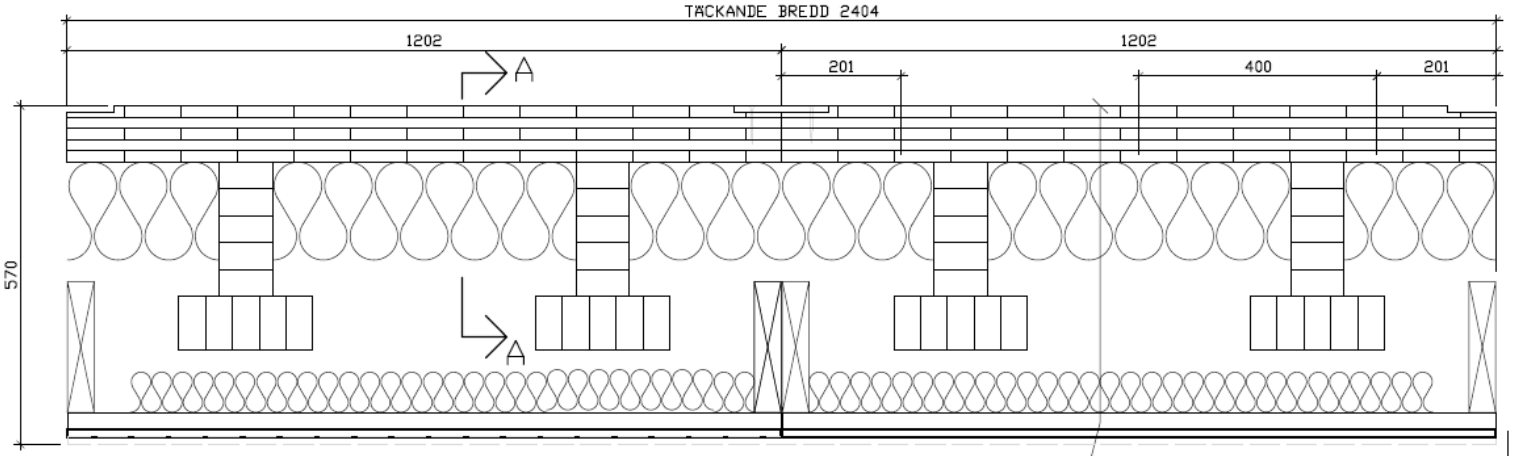

ELEMENTSKARV

MBK-12-02 Max tillverkningslängd 11,8m Egenvikt: 78 kg/m²

Statik

Karakteristisk last			Spännvidd[3]		Nedböjning[4]	
EKS	Last[1] [kN/m²]	BKR[2]	Typ 1 L [m]	Typ 2 L [m]	EK5[5] [mm]	[L/]
A	2,0	Vistelselast	8,5	8,5	14,3	L/596
B	2,5	Samlingslast	8,5	8,5	15,9	L/535
C:3	3,0	-	8,5	7,5	19,7	L/431
C:4	4,0	Trängsellast	8,5	6,0	23,6	L/360
C:5	5,0	Tung last	8,5	5,0	27,5	L/310

[1] EKS8, Tabell C-1. Lastvärden inkludera egt av flyttbara skiljeväggar: 0,5 kN/m² (SS-EN 1991-1-1)
[2] Laster, q_k (och Ψ) enligt BKR 2003 Tabell 3:41a. Egt = elementtypens egt + 50kg
[3] Egenfrekvens: 9,2 Hz. vid spännvidd 8,5 m. Nedböjning vid 1 kN punktlast på mitten: 0,45 mm
[4] Nedböjning vid spännvidd typ 1
[5] Nedböjning enligt karakteristisk kombination Bkv. 6.14a & 6.14b (SS-EN 1990)
[6] Nedböjning enligt lastkombination 9 BKR 2003 2:322c. Klimatklass 1

Byggnadsfysik

Brand: REI 60

Ljud: Ljudklass B för bostäder när den används i Martinsons byggsystem.

95 KL-TRÄ
90*225 LIV LK20
90*225 FLÄNS L40c
170 ISOLERING
45*220 REGEL
70 ISOLERING
LÄKT 28*70
cc300
13 GIPS
13 GIPS
(INGÅR EJ)

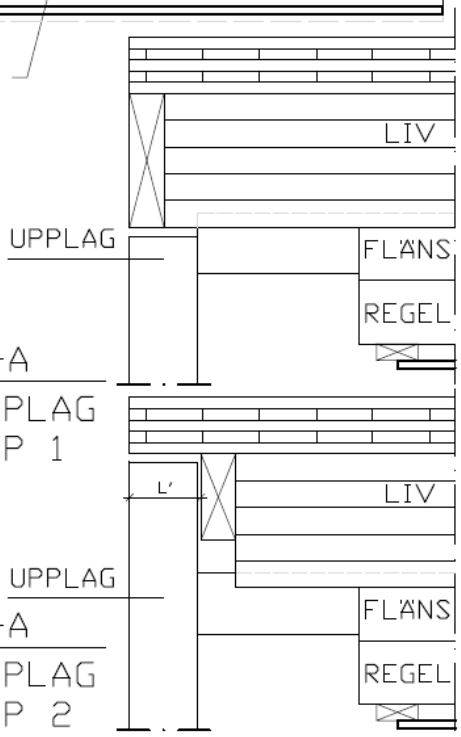

MBK-12-02

(2012-12-07)

Case study 2 - Calculation of eigenfrequency of MBK 12-02

Length of span

$L := 8m$

Width of one casette floor system

$B := 0.601m$

Width of different components

$b_{top} := 601mm$ Width of top flange

$b_{web} := 90mm$ Width of web

$b_{bot} := 225mm$ Width of bottom flange

Height of top flange

$h_{top} := 95mm$ Height of top flange

$h_{web} := 225mm$ Height of web

$h_{bot} := 90mm$ Height of bottom flange

Density of materials

$\rho_{GL30c} := 430 \frac{kg}{m^3}$ Density of gulam L40c (equivalent to GL30c)

$\rho_{GL24h} := 400 \frac{kg}{m^3}$ Density of glulam LK20 (equivalent to GL24h)

$\rho_{CLT} := 400 \frac{kg}{m^3}$ Density of CLT

Loads

$q_{imposed} := 5 \frac{kN}{m^2}$ Uniformly distributed imposed load

$q_{dw} := 2 \frac{kN}{m^2}$ Added dead weight due to installations and extra material

Bending stiffness per unit width (with reduction for shear deformation)

$EI_{unit} := 2.58 \cdot 10^7 \cdot N \cdot m$

Area of components

$A_{top} := b_{top} \cdot h_{top} = 0.057\,m^2$ Area of top flange

$A_{web} := b_{web} \cdot h_{web} = 0.02\,m^2$ Area of web

$A_{bot} := b_{bot} \cdot h_{bot} = 0.02\,m^2$ Area of bottom flange

Mass per square meter (without acoustic ceiling)

$$m_{unit} := \frac{A_{top} \cdot \rho_{CLT} + A_{web} \cdot \rho_{GL24h} + A_{bot} \cdot \rho_{GL30c}}{B} = 65.966 \frac{kg}{m^2}$$

Mass per square meter including added dead weight

$$m_{freq} := m_{unit} + \frac{q_{dw}}{g} = 269.909 \frac{kg}{m^2}$$

First eigenfrequency

$$f_1 := \frac{\pi}{2 \cdot L^2} \cdot \sqrt{\frac{EI_{unit}}{m_{freq}}} = 7.588 \cdot Hz$$